LEO-PNT Constellation Design through Multi-Objective Optimisation of Performance and System Feasibility

MSc Aerospace Engineering Thesis

by

Nikolaus Oliver Ricker Chong

for the degree of Master of Science in Aerospace Engineering
at Delft University of Technology,
under the supervision of the Examination Board,
to be defended in public on Nov. 14, 2025 at 11:00 AM

Student number:	5274737	
Repository:	GitHub Repository	
Project duration:	February, 2025 – November, 2025	
Thesis committee:	Dr. O. Çelik,	TU Delft, supervisor
	Ir. K.J. Cowan,	TU Delft
	Dr. S. Speretta,	TU Delft

TU Delft

Contents

SUMMARY

Navigation systems such as GPS, Galileo, and BeiDou have become essential to modern life, providing global coverage and reliability. However, challenges remain in addressing the limited geometric diversity, multipath propagation in urban areas, atmospheric distortions, and vulnerabilities to spoofing and jamming. Additionally, there is a growing demand for higher accuracy, faster convergence of techniques like Precise Point Positioning (PPP), and improved indoor coverage. To tackle these issues, Low Earth Orbit Positioning, Navigation, and Timing (LEO-PNT) systems have emerged as a promising alternative. Operating at lower altitudes, they offer advantages such as stronger link budgets, better geometric diversity, and compatibility with New Space principles, fostering innovation, cost reduction, and rapid deployment. Nonetheless, their design presents challenges in orbit determination within the complex LEO environment, precise clock synchronisation, system performance optimisation, constellation deployment strategies, and long-term sustainability considerations.

The objective of this thesis is to **assess the feasibility of a LEO-based PNT system that can provide comparable performance to existing GNSS systems while remaining cost-effective and leveraging New Space technologies**, operating independently from current constellations.

Constellations were modelled as Walker Delta and Walker Star configurations and evaluated from a geometric perspective using the Geometric Dilution of Precision (GDOP) metric. A simulator was developed, including Keplerian propagation and Earth's oblateness perturbation up to second degree zonal harmonic (J_2), and a user distribution following a Fibonacci lattice approach. Ground track repeating orbits adjusted for J_2 precession were analysed at altitudes of 700-1500 km, with limits given by drag and radiation exposure. Initial analyses showed that a minimum inclination of 68°-74° is required for full Earth coverage.

Optimisation was performed progressively, starting with a single-objective approach, minimising the number of satellites and advancing to multi-objective optimisations (MOO) using NSGA-III. The final optimisation minimised three objectives: manufacturing and launch cost, deployment time, and max 95th percentile GDOP ($GDOP_{95}$), using empirical and analytical models for satellite mass, cost scaling, and launcher capacity. Deployment strategies favoured maximising launcher capacity and indirect injection to minimise the time until the constellation is fully operational.

Results showed that higher altitudes yield better performance despite increased mass, with optimal designs around 1450 km. The most balanced configuration, the Equally Weighted Optimum, achieved a mean GDOP of 1.89, $GDOP_{95}$ of 2.69, cost below 3.5

B$, and deployment time of 16 months, using 150 satellites spread over 10 planes at a 79.3° inclination in a Walker Star formation. Additional analyses included End-of-Life (EOL) compliance (meeting ESA's 5-year reentry rule), debris risk ($\sim$ 20% probability of a collision avoidance manoeuvre per satellite), ground station visibility, and inter-satellite link (ISL) feasibility. A robustness assessment introduced a new metric, the Expected Performance Loss (EPL), quantifying performance degradation under random failures, showing 50-80% probability of at least one satellite failure.

Limitations include the restriction to Walker-type constellations, simplified cost and mass models, and assumptions in launcher cadence and regulatory aspects. Future work could expand the design space, refine feasibility models, incorporate alternative architectures, and explore augmentation with existing GNSS, as well as the ISL integration.

The study demonstrates that LEO-PNT constellations are technically and economically feasible, capable of achieving GNSS-level performance with reduced costs. The developed modular framework enables fast and adaptable mission design and optimisation, and establishes a foundation for future research in this emerging field. Access to the software and algorithms used throughout the thesis is provided via a public repository at `https://github.com/POTN1K/ConstellationOptimisation`.

Preface

This thesis marks the end of my five-year journey at TU Delft. It represents the goals I set for myself when I arrived here and brings together everything I've learned along the way. I never thought I would dive so deeply into navigation and mission analysis topics, but I am glad I did. Through courses, DSE, and an unforgettable internship at ESA, this thesis is a conclusion to that journey.

Writing this thesis turned out to be one of the best experiences of my studies. I had the chance to work on a topic I truly enjoyed and understood, one that challenged me, but also gave me the sense that my work could have a real impact. This project was ambitious, tackling multiple facets of the same problem, and I could not be prouder of the outcome.

I want to thank Onur for being an amazing supervisor. From the very beginning, you gave me the freedom to explore the topic as I pleased and you always asked the right questions. Your trust and reassurance, especially when I doubted my progress, made this process far more rewarding. I am also grateful to Alan and the entire LEO-PNT team at ESTEC for welcoming me so openly. I learned a great deal from all of you, and I hope that the insights from this work can be of value to the project.

Over these five years, Delft has seen me grow in more ways than I could have imagined. I am deeply thankful for the friends I've made here. When you leave your home, friends become your safety net, and I couldn't have done this without you. To those who have been here since the beginning and to those I met along the way, you made these years unforgettable.

To my friends back in Mexico, thank you for staying close despite the distance. Every summer you recharged my batteries and gave me the push to keep going. And above all, to my family, none of this would have been possible without you. Your sacrifices, encouragement, and unconditional support are the foundation of everything I have achieved. This is for you.

Looking back, I have learned much more than how to be an engineer. I want to thank my younger self for overcoming so many challenges to bring us here. It wasn't always easy, but it was definitely worth it.

Nikolaus Oliver Ricker Chong
Delft, November 2025

Nomenclature

Acronyms

2D-LFC	2D Lattice Flower Constellation
ARES	Assessment of Risk Event Statistics
C/A	Coarse/Acquisition code
CAM	Collision Avoidance Manoeuvre
CDMA	Code Division Multiple Access
CFRP	Carbon Fiber Reinforced Polymer
COTS	Commercial Off-The-Shelf
CROC	Cross Section of Complex Bodies
CSAC	Chip Scale Atomic Clock
DGNSS	Differential GNSS
DOP	Dilution of Precision [-]
DRMS	Root Mean Square of Range Errors [m]
ECEF	Earth-Centered, Earth-Fixed
ECI	Earth-Centered Inertial
ECSS	European Cooperation for Space Standardization
EGNOS	European Geostationary Navigation Overlay Service
ENU	East-North-Up coordinate system [-]
EOL	End of Life
EPL	Expected Performance Loss [%]
ESA	European Space Agency
FDMA	Frequency Division Multiple Access
FGUU	Frequency Generation/Upconversion Unit

FLVOP	Fibonacci Lattice Virtual Observation Points
FOC	Full Operational Capability
FSPL	Free Space Path Loss [dB]
GA	Genetic Algorithm
GCC	Galileo Control Centre
GDOP	Geometric Dilution of Precision [-]
GEO	Geostationary Earth Orbit
GMST	Greenwich Mean Sidereal Time
GNSS	Global Navigation Satellite System
GPS	Global Positioning System
HAS	High Accuracy Service
HDOP	Horizontal Dilution of Precision [-]
HFC	Harmonic Flower Constellation
HV	Hypervolume [-]
IGD	Inverted Generational Distance [-]
IGSO	Inclined Geosynchronous Orbit
IMU	Inertial Measurement Unit
IOC	Initial Operational Capability
IOD	In-Orbit Demonstrator
IoT	Internet of Things
IOV	In-Orbit Validation
ISL	Inter-Satellite Link
ISRO	Indian Space Research Organisation
JAXA	Japan Aerospace Exploration Agency
LEO	Low Earth Orbit
LLVOP	Latitude-Longitude Virtual Observation Points
MASTER	Meteoroid and Space Debris Terrestrial Environment Reference

MEO	Medium Earth Orbit
NaN	Not a Number
NASA	National Aeronautics and Space Administration
NSGA	Non-dominated Sorting Genetic Algorithm
NSGU	Navigation Signal Generation Unit
ODTS	Orbit Determination and Time Synchronization
OS	Open Service
OSCAR	Orbital Spacecraft Active Removal
P(Y)	Precise (Y) code
PDOP	Position Dilution of Precision [-]
PM	Polynomial Mutation [-]
PNT	Positioning, Navigation and Timing
POD	Precise Orbit Determination
PPI	Producer Price Index
PPP	Precise Point Positioning
PRN	Pseudo-Random Noise code
PRS	Public Regulated Service
PSO	Particle Swarm Optimisation
PVT	Positioning, Velocity, and Time
QZSS	Quasi-Zenith Satellite System
R&D	Research and Development
RAAN	Right Ascension of Ascending Node
RGT	Repeating Ground Track
RTU	Remote Terminal Unit
SAR	Search and Rescue
SBX	Simulated Binary Crossover [-]
SH	Spherical Harmonics

SISRE Broadcast Ephemeris Errors [m]

SNR Signal-to-Noise Ratio [dB]

SNR Signal-to-Noise Ratio

SOC Streets of Coverage

SoOp Signal of Opportunity

SPENVIS Space Environment Information System

SPP Single Point Positioning

SRP Solar Radiation Pressure [-]

SSCM Small Satellite Cost Model

SSO Sun-Synchronous Orbit

TDOP Time Dilution of Precision [-]

TFU Theoretical First Unit

TLE Two-Line Element

TOA Time of Arrival

TT&C Telemetry, Tracking and Command

TWTA Traveling Wave Tube Amplifier

UEE Pseudorange Noise and Multipath Error [m]

UERE User Equivalent Range Error

UHF Ultra High Frequency

ULS Uplink Station

UTC Coordinated Universal Time

VDOP Vertical Dilution of Precision [-]

WGS84 World Geodetic System 1984

Constants

μ Standard gravitational param. of the Earth [$3.98589196 \times 10^{14}$ m^3/s^2]

ω_{Earth}/ω_e Angular velocity of the Earth [7.2921159×10^{-5} rad/s]

c Speed of light [299,792,458 m/s]

g_0 Standard gravity [9.80665 m/s^2]

Greek Symbols

α Elevation angle [deg]

$\Delta\Omega$ Change in Right Ascension of Ascending Node (RAAN) [deg]

δ Angular separation [deg]

$\dot{\Omega}_{J_2}$ Rate of change of RAAN due to J_2 perturbation [deg/s]

$\dot{\omega}_{J_2}$ Rate of change of Argument of Perigee due to J_2 perturbation [deg/s]

$\dot{\theta}$ Rate of change of True Anomaly [deg/s]

$\dot{\theta}_{J_2}$ Rate of change of True Anomaly due to J_2 perturbation [deg/s]

ϵ Excess loss [dB]

ϵ_i Observation error [m]

η Efficiency [-]

η (NSGA) Distribution index [-]

λ Geodetic longitude [deg]

λ Wavelength [m]

Ω Right Ascension of Ascending Node (RAAN) [deg]

ω Argument of Perigee [deg]

ϕ Golden ratio [-]

ψ Azimuth angle [deg]

ρ Pseudorange [m]

σ_p Position error [m]

σ_{UERE} User Equivalent Range Error (UERE) [m]

θ True Anomaly [deg]

θ_{GMST_0} Local meridian at GMST reference time [deg]

ε Error term [-]

φ Geodetic latitude [deg]

Roman Symbols

Δt Change in time [s]

Δv Change in velocity [m/s]

$\mathbb{E}$ Expected value []

ρ Density [kg/m^3]

A Area [m^2]

A Availability [-]

a Semi-major axis [m]

C/N_0 Carrier-to-Noise Ratio [dB-Hz]

d Distance [m]

e Eccentricity [-]

F Relative spacing between satellites in adjacent planes in a Walker constellation [-]

f Frequency [Hz]

F_r Radial Force [N]

F_θ Tangential Force [N]

G Gain [dB]

H Design Matrix [-]

h Altitude above Earth's surface [m]

i Inclination [deg]

I_{sp} Specific Impulse [s]

J_2 Second zonal harmonic coefficient of the Earth's gravitational potential [-]

K Number of orbits [-]

L Loss [dB]

m Mass [kg]

n Mean motion [deg/s]

N (days) Number of days [-]

N (general) Number of units [-]

N_{sats} Number of satellites [-]

N_{users} Number of users [-]

P Number of orbital planes in a Walker constellation [-]

P Power [W]

p Probability [-]

P_{95} 95th percentile [-]

Q Cofactor Matrix [-]

R Radial [m]

R_e Earth's radius [m]

S Along-track [m]

S Number of satellites per plane in a Walker constellation [-]

s_i Satellite position vector [m]

T Orbital period [s]

T Thrust [N]

T Total number of satellites in a Walker constellation [-]

t Thickness [m]

t Time [s]

t_u Time offset of the user clock [s]

u User position vector [m]

V Volume [m^3]

W Cross-track [m]

List of Figures

List of Tables

1

Introduction

Satellite navigation is a concept that has revolutionised the way humanity perceives and interacts with the world. From its introduction through the Transit system in the 1960s, satellite navigation has continuously evolved to become an integral part of modern life. In the current era, systems like the Global Positioning System (GPS), GLONASS, Galileo, and BeiDou provide global coverage and have critical applications in various fields, including transportation, agriculture, military operations, and emergency response.

Nevertheless, the increasing reliance on satellite navigation systems has also highlighted areas of opportunity: signal interference, urban canyons, and the need for higher precision in certain applications. Several solutions have been proposed to address these challenges, and one of them has taken traction worldwide: the creation of a Low Earth Orbit (LEO) Positioning, Navigation and Timing (PNT) system. The so-called LEO-PNT systems leverage the advantages of LEO satellites, such as lower latency, improved signal strength, and changing dynamics, to enhance the overall performance of satellite navigation.

Entangled with the LEO-PNT concept comes the New Space era. New Space refers to the emerging private sector in the space industry, which is transforming the traditional approach to mission and satellite design. Companies like SpaceX, OneWeb, and Amazon's Project Kuiper are deploying large constellations of LEO satellites to provide global internet coverage. These have opened the door for LEO-PNT constellations to be deployed with reduced costs and faster timelines, making them a viable alternative to traditional GNSS systems.

LEO-PNT systems present a promising solution to the limitations of traditional GNSS, but they also introduce new challenges. Among these challenges is the need for robust and efficient constellation structures capable of providing the required coverage and performance, while maintaining a lean design, minimising costs, and ensuring a realistic deployment strategy. The objective of this thesis is to explore and evaluate different constellation structures for LEO-PNT systems, with a focus on optimising performance metrics and feasibility concerns.

The thesis follows a chronological structure, building progressively from fundamental concepts to advanced analyses. It begins with a literature study in chapter 2, which covers the fundamentals of mission and constellation design, GNSS, LEO-PNT systems, and the current state of the art. This chapter also identifies the research gap and formulates the research questions that guide the study.

Following the literature review, chapter 3 details the development of the simulation tool designed for a navigation constellation analysis. It describes the simulator's architecture, the orbital mechanics and perturbations considered, and the key assumptions adopted throughout the study.

The optimisation process is presented across four chapters, progressing from preliminary analyses to a comprehensive feasibility-driven optimisation. chapter 4 introduces a heuristic analysis that explores the design space and identifies key parameters such as inclination, altitude, and number of satellites. chapter 5 presents a single-objective optimisation using a genetic algorithm to minimise the number of satellites while satisfying performance constraints. chapter 6 extends this to a multi-objective framework with the NSGA-III algorithm, optimising both constellation size and performance metrics.

Building on these results, chapter 7 performs an integrated feasibility optimisation, extending the analysis to include satellite design aspects, ΔV requirements, launch and deployment strategies, and cost modelling within the optimisation framework. Additional elements such as space debris mitigation, ground segment design, inter-satellite links, and robustness are evaluated on the optimised constellations to provide a comprehensive assessment. This chapter combines the previous optimisation outcomes into a framework for LEO-PNT constellation design, offering the most complete and realistic evaluation of the system's overall feasibility.

Finally, chapter 8 presents the results of the feasibility optimisation and discusses their implications in the context of existing literature, highlighting representative constellation designs and key trends. The thesis concludes with chapter 9, which summarises the main findings, revisits the research questions, discusses the limitations, and outlines directions for future work.

Throughout the thesis, preliminary results are presented in earlier chapters where relevant to the corresponding methods or analyses. Consequently, certain findings may not be repeated in later sections if they have already been discussed in detail within a related context. This structure is intended to ensure clarity and continuity, allowing each chapter to build naturally upon the previous ones.

2

Literature Study

This chapter introduces the reader to the basic concepts of mission design, discussing relevant perturbations, orbits and design methodologies in section 2.1. It then provides an overview of GNSS fundamentals in section 2.2, including its operation principles, relevant performance metrics, the current systems in operation, as well as the challenges faced by them. The concept of LEO-PNT is introduced in section 2.3, discussing the idea and implementation, its potential performance improvements, as well as its challenges. The state of the art in LEO-PNT missions is reviewed in section 2.4, including existing missions, optimisation approaches, and other relevant information. Finally, the chapter concludes by summarising the key findings and proposing research directions for the thesis in section 2.5.

2.1. Fundamentals of Mission Design

Designing a mission has many aspects, and most segments and subsystems affect each other deeply. The mission profile, the orbit, the spacecraft design, and the ground segment are all interrelated and must be considered together. Generally, these are studied in parallel and developed iteratively. This section provides an overview of the basic concepts of mission design as seen from a higher level, where the focus is on the mission profile and orbit design. These are generally the first steps in the mission and drive the spacecraft's mass, power, and other requirements. They also carry the most significant economic impact, as they define the backbone of the mission. In the following subsections, the mission profile is discussed, relevant perturbations for the current mission, and the design methodologies used for constellation design.

Mission Profile and Types of Orbits

The mission profile defines the path followed by a satellite in space. This profile can vary greatly based on the mission objective, from fly-bys and landers to orbiters around a particular body. Depending on the profile, the mission is designed differently and affects all segments, from launch to operations. For the current study, a particular interest is placed on the orbits around the Earth. These orbits can generally be simplified using Keplerian motion for short periods or using averaged values. These orbits are described as such [173].

Earth orbits can be classified into a set of continuously varying eccentricities, inclinations, and altitudes ranging from low altitudes up to interplanetary orbits. The most common classes and their characteristics are summarised as follows: [6, 114, 173]

- Low Earth Orbit (LEO). A class of orbits located below 2000 km from Earth's surface. These orbits are used mainly for Earth observation, communication, transportation, and resupply. This is because of their proximity to Earth, allowing for high-resolution imaging, low-latency communication, and easy access for resupply missions. Their main drawback is the high atmospheric drag, leading to potentially frequent stationkeeping and a shorter lifetime. The upper limit is set by the Van Allen belts, areas with a higher concentration of high-energy particles. LEO orbits are the most populated due to their easy access. As of March 2025, LEO houses 84% of all satellites in space, and with the increase of constellations such as Starlink, these numbers are expected to rise. The International Space Station (ISS) is a well-known example of a LEO satellite.

- Medium Earth Orbits (MEO). Orbits located right above LEO, ranging from 2000 km to 35786 km (GEO). These orbits are used mainly for navigation and communication satellites. The main advantage of MEO orbits is the higher altitude, leading to a larger coverage area. This is particularly useful for navigation satellites, as they can cover a larger area with fewer satellites. The main drawback is the lower signal strength, as well as the cost of launching to these orbits. Only 3% of satellites are located in this region. Galileo, as a navigation system, is a well-known example of MEO satellites.

- Geostationary Earth Orbits (GEO). Orbits located at 35786 km from Earth's surface. These orbits have the characteristic of maintaining a "nearly fixed position with respect to the surface of the Earth" [173]. This is achieved by matching the orbital period with Earth's rotational period. In reality, the satellite is not perfectly aligned with the equator and will therefore move relative to the Earth, forming an 8-shaped pattern. Approximately 12% of satellites are located in this region.

Within these orbits, there is a second group defined as specialised orbits, given their particular characteristics. Some of the most famous orbits are defined here:

- Sun-Synchronous Orbits (SSO). Orbits that are approximately fixed with respect to the Sun. It takes advantage of the Earth's oblateness near the equator, commonly described using spherical harmonics using the term J_2, explained in more detail in section 2.1, to precess the orbit such that the Right Ascension of the Ascending Node (RAAN) of the satellite can rotate 360° in one year. To achieve this, there is a combination of altitude and inclination that must be met. They typically orbit at 600-800 km but can reach up to 5974 km. They are used for Earth observation satellites, monitoring weather patterns. The main advantage is the constant lighting conditions, as the satellite will always see the same area at the same time of day.

- Repeating Ground Track. Orbits that follow the same path as seen from Earth every certain number of orbits. It is achieved by defining the period as $T = N/K$, where K is the number of orbits and N is the number of days. This is useful for Earth observation satellites, as they can observe the same area at the same time of day.

- Polar Orbits. Orbits close to 90° in inclination. They are used for Earth observation satellites, as they can cover the entire Earth's surface. The main advantage is the coverage, as they can see the entire Earth's surface. The main drawback is the higher cost of launching to these orbits, as they require a higher inclination.

- Frozen Orbits. Orbits where one of the orbital parameters is fixed by taking advantage of certain perturbations. Circular orbits have eccentricity oscillations. By setting a low eccentricity, we eliminate variations and fix the apogee, taking advantage of the high spherical harmonics (section 2.1).

- Molniya Orbits. Orbits with a high eccentricity and inclination of 63.4°. Under these constraints, the apogee and perigee in the orbit are fixed. It is achieved by reducing the J_2 effect on the argument of perigee to zero. This is useful for communication and remote sensing, covering the northern hemisphere for longer periods.

- Lagrange Points. Points in space where the gravitational forces of two bodies (e.g. Sun and Earth) cancel each other out, maintaining a fixed position with respect to them. Space observatories, such as the James Webb Space Telescope, are located at these points.

This is not an exhaustive list, but it provides an overview and application of some of the most considered orbits. Some of them are taking advantage of perturbations, such as SSO and frozen orbits, but others do not consider them and are idealisations of what can be expected. It is therefore relevant to understand the perturbations affecting the mission.

PERTURBATIONS

Perturbations are the external forces affecting the satellites. When designing a mission, it is common to use a reference orbit and then consider the perturbations affecting it. This reference orbit is a simplification of what is to be expected and desired. It always includes a central body exerting at least a point mass gravity on the satellite. For example, in LEO orbits, the orbits are generally modelled as Keplerian orbits with a precession rate on the RAAN to account for the constant pull of the Earth's oblateness. Orbit perturbations are the deviations from such an orbit, creating the real orbit, which is the best estimate of the satellite's position [173].

The altitude has a large impact on the type of perturbations affecting a satellite. Closer to the Earth, atmospheric drag is dominant, and as the altitude increases, radiation and other bodies become more important. Figure 2.1 provides the relative importance of the perturbations as a function of altitude.

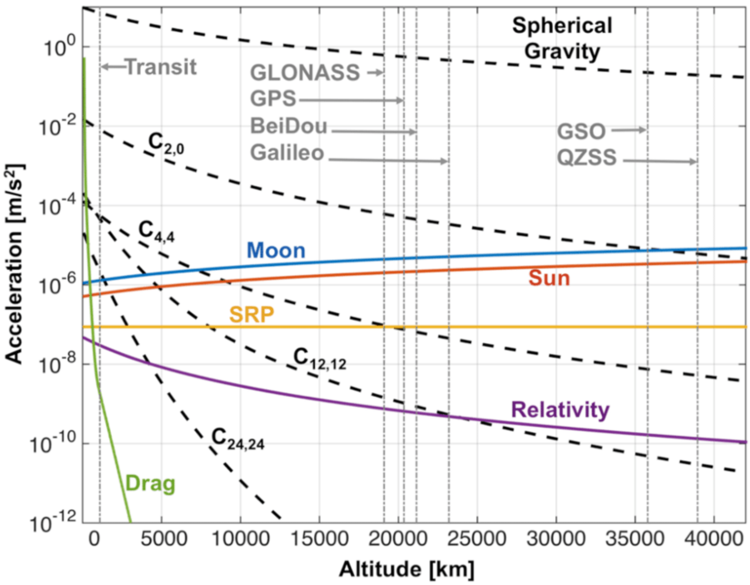

Figure 2.1: Orbital perturbations as a function of altitude. Source: [136]

The main perturbations affecting the satellite are introduced by Wertz (2001)[173]. There is a special focus on LEO orbits, as they are the focus of the current study. These are Earth's gravity, as well as third bodies, atmospheric drag, solar radiation pressure, and relativistic effects.

Earth Gravity. The main perturbation affecting the satellite is the Earth's gravity. When modelling it as a point mass, the Keplerian elements arise. However, the Earth is not perfectly spherical, leading to deviations from the ideal orbit. The perturbations causing this are referred to as spherical harmonics, and they have a larger effect the closer the satellite is to Earth. Spherical harmonics are defined by a certain degree and order, later expressed as SH(degree, order). Details on their calculations can be found in section 3.2. The main effect is the J_2 term, also known as the oblateness of the Earth. It represents a bulge found near the equator, leading to a precession of the orbit. The effect varies depending on the orbit, but for a circular LEO orbit at 500 km and close to the equator, the precession is $> 7.5 deg/day$.

Third Bodies. The gravitational pull of other bodies in the solar system also affects the satellite. The main bodies for Earth's orbits are the Sun and the Moon, and their spherical harmonics tend to be ignored. These bodies cause periodical variations in the orbital elements. It is relatively small, and for LEO this effect is diminished by Earth's spherical harmonics.

Solar Radiation Pressure. Also known as SRP, this perturbation also generates periodical variations, affecting mostly satellites with low mass and large cross-sectional area. It has an important impact above 800 km [173].

Atmospheric Drag. The main non-gravitational perturbation in LEO. It opposes the direction of the velocity, causing satellite decay. It is dependent on the density of the atmosphere, which is a function of altitude and solar activity, the satellite's cross-sectional area, and drag coefficient. Drag can vary by an order of magnitude depending on the spacecraft's attitude and up to two orders depending on the solar cycle. It is the main driver for stationkeeping in LEO.

Relativistic Effects. These are small, but they are important for high-precision missions. It is important for other GNSS subsystems, as it affects the clock rate.

During the mission design, it needs to be discussed which perturbations are acceptable and which ones have to be periodically corrected through stationkeeping. This, among several other aspects of the mission, requires trade-offs and optimisation.

CONSTELLATION DESIGN

Wertz (2001)[173] defines a constellation as "a set of satellites distributed over space intended to work together to achieve a common objective." When they are close to each other, they are called clusters or formations. The objectives of a constellation can be coverage, revisit time, and availability, among others. Some well-known constellations are GPS, Galileo, and Starlink. There is no rule when designing a constellation; the individual parameters may vary between satellites, but in general, some are kept constant (altitude, inclination, eccentricity) or follow a pattern (initial anomaly, RAAN).

A common simplification is to have circular, co-altitude constellations. In this scenario, the relative motion between satellites depends solely on their relative phase and relative inclination, forming analemmas with respect to each other. The relative inclination is not equal to the orbit inclination, but rather the angle formed between the two planes while crossing each other. The relative phase is the angle between the two satellites when crossing the equator. The relative phase is defined as the angular separation at the time of crossing the intersection [173].

As mentioned earlier, constellations work on a constant trade-off between performance and cost. Table 2.1 outlines the main aspects of constellation design.
Regarding coverage, it is very dependent on the mission. Some missions may allow for discontinuous coverage, others need continuous global or regional coverage, and systems used for navigation need fourfold coverage, meaning that at least four satellites are visible at all times. There has been a large number of studies on global coverage constellations. Among them are the Streets of Coverage (SOC) [103], Walker star and delta [169], Flower [112], among others. The ones mentioned here are generally the most commonly used because of their simplicity and performance.

Table 2.1: Main aspects in constellation design. Source: [173]

Aspect	Relevant Orbital Parameters	Relevance
Coverage	Altitude, elevation angle, inclination, constellation pattern	Principal performance parameter
Number of Satellites	Altitude, elevation angle, inclination, constellation pattern	Principal cost parameter
Launch	Altitude, inclination, satellite mass	Major cost driver
Environment	Altitude	Lifetime and hardness requirements
Perturbations	Altitude, inclination, eccentricity	Dephasing between satellites and stationkeeping
Collision Avoidance	Constellation pattern, orbit control	Snowball effect
Build-Up, Replenishment, and End-of-Life	Altitude, constellation pattern, build-up philosophy	Level of service over time and outage impact
Number of Orbit Planes	Altitude, inclination	Fuel consumption and graceful degradation

STREETS OF COVERAGE (SOC)

Developed by Luders (1961)[103], the SOC is the most common analytic constellation. It consists of circular orbits with a constant altitude in a single plane, creating a "street" that is continuously covered by the satellites. Figure 2.2a shows the concept of the SOC. Defining such a street is given by the maximum central angle, λ_{max}, and the distance S/2 from the satellite to the overlap point. The street angle is defined by Equation 2.1

$$\cos(\lambda_{street}) = \frac{\cos(\lambda_{max})}{\cos(S/2)} \tag{2.1}$$

The number of planes required for global coverage is given by $N = 360/\lambda_{street}$ for inclined orbits, and $N = 180/\lambda_{street}$ for polar orbits [99, 138].
Furthermore, when working with adjacent planes in a corotating constellation, the phasing between them can be adjusted to fill the gaps between the streets, as shown in Figure 2.2b. It leads to a max coverage per satellite of $D_{maxS} = \lambda_{street} + \lambda_{max}$. This schematic is a simplification, as in reality, closer to the poles, there will be clear overlapping between the streets [173].

WALKER CONSTELLATIONS

Created by Walker (1970)[169], this constellation methodology is probably the most well-known for global coverage. A reason for this is its flexibility and varied range of applications. It consists of a set of satellites in a circular orbit, with a constant altitude and a

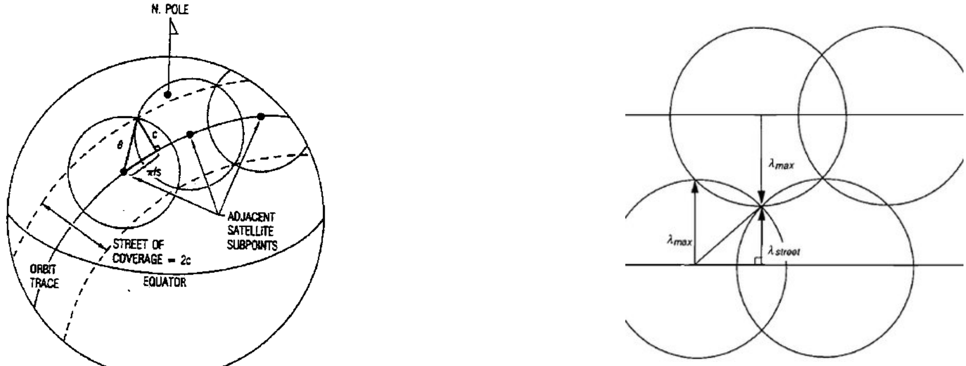

(a) Street of Coverage. Source: [99]

(b) Adjacent Streets of Coverage. Source: [173]

Figure 2.2: Streets of Coverage Concept

constant phasing between them. The symmetrical constellations are then commonly varied numerically to obtain optimal results. There have been multiple theoretical and practical constellation designs following this methodology, such as Galileo [18], GPS [85], and Starlink [28].

There are two types of Walker constellations, Delta and Star. Walker constellations use the notation $i : T/P/F$, where i is the inclination, T is the number of satellites, P is the number of planes, and F is the relative phase between adjacent planes. This constellation divides satellites equally among all planes and distributes the planes evenly over the entire RAAN range. Mathematically, the RAAN distribution for a Walker Delta is represented as follows Equation 2.2:

$$\Omega_p = \Omega_0 + \frac{360°}{P} \cdot p \tag{2.2}$$

where p is the plane number. On the other hand, Walker Star works mainly with near-polar inclinations and distributes the planes only over 180° rather than 360°, requiring a modification of Equation 2.2. This leads to a higher coverage of the poles, and satellites going towards the North on one side of the Earth, and towards the South on the other. The name is due to the star-link pattern formed at the poles [169].

The mean anomaly per satellite is then defined as shown in Equation 2.3

$$\theta_i = \frac{360°}{S} \cdot s + \frac{360° \cdot F}{T} \cdot p \tag{2.3}$$

where $S = \frac{T}{P}$. Figure 2.3 shows the concept of Walker constellations.
Lang and Adams (1997)[99] performed a comparison between SOC and Walker constellations. The first conclusion was that the required number of satellites increases as altitude decreases, although not necessarily in a monotonic way. It also showed that increasing the number of folds (satellites in view at all times) is not linear, as a two-fold

2

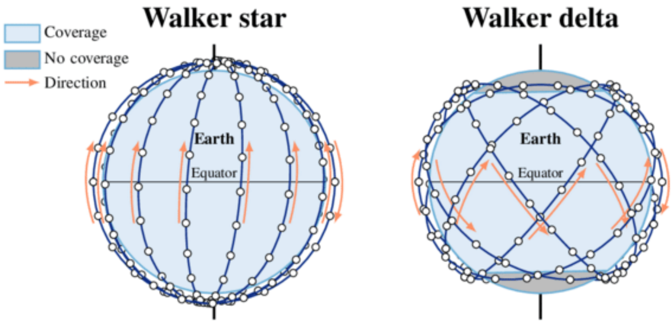

Figure 2.3: Walker Constellations. Source: [100]

constellation will not require double the satellites of a single-fold constellation. However, the most important conclusion drawn was that an optimally phased, non-symmetric polar SOC constellation outperforms Walker only when there is one-fold coverage required with more than 20 satellites. For any other scenario, such as multiple folds, Walker constellations are preferred.

Turner (2002)[166] performed an analysis on Walker for constellation design. They compared several cases and studied the phasing parameter, concluding that optimal coverage tends to occur following Equation 2.4, where the mod ensures the value of F is positive. When defining this parameter, it is important to also maximise the minimum miss-distance to prevent collisions at the intersection between two planes (usually at the poles) and radio frequency interference. Finally, they concluded that Walker is not the most efficient pattern if the number of satellites per plane equals the number of orbit planes, improving coverage when fewer satellites per plane are allocated.

$$F = [(P-1) - (T/P)] \mod P \tag{2.4}$$

FLOWER CONSTELLATIONS

A concept first defined in Mortari, Wilkins, and Bruccoleri (2004)[112] known as the Flower Constellation is a generalisation of several types of constellations. Ruggieri et al. (2008)[144] defines them as "special satellite constellations whose satellites follow the same 3-dimensional space track with respect to the assigned rotating reference frame". They take advantage of repeating tracks to create petals in the Earth Centred Earth Fixed (ECEF) frame, but can be extended to the implementation of J_2 perturbations under critical inclinations.

In contrast to the previous constellations, flower constellations do not need to be circular, allowing for extra flexibility. They are parametrised using five integer elements: number of petals N_p, number of days N_d, phasing F_n, F_d, and F_h, as well as three continuous orbital parameters: argument of perigee ω_p, inclination i, and perigee altitude h_p or eccentricity e. To ensure repeating ground track orbits, the constellation must meet $N_p t = n_d \frac{2\pi}{\omega}$, where T is the orbital period, and ω is the angular velocity of the reference frame. Figure 2.4 shows an example of a flower constellation around Earth with three petals in one day. It represents an eccentric orbit in a rotating frame, causing the appearance of petals as the satellite moves with respect to Earth's frame.

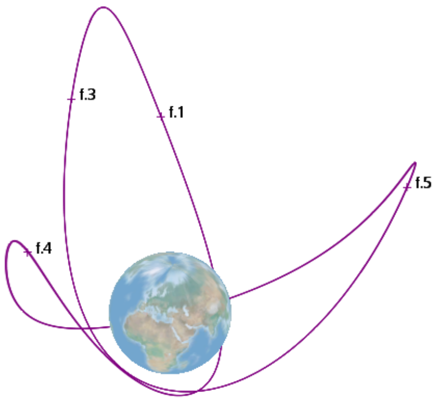

Figure 2.4: Flower Constellation Example. Source: [81]

The satellites then need to be distributed over the orbit node and anomaly lines based on Equation 2.5 and Equation 2.6

$$\Omega_k = 2\pi \frac{F_n}{F_d}(1-k) \tag{2.5}$$

$$M_k = 2\pi \frac{F_n N_p + F_d F_h}{F_d N_d}(k-1) \tag{2.6}$$

where $k = 1, 2, ...N_s$, with N_s being the total number of satellites. There is also the restriction $\frac{F_n}{F_d} < 1$, and $F_h \leq N_d - 1$. F_h is not limited to being constant. Finally, $N_s \leq F_d N_d$. The allocated path can then be filled with the satellites. However, if a satellite is meant to be placed in the position of an already occupied body, then it will be placed in a secondary path.

A flower constellation is known as Harmonic Flower Constellations (HFCs) when all the available slots are taken by a satellite. Avendaño, Davis, and Mortari (2013)[17] introduced a simplified approach to computing these scenarios, making use of integer parameters. It works on a lattice where the satellites are placed in a grid-like pattern in the (Ω, M)-space. The satellites' placement is then solved by following Equation 2.7:

$$\begin{bmatrix} N_o & 0 \\ N_c & N_{so} \end{bmatrix} \begin{bmatrix} \Omega_{ij} - \Omega_{00} \\ M_{ij} - M_{00} \end{bmatrix} = 2\pi \begin{bmatrix} i \\ j \end{bmatrix} \tag{2.7}$$

Where i goes from 0 to $N_o - 1$ and j goes from 0 to $N_{so} - 1$, giving the locations of satellite (i,j) in the plane. N_o, N_{so}, and N_c are the number of orbits, satellites per orbit, and phasing distribution. The zero parameters are the reference point of the first satellite. The repeating condition should also be enforced separately, following the rules previously given.

The 2D Lattice Flower Constellation (2D-LFC) is a development of the HFC [17]. A 2D-LFC is described by four integer parameters and six continuous ones. The integer parameters are given in matrix L, while the remaining are the Keplerian elements. The formulation is shown in Equation 2.8. The extra element $l_{1,2}$ allows for skewed lattices.

$$L \begin{bmatrix} \Delta\Omega \\ \Delta M \end{bmatrix} = \begin{bmatrix} l_{1,1} & l_{1,2} \\ l_{2,1} & l_{2,2} \end{bmatrix} \begin{bmatrix} \Delta\Omega \\ \Delta M \end{bmatrix} \tag{2.8}$$

However, for this case, there is not necessarily a constraint on the repeating time, expanding the constellation design space. It was also demonstrated to be mathematically equivalent to the Walker constellations when circular orbits are used.

A final option is known as the 2D Necklace Flower Constellation, a generalisation of the 2D-LFC. It is a more flexible version; instead of filling all spaces available, only a subset is considered. This allows to study different formations and design a better build-up, spares, and replenishment [15].

For both scenarios, lattice and necklace, there is the option to work with a 3D version. This adds a new degree of freedom, generally the argument of perigee to account for eccentric orbits [16, 37]. Although eccentric orbits were already used in 2D, they suggested working with them only at critical inclinations, while with these methods, that is no longer a constraint.

2.2. FUNDAMENTALS OF GNSS

Global Navigation Satellite System (GNSS) is a collection of all systems providing Positioning, Navigation, and Timing (PNT) services. These systems provide global or regional, accurate, continuous three-dimensional position and velocity to users, as well as distribute precise timing information following the Coordinated Universal Time (UTC) [85]. Among these systems, there are GPS, Galileo, GLONASS, and BeiDou. Such constellations are generally composed of approximately 30 satellites in MEO, providing 8-10 satellites in view of most points on the globe. This is a vital technology for the current world, with global revenues of €260 billion by 2023 [56], supporting in navigating ships, landing aircraft, providing precise timing, mining, and agriculture, among others [65].

FUNDAMENTALS OF SATELLITE NAVIGATION

Navigation systems work based on the principle of one-way time of arrival (TOA) ranging. It can provide service to unlimited users as the receivers operate passively. Depending on the system, there may be small differences, which are discussed in the following subsections, but the general concept works by measuring the time it takes for a user to receive a signal transmitted from a known location. This time interval can then be converted into a ranging distance from the reference point (satellite). When sufficient satellites are in view, and all signals are broadcast to a user, the receiver can determine its position [85].

GNSS satellites work as orbiting atomic clocks. They broadcast orbital parameters, precise timing of when the signal was broadcast, as well as corrections, health status, etc. For the user to know their location, they need to solve for the position and time, four unknowns. Consequently, at least four satellites should be in view [173]. The last unknown needs to be corrected because the user does not possess a sufficiently accurate clock on their device. On the contrary, systems like GPS or Galileo have agreed on expected time accuracies within the order of nanoseconds (10^{-9}) [18]. By adding a fourth satellite, this element can be solved, further reducing errors. To get an idea of the clock impact, an error of one nanosecond already accounts for a 30cm deviation in range.

The basic message structure varies, but taking GPS as an example, it takes approximately 12.5 minutes to transmit all information. This information consists of 25 frames, further subdivided into 5 subframes. Figure 2.5 graphically shows how a frame is constructed. The first three subframes contain the clock information and precise satellite ephemeris. These are the main elements required for computing a user's location and are repeated in every frame. Therefore, a receiver could compute its location within 30 seconds, the duration of a frame, after acquiring the signal. The final two subframes change every frame and give information on the health of the satellite, further corrections on the ionosphere and time, as well as global information on the constellation, known as the almanac. The almanac stores rough approximations of the neighbouring satellites, indicating to the user where to look. This information is valid for weeks, while the ephemeris sent in the first two frames is usually corrected every couple of hours [173, 150]. GPS uses this structure for its civilian and military codes. The first one is referenced as the Coarse/Acquisition (C/A) code, while the more precise one is the P(Y) code. The C/A code is available to all users, while the P code is encrypted and only available to authorised users. It works at a higher rate, making it less susceptible to jamming and capable of transmitting more precise data.

The receiver observes multiple signals, some by GNSS, but others may come from other sources, all at the same frequency. To mitigate interference and separate signals, GNSS employs Code Division Multiple Access (CDMA), where each satellite transmits the data using a unique Pseudo-Random Noise (PRN) code. These codes modulate the carrier wave, aiding the user in recognising the signal. As well, depending on how far it has travelled, the user might not know where in the 25 frames it is located, increasing the complexity of extracting the information. That helps discriminate relevant signals and locate themselves within them [150, 90].

SINGLE POINT POSITIONING

To determine the positions of the user in three dimensions, it follows Equation 2.9.

$$\rho_i = ||\mathbf{s}_i - \mathbf{u}|| + c \cdot t_u + \epsilon_i \tag{2.9}$$

where i ranges from 1 to n satellites, $\mathbf{s}$ is the satellite position, $\mathbf{u}$ and t_u are the position and time offset unknowns to solve, and c is the speed of light. ϵ_i are the errors of the

2

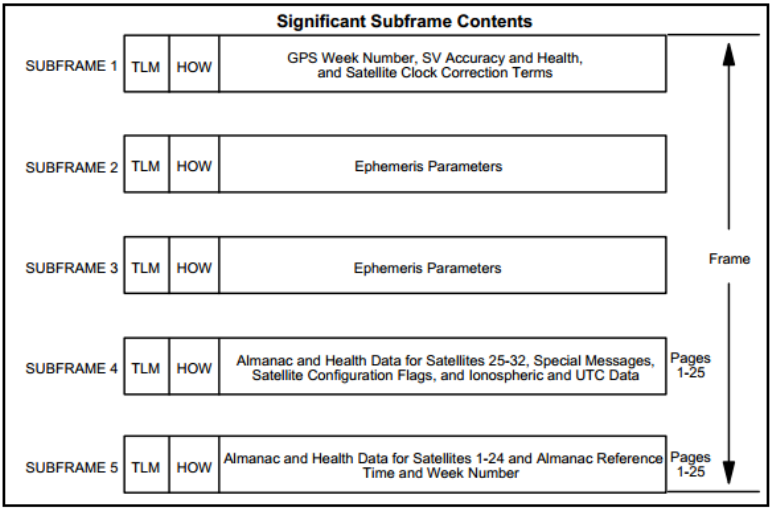

Figure 2.5: Structure of the GPS Message. Source: [82]

observation caused by the atmosphere, multipath, noise, etc. This vector equation can be expanded into at least four non-linear equations, which can be solved using closed-form solutions, iterative methods using linearization, or Kalman Filters. Kalman filters improve positioning by combining prediction and estimation. Furthermore, velocity can also be estimated using derivatives of the user position $\dot{\mathbf{u}} = \frac{d\mathbf{u}}{dt}$. This is a valid approach for nearly constant scenarios, but for more complex cases, more precise Position, Velocity and Time (PVT) methods have been devised, such as the use of the carrier wave, dual-frequency, or reference stations [85]. This method is known as Single Point Positioning (SPP), and can be used through single- or dual-frequency systems.

Table 2.2: GNSS Sources of Errors. Source: [85]

Contributing Source	**Single-Frequency Error (m)**	**Dual-Frequency Error (m)**
Satellite clocks	0.4	0.4
Differential Group Delay	0.15	-
Orbit errors	0.3	0.3
Ionospheric delays	7.0	0.1
Tropospheric delays	0.2	0.2
Receiver noise	0.1	0.1
Multipath	0.2	0.2
Total UERE (σ_{UERE})	7.03	0.6

Table 2.2 shows the typical error sources and effects using a one-standard-deviation approach. It contains the total pseudorange error (UERE), typically computed using the residual sum of squares method. The clock error has been mentioned earlier, but it is

related to the drift of atomic clocks on board satellites. Differential group delays are hardware biases between different signals and appear when the system is not well calibrated. Ephemeris estimates are computed by ground stations and regularly uplinked to the satellites; the residual errors are orbit errors. Ionospheric and tropospheric delays are caused by the atmosphere having different speeds of propagation. The ionosphere, located between 70 km and 1000 km, contains ionised gas molecules that affect electromagnetic waves. This delay will be different depending on the frequency of the carrier wave. By using a dual-frequency system, the error can be solved and corrected. Ionospheric errors are highly correlated between satellites, leading to smaller position errors than predicted by the UERE. The tropospheric error occurs in the lower part of the atmosphere and depends on its temperature, pressure, and relative humidity. The receiver noise is related to thermal noise, jitter and interference. Finally, multipath errors depend on the environment, occurring when a signal reaches the receiver from two or more paths, due to reflection, increasing the apparent distance to the satellite [85].

ADVANCED PVT METHODS

There are several techniques to improve the accuracy of a user's positioning. One has already been shown before, using two frequencies to solve for atmospheric delays. This technique is generally superimposed with others, such as Precise Point Positioning (PPP) and Differential GNSS (DGNSS). They both make use of reference stations, but in a slightly different way. PPP receives the clock and ephemeris estimates directly from the ground network, rather than as a satellite broadcast, as well as additional error modelling, and uses sequential filtering of both pseudorange and carrier-phase measurements. DGNSS uses a reference station at a known location transmitting corrections to nearby receivers. The European Geostationary Navigation Overlay Service (EGNOS), essential for aircraft landing, is an example of such technology [125].

Carrier-phase measurements track the carrier wave rather than the code. The wave has a higher frequency, making it more accurate. This has a double purpose, for position and velocity. The user tracks the carrier's fraction of a wavelength at any instant. There is an ambiguity N, the number of full wavelengths between the satellite and user, which can be solved by combining the pseudorange computations with the carrier wave. This allows us to reach centimetre-level accuracy. Furthermore, by tracking the Doppler shift of the carrier phase, the velocity can be computed [85].

DILUTION OF PRECISION

The user-satellite geometry also affects the PVT solution accuracy through a concept known as Dilution of Precision (DOP). DOP is a dimensionless metric that quantifies how satellite geometry amplifies measurement errors in the final position solution. When satellites are well-distributed across the sky, measurement errors have minimal impact on positioning accuracy. However, when satellites cluster in one region of the sky, the same measurement errors result in significantly larger position uncertainties [85].

This geometric effect is best illustrated in Figure 2.6. In an ideal case without measurement errors, the intersection of the ranging circles would yield a precise position (scenario A). However, real measurements contain uncertainty, creating overlapping areas between the ranging rings. When satellites are evenly distributed (scenario B), these overlapping areas are minimised, leading to better position accuracy. In contrast, when satellites concentrate over one region (scenario C), the overlapping uncertainty areas become much larger, degrading position accuracy. GNSS systems aim for lower DOP values to ensure optimal positioning performance.

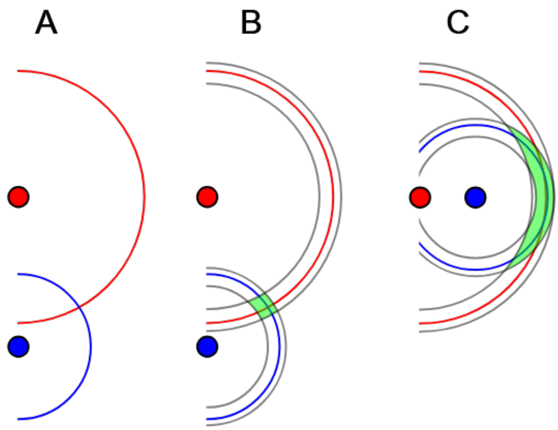

Figure 2.6: Relative Geometry and Dilution of Precision. Source: [178]

There is no exact agreement on what values of DOP are considered good or bad, as it depends on the application. However, lower values are always preferred. According to various sources, DOP values can be categorised as follows [111, 11, 80, 161]:

- Ideal: DOP < 1
- Excellent: $1 \leq$ DOP < 2
- Good: $2 \leq$ DOP < 5
- Moderate: $5 \leq$ DOP < 10
- Fair: $10 \leq$ DOP < 20
- Poor: DOP ≥ 20

To compute the DOP, at least four satellites are needed. A first step is to obtain the Jacobian after linearising Equation 2.9, known as the design matrix H. This matrix looks as

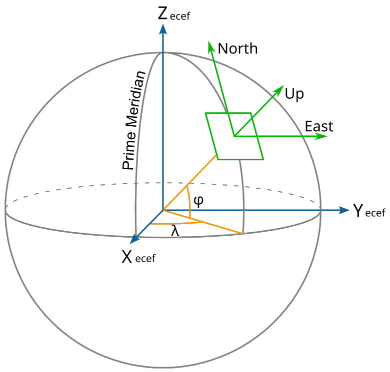

Figure 2.7: ENU coordinate system. Source: [108]

seen in Equation 2.10.

$$H = \begin{bmatrix} \frac{x_u - x_{s_1}}{\rho_1} & \frac{y_u - y_{s_1}}{\rho_1} & \frac{z_u - z_{s_1}}{\rho_1} & 1 \\ \frac{x_u - x_{s_2}}{\rho_2} & \frac{y_u - y_{s_2}}{\rho_2} & \frac{z_u - z_{s_2}}{\rho_2} & 1 \\ \vdots & \vdots & \vdots & \vdots \\ \frac{x_u - x_{s_n}}{\rho_n} & \frac{y_u - y_{s_n}}{\rho_n} & \frac{z_u - z_{s_n}}{\rho_n} & 1 \end{bmatrix} \tag{2.10}$$

where the position components are in an ECEF frame, generally using coordinates defining East, North, Up (ENU). An example of such is seen in Figure 2.7. From this matrix, the cofactor matrix Q is easily derived, as seen in Equation 2.11.

$$Q = \left(H^T H\right)^{-1} = \begin{bmatrix} \sigma_x^2 & \sigma_{xy}^2 & \sigma_{xz}^2 & \sigma_{xct}^2 \\ \sigma_{xy}^2 & \sigma_y^2 & \sigma_{yz}^2 & \sigma_{yct}^2 \\ \sigma_{xz}^2 & \sigma_{yz}^2 & \sigma_z^2 & \sigma_{zct}^2 \\ \sigma_{xct}^2 & \sigma_{yct}^2 & \sigma_{zct}^2 & \sigma_{ct}^2 \end{bmatrix} \tag{2.11}$$

These equations contain all relevant components for all DOP values. The DOP values are then computed from Equation 2.12 to Equation 2.16

$$GDOP = \sqrt{\sigma_x^2 + \sigma_y^2 + \sigma_z^2 + \sigma_{ct}^2} \tag{2.12}$$

$$PDOP = \sqrt{\sigma_x^2 + \sigma_y^2 + \sigma_z^2} \tag{2.13}$$

$$HDOP = \sqrt{\sigma_x^2 + \sigma_y^2} \tag{2.14}$$

$$VDOP = \sigma_z \tag{2.15}$$

$$TDOP = \sigma_{ct} \tag{2.16}$$

These values represent the geometric dilution of precision, using all elements, 3D-position, horizontal position, vertical position, and time, respectively [85].

2

PERFORMANCE METRICS

As a non-dimensional metric, DOP can be difficult to interpret. Therefore, other metrics help the mission analyst understand the performance of a system. Kaplan and Hegarty (2006) [85] defines accuracy, availability, integrity, and continuity as complementary to DOP. Accuracy is measured by the standard deviation. It represents the bias between the true and measured position. It is computed in Equation 2.17. It is also known as position error.

$$\sigma_p = DOP \cdot \sigma_{UERE} \tag{2.17}$$

It can also be used for any DOP measure. By taking two or three sigma, the user can have a 95% or 99% confidence interval, effectively working with the percentile of the error. Availability is the function to provide a certain accuracy level at a certain time and location. It is a function of the number of satellites in view and geometry, as well as other characteristics of the satellite and user. It is represented by Equation 2.18. The requirements will depend on the objectives and can be per region, latitude, time, or other factors.

$$A = P(\sigma_p \leq \sigma_{req}) \tag{2.18}$$

Integrity is a measure of the trust that can be put in a system. If it is not working properly, it should be able to provide the user with warnings. There are four main sources of anomalies causing Signal-in-Space aberrations: by the system, space segment, control segment, and user. The most common ones are due to clock deviations. To ensure integrity, enhancement techniques can be used, such as EGNOS in the aviation sector [125]. Finally, continuity is the ability of a system to maintain a specified performance for a certain period. It is a measure of the system's robustness and reliability.

GNSS SYSTEMS OVERVIEW

Currently, there are several GNSS worldwide. Each system follows similar principles, but has particular objectives for which they were optimised. Some have global coverage, while others are regional or enhanced over certain areas. Among these systems, there are GPS, Galileo, Beidou, GLONASS, and NavIC. In this subsection, a brief overview of each system is provided.

According to Kaplan and Hegarty (2006) [85], GNSS designs follow some major constraints and considerations. These considerations are mainly applicable to GPS and similar missions which aim for global coverage. It should only be considered a guideline followed in the past, rather than a recipe to use in the present. The considerations are:

1. Coverage needs to be global.
2. At least six satellites need to be in view of the user at all times. This increases robustness.
3. The constellation needs to have good geometry, with satellites uniformly distributed over the sky.
4. The system should be robust against a single satellite failure.

5. The constellation should be maintainable, with a low cost of replacement or repositioning.
6. The system shall minimise stationkeeping.
7. Altitude shall be chosen to minimise the size of the constellation, while managing complexity and payload size.

Table 2.3 shows a comparison made as part of a study by Montenbruck, Steigenberger, and Hauschild (2020)[110] in Wettzell, Germany, for dual-frequency, single-point positioning. The table shows the pseudorange noise and multipath (UEE), broadcast ephemeris errors (SISRE), total user range error (UERE), horizontal dilution of precision (HDOP), and the root mean square of the range errors (DRMS). The table shows that Galileo and BeiDou-3 have the best performance, with GPS following closely. GLONASS has the worst performance. Relevant to consider is that Galileo was not yet under Full Operational Capabilities (FOC) at the time of the experiment (Feb. 2020). The test also took place in Europe, for which Galileo had an advantage, as its design was to cover European soil, even if global coverage was also expected.

Table 2.3: Comparison of GNSS Systems using SPP. Source: [110]

System	Sats	Signals	UEE [m]	SISRE [m]	UERE [m]	HDOP	DRMS [m]
GPS	31	L1/L2 P(Y)	0.7	0.6	0.9	1.1	1.2
GLONASS	22	L1/L2 P	0.9	1.7	1.9	1.3	2.0
Galileo	22	E1/E5a	0.5	0.2	0.5	1.3	0.7
BeiDou-3	24	B1C/B2a	0.5	0.4	0.6	1.3	0.9

GLOBAL POSITIONING SYSTEM (GPS)

GPS was created in the 1970s by the US Department of Defense. It was initially designed for military purposes, but expanded for civilian use. The nominal constellation consists of 24 satellites in six MEO orbital planes. The system is composed of a space, control and user segment. It provides two services, the Standard Positioning Service (SPS) and the Precise Positioning Service (PPS). The SPS is available to all users, while the PPS is encrypted and only available to authorised users. Both use the L1 band, but PPS also uses L2. Recently, a variation of L2, L2C, has been introduced for civilian use. Finally, the L5 band is used for safety of life applications. Figure 2.8 shows the frequency bands used by GPS [85, 175].

The space segment is made up of a baseline 24-satellite constellation. They are circular, semi-synchronous orbits, such that their ground tracks repeat after every orbit, approximately every 12 hours. They are at an altitude of 20,200 km, an inclination of 55° and evenly distributed RAAN. As of July 2023, 31 operational 95% global accuracy for GPS is $<$ 100 m horizontal and $<$ 156 m vertical using single frequency C/A code. Using precise code, these values reduce to $<$ 36 m and $<$ 77 m respectively, even though better values are usually achieved [5].

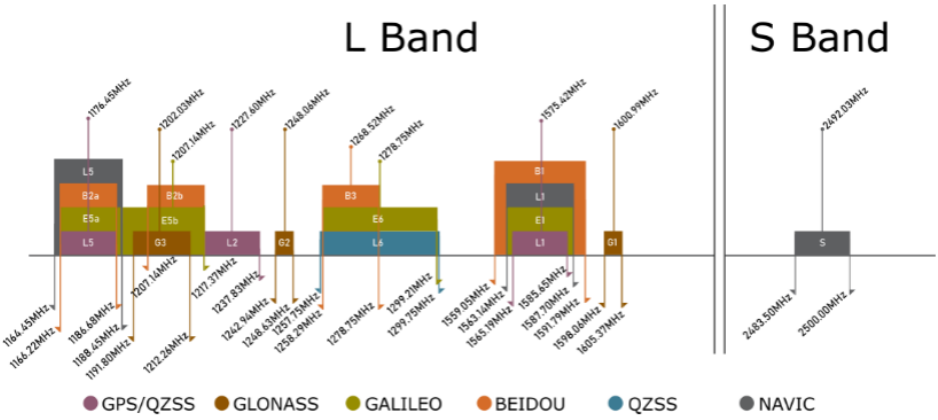

Figure 2.8: GNSS Frequency Bands. Source: [65]

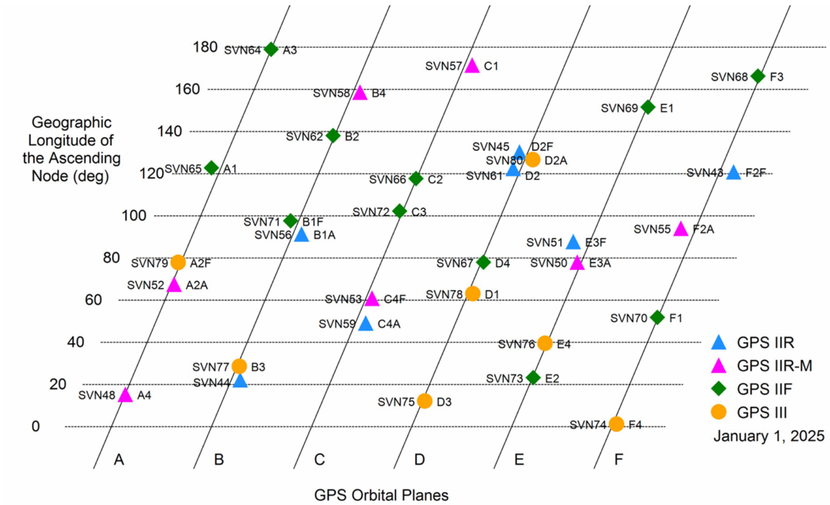

Figure 2.9: GPS Constellation. Source: [27]

GALILEO

In 1998, the European Union started the development of their own GNSS, focused on civilian use. It consists of space, launch, mission, control, and user segments. As of March 2025, the constellation has 32 satellites, of which 27 are operational, four are spares, and one is decommissioned [57]. The FOC has been reached, following a Walker Delta pattern 27/3/1 at an altitude of 23,222 km and inclination of 56° [8]. Galileo provides four services: Open Service (OS), High Accuracy Service (HAS), Public Regulated Service (PRS), and Search and Rescue Service (SAR). The system uses E1, E5a, E5b, and E6 bands, as shown in Figure 2.8. The performance levels expected by Galileo for 95%

global accuracy are < 15 m horizontal and < 35 m vertical using single frequency. With dual-frequency, these values reduce to < 4 m and < 8 m respectively [4].

BEIDOU

The Beidou satellite system was developed by China in a three-step process to provide navigation services to Asia and the world. It is comprised of the space, ground, and user segment. The project started in 1994 and has since developed from BDS-1 to BDS-3. Since 2020, it has provided FOC. The space segment is composed of 30 satellites. Three are located at GEO, specifically at 80°E, 110.5°E, and 140°E. Three satellites are in Inclined Geosynchronous Orbit (IGSO) near China, and the remaining 24 are MEO satellites. A combination with BDS-2 is shown in Figure 2.10. The accuracy aimed to be achieved 95% of the time is < 10 m horizontal and vertical globally, while 5 m is the objective for the Asia-Pacific region. They provide PNT services worldwide, as well as short message communication, SAR, and precise information [123, 122].

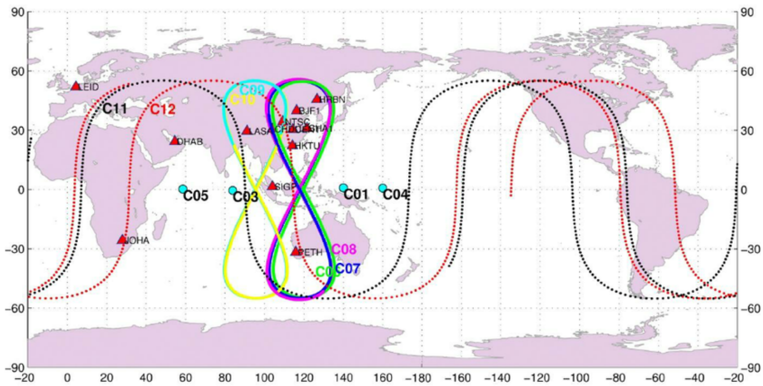

Figure 2.10: Beidou Constellation. Source: [75]

GLONASS

The Global Navigation Satellite System (GLONASS) was developed by the Soviet Union in the 1970s. It is composed of the space, control, and user segments. The constellation is composed of 24 satellites divided equally along three uniformly distributed planes. They are at a height of 19100 km and 64.8° inclination. They provide public and restricted services in L1 and L2. A key difference between GLONASS and other systems is the use of Frequency Division Multiple Access (FDMA), rather than through code (CDMA). This forces each satellite to use one unique frequency. In recent years, the system has been modernised, and the latest satellites, known as GLONASS-K, provide both signals. It is said that their accuracy is now comparable to GPS, between five and seven meters [137].

2

REGIONAL SYSTEMS

Regional systems are the Quasi-Zenith Satellite System (QZSS), developed by Japan Aerospace Exploration Agency (JAXA). It is a GNSS enhancement system. It is composed of four satellites, one in GEO and three in IGSO. The three follow the same analemma pattern, providing a longer visibility time over Japan, seen in Figure 2.11. It is mainly used for the Asia-Oceania regions [133].

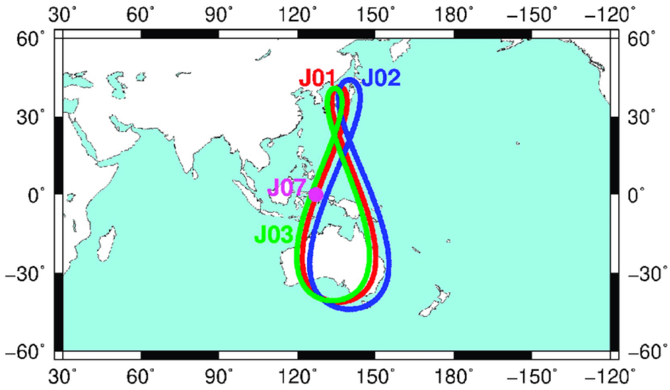

Figure 2.11: QZSS Constellation. Source: [176]

A second example is the Navigation with Indian Constellation (NavIC), developed by the Indian Space Research Organisation (ISRO). It is composed of seven satellites in GEO and IGSO. The three GEOs are located at 32.5°E, 83°E, and 131.5°E. Two IGSOs cross the longitude 55°E, while the remaining two cross 111.75°E and incline 29°. It is a regional military and civil service [85].

LIMITATIONS AND CHALLENGES

Even though GNSS has seen improvements in their signal, transmission and constellation size when compared to its beginning, some limitations and challenges still need to be addressed. These may be fixed through continuous development of MEO GNSS constellations, but also through the development of new systems. Some of the main challenges are:

- Atmospheric Distortions. Already mentioned above, modelling the ionosphere and troposphere is a complex task. The ionosphere is highly variable, and the troposphere is dependent on weather conditions. These errors can be corrected using dual-frequency systems, but they are still a source of error. This type of error is also a source of correlation between satellites, making convergence of precise positioning methods slower [141].
- Multipath Propagation. Areas with high reflectivity, such as cities, can cause the signal to reach the receiver through multiple paths. These can be known as urban canyons and are a source of error. The signal can be reflected off buildings, trees, or other structures, leading to a longer apparent distance [79].

- New Applications. Technology such as autonomous vehicles requires a highly accurate and reliable PNT system to operate. Ensuring the required availability is proving to be extremely complex with the current number of satellites and in dense urban areas [65]. Other technologies are IoT or 5G/6G network interaction [141].

- Low power signals. Due to the large distance to ground users, the signal received is weak and has limitations for indoor or urban use. It is also greatly affected by noise. This is further complicated by the security threats that can be posed by jamming or spoofing [79, 136].

- Satellite Geometry. The positioning of the satellites affects the performance, as well as limiting higher latitudes.

- Jamming and Spoofing. The signal is said to be jammed when an external source transmits a signal at the same frequency as the GNSS signal. This can be done to prevent the user from receiving the signal or to provide false information. This can be done by governments, but also by individuals. Spoofing is a more complex form of jamming, where the signal is not only blocked but also replaced by a false one. This can be done by creating a signal that is stronger than the original or by creating a signal that is more accurate than the original. Spoofing can make the user believe they are in a different location [65, 79].

Loss of GNSS in the UK and USA has been estimated to have an economic impact of a billion dollars daily [66, 63]. Loss of GNSS affects multiple sectors of the economy, from agriculture to military and science. This encourages the development of new systems, such as LEO-PNT, to provide a more robust and reliable system.

2.3. Low Earth Orbit (LEO) Positioning, Navigation and Timing (PNT)

Low Earth Orbit (LEO) Positioning, Navigation and Timing (PNT) has recently become one of the most researched projects in the PNT sector. It is considered a way to tackle the current challenges experienced and expected. These constellations would provide certain advantages concerning current MEO constellations. They also have several challenges to overcome, one of their main ones being the number of satellites and the space environment at that altitude. In the next subsections, the concept of LEO-PNT is introduced, and reasons for its development, potential applications, and challenges are discussed. In the next section, the state-of-the-art in LEO-PNT missions is reviewed.

2.3.1. New Space Environment

Before diving into LEO-PNT, a closely related concept that needs to be introduced is New Space. New Space is a term that refers to the transformation of the space industry from being dominated by government agencies and large corporations (Old Space) to a more commercial and entrepreneurial sector. New Space companies focus on innovative Research and Development (R&D), cost reduction, and rapid deployment of space technologies. This has led to the development of new technologies, such as small satellites, reusable launch vehicles, and satellite constellations [60].

Ferrara et al. (2025)[60] studies the design drivers and enablers for New Space missions. The main design drivers found are cost reduction, short time-to-market, function-specific performance, reliability, system and production scalability, debris mitigation, and environmental impact. These drivers are aligned with the main constellation projects in LEO, such as Starlink, OneWeb, or Kuiper. The main enablers for these drivers are the use of COTS components, miniaturisation, microfabrication, standardisation, additive manufacturing, mass production, design for demise and EOL, in-situ resources utilisation, and regulatory-aware design.

As discussed in the following subsection, LEO-PNT missions can take advantage of the New Space environment to provide a more cost-effective and efficient solution to PNT needs. The use of small satellites, COTS components, and rapid deployment can lead to a more agile and responsive system. However, it is essential to consider the challenges that come with this new approach, such as reliability, debris mitigation, and regulatory compliance.

2.3.2. MOTIVATION FOR LEO-PNT

The exploitation of LEO has been increasing in recent years. According to Kulu (2021)[94], the increase in satellite constellations was imminent in 2021, and has become a reality as of 2025. Table 2.5 summarises the current projects in LEO for communication purposes. The article studied 251 constellations, coming to the following conclusions. By 2021, most constellations had a focus on IoT and machine-to-machine (M2M) communications, followed by Earth observation, internet, and Synthetic Aperture Radar (SAR). Cubesats and microsats are the most common satellite types, and 236 out of the 251 (94%) are planned for LEO. This is likely because of the reduced launch costs appearing thanks to the reusability of the launcher, and the trend towards smaller satellites [26]. Ries et al. (2023)[141] studied the motivation for LEO-PNT by comparing it to traditional GNSS. The diversity in constellation, signals and technology opens a new range of possibilities. The main reasons for the development of LEO-PNT are:

Geometric Diversity. The new orbits, both in terms of altitude and inclination, would have a great impact on the geometric diversity. The orbital periods are shorter, which translates to less waiting time when an obstacle blocks the Line-of-Sight, or improves convergence for PPP.

Complement GNSS Coverage. LEO-PNT can provide coverage not initially considered by GNSS. This includes high latitudes, urban canyons, and potentially indoor environments. It also works as a backup system in case of GNSS failure.

Link Budget. By locating a constellation closer to Earth, the requirements on the system are lower, as the signal strength is higher. This allows for simpler systems or stronger signals. It is relevant to consider the regulatory environment, which can limit the use of certain frequencies or power levels.

Frequency Diversity. The signal diversity can also be used to improve accuracy or against interference. Signals outside L and S are already being tested, mainly C and UHF. These signals can deliver more accurate measurement codes or improve the link budget.

Two-Way PNT. The short distance between ground, space, and the user segment can be used to provide two-way communication. This can be used to provide more accurate positioning or to provide additional services, such as messaging. The latency is also greatly reduced, aiding in the spread of instructions or messages promptly.

Lean Design. Finally, the systems can be designed in a simpler way than GNSS. They can take advantage of already existing systems such as GPS or Galileo for Orbit Determination and Synchronisation (ODTS), rather than carrying their own atomic clocks and constant contact with ground stations. These simplified scenarios allow for the implementation of New Space approaches, more effective and efficient. New Space has a focus on commercialisation, privatisation, and the use of new technologies, taking higher risks through agile processes. As well, the cost of launching to LEO has been greatly reduced, visible in Figure 2.12.

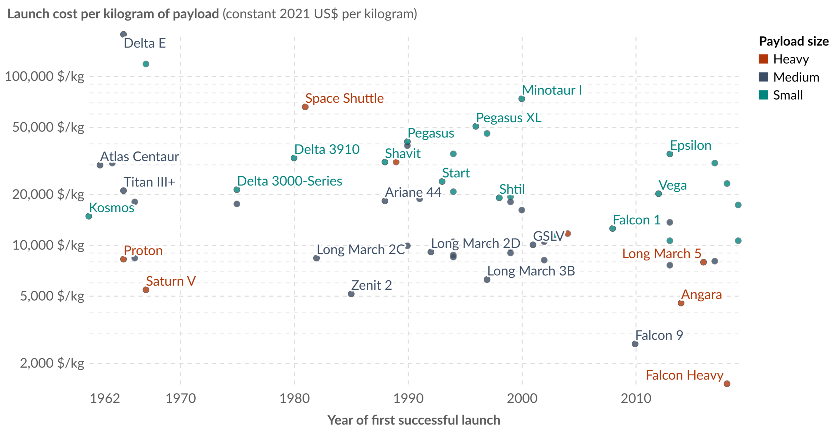

Figure 2.12: Cost of Space Launches to Low Earth Orbit. Data adjusted for inflation. Source: [130]

A further comparison with traditional GNSS can also be made to clarify the point. The main difference between MEO GNSS and LEO-PNT is the altitude, going from approximately 20,000 km to 1,000 km. This has a large impact on the orbital period, reducing from 12 hours to 1-2 hours in LEO. This affects the horizon-to-horizon pass being of 15min instead of 6-8 hours. That has a great advantage in geometric diversity. GNSS have 8-10 satellites in view at all times, except for polar regions. To achieve similar performance, LEO-PNT would require 200-300 satellites. The satellites in LEO will likely be micro (20 kg) or mini (200 kg), compared to traditional GNSS, weighing 2000 kg [65].

Geometrical diversity will have a large benefit on urban canyons and areas with limited visibility. The constant change in position and addition of satellites will provide a more robust system. The DOP values are also expected to be reduced. As mentioned earlier, higher latitudes can be targeted either through a multi-inclination system or using high inclination shells. A final improvement due to the geometry is the fast passing of the satellites. Ries et al. (2023)[141] explains that if the satellites move faster, observation errors can be decorrelated more easily by comparing measurements at different epochs. This is particularly useful for integer ambiguity resolution, improving the time for PPP convergence. This has been proven through simulation, confirming a drastic reduction in convergence time [101].

On the signal aspect, LEO-PNT has key advantages. A key aspect to improve is resistance against jamming and spoofing, which can be done thanks to the higher link budget. While GNSS has a carrier-to-noise ratio C/N_0 of 37-45 dB-Hz in the L1 band [69], LEO-PNT can reach much higher values. A study made on Starlink showed C/N_0 could reach 70 dB-Hz [92]. As well, using new frequencies diversifies the signal, making it more difficult to jam the entire spectrum. These new frequencies can also be used for extended purposes. Frequencies below the L band can penetrate trees and indoors better, potentially allowing for Indoor PNT, and combining them with the S band can improve ionosphere errors. Higher frequencies can be used for more precise measurements thanks to their shorter wavelength. If they are above 4 GHz, the ionosphere plays a minor role and accurate single-frequency measurements can be achieved [141].

New technology is also being developed in different areas. Anti-spoofing mechanisms can be implemented in the signals, as well as authenticity locks [65]. As well, the system can make use of 5G/6G Non-Terrestrial Networks as enablers for PNT uses. The latest generation of cellular network technology can be worked in collaboration with GNSS to design 5G-compatible signals and provide positioning and communication capabilities [141]. The possibility of using inter-satellite links (ISL) is also in the process. This technology is not new, but its implementation in the navigation sector is, and may be essential for the new constellations.

2.3.3. SYSTEM CONCEPTS

LEO-PNT is a system that provides navigation capabilities or enhancements to users on Earth. These systems have been explored through three options: dedicated systems, signals of opportunity, and integrated communication-navigation systems. A brief overview of these systems is provided, but special focus is given to dedicated systems, as they are the most relevant to this study.

DEDICATED CONSTELLATIONS

Dedicated services are constellations designed for PNT, which provide high-accuracy services. These can be either independent of MEO GNSS or enhancements to the current services. In the state-of-the-art section, both scenarios are discussed, as their optimisation approach will differ greatly. Table 2.4 shows a summary of the LEO-PNT constellations that are currently being developed. These constellations are designed by both private companies, such as Iridium or Xona, as well as public institutions, like JAXA and

ESA. The constellations vary depending on their objectives, but they are all expected to require 100s of satellites to provide global coverage.

Table 2.4: LEO-PNT Satellite Systems Overview. Source: [65]

Company	Country	First Launch	Launched	Frequency Band	Total Planned
Iridium	USA	2017	66	L	66
Xona Space	USA	2022	1 tech demo	L	258
TrustPoint	USA	2023	2 tech demos	C	300
JAXA	Japan	-	0	C	480
ArkEdge Space	Japan	-	0	VHF	50-100
Centispace	China	2018	5 tech demos	L	190
Geely	China	2022	0	L	240
SatNet LEO	China	2024	0	L	506
ESA's FutureNAV LEO-PNT IoD	Europe	-	0	L, S, C, UHF	10 demos (up to 263)

Further information about the constellations is given as follows. It complements what is found in the table and is extracted from a State of the Market report by FrontierSI (2024)[65].

Iridium. Designed as a communications constellation. The second generation, Iridium NEXT, will communicate with neighbouring satellites in the Ka-band using ISL, and host a payload by Satelles, providing Satellite Time and Position (STL). They aim for polar orbits at 780 km, with a mass of 860 kg per satellite. The expected accuracy is 10 – 20 m and time stability of 20 – 100 ns.

Xona Space. The American company is developing a constellation through three phases: the Initial Operating Capability (IOC) with one satellite augmenting GNSS, Phase 2 providing coverage of mid-latitude regions, and Phase 3 offering Full Operational Capabilities (FOC) globally and independently from GNSS. It will be located at high LEO.

JAXA. The Japanese space agency is working on improving PPP convergence from tens of minutes to under one minute. It will launch in two phases, launching half by 2030 and the rest by 2035. The constellation will be at 975 km and 55° inclination.

Centispace. A commercial Chinese company is working in collaboration with the Chinese government to improve PPP convergence to less than a minute. It will consist of three shells: (120 sats 975 km 55 deg), (30 sats 1100 km 87.4 deg), and (40 sats 1100 km 30 deg).

ESA's FutureNAV LEO-PNT IoD. The European Space Agency is working on a demonstration mission to provide PNT services. There are three phases planned: an In-Orbit Demonstrator (IOD) of 10 satellites, an In-Orbit Validation (IOV), and FOC. The IOD is planned at 550 km Quasi-polar orbits.

2

SIGNALS OF OPPORTUNITY

The second option is the Signal of Opportunity (SoOp) systems. These systems use radio signals from satellites that were not designed to provide PNT services. Some of the most famous ones can be found in Table 2.5. In most cases, these would be satellites used for communications. It works by extracting Doppler shift, pseudorange, and/or carrier phase measurements from the signals to compute the user's position. This would present opportunities to use the signals already in space, rather than develop new ones. The main challenge is that the signals were not designed for PNT, and therefore may not provide the required accuracy. First, these signals are not standardised, causing the user to decode the signal. The onboard clocks in the satellites is not stable [88], and ephemeris not as accurate [89].

Table 2.5: LEO Satellite Constellations Overview. Source: [65]

Company	Constellation	Country	First Launch	Launched	Total Planned
SpaceX	Starlink	USA	2019	7000+	42,000
China SatNet	Guowang	China	2024	10	12,992
SSST	G60	China	2024	36	12,000
Hongqing Technology	Honghu-3	China	-	0	10,000
GeeSpace	GEESATCOM	China	2022	30	5,676
Lynk	Lynk	USA	2022	6	5,000
Amazon	Kuiper	USA	2023	2	3,236
Skykraft	Skykraft	Australia	2023	10	2,976
EutelSat OneWeb	OneWeb Gen I	France, UK	2019	634	648
Rivada	OuterNET	USA	-	0	576
CASC	Hongyan-1	China	2018	1	320
SpaceRise	IRIS^2	EU	-	0	290
Sateliot	Sateliot	Spain	2023	6	250
Telesat	Lightspeed	Canada	-	0	198
AST SpaceMobile	Bluebird	USA	2023	5	168
ArkEdge	ArkEdge	Japan	-	0	50-100
Iridium	NEXT	USA	2017	80	80
Globalstar	Globalstar	USA	1998	48	65
Orbcomm	Orbcomm	USA	1995	31	31

Prol et al. (2023)[131] performed a survey of LEO-PNT. One of the focuses was on the studies done on the SoOp accuracies achieved. The first aspect to consider is that they all relied on Two-Line Elements (TLEs) to provide rough approximations. This occurs because there is no navigation message sent by the constellations. As well, they generally work as time-free solutions, greatly damaging the final results. These systems generally use an altimeter or IMU from the receiver's side to help the solution. The best solution converged to 7.7 m accuracy, benefiting from carrier-phase measurements and high satellite density by Starlink. Other solutions vary up to 1000 m.

FUSED COMMUNICATIONS AND NAVIGATION SYSTEMS

Finally, integrated systems are also in development. They do not have navigation as their primary payload, but carry sufficient technology to provide PNT services. According to

FrontierSI (2024)[65], Iridium NEXT will host a PNT payload from Satelles, providing satellite positioning and timing, independently of their main mission. Globalstar will also host an Augmented Positioning System (APS) payload, providing a low-accuracy service. A third example is the Guowang mega-constellation, developed by China SatNet, the same institution working on China's LEO-PNT service.

2.3.4. CHALLENGES

There are several challenges to be faced when developing LEO-PNT systems. These can be due to the harsh environment or the development of the system itself. Some of the main ones found in the literature are:

Precise Orbit Determination (POD) is one of the main aspects to consider in the design. Especially for dedicated systems, computing an accurate spacecraft position is essential to provide PNT services. The main approaches for POD are known as "dynamic", which works by solving the equations of motion considering the forces acting on the system; "kinematic", using the measurements directly; and "reduced-dynamic", combining both. In LEO, modelling the forces acting on the satellite for dynamic POD is complex. There is a presence of atmospheric drag, radiation pressure, albedo, and higher-order gravitational forces. Time variable effects, such as tides or third-body perturbations, also have to be considered. Perturbations are explained in more detail in section 2.1. On the other hand, "kinematic" methods rely solely on GNSS observations, which have their own set of challenges. These vary from eliminating ionospheric effects, inability to propagate between observations, multipath effects caused by the satellite itself and depend on the quality of the GNSS signal. The reduced-dynamic approach combines both, using the dynamic model to propagate the state vector and the GNSS observations to correct it. This approach presents itself as the best option for LEO-PNT systems [65].

Xie et al. (2018)[177] studied the required POD calculations for dedicated systems in LEO. The current GPS broadcast ephemeris works on 16 parameters (Keplerian, perturbations, time, harmonic corrections, among others), which is insufficient for LEO, causing a range error of 30-60 cm. Increasing the complexity of the Keplerian models to 22 coefficients solved the situation, improving the solution to less than 10 cm.

Another aspect to consider is the clocks. The lack of accuracy in them could affect both the POD of the satellite and the PNT service to the users. As mentioned earlier, because of the large quantity of satellites, it is not feasible to carry atomic clocks on the satellites, as they increase weight and cost. Even when using high-accuracy clocks, there is a linear relationship between orbits and clocks affecting the time error. There are several developments and methods to correct this error. A clear approach is to use atomic clocks on ground stations and synchronise them with the transmitting satellites. However, there are communication gaps, for which stable clocks are required. Providing the satellites with clocks that drift below the required threshold will probably also be possible for short periods. To maintain stable time for longer periods, there are three options: a dense ground network, GNSS satellites, or ISL. A dense ground network would send updated signals continuously, but it is logistically complicated and expensive, and the ground tracks of the satellites need to be designed accordingly. Using GNSS or GEO satellites reduces the number of ground stations, but creates a dependence on already existing systems, impacting the resilience. Finally, the use of (Optical) Inter-Satellite Links appears as a potential solution, by allowing for communication between satellites and a ground station. Synchronisation between satellites can be achieved, improving relative POD and timing. However, the development of the technology and implementation creates new challenges [65], such as geometrical feasibility, trading off temporal and permanent links, a communication strategy, and very high accuracy from the terminals.

Launch cost is a major design driver. Even if its price has dropped since the arrival of SpaceX to the market, the large number of satellites requires a major optimisation procedure of the constellation and its deployment. The satellite design choices will also be affected by it, as the weight and size have a major effect [65]. The study of constellation deployment is not new. Cornara et al. (1999) [35] developed a case study of a small Walker constellation in LEO (57°:24/6/x). There is no information on the phasing factor. For the plane population, there are two approaches: direct and indirect injection. Direct injection takes the satellites to the final orbit and allows for a quicker start of operations. It is generally more expensive and may not be feasible for certain altitudes/inclinations. Indirect injection sets the satellite at a lower altitude and uses Earth's oblateness to change the node of the satellite, potentially populating several planes in one launch. In this study, at least one full plane is populated per launch. When more satellites can be carried than required per plane, indirect injection is preferred. Nevertheless, the Δv and time required by the satellite to reach its final orbit should also be considered. Inspired by this article, an optimal deployment tool has been developed for mega-constellations, considering time, target orbits, and launch vehicles [158].

The constellation build-up should also be considered. Given that the total number of satellites is large, it will take a longer period to populate the constellation. The aim would be to provide service since the first deployment. This is usually achieved by populating a small number of planes, as they provide accurate regional coverage if placed nearby, or reduced global coverage if spread over the entire range. As well, in case of a satellite failure, rephasing the plane is easier and does not degrade the service as much. Regarding a replacement strategy, there are four options: overpopulation of the planes or constellation, in-orbit spares in parking orbits or aligned with the planes, and ground spares. Depending on the purpose, one is generally preferred and is due to the reliability and performance levels required. In-orbit spares will always be the best as seen from the performance perspective [35].

A final aspect is the End-of-Life of constellations. At the time of the study by Cornara et al. (1999) [35], regulations were more flexible and allowed for several options: controlled or uncontrolled reentry manoeuvres, non-propulsive orbit lifetime reduction. Since the development of the *ESA Space Debris Mitigation Requirements* in 2023 [7], the regulations have become stricter for Europe. Similar documents have been written for other countries, but among their requirements state that safe disposal shall have a probability of 90% or higher, disposal shall occur within five years after End-of-Mission, robust passivation techniques and proper demise at end of life are required, as well as minimise impact on astronomy. A study on optimisation of LEO constellations for space debris concluded that maximising the lifetime of the satellites optimises the constellation's contribution to space debris [124].

2.4. State-of-the-Art in LEO-PNT Missions

In this section, the state-of-the-art for LEO-PNT missions is reviewed. The main focus is on constellation design and optimisation, as well as the performance of the systems. Not all papers are specific to LEO-PNT, but they may have relevant information for the development of the thesis. It is divided into the general optimisation strategies for LEO-PNT related missions, followed by relevant related work.

2.4.1. Optimisation of LEO-PNT Constellations

Several papers have approached the optimisation of LEO-PNT constellations from different perspectives. In this subsection, they are explained, with a focus on their objectives, methodology, and results. The main focus is on the design of the constellation, generally taking some performance metrics as a basis. They are divided depending on the type of optimisation followed, first into analytical methods, then genetic algorithms, and finally other optimisation methods that could be related to the topic.

Analytical Methods

Analytical methods are the first step in developing an optimisation problem. They simplify the problem into a manageable one and help the reader understand the effect of the parameters on the results. They are generally used to provide a first approximation of the problem, and are then followed by more complex methods.

Wei, Li, and Du (2020)[172] studied the current methods for designing a constellation. The main focus is on Walker constellations, which are strong analytical solutions to achieve large-scale continuous global coverage. There is also a reference to SOC, an intuitive method, and Flower constellations, but the complexity of the latter makes the maintenance and operation more difficult, reducing the applicability. The paper proposes an optimal analytical solution by setting constraints on different parameters. Setting a four-fold coverage as the minimum, an analytical formula is developed to compute the Walker parameters. At a height of 1500 km, and an elevation angle of 10°, the results are 69.36°: 170/17/13. The phasing parameter F between planes was solved by iterating the phasing between satellites and minimising PDOP. This configuration gives ensures a $PDOP < 4$ for 94% of the time, and $PDOP < 8$ for 98.9% of the time as an independent system of other GNSS.

Ge et al. (2020)[67] studied the possibility of enhancing current GNSS with LEO constellations, known as LeGNSS. They statistically analysed the number of satellites, the number of planes and inclinations to find near-optimum solutions. To quantify the results, GDOP and availability are the objectives to minimise. They simulate GPS, Galileo, GLONASS, and BDS, along with a reference LEO constellation in a polar orbit. This reference is modified, first varying one parameter at a time, and then combining them. The most important conclusions from the study are:

- Increasing the number of planes improves the availability of the system, but does not improve the unequal distribution around the world. This is done by maintaining the total number of satellites, but distributing them in more planes. There is also an optimum within the number of planes.
- More satellites will reduce the total GDOP, but the effect is not linear, and the distribution is unequal. For a polar constellation, 180 satellites were found to reach an availability of 100%.
- The inclination in LEO plays an important role, and several should be used to cover the entire globe equally.
- If the near-optimum constellations are adopted, as shown in Table 2.6, PPP convergence can be achieved in less than one minute. The naming convention comes straight from the article.

Table 2.6: Ge Augmented-GNSS Optimal Constellation. Source: [67]

Constellation	Altitude	Walker 1 (i:T/P/F)	Walker 2 (i:T/P/F)	Walker 3 (i:T/P/F)	Error (E/N/U)
S240_w/	1000 km	90°:60/6/1	60°:90/6/1	35°:90/6/1	2.4/3.0/8.3 mm

Al-Hourani (2021)[78] discusses the optimal altitude for satellite constellations in order to meet a certain coverage probability, defined as users being able to see at least one satellite. The study used stochastic geometry and randomly distributed satellites in a constellation sphere to then propagate, maintaining the pattern. The users were also placed randomly. It ran three scenarios studying the Signal-to-Noise Ratio (SNR). The first was an ideal scenario, where a connection is made if the satellite is in view; a SNR scenario, where a minimum SNR is required (0dB); and a SNR with mutual interference scenario, where the SNR is reduced by the presence of other satellites. There is an optimum altitude when SNR is considered, as the higher altitudes require a stronger signal strength. It was also noted that the optimal altitude for SNR+interference is lower than for SNR, as at higher altitudes, more satellites are needed, creating more interference.

Gui et al. (2023)[72] developed a new analytical method for designing Walker constellations with multiple shells capable of meeting arbitrary coverage performance requirements per latitude. They devised a formula to compute the number of satellites in view per latitude. By reparametrising the formula, it can be written as a function of the number of satellites and inclination. By setting the number of shells, the problem can be written as a Non-Negative Least Squares (NNLS), and iterated over n times, aiming for convergence. This process is less computationally intensive in finding a near-optimal solution.

GENETIC ALGORITHMS

Çelikbilek, Lohan, and Praks (2025)[26] recently analysed the current state and challenges of the design of LEO-PNT constellations. It performs a similar state-of-the-art review as this one. Then it discusses the approaches to constellation optimisation. The most popular approach is performance-based, and it considers metrics such as DOP for navigation or latency for communication. A second, less explored approach is feasibility-based, focusing on the practical, non-performance metrics, such as costs, launching, and regulations. These scopes are usually left out in academic studies. The metrics used for their optimisation are: four-fold coverage, GDOP, and carrier-to-noise ratio (C/N_0). Other complementary metrics are atmospheric drag, orbit stability, altitude, and number of satellites. The solution is found among Walker constellations, using a novel genetic algorithm, the non-dominated sorting genetic algorithm-III (NSGA-III) [38], in combination with an adaptive weighting algorithm (aDaW). Regarding the signal strength, it is run in indoor and outdoor, urban and rural, with and without line-of-sight. The results indicate that multiple-shell constellations have better performance. There is a need for at least one high inclination shell to cover high latitudes. The number of satellites ranges between 281 and 404. The recommended configuration for a dedicated independent LEO-PNT system is shown in Table 2.7. It provides 99.1% four-fold coverage, a GDOP of 2.71, C/N_0 of 27.6 db-Hz, and drag of 4.87e-8 N.

Table 2.7: Çelikbilek Independent Optimal Constellation. Source: [26]

Shell	**Altitude (km)**	**Walker (i:T/P/F)**	**Topology**
1	1835	34°:133/19/x	Walker Star
2	1550	86°:99/3/x	Walker Delta
3	1477	80°:150/30/x	Walker Delta

As mentioned earlier, considering feasibility aspects is as relevant as performance, but it is not often done. Marchionne et al. (2023)[106] performed a study combining performance and cost in a simplified way. As performance metrics, the average and worst location GDOP were used, as well as the total number of satellites and planes. The last two are representatives of the cost of the system. Using an NSGA-II algorithm, they optimised on three parallel scenarios: a dedicated LEO-PNT system, a hybrid system with GNSS in urban, and a hybrid system with GNSS in open sky. The altitude was set to 1250 km, and up to three shells were considered. Free variables are the number of planes, satellites, and inclination within ranges. The best performing constellation is shown in Table 2.8. A small, medium and large constellation are shown. If the inclination is larger than 86°, the constellation is considered a Walker Star, while if it is lower, it is a Walker Delta. It shows the worst user location 95% percentile GDOP for all scenarios in order (dedicated, augmentation urban, augmentation open sky).

Guan et al. (2020)[71] studied the optimisation of dedicated LEO-PNT systems. It analyses LEO-PNT as a system independent of GNSS, or as an augmentation to it. It also studies single- or multi-objective optimisation. As an optimisation method, it works with NSGA-III. Some parameters were set before the optimisation. The altitude should be

Table 2.8: Marchionne Optimal Constellations. Source: [106]

Constellation	Altitude	Walker 1 (i:T/P/F)	Walker 2 (i:T/P/F)	Walker 3 (i:T/P/F)	GDOP
Large (484)	1250 km	0°:44/1/1	36°:192/8/1	80°:248/8/1	1.31, 4.69, 1.00
Medium (326)	1250 km	12°:80/4/1	50°:120/6/1	82°:126/6/1	1.62, 4.8, 1.17
Small (246)	1250 km	6°:36/2/1	46°:114/6/1	82°:96/6/1	1.87, 4.94, 1.40

above 900 km due to drag and below 1500 km to avoid the radiation belts. For single shells, the inclination was set as near-polar. Free variables were altitude, inclination, number of planes, and satellites. 1800 ground stations were placed on the ground.

As a system independent of GNSS constellations, the optimal solutions found for two and three-parameter objectives are shown in Table 2.9. The objectives to minimise were GDOP (*fit1*), number of satellites (*fit2*), and number of planes (*fit3*). The last one is only used in the three-objective case. These values were selected from a Pareto front, giving the same weight to all objectives.

Table 2.9: Guan Independent Optimal Constellations. Source: [71]

Altitude (km)	Walker (i:T/P/F)	Visible Satellites	GDOP	Opt. Type
900	88.54°:264/12/1	14.55	2.36	two-obj
1000	85.64°:240/10/9	14.49	2.80	two-obj
1100	85.64°:210/10/7	13.83	2.47	two-obj
1200	85.64°:210/10/8	14.96	1.87	two-obj
1300	86.72°:200/10/1	15.32	1.69	two-obj
1400	88.55°:190/10/8	15.57	2.51	two-obj
1500	85.64°:180/10/1	15.55	2.81	two-obj
1008.23	85.64°:252/12/1	18.31	1.54	three-obj

As a single-objective dedicated problem, two scenarios were tested. The objective is to reach a specific global average of visible satellites (*fit4*). The first considers only one shell and leaves altitude, inclination, number of planes, and number of satellites as constrained free variables. The second case works with two shells to have a more evenly distributed solution. It constrained the altitude and inclination of one shell to 900 km and between 0° and 45°, while the second shell is at 1200 km, and 45° to 90°. The remaining three parameters are left free, though inclinations are divided in a range of 0° to 45°, and 45° to 90°. The hybrid scenario gave better results in terms of availability, but generally worse GDOP. Each one shell, fold-coverage scenario found a unique altitude where the GDOP was also minimised.

The augmented optimisation considers the four main GNSS constellations. Optimising using *fit1* and *fit2*, the best performing constellation is shown in Table 2.10. It is a hybrid constellation, requiring few satellites. This is because the improvement in terms of GDOP is small when the entire network is present. The maximum decreased from 1.62

to 1.56, and the average from 0.95 to 0.80.

Table 2.10: Guan Augmented-GNSS Optimal Constellation. Source: [71]

Altitude (km)	Walker (i:T/P/F)
900	34.28°: 16/4/1
1200	70°: 40/5/1

Han et al. (2021)[73] modelled the LEO-PNT design problem as a multi-objective optimisation problem and solved it using Multi-Objective Particle Swarm Optimisation (MOPSO). The objectives to optimise were PDOP, visible satellites and altitude. It works with two-dimensional Lattice Flower Constellations, having altitude, inclination, number of planes, and phasing number as free variables, setting the number of satellites to 144 or 288. There is no detail on other parameters, which suggests zero eccentricity and equally distributed satellites. Three scenarios were considered: polar, single inclined shell, and two shells. An optimised inclined constellation is 7.5% and 5.2% better than the polar for the 144 and 288 satellites, respectively. The two shells constellation is 75.7% and 42.7% better. These best-performing constellations are shown in Table 2.11. The table shows the PDOP considering all four GNSS constellations, and the minimum number of satellites visible at any time. The constellation reduces the PDOP by 15 – 33%.

Table 2.11: Han Optimal Constellation. Source: [73]

Constellation	Num. Sats	Altitude(s) (km)	Inclination(s) (deg)	$N_o/N_{SO}/N_C$	PDOP	Sats. Visible
144L-2	81, 63	1361, 1260	92.7, 35.1	9/9/7, 7/9/3	0.825	7.33
288L-2	160, 128	1012, 1304	83.9, 38.2	10/16/1, 8/16/3	0.767	12.69

Pan et al. (2018)[126] approached the problem from a different perspective. They aimed for a uniformly distributed Walker over a limited RAAN range other than 180° or 360°. Even if the name refers to LEO-PNT, the selected orbit is in MEO. They ensured GDOP was below 10 for key cities globally. They considered the cost outside the Genetic Algorithm. They created a function of cost using a virtual currency, $N_D C_D + N_P C_P + N_s C_s$, where N_D are dedicated launches with a normalised cost of 1.2, N_P are piggyback launches costing 0.2, and N_s meant the number of satellites costing 0.05 each. Before running the optimisation, a constraint on the total cost was set below 10. They also defined a certain set of orbits to launch to and made use of the J_2 effect to modify the RAAN. Free variables were altitude, Walker parameters, and RAAN range. A constellation distributed between 105° and 308° showed the best results.

A similar study on the optimisation of constellation was done by Casanova, Avendaño, and Mortari (2014)[25]. It is a 2D-LFC optimisation for GNSS on MEO using a Genetic Algorithm (GA) and Particle Swarm Optimisation (PSO). It works with a predefined number of satellites and altitude, varying the remaining parameters (inclination, eccentricity, argument of periapsis) to find the lowest GDOP worldwide. They showed how the propagation time could be reduced by propagating to a defined Δt, rather than the entire period, due to the symmetry of the constellation.

$$\Delta t = \frac{T_p}{N_o N_{so}} \gcd(N_o, N_c) \tag{2.19}$$

Equation 2.19 gives an expression for the propagation time, where T_p is the orbital period, N_o and N_{so} are the number of orbits and satellites per orbit, and N_c is the configuration number as defined by the flower constellation. In addition, they show that the search space can be reduced without losing any configuration by taking inclinations up to 90° instead of 180°, as well as N_c up to $\frac{N_o}{2}$ instead of $N_o - 1$. Among the configurations, sometimes an eccentric set of orbits outperformed circular ones, and better results were achieved with the PSO.

On a slightly different objective, Chen et al. (2024) [29] developed a constellation for communication and navigation on the Moon. It uses multi-objective optimisation and solves it with the NSGA-II algorithm. It proposes the use of multiple inclinations to build shells of Walker constellations at the same altitude. They refer to it as Hybrid Inclination (HyInc) Walker. This is not a new concept, but here it is formally defined using an inclination vector. The optimisation is done taking average GDOP, four-fold, average coverage time, as well as average coverage power. The results of a HyInc Walker were more general and improved against a traditional Walker constellation.

In Table 2.12, a summary of the different optimisation methods is shown. It shows the most relevant aspects researched in the papers, useful for a quick study of what has already been accounted for and to find gaps. It follows typical nomenclature used by Walker constellations and Keplerian motion: inclination (i), total number of satellites (T), number of planes (P), phasing factor (F), altitude (h), initial RAAN (Ω_0), RAAN change ($\Delta\Omega$), eccentricity (e), argument of periapsis (ω), elevation angle (el), and arbitrary cost function ($f(\$)$).

Table 2.12: Summary of LEO-PNT Constellation Optimisation Methods

Paper	Opt. Type	Cons. Type	Objectives	Free Params	Constraints	Method	Constellation Type
[172]	Analytical	Walker	4Fold, PDOP	i, T, P, F	h, el	Formula, Iteration	Independent
[67]	Analytical	Walker(s)	GDOP, Availability	i, T, P	-	Trade-off	Augmentation
[78]	Analytical	-	1Fold	h	-	Stochastic geometry	-
[72]	Analytical	Walker(s)	nFold	i, T	-	NNLS, Iteration	-
[26]	Genetic Alg.	Walker(s)	4Fold, GDOP, C/N_0, F_{drag}	i, T, P, F, h	h, i	NSGA-III	Independent
[106]	Genetic Alg.	Walker(s)	GDOP, T, P	i, T, P	h, i, F	NSGA-II	Combined
[71]	Genetic Alg.	Walker(s)	nFold GDOP, T, P	i, T, P, F, h	h, i	NSGA-III	Ind./ Aug.
[73]	Genetic Alg.	2D-LFC	nFold, PDOP, h	i, P, F, h	T	MOPSO	Augmentation
[126]	Genetic Alg.	Mod. Ω Walker	GDOP	T, P, F, h, Ω_0, $\Delta\Omega$	i, e, $f(\$)$	GA	Independent (MEO)
[25]	Genetic Alg.	2D-LFC	GDOP	i, e, ω	h, T	GA, PSO	Independent (MEO)
[29]	Genetic Alg.	HyInc Walker	4Fold, GDOP, CovTime, CovPower	i, T, P, F, h	h, i	NSGA-II	Independent (Moon)

OTHER METHODS

Prol et al. (2024)[132] studied the LEO-PNT system as a whole, with particular interest in the PPP improvement. The most common observations were modelled, including clock, pseudorange, carrier, etc. A constellation of approximately 400 satellites at 800 km was selected arbitrarily because of its good GDOP and eight satellites in view. Using the constellation, a reduced impact on the signal effects was proved, between 15 – 97% depending on the altitude. Therefore, mismodelling of the signal will influence it less than in MEO. As an independent system, it reached accuracies of 1 cm in POD and 28 cm using the L1-Band.

Yue et al. (2022)[179] performed a study on the augmentation performance of a combined LEO-PNT system with Beidou-3. It arbitrarily chose a set of 60 near-polar orbits and 108 inclined orbits. It assessed the performance of orbit determination, coverage, and GDOP. It also studies the use of a Kalman filter for improving LEO errors and sending corrections for GNSS to the users.

Zhang et al. (2018)[180] worked on a constellation for observing multiple targets. Using grid search, they constructed a database of repeating ground track orbits that visit the targets. They were optimised using a pruning method. Finally, a constellation is built with these results, meeting the constraint on maximum visit time. The results yield a rapid revisit frequency and the least number of satellites.

The impact of the number and type of shells in a LEO constellation is analysed by Lohan and Çelikbilek (2024)[102]. They work on a regional African LEO-PNT constellation. It created five heuristic constellations fixing the number of satellites (240), and changing the altitude, number of planes, and inclinations. It is analysed for GDOP, carrier-to-noise-ratio, and coverage over the desired region. It showed that for indoor scenarios to have a C/N_0 of at least 20 dB-Hz, an altitude of 800 km already poses a constraint in most cases. On the other hand, a GDOP of 4 is only reached with at least 800 km. Their main recommendation is to focus solely on two to three shells.

A potential relevant aspect to optimise in a LEO-PNT constellation is the inter-satellite link (ISL) topology. Zhu et al. (2022)[182] studied the optimisation of the phasing parameter in a Starlink shell, maximising the shortest distance between satellites, and ensuring no collisions between them occur.

2.4.2. RELEVANT RELATED WORK

When working on the mission analysis, there are multiple aspects to consider further than the performance and feasibility aspects. The orbit selection affects the entire satellite design. Shi et al. (2018)[149] studied multidisciplinary design optimisation (MDO), taking a Walker delta constellation and optimising in parallel with the spacecraft subsystems using surrogate models, aiming for minimal mass. By approaching the optimisation in this way, the mass was reduced by 28% compared to traditional methods, as well as a saving in computational budget of 85% against a common integer coding genetic algorithm (ICGA).

There is one article focusing more in detail on the cost of the system. Pereira and Selva (2019)[128] studied the next generation of GNSS in LEO and MEO, considering GDOP and the total mission cost over 30 years. It used an optimisation algorithm after constraining the design space, and developed several empirical relations for explaining the costs. They went over satellite cost due to mass and power, the effect of radiation on the mass, propellant for manoeuvres, and launch costs. There is also an analysis on the ground segment, even if not considered in the objective function. It found that Low MEO could be a better option for the next generation of GNSS, as it has a lower cost and better performance. LEO would always give the best GDOP, but the cost would be too high, mainly because of the number of satellites and associated ground costs.

2.5. IDENTIFIED GAPS AND RESEARCH OPPORTUNITIES

As seen in the previous section, there has been an advancement in the design of LEO-PNT constellations in the last five years. There have been varied studies on the approach to the problem, ranging from analytical to statistical and genetic algorithms. The most common approach is to optimise the performance of the system, generally defined by metrics like coverage or GDOP. However, there are still several aspects that have not been studied in detail, and could be relevant for the development of a LEO-PNT system.

The first aspect that needs to be paid more attention to is the feasibility of the systems. Most studies are clear that the cost of the system is a relevant aspect, but given the complexity of the problem, it is often left out. Papers like Çelikbilek, Lohan, and Praks (2025)[26] and Pan et al. (2018)[126] studied the effects superficially or constrained the cost to a certain value. Others, like Marchionne et al. (2023)[106], considered the cost of the system through the number of satellites and planes. However, the cost and feasibility are more than the number of satellites. It is also related to the launchers used and their quantity, the type of orbit, the mission lifetime, ground stations, and even its buildup. An analysis in the direction of what Pereira and Selva (2019)[128] did could be a source of inspiration.

A second aspect to improve is within the design space. Except for a small portion of the studies, most of them work with a typical Walker constellation. It has been shown that for the case of LEO-PNT, two or three shells are more beneficial, but they depend on the application. However, other constellations, such as the Flower constellation, have not been thoroughly considered. Casanova, Avendaño, and Mortari (2014)[25] used it for MEO orbits, and Han et al. (2021)[73] used a simplified version without eccentricity, cost or multiple inclinations. It is a more complex constellation, but could provide better behaviour and performance. Making use of repeating ground track orbits could benefit the ground stations and emulate current GNSS constellations. As well, ISL networks may be more easily implemented in such a case. On the other hand, it could also have a more limiting effect on the stationkeeping. No design was found using eccentric orbits in LEO.

The study of more creative solutions could also help to find more optimal results. Pan et al. (2018)[126] looked into asymmetrical RAAN in Walker, as well as a recommendation from Casanova, Avendaño, and Mortari (2014)[25] to use Necklace Flower constellations to reduce the number of satellites per orbit while maintaining the symmetry of the constellation, simplifying the design and operations. Integration with ground stations has also been generally ignored, but for a large constellation, it needs to be a key parameter to optimise, as it will result in either more lenient latency and communication requirements, or a large number of stations will be required on the ground.

The objectives of the optimisation may also be improved. Some missions focus on the geometrical performance, while others focus on the signal aspect. However, focusing on a more realistic mission, aspects related to cost, space debris, ISL, mission timeline, sustainability, and space environment could be considered. For example, a deeper study on the cost of launch as a function of the number of satellites, planes to be reached, and the satellite's mass at different altitudes gives better results on the total cost. The topic of space debris and demisibility also has a high importance, especially in the design of a large constellation like LEO-PNT. This should also be a priority in the optimisation. On the topic of ISL, latency, and the type of connections are also important.

The techniques to optimise the constellation are similar. In most cases, a genetic algorithm like GA or NSGA is used. However, other methods could be used, such as MDO, semi-analytical, or even other genetic algorithms could find an optimal solution using less computational power. Performing a trade-off at the beginning of the design could help find better solutions at a lower computational cost.

A third gap in the design of the constellation is the scenarios considered. Depending on whether the design is independent of GNSS or an augmentation system, the objectives will vary. So far, only Marchionne et al. (2023)[106] has optimised for different scenarios simultaneously. In a real design, the system should be able to work in both scenarios. The augmentation system should be able to work independently, and the independent system should be able to augment the current GNSS. This is not only a matter of performance, but could also lead to a cost reduction by defining a limited independence without fully relying on the GNSS. A key scenario to consider is also the resilience against failures, either through in-orbit spares or decreased performance.

Finally, the last gap is the study of the subsystems. Most studies focus on the constellation design, but do not consider the spacecraft design. The spacecraft design is as relevant as the constellation design, as it will affect the performance of the system. A study on the subsystems could help understand how they affect the overall performance of the system, and how they can be optimised together with the constellation design.

From these gaps, some research questions can be derived:

RQ1 How do geometric performance metrics (e.g., DOP, availability) trade off with practical constraints (e.g., cost, deployment time) in a LEO-PNT system designed as an independent GNSS alternative?

RQ1.1 How do altitude and inclination selection influence both GDOP performance and practical constraints such as orbital lifetime or launch requirements?

RQ1.2 What is the Pareto front between GDOP and the number of satellites, or other relevant design constraints?

RQ1.3 How does the inclusion of deployment aspects (e.g., launch strategy, deployment timeline) influence constellation selection?

RQ1.4 What is the impact of partial constellation failure on LEO-PNT geometrical performance (e.g., DOP, availability)?

RQ1.5 What considerations would be needed to adapt the independent LEO-PNT system into a Galileo augmentation role?

RQ2 How do variations within Walker constellation configurations affect navigation performance and system complexity?

RQ2.1 How do specific Walker constellation parameters affect navigation performance metrics such as GDOP and availability?

RQ2.2 What qualitative implications do these configurations have for ground segment operations?

RQ2.3 How do these configurations influence inter-satellite link feasibility?

RQ3 How can sustainability constraints (e.g., debris mitigation, post-mission disposal compliance) be included in the LEO-PNT constellation design and optimisation process?

RQ3.1 What is the risk of collision for optimal constellations?

RQ3.2 How can the disposal strategy be implemented in the optimal constellation?

3
Simulator Development

To answer the research questions posed in chapter 2, a simulator is developed. The simulator is designed to be a tool for analysing the performance and other characteristics of the constellation. It is used as a mission design tool, including orbit design, constellation design, optimisation, verification, and analysis of the constellation. The simulator is developed in Python and is mostly built from scratch using basic libraries such as NumPy [121] and Scipy[147]. For the optimisation algorithms, the Pymoo library is used [22]. The simulator is designed to be modular, allowing for easy addition of new features and functionalities. It is also designed to be flexible, allowing for different types of constellations and mission scenarios to be simulated. In the following sections, the development of the simulator is described, including the design choices, implementation, assumptions, and limitations.

3.1. Earth Gravity Field Modelling

In later sections of this chapter, the different perturbations experienced by a satellite in low Earth orbit (LEO) are discussed. However, the most relevant aspect when designing a constellation is the effect of Earth's gravity field. The interaction between the Earth and the satellite is the primary force acting on the satellite, and it determines the orbit's shape, size, and orientation. Therefore, it is essential to understand one of the most common approaches to modelling Earth's gravity field, which is done through point mass and spherical harmonics. This section provides a brief overview of these concepts, which are later used in the simulator development.

3.1.1. Point Mass Model and Keplerian Orbits

The simplest model for orbit propagation is the Keplerian orbit, which assumes a two-body problem with a central point mass. Vallado (2013)[168] defines the Keplerian motion as the motion of a body in a gravitational field, which is given by Newton's law of gravitation, shown in Equation 3.1.

$$\mathbf{F} = -G\frac{m_1 m_2}{r_2^3}\mathbf{r_2} \tag{3.1}$$

In this equation, G is the gravitational constant with a value of $6.67428\times10^{-11}\ \mathrm{m^3kg^{-1}s^{-2}}$, m_1 and m_2 are the masses of the two bodies, $\mathbf{r}$ is the vector from one body to the other, and r_2 is its magnitude. In the case of a satellite orbiting Earth, m_1 is the mass of Earth, approximated as 5.97219×10^{24} kg, and m_2 is the mass of the satellite, which is negligible compared to Earth. Therefore, the acceleration of the satellite can be simplified to Equation 3.2.

3

$$\mathbf{a} = -\frac{\mu}{r_2^3}\mathbf{r_2}, \text{ with } \mu = Gm_1 \tag{3.2}$$

Here, μ is known as the standard gravitational parameter of Earth. This equation describes the motion of a satellite under a central gravitational field. A convenient way to represent this motion is through the set of Keplerian orbital elements, defined by Kepler in the early 17th century. These six parameters uniquely describe the geometry and orientation of the orbit, as well as the position of the satellite along it. The elements are [173]:

- a: semi-major axis, representing the size of the orbit,
- e: eccentricity, defining its shape,
- i: inclination, the tilt of the orbital plane with respect to the equatorial plane,
- Ω: right ascension of the ascending node (RAAN), indicating the orientation of the orbital plane,
- ω: argument of perigee, locating the orientation of the ellipse within the orbital plane,
- θ: true anomaly, defining the satellite's position along the orbit at a given time.

The position and velocity of the satellite at any point in time can be obtained by propagating the true anomaly θ. For a two-body Keplerian system, θ evolves according to the conservation of angular momentum and energy, which yields the following relation between time and position [173]:

$$r = \frac{a(1-e^2)}{1+e\cos\theta} \tag{3.3}$$

The motion is periodic, and θ increases as the satellite moves around the Earth. To relate θ to time, it is convenient to define the mean anomaly M and eccentric anomaly E, which satisfy Kepler's equation [173]:

$$M = E - e\sin E = n(t-t_0) \tag{3.4}$$

where $n = \sqrt{\mu/a^3}$ is the mean motion, and t_0 is the time of perigee passage. Once E is found by solving Equation 3.4, the true anomaly θ can be obtained from [173]:

$$\tan\frac{\theta}{2} = \sqrt{\frac{1+e}{1-e}}\tan\frac{E}{2} \tag{3.5}$$

Together, these equations fully describe the evolution of a satellite in a Keplerian orbit. In this idealised model, the orbit remains fixed in space, and the satellite's position repeats periodically with an orbital period $T = 2\pi/n$. The equations are simplified when working with circular orbits ($e = 0$), where the eccentric anomaly E equals the mean anomaly M, and the true anomaly θ increases linearly with time. In such cases, most parameters become constant, except for θ, which evolves uniformly following Equation 3.6.

$$\theta(t) = \theta_0 + n(t - t_0) \tag{3.6}$$

3.1.2. SPHERICAL HARMONICS AND J_2 PERTURBATION

While the Keplerian model provides a first approximation of satellite motion, it neglects several important perturbations that affect real orbits. One of the most significant perturbations arises from the non-uniform distribution of Earth's mass, which causes deviations from the idealised point mass gravitational field. To account for these effects, Earth's gravity field is often modelled using spherical harmonics, which provide a more accurate representation of the gravitational potential.

The gravitational field from an uneven Earth is commonly modelled using spherical harmonics. Spherical harmonics are "functions formed by the product of the Associated Legendre Functions with $\cos m\lambda$ and $\sin n\lambda$" [116]. They can then be used to represent the gravitational potential with increasing accuracy as the degree and order are higher.

$$V = \frac{\mu}{r}\sum_{l=0}^{\infty}\left(\frac{R_e}{r}\right)^l \sum_{m=0}^{l} P_{l,m}(\sin\phi)\left[C_{l,m}\cos m\lambda + S_{l,m}\sin m\lambda\right] \tag{3.7}$$

The gravitational potential is then represented by Equation 3.7, where μ is the standard gravitational parameter, R_e is Earth's radius, r, ϕ, λ are the distance, latitude and longitude of the satellite, l and m are the degree and order, and $P_{l,m}$ is the associated Legendre Function. In a numerical model, the degree and order can be truncated to a limiting accuracy, as the coefficients $C_{l,m}$ and $S_{l,m}$ decrease in magnitude. The Legendre polynomial before normalisation is given by Equation 3.8.

$$P_{l,m}(x) = \frac{(1-x^2)^{m/2}}{2^l}\sum_{k=0}^{\frac{l-m}{2}}(-1)^k \frac{(2l-2k)!}{k!(l-k)!(l-m-2k)!}x^{l-m-2k} \tag{3.8}$$

To deal better with such functions, it's advantageous to normalise the Legendre polynomial, as well as potential coefficients. This normalisation depends on the degree and order and is given by Equation 3.9

$$\begin{Bmatrix} \bar{P}_{l,m} \\ \frac{1}{\bar{C}_{l,m}} \\ \frac{1}{\bar{S}_{l,m}} \end{Bmatrix} = \left[(2-\delta_{m0})(2l+1)\frac{(l-m)!}{(l+m)!}\right]^{1/2} \cdot \begin{Bmatrix} P_{l,m} \\ \frac{1}{C_{l,m}} \\ \frac{1}{S_{l,m}} \end{Bmatrix} \tag{3.9}$$

$$\delta_{m0} = \begin{cases} 1, & \text{if } m = 0 \\ 0, & \text{if } m > 0 \end{cases} \tag{3.10}$$

Spherical Harmonics are usually written in the form SH(degree, order), where the degree is l and the order is m. The most basic model is SH(0,0), which represents a point mass. The next most dominant component when modelling Earth's gravity is Earth's oblateness SH(2, 0), also referred to as the J_2 effect. This arises from Earth's equatorial bulge due to its uneven mass distribution. Although station-keeping addresses many such effects, the J_2 perturbation is significantly larger, often several orders of magnitude above other harmonics [116].

The J2 effect has a substantial impact on satellite orbits, causing secular changes in the orbital elements over time. These changes are mainly visible in the precession of the orbital plane and the rotation of the orbit within that plane.

The effect of Earth's bulge (J_2) is given by combining normalised coefficient $\bar{C}_{2,0} = -4.84 \times 10^{-4}$ with the Legendre function normalisation being $\sqrt{5}$ as derived from Equation 3.9, leads to the standard value $J_2 = 1.08263 \times 10^{-3}$. This value is two orders of magnitude larger than the second highest coefficient SH(2,2), which has a coefficient of $\bar{C}_{2,2} = 2.44 \times 10^{-6}$ [116].

Vallado (2013)[168] mentions that zonal harmonics ($m = 0$) do not influence the longitudinal component of the acceleration and will produce secular motion in three orbital elements: RAAN ($\dot{\Omega}$), argument of periapsis ($\dot{\omega}$), and mean anomaly ($\dot{\theta}$). Other elements have a periodic variation and are therefore equated to zero. The linear perturbations can be represented by Equation 3.11 and Equation 3.12, and Equation 3.13 [168].

$$\dot{\Omega}_{J_2} = -\frac{3}{2} J_2 \left(\frac{r_{\text{earth}}}{p}\right)^2 n \cos(i) \tag{3.11}$$

$$\dot{\omega}_{J_2} = \frac{3}{4} J_2 \left(\frac{r_{\text{earth}}}{p}\right)^2 n(4 - 5\sin^2(i)) \tag{3.12}$$

$$\dot{\theta}_{J_2} = -\frac{3}{4} J_2 \left(\frac{r_{\text{earth}}}{p}\right)^2 n\sqrt{1-e^2}(3\sin^2(i) - 2) \tag{3.13}$$

In these equations, $p = a(1-e^2)$, where a is the semi-major axis and e the eccentricity, $n = \sqrt{\frac{\mu}{a^3}}$ being the mean motion, and finally i representing the inclination. These equations can then be used to simulate a satellite constellation in combination with the

Keplerian orbit, updating the relevant orbital elements at each timestep.

Once the most dominant perturbation has been described, the next section discusses the analysis of other perturbations that could be relevant for the simulator development, including the higher-order spherical harmonics.

3.2. PERTURBATIONS ANALYSIS

Taking the explanation of the perturbations in section 2.1 as a starting point, the perturbations that could affect the constellation are Earth's gravitational field, atmospheric drag, third-body perturbation, and solar radiation pressure. A simple assessment is performed using the orbit propagation library Tudat [162]. Since the expected operational altitudes for optimisation are between 700 km and 1500 km, the perturbations are evaluated for circular orbits at an inclination of 45 degrees, representing the limiting scenarios. The specific orbital mechanics of these scenarios are discussed in subsection 3.1.1 and subsection 3.1.2, after the perturbations have been selected.

The comparison is carried out by taking a high-fidelity propagation over one day (short-term) and 100 days (long-term) as a baseline and comparing it with simplified models. The high-fidelity model includes Earth's gravity field with SH(48, 48), Sun and Moon point masses, atmospheric drag, and SRP. The simplified models are truncated versions of it, neglecting or simplifying one or more perturbations. The results of this comparison for the 700 km case are shown in Figure 3.1, while additional results for the 1500 km altitude can be found in Appendix A. Both scenarios exhibit similar behaviour, although at 1500 km, the higher spherical harmonics (SH(24,24)) and atmospheric drag show smaller relative errors, approximately one order of magnitude lower. Given that the 700 km case is more constraining, it is used as a reference for the analysis.

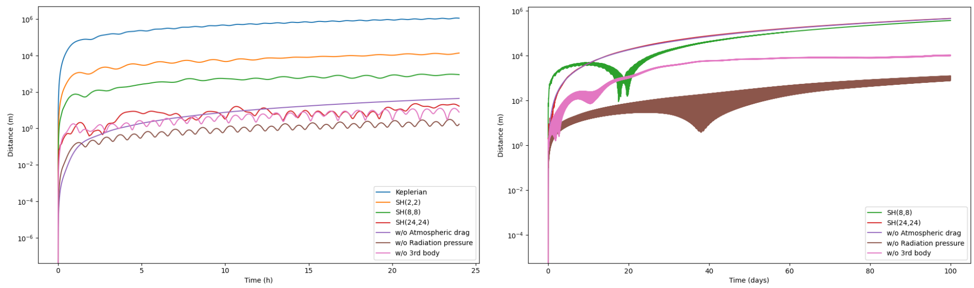

(a) Short Term Effect

(b) Long Term Effect

Figure 3.1: 700 km Orbit Error with respect to High Fidelity Scenario

From Figure 3.1a, it is clear that several perturbations, such as drag or spherical harmonics, have a significant impact on the orbit evolution. A purely Keplerian model or a simple SH(2,2) expansion is insufficient, leading to position errors of approximately 1000 m after one day. Truncated models without SRP or third-body effects contribute errors on the order of one meter, while neglecting atmospheric drag introduces errors of roughly 10 m, even when the gravitational field is modelled with high fidelity, as indicated by the purple line. The atmospheric contribution shows a continuous increase over time.

The long-term propagation in Figure 3.1b further highlights the importance of atmospheric drag. While other perturbations, such as SRP and third-body perturbation, fix at a constant error of 100 m and 1000 m, respectively, orbits without drag (green, red, and purple lines) diverge steadily and increasingly. This poses the question of the relevance of the specific spherical harmonic order and degree, given the similarity between results. In order to answer that question, the different spherical harmonics are propagated in combination with drag to study their effects. These results can be seen in Figure 3.2, where the Keplerian elements are compared.

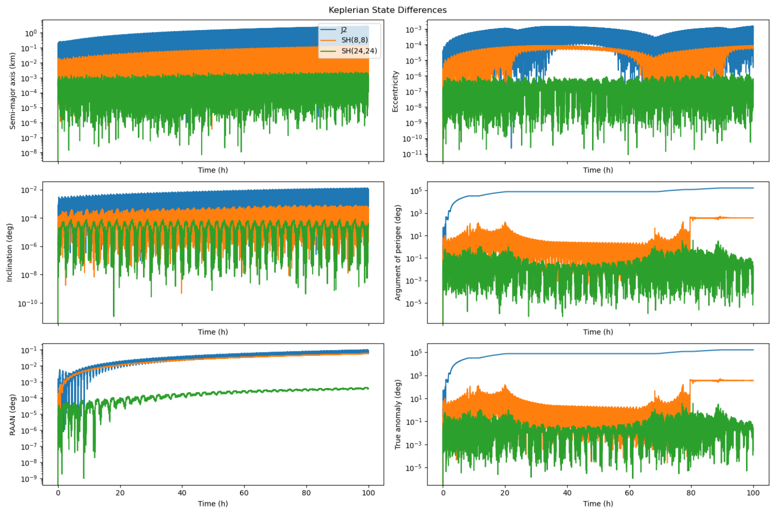

Figure 3.2: 700 km Keplerian Elements Error with Atmospheric Drag for Different Spherical Harmonics

From these results, it can be seen that the errors in each orbital element remain small. Even in a simplified scenario considering only Earth's oblateness, represented by the J_2 term, the semi-major axis varies by roughly one kilometre. As these small discrepancies accumulate, the true anomaly begins to dephase, producing large apparent position errors. However, if all satellites experience this effect consistently, the relative geometry of the constellation remains largely unaffected. It is therefore concluded that the dominant perturbations for LEO navigation satellites are atmospheric drag and the basic gravitational harmonics. In the long term, the difference between high-degree gravity models (e.g., SH(48,48)) and lower-degree ones (e.g., SH(2,0), SH(8,8), or SH(24,24)) becomes negligible. Consequently, a reduced-order gravity model combined with atmospheric drag provides a sufficiently accurate representation. Third-body perturbations and solar radiation pressure have a measurable but secondary effect.

For navigation missions, maintaining accurate orbit knowledge and alignment between satellites is critical, as any deviation propagates directly to the user's positioning error. The constellation geometry must also remain stable to prevent collisions and ensure optimal performance. These requirements imply continuous orbit corrections through station-keeping, which compensate for most perturbations such as drag, solar radiation pressure, third-body effects, and higher-order gravitational terms. Among the remaining uncorrected forces, Earth's oblateness (J_2) is the most significant. Although its effect is substantial, it would be too costly to counteract and does not necessarily degrade the orbit. Consequently, for the remainder of the thesis, the perturbation model will include point-mass effects (PM) and the J_2 term.

3.3. CONCEPT

In this section, the simulator design is explained, starting from the general overview, discussing the propagators, classes, and metrics computations.

The simulator is designed to be modular and flexible, allowing for easy addition of new features and functionalities. In its most basic form, it is composed of a set of general utility functions and constants, classes representing the satellites and users, followed by the constellation class, capable of handling multiple satellites in parallel. Finally, a set of analysis tools computes the relevant metrics to assess the constellation's performance. In later stages, this tool is expanded upon to include feasibility analysis tools, along with optimisation algorithms. In the next subsections, the main classes and functions are discussed.

Steps in the LEO-PNT Simulator

1. Create a satellite constellation using the "Constellation" class.
2. Propagate the network in an inertial frame and convert it to a rotating Earth reference frame.
3. Create a set of Earth users to measure performance.
4. Compute a visibility mask between users and satellites at all epochs.
5. Compute the DOP per user at each epoch using a local East-North-Up frame.
6. Depending on the type of analysis, perform statistical analysis on the results, such as a maximum 95th Percentile GDOP computation.

The software and algorithms used throughout the entire thesis are accessible in a public repository. The repository can be found at `https://github.com/P0TN1K/ConstellationOptimisation`. The structuring of the repository is found in the README file of the repository.

3.3.1. COORDINATE SYSTEMS

The software is developed using different coordinate systems depending on the case. The reference frame used is an Earth-Centred Inertial (ECI) frame. In this frame, the 'i' axis points to the vernal equinox, 'j' is located 90 degrees to the East of the Equator, and 'k' points towards the North Pole. Given the small variations in this frame in time, a specific system is considered: J2000. This works both as a time and space system; it has an initial date on Jan 1st, 2000, 12:00:00. The axes are set at this time[168].

The second frame used is an Earth-Centred, Earth-Fixed (ECEF) frame. A proper implementation of such a framework includes the precession, nutation, sidereal motion and polar motion of the Earth. The largest impact in a short period is the sidereal motion, which represents the sidereal day. The precession effects of planetary and lunar bodies have an effect of $\sim 50''$ per year, nutation has an amplitude of $17''$ and a period of 18.6 years, and polar motion has a maximum amplitude of $0.3''$, where $1'' = 0.000028\,\text{deg} = 3.09$ m. These effects are negligible in the short term and can therefore be ignored to improve computation time. The remaining element, the sidereal motion, is calculated using Earth's rotation velocity ($\omega_e = 7.292115 \times 10^{-5}$ rad/s). For this transformation, the Greenwich Mean Sidereal Time is considered, shown in Equation 3.14.

$$ECI \rightarrow ECEF : \mathbf{R}(t) = \mathbf{R}^{GMST}(t) = \mathbf{R}_z(\theta_{GMST_0} - \omega_e \cdot (t - t_{J2000})) \tag{3.14}$$

In this equation, there is a rotation around the z-axis using the angle between the vernal equinox and the local meridian at the reference epoch (θ_{GMST_0}) and the deviation in time from this angle ($\omega_e \cdot \Delta t$) [168].

From an ECEF frame, the next step is to compute a geodetic frame. The World Geodetic System 1984 (WGS84) is the standard for navigation [98] and the conversion can be computed using Ferrari's solution [76], as it is the most accurate[181]. Equation 3.15 shows the procedure. The most relevant parameters are a, b representing the WGS84 semi-major and semi-minor axes, e is the eccentricity, and φ, λ, h are the geodetic latitude, longitude, and altitude.

$$ECEF \rightarrow Geodetic: \tag{3.15}$$

$$e^2 = \frac{a^2 - b^2}{a^2}, \quad e'^2 = \frac{a^2 - b^2}{b^2}, \quad p = \sqrt{x^2 + y^2}$$

$$F = 54b^2z^2, \quad G = p^2 + (1 - e^2)z^2 - e^2(a^2 - b^2)$$

$$c = \frac{e^4 F p^2}{G^3}, \quad s = \left(1 + c + \sqrt{c^2 + 2c}\right)^{1/3}, \quad k = 1 + s + \frac{1}{s}$$

$$P = \frac{F}{3G^2k^2}, \quad Q = \sqrt{1 + 2e^4 P}$$

$$r_0 = -\frac{Pe^2 p}{1 + Q} + \sqrt{\frac{a^2}{2}(1 + \frac{1}{Q}) - \frac{P(1 - e^2)z^2}{Q(1 + Q)} - \frac{Pp^2}{2}}$$

$$U = \sqrt{(p - e^2 r_0)^2 + z^2}, \quad V = \sqrt{(p - e^2 r_0)^2 + (1 - e^2) z^2}$$

$$z_0 = \frac{b^2 z}{aV}$$

$$h = U\left(1 - \frac{b^2}{aV}\right), \quad \varphi = \arctan\left(\frac{z + e'^2 z_0}{p}\right), \quad \lambda = \arctan\left(\frac{y}{x}\right)$$

Finally, for the DOP computations, the topocentric East-North-Up (ENU) frame is required [157]. It is shown in Equation 3.16.

$$ECEF \rightarrow ENU : \mathbf{R}(\phi, \lambda) = \begin{pmatrix} -\sin\lambda & \cos\lambda & 0 \\ -\cos\lambda\sin\varphi & -\sin\lambda\sin\varphi & \cos\varphi \\ \cos\lambda\cos\varphi & \sin\lambda\cos\varphi & \sin\varphi \end{pmatrix} \tag{3.16}$$

VERIFICATION AND VALIDATION

All functions were verified against known use cases or analytical formulas. For the conversion from ECI to ECEF, two approaches were taken. The first was to perform a conversion by hand and compare it against the computed scenario. Afterwards, a simple repeating non-perturbed orbit was considered. Repeating orbits are discussed in detail in section 4.3. Figure 3.3 shows a three-day repeating orbit with eight revolutions, a high eccentricity (0.6) and mid-inclination (45 degrees). The state after the repeating period is computed and compared to the initial state. The error between them is $\varepsilon = \mathcal{O}(10^{-6})$ in meters.

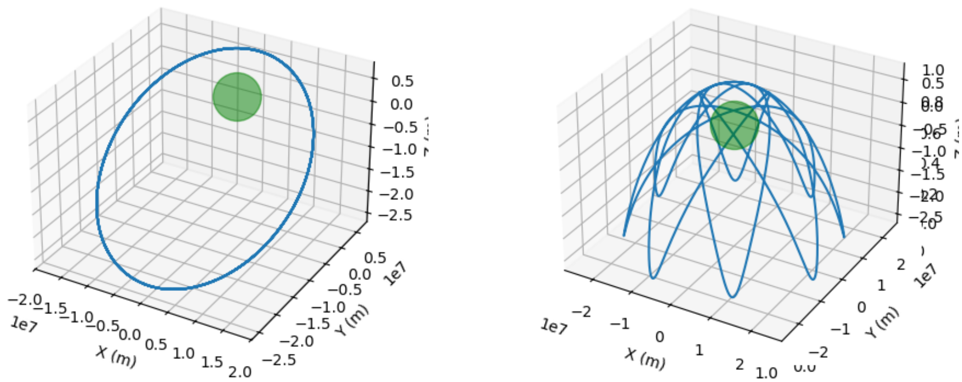

(a) ECI Frame

(b) ECEF Frame

Figure 3.3: Propagated Satellite in Inertial and Rotating Frame

To validate the conversion from ECEF to geodetic, an alternative algorithm is used. It is known as Bowring's irrational geodetic-latitude equation [23], and can be solved following an iterative approach. The differences of $\varepsilon = \mathcal{O}(10^{-9})$ in meters. Extreme cases were also tested to find asymptotes. Ferrari's solution performed better than Bowring's in all scenarios, including different points at the equator and the poles.

For the ECEF to ENU transformation, the rotation matrix was first validated for orthogonality. Then, the matrix creation was validated for several points on Earth. Finally, a manual check was performed by placing a reference point at geodetic coordinates $(\varphi, \lambda, h) = (0°, 0°, 0\text{ m})$ and defining test points in known directions around it. These include pure displacements in the east, north, and up directions, as well as along the equatorial plane. The resulting ENU coordinates confirm that the transformation correctly maps local directions: east aligns with increasing y, north with increasing z, and up with increasing x in ECEF at the equator.

3.3.2. UserGroup and User classes

The first step in the simulator is to create users capable of measuring the performance of the constellation. The User class creates a point object in the simulation space. It is defined by a set of three arguments: latitude, longitude, and altitude, according to the WGS84 system, or Cartesian coordinates in ECEF. The users can be positioned on or above the Earth's surface, representing ground stations, people, aeroplanes, satellites, etc.

In order to facilitate the creation and handling of users, the UserGroup class clusters several users. There are also multiple ways to create several users in a sphere. Research has focused on this topic to distribute the points along the sphere equally in all latitudes and longitudes. A new approach uses the Fibonacci lattice virtual observation points (FLVOP), which distribute the points over the sphere using the golden angle, giving better uniform and stochastic distributions compared to the traditional latitude-longitude VOP (LLVOP) [29]. For this simulator, a variation of this approach is taken to adapt the sphere to a geodetic Earth, using Equation 3.17. It works with the golden ratio (ϕ), N_{users} defines the number of users on the ground, and a Boolean variable $half\_sphere$ distributes the users throughout the globe or only the Northern Hemisphere. Both cases can be seen in Figure 3.4. The distribution is slightly different between them due to the different number of total users. More information on the validity of half a sphere can be read in subsection 3.4.2.

$$\forall i \in \{1, \ldots, N_{users}\}: \tag{3.17}$$

$$z = \begin{cases} \dfrac{i-1}{N_{users}-1} & \text{if } half\_sphere = True \\[2ex] \dfrac{2i-1}{N_{users}} - 1 & \text{if } half\_sphere = False \end{cases}$$

$$r = \sqrt{1 - z^2}, \quad \theta = \frac{2\pi i}{\phi}$$
$$x = r\cos\theta, \quad y = r\sin\theta$$
$$\varphi = \sin^{-1}(z), \quad \lambda = \tan^{-1}(y/x), \quad h = 0$$

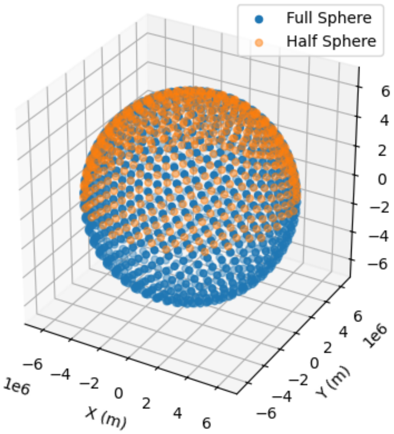

Figure 3.4: User Distribution over the Earth or Northern Hemisphere

VERIFICATION

The creation of the geodetic sphere is verified mainly on the coding side, as the geodetic transformation has already been validated. For this, using a small number of users, the computations are done by hand and compared. As well, given that the algorithm has been modified to meet the geodetic requirement, it is verified that the latitude and longitude locations are maintained, while the altitude is limited to the geodetic surface. A visual example for 1000 users is visible in Figure 3.5. As expected, the altitude does not vary, meaning the users are on the surface, and the latitude and longitude match perfectly, maintaining the advantageous performance of the users' distribution.

3.3.3. CONSTELLATION CLASS

Similarly, the "Constellation" class is defined by a set of "Satellite" objects. Each satellite is created using the set of six basic Kepler parameters, the central body, and the starting epoch. The satellite class stores the states in ECI and ECEF frames, as well as propagating, implementing the conclusions from subsection 3.1.2. The propagator allows for J_2 perturbations or ideal Keplerian orbits, timestep definition, and if the final epoch should be exact or not.

The constellation accesses all satellites stored in it, as well as handling a $(N_{sat} \times t \times 6)$ matrix containing all states for all satellites at all epochs. A subclass is the Walker con-

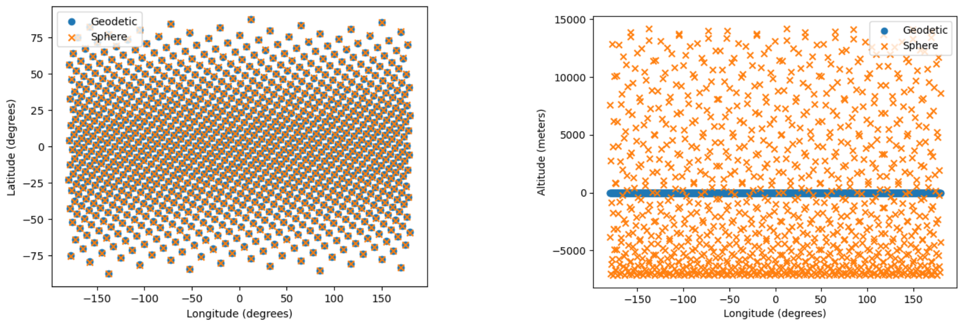

(a) Latitude and Longitude Similarity

(b) Altitude Difference

Figure 3.5: Comparison between normal sphere and geodetic sphere

stellation, which is the main focus of this thesis. It allows the creation of Walker constellations as defined by Walker (1970)[169]. As a brief reminder, these constellations distribute satellites evenly in a plane and between planes to provide optimal coverage.

These constellations have already been defined in section 2.1, but reevaluated here for clarity. They are defined by the total number of satellites (T), the number of planes (P), a phasing parameter (F), the semi-major axis (a), and the inclination (i). It also allows for the selection of a Walker delta or star, which defines the RAAN range to either (0, 360°) or (0, 180°). The functions to create the constellation are Equation 2.2 and Equation 2.3. The class can create one or multiple shells, where there are different inclinations and/or altitudes.

As mentioned in the previous chapter, Turner (2002)[166] suggested the optimal coverage for a given number of satellites and planes can be found using an analytical function for the phasing parameter (F). This was implemented and its validity analysed in section 4.4.

VERIFICATION AND VALIDATION

As a verification of the propagator, it was compared to hand-written results and alternative software. The software used is Tudat [162], which has an analytical propagator, as well as several numerical ones. The analytical propagator outputs no difference between ideal Keplerian orbits. It also validated the conversion between Keplerian and Cartesian coordinates, giving an error of order $O(10^{-9})$ m. For the J_2 perturbed orbit, it was validated by hand and compared results to Vallado (2013)[168], as there is no analytical implementation on Tudat of the J_2 perturbations.

3.3.4. DILUTION OF PRECISION FUNCTIONS

The dilution of precision (DOP) functions are based on Equation 2.10-Equation 2.16. They can be divided into *visibilityCriteria*, *computeVisibilityMask*, *computeDOP*, and several statistical functions.

The visibility criterion is purely based on geometrical aspects. Figure 3.6 presents a satellite and a user on the Earth's surface. In order to have a direct line of sight between the satellite and the user, there must not be an obstacle between them, such as the Earth or a building. This is commonly defined as the elevation angle (α), and it is the minimum angle between the horizon and the satellite. For practical scenarios, according to Kaplan and Hegarty (2006)[85], a practical constraint in GNSS is five degrees for users. However, for urban environments and ground station antennas, this requirement can be higher, limited to a minimum angle of 15 degrees. Rider (1986)[139] was the first one to define these angles and distances. The distance 'x' defines a maximum limit which can be solved for, giving Equation 3.18 as a result.

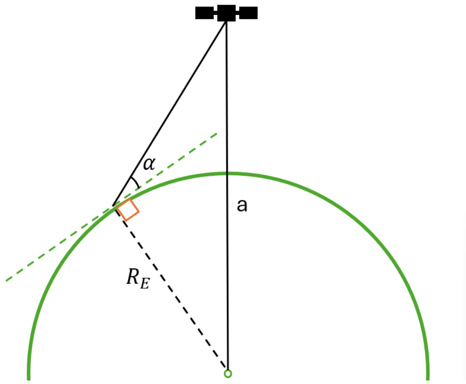

Figure 3.6: Visibility Criterion

$$x = -R_E \sin\alpha + \sqrt{a^2 - R_E^2 \cos^2\alpha} \tag{3.18}$$

This criterion is used to compute a visibility mask, a boolean matrix of shape (N_{sat}, N_{user}, t), where true implies a pair connection at the given epoch. In order to be more computationally efficient, the matrix operation is done in smaller batches in parallel, reducing the RAM storage required. The matrix can then be used in the computation of the DOPs. The process requires the visibility matrix, the constellation and users' positions in an ECEF frame, as well as the rotation matrix for each user from ECEF to ENU.

The process uses several loops to traverse each user and each epoch, as they are independent of each other. The outer loop is run in parallel to reduce the computation time. The DOPs are initialised to type NaN, meaning Not a Number, and a first check is made to ensure there are at least four satellites visible to proceed. Then, at each epoch, the vectors connecting the ground station to the satellite are transformed to an ENU frame, and subsequently, the observation matrix is created. The cofactor matrix is obtained if the determinant is non-zero to compute all DOP variations from its diagonal, finally.

The final aspect is the result processing. There are different approaches depending on the objectives to minimise in future steps. However, there are three main functions. The

3

first one computes the min, max, mean, and standard deviation of the visibility. It also computes the availability as Equation 2.18, where a minimum of four satellites is required to consider it available. A second function performs similar statistics but for the DOPs. Some DOP values will be recorded as NaN, which are ignored.

An interesting statistical measure to consider is the percentile. Previous papers, such as Marchionne et al. (2023)[106] have used it, as it gives an upper limit on the capabilities. Navigation missions need to provide a reliable service for a long period. However, there might be times when the performance drops momentarily, which is generally acceptable. A way of quantifying this behaviour is by taking the 95th percentile of a user's performance. It refers to the DOP value under which 95% of the data lies. This final function can also compute the maximum over the user grid, giving the worst performing location value without considering outliers within it, shown in Equation 3.19, using GDOP as an example.

$$\max_{u \in N_{users}} P_{95}(\mathrm{GDOP}_u) \tag{3.19}$$

Verification and Validation

Similarly, the DOP functions are validated. The visibility criterion was solved by hand and compared to computed results, as well as the creation of a smaller visibility mask. For the DOP creation, it was modularly tested, starting from the observation matrix. Starting from simple test cases, it was checked that when four satellites are set directly above, the observation matrix looks like Equation 3.20.

$$\mathbf{A} = \begin{bmatrix} 0 & 0 & 1 & 1 \\ 0 & 0 & 1 & 1 \\ 0 & 0 & 1 & 1 \\ 0 & 0 & 1 & 1 \end{bmatrix} \tag{3.20}$$

A second scenario worked with a user at an imaginary location $(x, y, z) = (1, 5, 3)$, and four satellites visible at random locations, as seen in Equation 3.21. The observation matrix was computed both by hand and using code, giving the same result.

$$\mathbf{sats} = \begin{bmatrix} 2 & 5 & 3 \\ 1 & 6 & 5 \\ 3 & 5 & 4 \\ 1 & 7 & 3 \end{bmatrix} \qquad \mathbf{A} = \begin{bmatrix} 1 & 0 & 0 & 1 \\ 0 & 0.45 & 0.89 & 1 \\ 0.89 & 0 & 0.45 & 1 \\ 0 & 1 & 0 & 1 \end{bmatrix} \tag{3.21}$$

Another example of a user located at the centre of Earth and four satellites located in a tetrahedron shape, creating the satellite matrix shown in Equation 3.22, gives the expected DOP result of 1.58, verified by hand.

$$\mathbf{sats} = \begin{bmatrix} 1 & 1 & 1 \\ 1 & -1 & -1 \\ -1 & 1 & -1 \\ -1 & -1 & 1 \end{bmatrix} \tag{3.22}$$

As a final validation, Lab (2024)[95] created an open-source library for GNSS known as NAV Lab. Several comparisons were made with individual users and varying numbers of satellites, yielding the same results.

3.4. SIMULATOR TUNING AND PERFORMANCE

Once the whole set of functions has been created, the simulator is almost ready to run. The final objective is to perform different types of optimisation, such as minimising satellites or maximising performance. But before it can be used to optimise the constellation, some parameters need to be tuned to achieve sufficient precision without sacrificing time. The optimal performance will vary per device; however, the device specifications can be found in Table 3.1.

Table 3.1: Relevant system specifications for Python optimisation tasks

Component	Specification
Processor	Intel Core i7-10510U @ 1.80 GHz (2.30 GHz Turbo)
RAM	16.0 GB (15.8 GB usable)
System Type	64-bit OS, x64-based processor

3.4.1. DURATION AND TIMESTEP

The propagation time and timestep are crucial parameters in the simulation. They represent the discretisation of continuous satellite motion and determine the duration of the study period. The propagation time involves a trade-off between computational efficiency and result validity. For LEO-PNT optimisation, this means ensuring that the computed DOP values represent the typical service quality that ground users will experience. The timestep selection is equally important, as DOP depends on the relative satellite-user geometry, which changes rapidly due to the high orbital velocities in LEO systems.

For all papers discussed in the state-of-the-art, the propagation time and timestep vary without deeper reasoning. Marchionne et al. (2023)[106] mentions 30 days at 120 seconds to have "sufficient spatial and temporal statistical significance"; Pan et al. (2018)[126] propagated for two years and gave no information on their timestep; finally, Çelikbilek, Lohan, and Praks (2025)[26] propagates for 12 hours to "guarantee that the simulated scenario will include several revisits from all LEO satellites" and no mention of the timestep.

Aiming for a more robust simulator, the duration and timestep have been carefully chosen. Selection of the duration is straightforward. In section 4.3, it is defined that for this optimisation, all orbits considered will be repeating orbits for several performance-related reasons. However, this is also beneficial for the modelling, since a repeating orbit ensures a repetition of DOP or other metrics after a cycle. Therefore, the duration is set to one or two days, depending on the repeating orbit considered.

Figure 3.7 compares the difference in the 95th percentile GDOP values per latitude as a function of the propagation duration for a one-day repeating constellation. It can be seen that if the propagation is less than one day, the errors increase drastically, up to 30% for half a day and 60% for a quarter of a day. In contrast, propagating for two days does not show any improvement and the small differences are numerical or caused by a small offset in the sampling times, proving that there is no need for longer simulations.

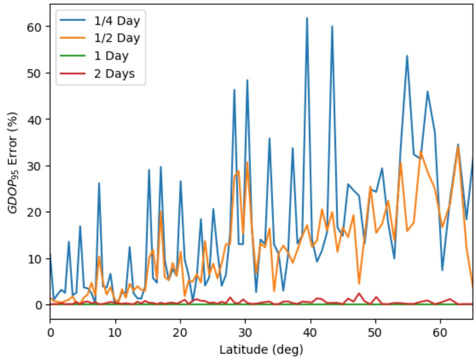

Figure 3.7: DOP Error against a 1-day repeating orbit for an arbitrary 1200 km constellation

Similarly, a trade-off was performed to find the fastest performing timestep with a minimal error. To have a more physical meaning for this timestep, it was converted to observations. Figure 3.8 represents a satellite passing above a user's zenith point. Assuming a minimum observation angle (α) of 5°, the angle θ can be derived following Equation 3.23, which requires Equation 3.18 to find x. The time spent above the zenith is then approximated using the mean motion: $t_{vis} = \frac{\theta}{n}$. Finally, by dividing this time over integer values, it can represent how many samples are taken by each user.

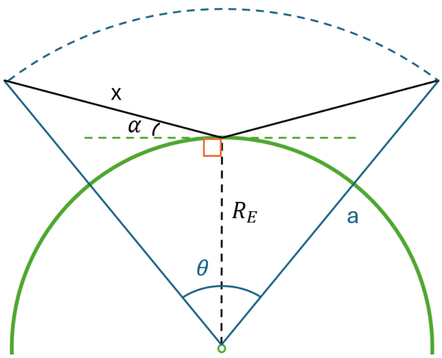

Figure 3.8: View of a Satellite by a Ground User Geometry

$$\frac{x}{\sin\frac{\theta}{2}} = \frac{a}{\cos\alpha} \Rightarrow \theta = 2\cdot\sin^{-1}\left(\frac{x}{a}\cos\alpha\right) \tag{3.23}$$

With this in mind, different numbers of samples were taken and compared to a high-fidelity 100 samples. The same arbitrary repeating orbit as for the duration was taken, and the results can be seen in Figure 3.9.

3

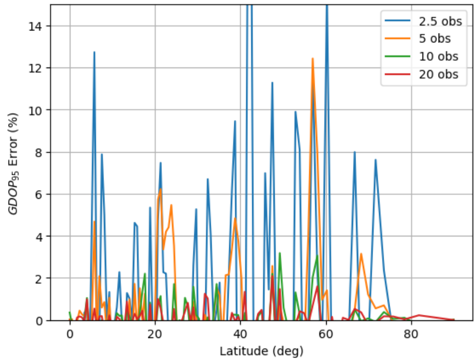

Figure 3.9: 95th Percentile GDOP Error with respect to 100 observations

Taking a few observations does not allow for capturing the DOP behaviour properly, giving errors of up to 12% and 22%. Taking 10 to 20 observations already reaches high accuracies, with errors smaller than 3% and 2%, respectively. To work on a conservative side, 20 observations are selected. This leads to an altitude-dependent timestep, ranging between 34.78 s (700 km) and 60.34 s (1500 km).

3.4.2. NUMBER OF USERS AND DISTRIBUTION

The number of users also has a large effect on the computational time and how realistic the DOP values obtained are. If the DOP is excellent but only a couple of points are considered, there might be large holes without satellites. Therefore, studying them provides a robust system.

When propagating a constellation, there is a scenario where the DOP computation can be simplified. This occurs when the Walker constellation orbits are circular, no perturbations exist, and the Earth is symmetric about the Equator. Only under this combination, the DOP produced by the constellation should be symmetrical around the Equator.

In order to test this theory, the Galileo mission is modelled, positioning 500 users around the globe. Figure 3.10 visually shows this scenario. There is a symmetry visible over the Equator. Then, a second scenario is tested with 250 users only in the Northern Hemisphere, to further investigate the symmetry over the latitudes.

3

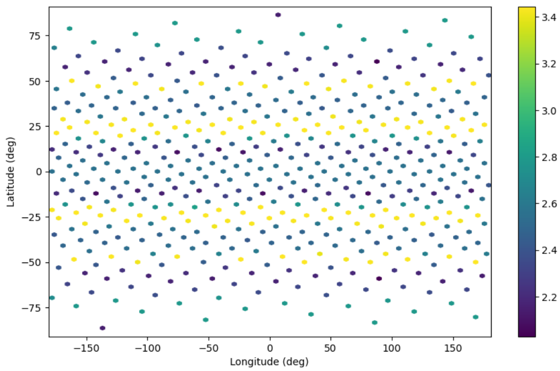

Figure 3.10: Galileo $GDOP_{95}$ heat map

A numerical demonstration is shown in Table 3.2. It shows the difference between a full and a half sphere configuration. The results indicate that the errors in DOP are of power 10^{-3} or less. This is no proper formal demonstration, but for practical purposes, it can be considered valid. Given the accuracy required is generally in the order of 10^{-1}, the assumption holds.

Table 3.2: DOP Differences between Full and Half Sphere

DOP Type	P95	Mean	Max
GDOP	7.4×10^{-3}	5.2×10^{-4}	-5.0×10^{-3}
PDOP	-5.1×10^{-3}	4.7×10^{-4}	-3.7×10^{-3}
TDOP	-5.8×10^{-3}	2.3×10^{-4}	-3.6×10^{-3}
VDOP	-1.5×10^{-3}	-4.6×10^{-4}	-1.2×10^{-3}
HDOP	3.7×10^{-3}	8.1×10^{-4}	-2.9×10^{-3}

The second aspect is determining the optimal number of users to distribute across the Northern Hemisphere. For this analysis, the Galileo constellation is propagated for one day using 10-second timesteps, and the 95th percentile GDOP is computed for all ground users. The resulting DOP distributions are then compared against a high-fidelity reference scenario using 1000 users to assess convergence and accuracy.

Figure 3.11 shows a whisker plot, including the min, max, 25th and 75th percentile, mean, and outliers. It shows how, as the number of users increases, there is a convergence in the GDOP. The first case to align in the interquartile range and mean is 100 users, suggesting this is a sufficient number. Increasing users does not show any real improvement compared to 1000 users. As a second validation, an arbitrary LEO constellation was run, and the same conclusion was achieved. Therefore, it has been selected to work with 100 users distributed over the Northern Hemisphere.

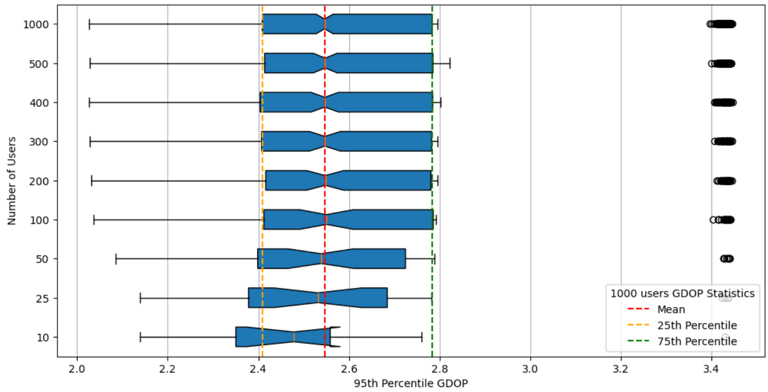

Figure 3.11: Whisker plot of 95th percentile GDOP for different numbers of users for the Galileo mission

3.4.3. RUNNING PERFORMANCE

To get an idea of the optimisation time, a simple analysis was made on the running time per simulation. The simulation consists of the user and constellation creation, propagation, visibility masks and DOP computation, along with some statistics.

The most intense part is in the visibility mask and DOP computation. This occurs because of the large matrix size (N_{sat}, N_{users}, t), of order $10e7$. These functions are processed using parallel methods from the Numba library[34], and for the visibility mask, it is preferred to run in batches, a task that can be done because each point is independent from the other, in contrast to the DOP matrix. Table 3.3 shows the runtime for processing the visibility matrix as a function of the batch size for an arbitrary constellation. A batch of 16 elements is chosen as the optimal.

Table 3.3: Visibility Matrix Batch Processing Time

Batch Size	4	8	16	32	64	128	256	512
Time (s)	0.10	0.09	0.09	0.12	0.14	0.18	0.18	0.18

Once the most demanding parts of the simulator have been optimised, a test run is done for different altitudes and numbers of satellites for one day. The running time will be larger for lower altitudes because of the shorter timesteps, as well as when there are more satellites propagated. Results are shown in Table 3.4, showing the fastest and slowest possible runs. The computation time is almost 4x larger for low altitudes with many satellites. In summary, for the optimisation, it can be expected that in a day, between 37,000 and 163,000 evaluations can be done.
This chapter summarises the development of the simulator used for the constellation optimisation. It is the backbone of the optimisation process and the results obtained. Each class has been carefully verified and validated to ensure no errors are present. Finally, the simulator has been tuned to achieve a balance between performance and com-

Table 3.4: Computation times for different constellation scenarios

Task	**700 km, 500 sats**	**1500 km, 150 sats**
User Creation	0.005 s	0.005 s
Constellation Creation	0.056 s	0.005 s
Constellation Propagation	0.430 s	0.072 s
Visibility Mask Computation	0.969 s	0.150 s
DOP Computation	0.754 s	0.285 s
Statistics Computation	0.014 s	0.012 s
Total elapsed time	**2.227 s**	**0.529 s**

putation time, allowing for fast evaluations during the optimisation process. This tuning includes a varying timestep depending on the altitude, a propagation duration equal to the repeating orbit period, and a user distribution only in the Northern Hemisphere with 100 users. In the next chapter, a first analysis of the problem is performed using the developed simulator, along with some constraints and objective selection.

4

Heuristic Analysis and Simulator Tuning

In this chapter, two of the main parameters in the constellation design are studied to understand the connections between the mission performance and the design choices: inclination and altitude. The mission performance can be measured using different metrics, such as the average GDOP, the 95th percentile HDOP, or simply the visibility. There is no perfect metric, and they may also miss other non-performance aspects. However, performing an initial heuristic analysis can give some constraints on the mission design and present insight into their relevance.

4.1. Inclination

A first aspect to consider is the inclination. If the constellation is meant to provide navigation services to the entire globe, there will be a minimum inclination required to observe the poles. This does not mean that all satellites need to be above such an inclination, but some must be located there. Figure 4.1 shows the geometry formed between them, where α is the minimum user elevation. The expression that comes out is Equation 4.1. When aiming to solve for the inclination, it becomes an intrinsic equation that needs to be solved iteratively.

$$a^2 + \frac{a^2 \cos^2 i}{\cos^2 \alpha} - R_E^2 - \frac{2a^2 \cos i \cos(\alpha - i)}{\cos \alpha} = 0 \tag{4.1}$$

Figure 4.2 shows such results for changing elevations. Historically, polar regions have received less attention in GNSS constellation design, leading to more relaxed performance requirements in these areas, generally due to limited infrastructure and lower user density. However, solving Equation 4.1 reveals the challenging orbital mechanics involved: even for a minimum elevation angle of 5°, satellites must be positioned at inclinations of at least 60° for a 1400 km altitude, with even higher inclinations required at lower altitudes to maintain polar coverage.

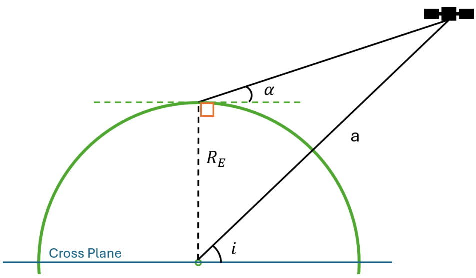

Figure 4.1: Minimum Inclination for Pole Coverage

It is important to note that satellite visibility alone does not guarantee high positioning performance. When satellites are concentrated near the horizon, the resulting geometry yields favourable horizontal dilution of precision (HDOP) but poor vertical dilution of precision (VDOP), creating an unbalanced accuracy profile.

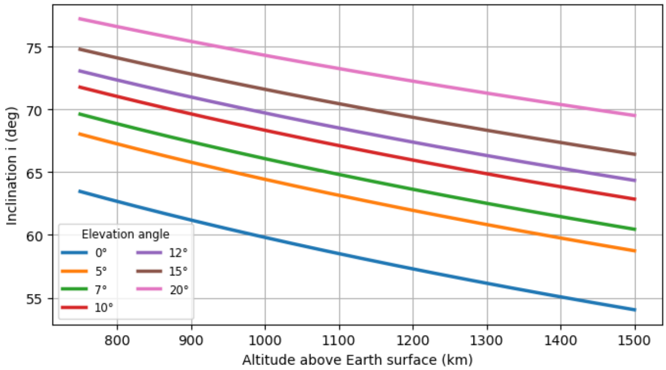

Figure 4.2: Minimum Inclination Required for Pole Coverage

Therefore, to have a more representative minimum inclination, a performance assessment could be done considering GDOP. As mentioned in the literature study, a $GDOP <$ 4 is considered acceptable, so this can be used as a benchmark. As there has not yet been any optimisation for the number of satellites, the simulation employs 600 satellites, a number significantly larger than what preliminary studies suggest [65, 106, 71]. This approach is intentional to ensure that the performance evaluation focuses solely on the effects of inclination, without influence from the satellite count itself. It is a static simulation, with results shown in Figure 4.3. It shows that for an elevation of 5 degrees, it requires an increase in inclination between $8° - 10°$. The overall conclusion is that there is a minimum inclination required of 68° to cover the poles, and that it can be larger for more limiting elevation angles or altitudes lower than 700 km.

A final assessment examines the GDOP distribution across different inclinations. This

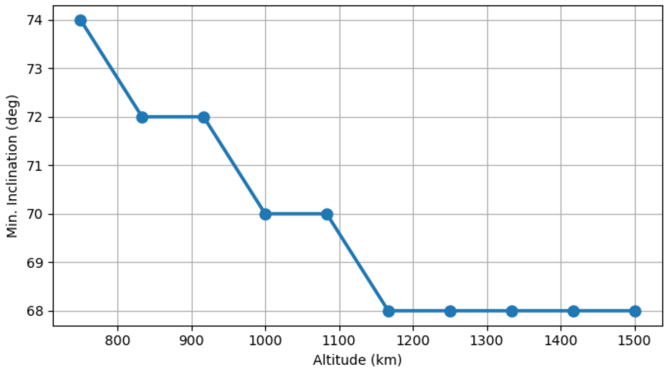

Figure 4.3: Theoretical Minimum Inclination for a global $GDOP < 4$ at $\alpha = 5°$

analysis evaluates the GDOP values achievable at various latitudes using a test Walker Delta constellation positioned at 1200 km with configuration i:204/12/6, which aligns with feasible configurations identified in the literature. Figure 4.4 displays the 95th percentile distribution by location.

Three key observations emerge from this analysis. First, the distribution exhibits clear symmetry about the equator. Second, inclinations below 70° form asymptotes in the maximum coverage latitude. Third, a key trade-off appears: constellations capable of covering high latitudes show degraded performance at equatorial regions. This performance degradation occurs because satellites in high-inclination orbits spend relatively brief periods above equatorial areas compared to their low-inclination counterparts. This is shown by the spikes occurring near the equator. This trade-off represents a critical design consideration for single-shell constellations and justifies employing multiple-inclination constellation architectures.

4.2. ALTITUDE

The next parameter to study is the altitude. It is a defining parameter, as it has an effect on many aspects: launch costs, number of satellites, period, perturbations, etc. As an initial assessment, it is possible to start by setting limits on the minimum and maximum. Afterwards, a baseline can suggest how many satellites will be needed for different performance metrics. All cases are run using a minimum elevation of 5° unless explicitly stated otherwise.

4.2.1. LOWER BOUND - ATMOSPHERIC DRAG

As demonstrated in section 3.2, atmospheric drag significantly impacts the mission. This analysis assumes a spacecraft mass-to-area ratio of 41.7 kg/m² and a drag coefficient of 2.2. The mass-to-area ratio was refined through iterative calculations from subsequent results, while the drag coefficient represents a typical value for satellites according to Prieto, Graziano, and Roberts (2014) [129].

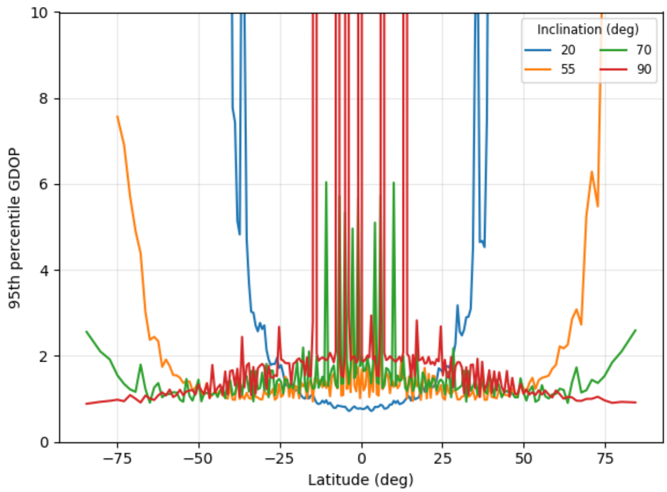

Figure 4.4: GDOP distribution over latitudes for different inclinations

4

When the satellite altitude is too low, it experiences substantial drag forces, primarily affecting the along-track motion. This leads to altitude loss and modifications to both semi-major axis and mean anomaly. As the satellite loses altitude, it accelerates relative to its intended position. For most missions, particularly navigation constellations, maintaining precise orbital positioning is essential to meet mission objectives. This is achieved through station-keeping manoeuvres, a series of corrective burns [173].

Drag also affects other orbital parameters, such as RAAN, causing altitude-dependent changes in precession rates and coupling between RAAN and inclination. To assess station-keeping requirements, perturbed orbits including drag and SH(48,48) perturbations were propagated at various altitudes. Assuming corrections every 20 days, the altitude loss and required annual Δv were calculated. The Δv estimates are approximations that do not account for specific mission requirements or out-of-plane corrections. Results are presented in Table 4.1. While these results vary with solar activity affecting atmospheric density, they demonstrate the general trend and enable altitude comparisons.

Table 4.1 shows the expected altitude loss and required annual Δv for station-keeping at various altitudes, considering both solar minimum and maximum conditions. According to European Space Agency (2025)[55], solar minimum and maximum refer to periods of low and high solar activity, respectively, which significantly influence atmospheric density and, consequently, drag effects on satellites. A solar cycle follows an 11-year period, affecting space weather conditions.

As expected, the altitude loss is larger at lower altitudes. Performing constant manoeu-

Table 4.1: Drag Effect on Altitude and Stationkeeping assuming corrections every 20 days

Altitude (km)	Solar Minimum		Solar Maximum	
	Altitude Lost (m)	Deltav Solar (m/s/year)	Altitude Lost (m)	Deltav Solar (m/s/year)
500	2565	25.97	2510	25.41
600	544	5.39	536	5.31
700	158	1.53	150	1.46
800	58	0.55	49	0.46
900	33	0.3	24	0.22
1000	30	0.28	21	0.19
1100	32	0.29	21	0.19
1200	39	0.34	17	0.15

vres and different altitudes could affect the LEO-PNT service in several ways. First, when a manoeuvrer occurs, the satellite goes offline for some time. Second, the differential drift between satellites, both in the along- and cross-track, can cause dips in the user performance, and in the case of using ISL, this connection could break. It is preferred to work on altitudes higher than 700 km, as the altitude drift stabilises. The lower bound for the altitude is set to 700 km. At this altitude, there is still significant drift, but it could be managed and gives some margin for the potential benefits of low LEO orbits to be studied.

4

4.2.2. UPPER BOUND - RADIATION AND FEASIBILITY

The upper bound of LEO is set around 2000 km, where the Van Allen Belt starts [6]. Starting at 1000 km and approaching this altitude, there is a rapid increase in the radiation. According to FrontierSI (2024) [65], most missions planned are between 500 km and 1200 km. In the state-of-the-art, the maximum altitude considered is 1500 km. A more detailed analysis is carried out by Ma et al. (2020) [104], who analyses the effect of such radiation. Making use of the SPace ENVironment Information System (SPENVIS) [54], they compute the total ionising dose over five years for different altitudes. They use the ionising capability of a chip-scale atomic clock (CSAC) as a limiting value, given the large probability of using one. The results are shown in Figure 4.5. This limitation is at 50 krad(Si). This threshold is crossed at ~ 1200 km for equatorial orbits, and at ~ 1600 km for polar orbits. These are not absolute limits, as shielding and other measurements can improve the resistance of the component. Nevertheless, this comes at the expense of a higher mass and/or shorter lifetime. For a more conservative approach, and assuming most satellites will be found at a polar orbit, the upper limit is set at 1500 km.

4.2.3. SATELLITES REQUIRED FOR A LEO-PNT CONSTELLATION

Before diving into the optimisation algorithm, which is effectively a black box, a grid search will help understand how many satellites are required for each altitude. This produces a baseline for comparison. However, there are different ways of assessing performance, and they will converge to more or fewer satellites. The three cases considered here are:

- Visibility. If there are four or more satellites above the users on the ground.
- Max HDOP. A common dilution of precision to consider is the horizontal DOP. It

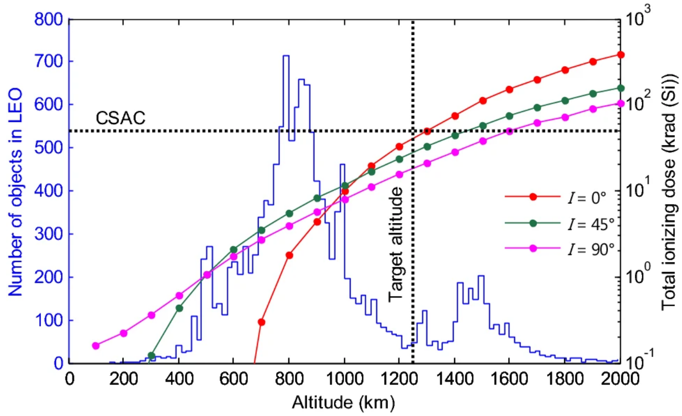

Figure 4.5: "Number and distribution of objects in LEO and radiation dosage in silicon over a 5-year mission as functions of orbital altitude and inclination" [104]

represents how well a user can place themselves in a horizontal plane, which is the most relevant metric for the general public, as there is little to no interest in the vertical placement. That is more relevant for aeroplanes or high-precision devices. An excellent HDOP is below two.

- Max GDOP. The more general DOP, considering both vertical and horizontal precision, is the GDOP. It is considered good if it is below four.

SINGLE-SHELL STATIC SIMULATOR

The simulator used for the heuristic analysis consists of 500 users on the ground spread on the ground and a static measurement at an initial epoch, without propagation. In this way, some initial assessment is computed at a fraction of the cost. Then a grid search is done, going through a variety of planes and satellites per plane for different altitudes. The search starts with the least number of satellites and then starts increasing. It stops once the objective has been met. The results for a single shell Walker constellation at an inclination of 80° are visible in Figure 4.6.

The first obvious aspect to consider is the inverse proportional relation between the number of satellites and altitude. It is interesting to see that the curve does flatten as the altitude increases, as if after 1200-1300 km, an asymptote is reached. It should be highlighted that these are not optimised configurations, and this flattening might mean simply that the reduction in the number of satellites is more difficult to achieve at higher altitudes, even if there is one.

On the other hand, very low altitudes require between 2.2 – 2.5 times more satellites than high altitudes. This seems excessive, but a trade-off can be made, considering performance, launch capabilities, and cost. The expected optimal value could be in between them, probably tending towards the higher altitudes. An interesting comparison is that with 200 satellites at low LEO, the mission can nearly meet visibility criteria, while at high

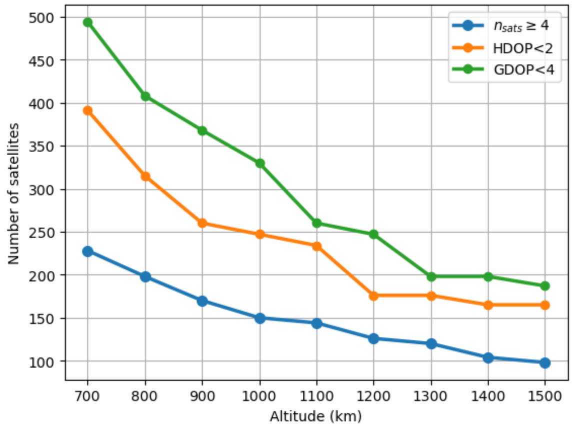

Figure 4.6: Grid Search for number of satellites vs altitude

LEO, it ensures a GDOP below four.

The first metric, visibility, can easily be met with 220 satellites, and with as few as 100. This is a lenient metric, which must be met, but is not sufficient. Keeping all HDOPs below 2 requires an additional 100-150 satellites. Both the HDOP and GDOP have four or more satellites in view at all times. Finally, the most limiting objective is keeping the GDOP below four. Even if not explicitly stated, in most cases, a GDOP under four will already fulfil an HDOP close to or below two. It will require between 50 and 100 more satellites.

COVERAGE PER LATITUDE

As shown earlier in Figure 4.4, depending on the inclination, the GDOP performance will change per latitude. In this analysis, 100 users were spread over the Northern hemisphere, and the constellations were propagated for one orbit, aiming to cover certain latitudes. This analysis combines inclination and altitude to understand the relation between them. Results are visible in Figure 4.7.

The figure shows three subplots, each aiming to cover a different part of the globe: low, medium or high latitudes. This is a first attempt at an optimisation, as the different inclination lines show which one works best to cover the designated area. These are: 30° for low latitudes ($< 30°$), 55° for medium latitudes ($30° - 60°$), and 80° for high latitudes ($> 60°$).

Requiring coverage only of certain parts of the Earth is a more lenient requirement compared to the previous analysis. To cover the entire Earth at 80° inclination and 700 km requires $\sim$ 420 satellites; focusing only on the high latitudes requires 150 satellites. From the diagrams, it seems that at the mid latitudes, the objective is not met as easily, requiring 240 satellites. From here, the possibility opens that using two or more shells could

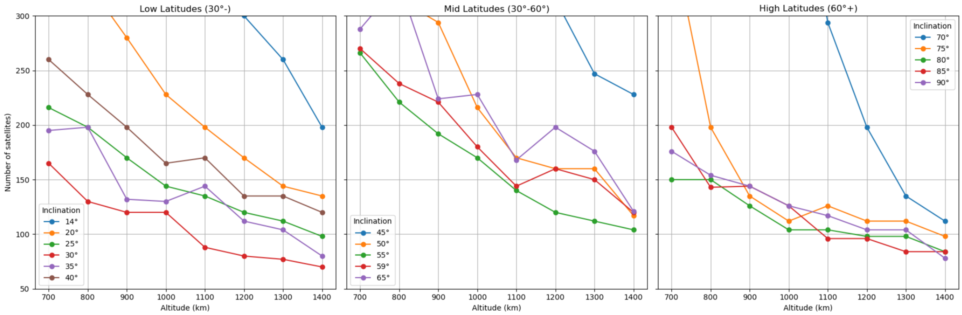

Figure 4.7: Number of satellites required to meet a Max $GDOP_{95} \leq 4$

potentially reduce the number of satellites required. This will be studied in the next sections and chapters.

TWO-SHELL SIMULATOR

If a certain inclination ensures that an area of the globe is covered, a second inclination can be used to fill in the gaps missed. However, it is not clear if this would actually provide a reduction in the size of the constellation. For this reason, a final analysis is done, where two shells are tested. The first shell will aim to provide a Max $GDOP_{95} \leq 4$ to all latitudes below a threshold, while the second shell will do the same for the higher latitudes. This was done for several thresholds using a grid search and allowing some limited freedom in the inclination variable. The results are visible in Figure 4.8.

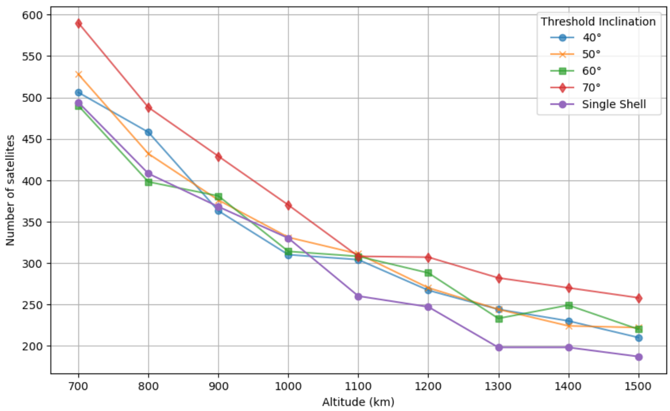

Figure 4.8: Number of Satellites vs Altitude required to meet a Max $GDOP_{95} \leq 4$ for a Two-Shell scenario

At first sight, the results are not very promising; compared to Figure 4.6, two shells would require more satellites for most scenarios. The exception is at low LEO setting a threshold at 60°, but providing a negligible improvement. These results are not completely comparable, however, since the first one is a static measurement, and this considers a full period of measurements. This shows the need for optimisation, where the combinations of inclinations, number of satellites and altitudes can be tested.

An example of how the shells are made is the 1200 km, where the shells are $35° : 117/9/4$ and $85° : 150/10/4$. This has the threshold at 40°, clearly visible in Figure 4.9, where the two sub constellations add to a better performing system.

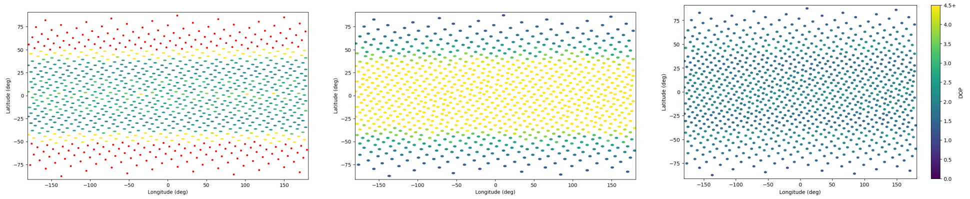

Figure 4.9: Max $GDOP_{95}$ performance per user for different constellation configurations: (a) low-inclination shell, (b) high-inclination shell, and (c) combined configuration.

4.3. Repeating Ground Track Orbits

In chapter 2, several types of orbits were discussed. An interesting one to consider is the repeating ground track orbit (RGT). RGTs have a specific combination of altitude and inclination to return to their initial position after N days and K revolutions around the Earth. Such situations can have several benefits to a LEO-PNT mission.

The first benefit is on the DOP. RGTs have better predictability of the performance, and the optimisation of the layout is easier as it can be simulated for n days, ensuring that the DOP does not change afterwards. This is especially useful for multi-inclination constellations, as they will be off-phase quickly unless they are realigned every certain intervals.

In the ground segment, over-ground passes simplify the contact schedule, enabling a potential reduction in ground stations and increased robustness. If the mission uses ISL and co-rotating shells, the relative positioning is better known, and the optimisation can be done more straightforwardly.

It will allow for a more deterministic service coverage, as well as predictable outage windows. This temporal repeatability is particularly valuable for LEO-PNT missions where maintaining consistent service quality is crucial. While Galileo operates on a 10-day ground track repeating cycle for a consistent performance and ground segment contact [85], LEO constellations can benefit from much shorter RGT periods due to their faster orbital dynamics.

For these reasons, along with the possibility of reducing the design space for the optimisation, it was decided to work purely with RGTs within the bounds found. The traditional repeating orbit is given by Equation 4.2.

$$T_{sat} = \frac{2\pi}{n} = 2\pi\sqrt{\frac{a^3}{\mu}}, \quad T_{Earth} = \frac{2\pi}{\omega_e}, \quad T_{sat}\cdot K = T_{Earth}\cdot N$$
$$\Rightarrow a = \sqrt[3]{\frac{\mu}{\omega_e^2}\cdot\left(\frac{N}{K}\right)^2} \tag{4.2}$$

In the equations, ω_e represents Earth's rotational speed, N and K represent the number of sidereal days and revolutions, respectively. For LEO, K is always larger than N, and specifically, the fractions that meet the requirement $700 \le h \le 1200$ km are $0.0687 \le \frac{N}{K} \le 0.0807$, leading to the potential orbits shown in Figure 4.10.

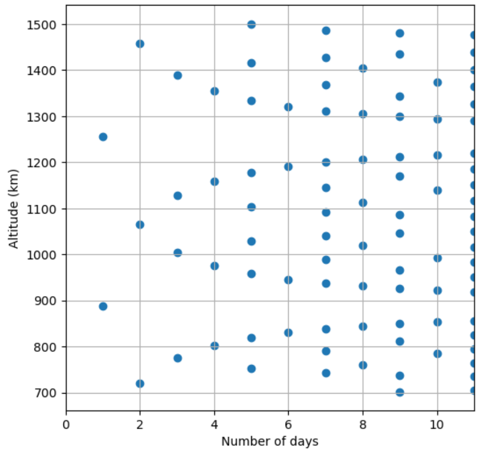

Figure 4.10: Repeating Ground Track Orbits with their Corresponding Altitude

However, in comparison to Galileo or higher altitude satellites, the effect of J_2 is much higher in LEO. Using the previous equation would slowly offset the orbits, meaning that they would not meet their purpose. Therefore, following Wei et al. (2023)[171], the J_2 effect can be incorporated into the formulation.

$$T_{sat} = \frac{2\pi}{n+\dot{\theta}_{J_2}+\dot{\omega}_{J_2}}, \quad T_{Earth} = \frac{2\pi}{\omega_e-\dot{\Omega}_{J_2}}, \quad T_{sat}\cdot K = T_{Earth}\cdot N$$
$$\Rightarrow a = \sqrt[3]{\frac{\mu}{\left((\omega_e-\dot{\Omega}_{J_2})\cdot\frac{K}{N}-\dot{\theta}_{J_2}-\dot{\omega}_{J_2}\right)^2}} \tag{4.3}$$

Equation 4.3 has a similar structure as its simplified version, but includes the J_2 rates for mean anomaly ($\dot{\theta}_{J_2}$), RAAN ($\dot{\Omega}_{J_2}$), and argument of periapsis ($\dot{\omega}_{J_2}$), which were first introduced in Equation 3.13, Equation 3.11 and Equation 3.12. These equations are functions of the semi-major axis and cannot be solved explicitly, so an initial guess is taken and solved iteratively. Convergence is shown after three iterations, with errors smaller than 10^{-7} m, but it is run until five iterations for robustness. The results are also dependent on inclination due to the rates and are shown in Figure 4.11.

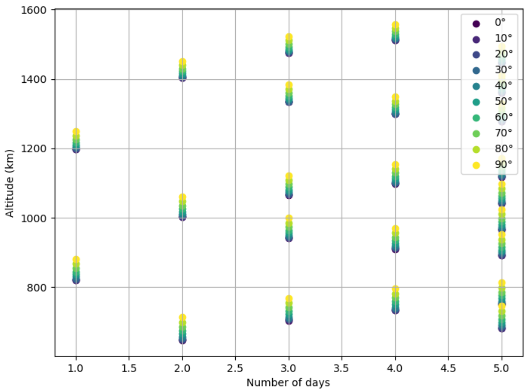

Figure 4.11: Altitudes for Repeating Ground Track Orbits with J_2 perturbation

The inclination produces changes of up to 80 km in altitude. The 90° case converges with the simplified repeating orbit because it does not precess, while other inclinations require lower altitudes. The new ratio range for this plot is $0.0700 \leq \frac{N}{K} \leq 0.0817$. All results were verified by propagating and ensuring they returned to the original point.

In LEO, satellites experience fast-changing orbital dynamics due to high angular velocity and stronger perturbations compared to higher orbits. This makes maintaining geometric consistency and network performance more challenging, especially for a dense constellation. For this reason, adopting repeating ground track orbits with tighter constraints could improve the stability and reduce operational conflicts.

Due to their lower altitude, LEO satellites pass more frequently over ground stations. By exploiting this, RGTs can help maximise contact opportunities predictably and periodically. This is particularly advantageous for uploading navigation corrections, downloading PNT data and satellites' telemetry.

Given these considerations, 1- or 2-day repeating ground track orbits are preferable for the LEO-PNT mission. They offer a trade-off between temporal repeatability, altitude, and operational feasibility. This leaves five candidate orbit sets. The lowest altitude set might encounter some problems with the large number of satellites and Δv required, while the highest altitude may also have problems with radiation and not provide a significant improvement in the number of satellites against the one at 1200 km. Nevertheless, they are worth taking a look at. The scenarios to be tested in the optimisation are in Table 4.2.

4

4

Table 4.2: Repeating Orbit Altitudes for Optimisation

ID	Altitude (km)	Number of Days	Number of Revolutions
a	~ 1250	1	13
b	~ 850	1	14
c	~ 1050	2	27
d	~ 700	2	29
e	~ 1450	2	25

4.4. OPTIMAL PHASING PARAMETER

In chapter 2, the Walker constellation was defined, and its implementation was discussed in chapter 3. A parameter that has not yet been discussed is the phasing between planes in a Walker constellation, denoted as F. This parameter is defined by Equation 2.3 and represents the angular displacement between neighbouring orbital planes, as illustrated in Figure 4.12.

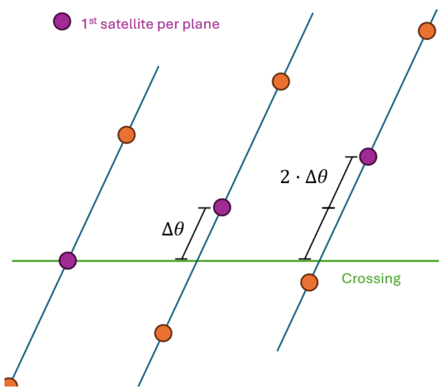

Figure 4.12: Representation of Displacement given by $\Delta\theta = 2\pi\frac{F}{T}$

Turner (2002)[166] claims that through Equation 2.4, repeated here for simplicity, the optimal F for visibility can be found. As a validation scenario, several random constellations at 80° are run using different F parameters and the availability between them is compared. The "optimum" is marked according to Turner.

$$F = [(P-1)-(T/P)] \bmod P$$

Figure 4.13 shows that in all cases, the point obtained using Turner (2002)[166] equation is either the optimum (green, purple, and pink cases), or very close to it, with a difference of less than 2%. Optimal points are marked with a black star. However, it is unclear whether this assumption still holds when considering the maximum 95th percentile GDOP. To verify this, the same analysis is conducted using constellations that achieve a GDOP below four, as identified in the grid search results from Figure 4.6.

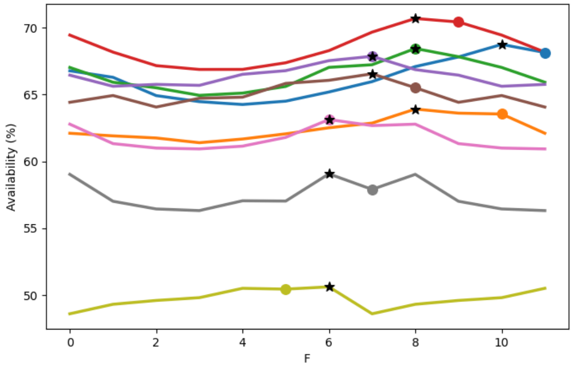

Figure 4.13: Optimal F for Arbitrary Constellations with Availability as Objective

The analysis in Figure 4.14a reveals that the F parameter selected by Turner's equation is rarely the true optimum for GDOP minimisation, but it remains reasonably close. The maximum difference between the actual optimum and Turner's selection reaches 22.8%, equivalent to 0.5 in GDOP units, while the average difference is 10.4%.

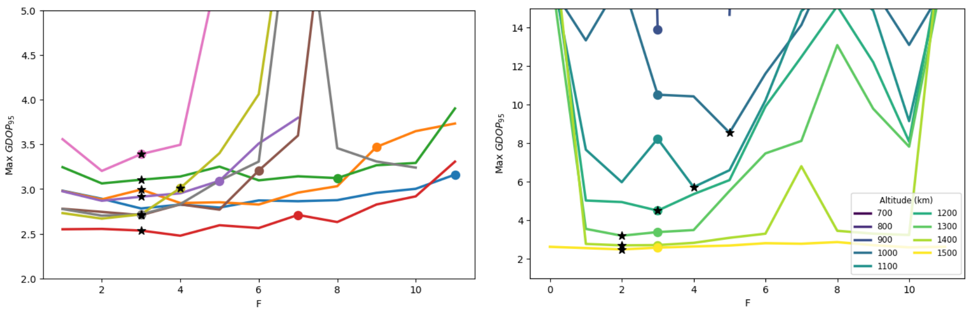

(a) Varying constellations

(b) 80° : 198/11/F constellation at different altitudes

Figure 4.14: Optimal F for Arbitrary Constellations with Max $GDOP_{95}$ as Objective

The plot is constrained to F factors up to 11 due to a repeating pattern in constellation geometry. Beyond a certain phasing, satellites realign themselves, recreating an earlier configuration. Equation 4.4 demonstrates this repetition pattern based on the number of planes, where N is an integer. This periodicity occurs when $F = N \cdot P$.

$$\Delta\theta = \frac{2\pi}{T/P} \rightarrow \text{Separation between sats in a plane}$$
$$\Delta\theta = 2\pi\frac{F}{T} \rightarrow \text{Offset between neighbouring planes}$$
$$2\pi\frac{F}{T} = N \cdot \frac{2\pi P}{T} \Rightarrow F = N \cdot P \tag{4.4}$$

To strengthen the analysis, the constellation $80^\circ : 198/11/F$ is evaluated at different altitudes to examine whether the optimal GDOP-F relationship remains consistent across varying performance conditions. By testing the same constellation configuration at multiple altitudes, it becomes possible to observe how the F parameter behaves when constellation performance deteriorates at lower altitudes.

Figure 4.14b demonstrates that Turner's equation does not consistently identify the optimal F value across all scenarios. For instance, at 1100 km altitude, the true optimal F value differs significantly from the predicted value. The maximum discrepancy reaches 43.8% for cases with large GDOP values, but when performance is maintained below a GDOP of five, this difference reduces to a maximum of 5.9%. Despite these limitations, Equation 2.4 continues to be employed in subsequent optimisation steps due to the relatively modest deviations and the significant computational simplification it provides.

5

SINGLE OBJECTIVE OPTIMISATION (SOO)

A single objective optimisation (SOO) problem is defined as a problem where the goal is to find the best solution according to a single objective function. In this chapter, the LEO-PNT mission is adapted to a single objective optimisation problem, where the objective is to minimise the number of satellites in the constellation while still meeting the mission requirements. The problem is first formulated in section 5.1, where the objective function, variables, and constraints are defined. The optimiser used to solve the problem is described in section 5.2, including the tuning process. The results of the optimisation are presented in section 5.3.

5.1. PROBLEM DEFINITION

When defining an SOO problem, it is essential to clearly outline the objective function, decision variables, and constraints. Depending on these definitions, the problem can be solved using various optimisation techniques, and the results can vary significantly. In this section, we will define the problem for the LEO-PNT mission.

Starting with the problem with some fixed parameters, we define the following:

- N and K: The integer parameters of the repeating orbit Walker constellation, where N is the number of days in the repeating period and K is the number of revolutions in the repeating period. These parameters are given in Table 4.2.
- α: The minimum allowed elevation angle of the satellites above the horizon, set to 5°.
- N_{obs}: The number of samples taken by a user from a satellite per orbit, which is set to 20.

The decision variables are defined as follows:

- S or S_1, S_2: The number of satellites per plane in a single shell or two shells, respectively. This is an integer variable. In the Walker constellation, it is more common to define the total number of satellites; however, here we define the number of satellites per plane to allow for more flexible optimisation. The ranges for S and S_1 are $S \in [10,25]$ and $S_2 \in [0,20]$. The range of S_2 starts from zero to allow for a single-shell constellation if the performance is better than a two-shell constellation.

- P or P_1, P_2: The number of planes in a single shell or two shells, respectively. This is also an integer variable. The ranges for P and P_1 are $P \in [5,20]$ and $P_2 \in [5,15]$. The range of P_2 is smaller because it covers the lower inclination range, expecting that the total number of satellites will be lower than for the higher inclination range.

- I or I_1, I_2: The inclination of the constellation, which is a continuous variable, but which can be discretised to a set of values. A deeper discussion on the inclination sensitivity analysis is provided in section 5.2. The ranges for I and I_1 are $I \in [68°,90°]$ and $I_2 \in [25°,68°]$. The dividing threshold is set by the heuristic analysis performed in the previous chapter, where it was found that an inclination of 68° is the minimum required to achieve a GDOP of 4. The shells are then divided into a high and low inclination shell, where the high inclination shell is defined as I_1 and the low inclination shell as I_2.

- Walker Type: The type of Walker constellation, which can be either Delta or Star. This is a categorical variable, and the choice of Walker type is made based on the inclination of the constellation. For the high inclination shell, both Delta and Star constellations are considered, while for the low inclination shell, only Delta constellations are considered. This is because Star constellations do not work well for low inclinations due to the geometry of the constellation. A deeper discussion on the Walker-type selection is provided in section 5.2.

5

From these free variables, there are other dependent variables that can be derived. Among the most important ones are:

- $a(N,K,i)$: The semi-major axis of the orbit, which is a function of the repeating orbit parameters N and K, and the inclination i.

- $dt(a,N_{obs})$: The timestep of the propagation, which is a function of the semi-major axis a and the number of observations N_{obs}.

- $T(S,P)$: The total number of satellites in the constellation, which is a function of the number of satellites per plane S and the number of planes P.

- $t_{prop}(N)$: The propagation time of the constellation, which is a function of the repeating period in days N.

- $F(T,P)$: The phasing factor of a Walker constellation, which is a function of the total number of satellites T and the number of planes P.

The objective function is to minimise the number of satellites in a one or two-shell Walker constellation. This objective is expressed mathematically by Equation 5.1.

$$\text{Minimise } f(x) = T \tag{5.1}$$

For a single-shell constellation, T is the number of satellites in the constellation, while for a two-shell constellation, it is the sum of the satellites in both shells, $T_1 + T_2$.

There is one constraint that must be satisfied, which is the maximum allowed GDOP. The metric used to measure it is the maximum 95th percentile of the GDOP over the entire constellation, which was defined in Equation 3.19. Several scenarios are then considered, where the maximum allowed GDOP is set to 2, 3.4, and 4. These values are chosen because a GDOP of 2 is considered excellent, 3.4 is the GDOP computed for the Galileo constellation using the same method, and 4 is a value that is still acceptable for PNT applications. The constraint can be expressed mathematically as follows:

$$g(x) = \max_{u \in \mathcal{U}} P_{95}(\mathrm{GDOP}_u) - \mathrm{GDOP}_{lim} \leq 0 \tag{5.2}$$

5.1.1. Naming Conventions

The optimised results need to be clearly defined to avoid confusion. Therefore, a clear naming convention is established. The results are named based on the number of shells, altitude, maximum allowed GDOP, objective, and the Walker type. An example of the naming convention used throughout this thesis is shown below:

1S4Ta or **2SD4Ta**

Each part of the label represents a design parameter:

- **1** or **2**: Number of shells used in the constellation.
- **S** or **SD**: Walker constellation type — Star (S) or Delta (D) or a combination of both (SD) in that order for the high and low inclination shells.
- **4**: Maximum allowed Geometric Dilution of Precision (GDOP). Options are 2, 3, and 4, where 3 refers to Galileo's performance (3.4).
- **T**: Primary optimization objective.
- **a**: Repeating orbit as given by Table 4.2. The options 'case'(N, K) are 'a' (1, 13), 'b' (1, 14), 'c' (2, 27), 'd' (2, 29), 'e' (2, 25), along with their corresponding repeating orbit parameters.

5.2. Optimiser

The optimisation problem defined in section 5.1 is solved using a genetic algorithm (GA). The GA is a population-based optimisation technique that mimics the process of natural selection. Making use of pymoo's available algorithms, a mixedGA is implemented, which allows for the use of both continuous and discrete variables. In this section, the GA is described, including its parameters and how it is applied to the problem.

5.2.1. GENETIC ALGORITHM

Genetic Algorithms (GAs) were introduced by Holland (1975)[77], and are a population-based optimisation technique that mimics the process of natural selection inspired by Darwin's theory of evolution. The basic idea is to evolve a population of candidate solutions over several generations, selecting the fittest individuals to create new offspring. It works in the following way:

Initialisation: A population of candidate solutions is randomly generated. They are encoded in a chromosome-like structure, where each individual represents a potential solution to the optimisation problem.

Selection: The fittest individuals are selected based on their fitness values, which are determined by the objective function. The probabilistic function is given by:

$$P(i) = \frac{f(i)}{\sum_{j=1}^{N} f(j)} \tag{5.3}$$

where $P(i)$ is the probability of selecting individual i, $f(i)$ is the fitness value of individual i, and N is the total number of individuals in the population. This ensures that fitter individuals have a higher chance of being selected for reproduction.

Crossover: Selected individuals are combined to create new offspring, which inherit characteristics from both parents.

Mutation: Random changes are introduced to the offspring to maintain genetic diversity.

Replacement: The new offspring replace the least fit individuals in the population, and the process is repeated until a stopping criterion is met.

Termination: The algorithm terminates when a stopping criterion is met, such as a maximum number of generations or convergence to a solution. The best individual in the final population is considered the optimal solution to the optimisation problem.

5.2.2. FIRST RESULTS

The first results of the optimisation are presented in this section. The optimisation algorithm is set to default settings, with a population size based on a rule of thumb given by Clerc (2008)[31] and Clerc and Kennedy (2002)[32] as shown in Equation 5.4.

$$S_1 = \mathrm{ceil}\left(10 + 2\sqrt{N}\right) \quad \text{or} \quad S_2 = \mathrm{ceil}\left(\frac{\ln\left(1 - 0.5^{1/N}\right)}{\ln(\alpha)}\right), \text{ where } \alpha = 0.17 \tag{5.4}$$

In the equations, N represents the number of decision variables, which is 3 for a single shell constellation and 6 for a two shell constellation. This leads to a recommended population S_1/S_2 size of 14/9 for a single shell constellation and 15/12 for a two-shell constellation. For simplicity, a value of 10 is used overall and in future steps, tuned again. The termination criteria are also left to the default, allowing for a maximum of

1000 generations and 100,000 evaluations, along with a tolerance of 10^{-6} for the convergence criteria and a period of 20 generations.

The results of this first iteration do not show the best performing constellations, but they do provide a good starting point for tuning, iteration and further analysis. For this reason, the results can be found in Appendix B. Nevertheless, some relevant aspects can be highlighted.

The first one is regarding the selection of constellation types. Even though for high inclination shells, both the Delta and Star constellations are considered, the results consistently show that the Star constellation works better than the Delta constellation. This is likely due to the unnecessary redundancy occurring in the Delta constellation, which is not needed for high inclinations. In low inclination shells, covering the entire RAAN range is necessary to ensure that the satellites are evenly distributed, but for polar orbits, the consequences of this would be to have satellites travelling almost the same path but in opposite directions. The results of the single shell optimisation show that Delta constellations require between 20 and 120 more satellites than Star constellations, which is a significant difference. With this in mind, the Star constellation is selected for the high inclination shell and the Delta constellation for the low inclination shell.

A second aspect is the inclination. Even if in the result tables, no more than two decimals are shown, the inclination is optimised to a much higher precision of the order of 10^{-6}. This is potentially unnecessary and requires extra computational time. Therefore, in an attempt to round the inclination to a more reasonable value, a sensitivity analysis is performed.

The sensitivity analysis is performed by adding and subtracting a small value to the inclination and checking if the performance of the constellation changes significantly. This test was done constraining the GDOP to 2 and 4 on the single shell case. The threshold for an allowable change in performance is set to 0.1 in the GDOP, which is the accuracy to which the optimisation is performed. The results of the sensitivity analysis are shown in Figure 5.1. The results show that the inclination can be rounded to the nearest 1° for the more constraining GDOP of 2, and to the nearest 0.5° for the less constraining GDOP of 4. Nevertheless, to have a more consistent and easier-to-read result, the inclination is rounded to the nearest 0.1° for all cases. This is done to ensure that the results are still accurate enough while being easier to interpret and faster to compute.

5.2.3. OPTIMISER TUNING

After defining what type of Walker constellation to use, as well as the inclination sensitivity, the next step is to tune the optimiser. The tuning is done by adjusting the parameters of the genetic algorithm to improve the performance of the optimisation. The objective is to converge to the optimal solution faster and with fewer evaluations. The tuning is done by running the optimiser for case "2SD2Tb" with different parameter values and comparing the results. This was the chosen scenario because it is one of the most complex ones to optimise, with a low altitude and two shells.

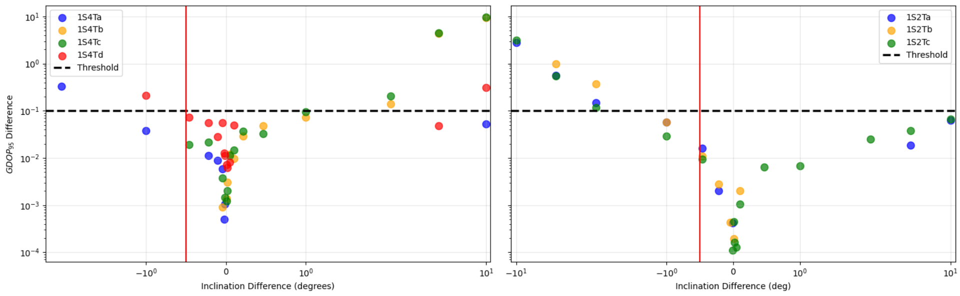

Figure 5.1: Sensitivity analysis of the inclination for different GDOP constraints. The red line indicates the last point below the threshold of 0.1 in GDOP.

The parameters to tune are both in the genetic algorithm and the termination criteria. The parameters are listed below, along with the reasoning for their selection:

- **Population size**: The population size represents the number of individuals looking for a solution. A larger population size allows for a better exploration of the search space, but it also increases the computational time. The default is set to 50, but it is tuned in the range of 5 to 75.

- **Number of offspring**: The number of offspring is the number of individuals that are created from the selected parents. If the number of offspring is too low, the algorithm may not explore the search space enough, while if it is too high, it may lead to premature convergence. It is set to None by default, meaning it is set to the population size, but it is tuned in the range of 5 to 10.

- **Period**: The period is the number of generations after which the algorithm is considered to have converged. If there is no improvement in the best solution after this number of generations, the algorithm stops. The default is set to 30, but it is tuned in the range of 5 to 50.

There are several more hyperparameters that can be tuned, such as the crossover and mutation rates, but these are left at the default values. The performance with these values is already acceptable, and tuning them further would require more computational time. Other parameters in the termination criteria are also modified, but without further tuning required.

Figure 5.2 shows the performance of the optimiser for different parameter values. The optimal point is marked in red, which is the leftmost point capable of reaching the minimum number of satellites. This corresponds to a population size of 50, the default offspring (50), and a period of 10. To be more conservative and generalise better, the period is increased to 20, as the time increase is minimal. These are the values used for the rest of the optimisation.

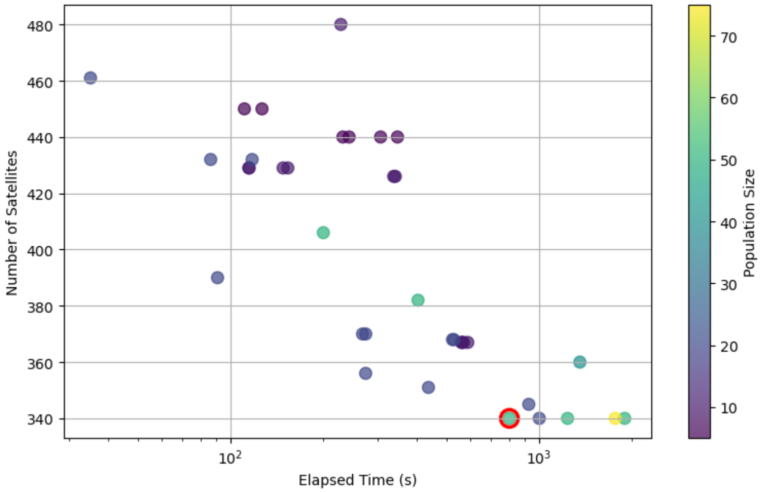

Figure 5.2: Tuning performance for the MixedGA using case "2SD2Tb". Optimal point marked in red.

Furthermore, since the inclination only needs to be accurate to the nearest 0.1°, the design variable is modified to work in an integer space by multiplying the inclination by 10. This transformation allows the optimiser to work solely with integers, which improves computational efficiency.

Given this integer-based approach, the termination tolerances can be adjusted to match the required accuracy. Since the design and objective variables are all integers, their tolerances are set to 1. The constraint tolerance is set to 10^{-2} because the GDOP performance metric has an accuracy of 0.1, and the constraint tolerance must be at least one order of magnitude smaller to ensure proper convergence. The final parameters used for the optimisation are summarised in Table 5.1.

Table 5.1: Optimiser and termination parameters for the SOO optimisation

Parameter	**Value**
Population size	50
Offspring	Default (50)
Period	20
Max generations	10^3
Max evaluations	10^5
Design Variable Tolerance (xtol)	1
Constraint Tolerance (cvtol)	10^{-2}
Objective Tolerance (ftol)	1

5.3. RESULTS OF THE SOO OPTIMISATION

The results of the SOO optimisation are presented in this section. The results are divided into two sections: single shell and two shell results. They are compared against each other, and the best-performing constellations are highlighted. The results are presented in tables, with the most relevant parameters shown. Finally, a comparison with some state-of-the-art constellations is made to highlight the performance of the optimised constellations. The results are also discussed in terms of their implications.

5.3.1. SINGLE SHELL RESULTS

The results of the single shell optimisation are presented in Table 5.2. All constellations are optimised to minimise the number of satellites in a Walker star constellation, while still meeting the maximum allowed GDOP. The first point to highlight is the lack of results for case "1S2td", which is the most limiting scenario in terms of GDOP and at the lowest altitude, close to 700 km. This occurred because it could not find a combination with fewer than 500 satellites, a limit set on the optimisation process. Nevertheless, the other cases show a significant improvement over the baseline analysis in chapter 4 and give potentially positive results for the LEO-PNT mission.

5

Table 5.2: Single Shell SOO Results

Max $GDOP_{95}$	Case	alt. (km)	inc. (deg)	T	P	F
≤ 2	1S2Te	1445.9	85.2	204	12	6
	1S2Ta	1241.2	83.5	240	12	3
	1S2Tc	1051.2	83.6	286	13	3
	1S2Tb	872.2	83.5	345	15	6
	1S2Td					
≤ 3.4 (Galileo)	1S3Te	1442.3	82.0	126	9	3
	1S3Ta	1240.4	82.8	150	10	4
	1S3Tc	1048.2	81.3	187	11	4
	1S3Tb	872.5	83.7	228	12	4
	1S3Td	702.6	82.8	294	14	6
≤ 4	1S4Te	1442.9	82.6	126	7	2
	1S4Ta	1238.6	81.3	150	10	4
	1S4Tc	1048.0	81.1	170	10	2
	1S4Tb	870.3	82.1	209	11	2
	1S4Td	705.6	84.8	260	13	5

When compared to the heuristic analysis, the reduction in the number of satellites is between 37% and 48% for high and low LEO, respectively. The reduction is more significant for the low LEO, where the number of satellites is higher simply because of the geometrical properties of the mission. The inclination is also optimised, finding that around 83° is the perfect inclination, but not varying more than 2°. For the high altitude, low constraining GDOP cases, they converge to the same constellations, which is the case of "1S3Ta" and "1S4Ta". They both converge to similar GDOPs, 3.40 and 3.36, respectively, and the same number of satellites, 150. The inclination is also similar, with a difference of 1.5°, suggesting the inclination has a larger range than previously expected.

In terms of the overall performance, the results show that the single shell Walker constellation can achieve a GDOP of 2 with a minimum of 204 satellites at an altitude of 1445.9 km and an inclination of 85.2°. However, there is a dramatic jump when the GDOP is relaxed to 3.4, where the number of satellites drops between 78 and 117. This suggests that if the mission allows for a higher GDOP, the overall mission cost and complexity could be reduced significantly.

In terms of the altitude, the lower the altitude, the more satellites are required to achieve the same GDOP. This also suggests there can be a trade-off between the altitude and the number of satellites, from a feasibility point of view. In this way, it can be discussed whether it is more expensive to launch more satellites at a lower altitude or fewer satellites at a higher altitude. Taking the Galileo performance as a reference, the satellite increases its range from 19% to 29% between altitudes.

5.3.2. TWO SHELL RESULTS

Similarly to the single shell results, the two shell results are presented in Table 5.3. In this table, the results are divided into two column groups, representing the two shells, followed by a total column group. The first column group shows the results for the high inclination shell, while the second column group shows the results for the low inclination shell.

Table 5.3: Two Shell SOO Results

Case	Shell 1 - Walker Star					Shell 2 - Walker Delta					Total
	alt. (km)	**inc. (deg)**	**T**	**P**	**F**	**alt. (km)**	**inc. (deg)**	**T**	**P**	**F**	**T**
2SD2Te	1443.7	83.3	150	10	4	1406.7	28.8	50	10	4	200
2SD2Ta	1242.6	84.6	216	12	5	1204.4	38.9	24	6	1	240
2SD2Tc	1052.1	84.3	273	13	4	1016.0	47.5	5	5	3	278
2SD2Tb	873.0	84.1	345	15	6						345
2SD2Td	705.9	85.0	425	17	8	653.0	30.1	24	8	4	449
2SD3Te	1440.0	79.9	126	9	3	1424.9	64.0	5	5	3	131
2SD3Ta	1238.7	81.4	150	10	4						150
2SD3Tc	1052.9	84.9	176	11	5	1021.8	55.7	10	5	2	186
2SD3Tb	873.7	84.6	216	12	5	827.3	35.1	5	5	3	221
2SD3Td	705.7	84.9	294	14	6						294
2SD4Te	1443.7	83.3	126	7	2						126
2SD4Ta	1237.8	80.6	150	10	4						150
2SD4Tc	1051.2	83.6	160	10	3	1006.3	26.3	7	7	5	167
2SD4Tb	872.1	83.4	198	11	3	831.3	42.5	7	7	5	205
2SD4Td	705.0	84.4	260	13	5						260

The results are similar to the single shell results, with slightly better performance in terms of the number of satellites. The two-shell Walker constellation allows for more flexibility in the satellite placement. The satellite distribution is more extreme than expected, having most satellites located at the high inclination shell(1), rather than the low inclination shell(2). There are some scenarios where the low inclination shell has no satellites. This is likely because the high inclination shell can cover a larger area of the Earth, and therefore requires fewer satellites to achieve the same GDOP, combined with the advantages of distributing the satellites in a star formation. The low inclination shell is only used when the high inclination shell fails to cover users near the Equator properly. An exception is seen for case "2SD2Te", where the low inclination shell accounts for 25% of the total number of satellites.

As mentioned earlier, the inclination and altitude are connected by the repeating orbit equation, which means that the two shells will have different altitudes. These altitude differences are between 15 and 53 km, or between 1% and 7%. Even though for most aspects this difference can be considered negligible (e.g. in terms of coverage and GDOP), it is still important to consider them on the feasibility aspect of the mission. If the mission works with ISL or needs optimisation for the signal propagation, these differences have to be considered. The first shell works with inclinations around 83.5°, while the second shell works with a larger range, between 25° and 65°. The closer the two inclinations are, the more similar the altitudes will be.

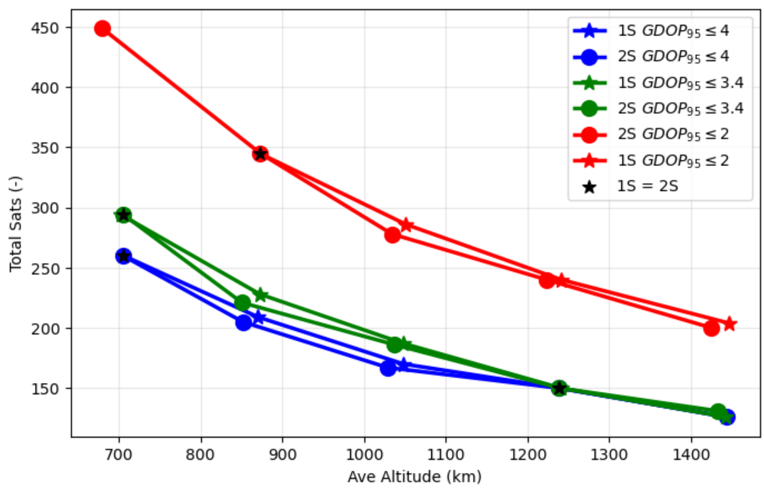

Figure 5.3: Comparison of the single shell and two shell Walker constellations

Figure 5.3 shows the comparison between the single shell and two-shell Walker constellations. The two-shell constellation has a lower number of satellites for the same GDOP, which is expected due to the increased flexibility in the satellite placement. However, this decrease is minimal. For comparable constellations, the improvement is between 1 and 8 satellite reductions, with an average reduction of 1.6. At the same time, to achieve this reduction, there is an increase in the complexity of the constellation, with up to 8 more planes, probably increasing launching costs and deployment time. The two-shell constellation is therefore not necessarily better than the single-shell constellation, but it does provide more flexibility in the satellite placement and can be beneficial for certain scenarios. Therefore, a feasibility analysis could provide better insights.

Furthermore, the black stars represent cases where the two-shell optimisation converged to a single-shell Walker constellation, reinforcing the viability of single-shell constellations for the LEO-PNT mission. The single-shell Walker constellation offers an optimal balance between satellite count and GDOP performance. The two-shell Walker constellation can be considered as an alternative, particularly when GDOP constraints become more stringent, but further analysis in this regard is performed in the multi-objective optimisation.

5.3.3. COMPARISON TO STATE OF THE ART

The results obtained do not necessarily align with the state of the art, as the literature presented two and three-shelled constellations as superior to single-shelled constellations. However, the results obtained in this chapter demonstrate that the single-shell Walker constellation can already meet the mission requirements in terms of geometric performance. A potential reason for this mismatch is the difference in objective functions used across studies.

As a validation step, several results from the literature are reproduced using the same objective function and compared to the results obtained in this chapter. Most results were of the same order of magnitude as presented in the source articles. However, many of the published results lack critical parameter specifications or clarifications, such as the constellation type (Star vs Delta) in Guan et al. (2020)[71], the phasing parameter F in Çelikbilek, Lohan, and Praks (2025)[26], or the type of GDOP metric considered (e.g., mean, maximum, 95th percentile).

Marchionne et al. also used the maximum 95th percentile GDOP metric, and for two out of three constellations, the results matched closely. For the third constellation, however, the reproduced GDOP is 0.4 higher than the published value. These comparisons are shown in Figure 5.4.

The first point to mention is that the results are generally in line with the findings of recent literature. Only the single shell Walker is presented for simplicity, and it shows that both the optimisations for a GDOP smaller than 2 and smaller than 3.4 are within the design space. Before performing a multi-objective optimisation, the analysis is limited to the values that have been obtained so far, but the results appear in the expected area. One point to highlight is from Marchionne et al. (2023)[106], marked by 1.87. This is the value given in the paper, but when run by the authors, the result of the constellation gives 2.27. This is probably a wrong configuration, since the other two results match the ones given in the paper. Therefore, this suggests an error in the paper, potentially in the writing phase.

Another point to consider is that every paper except for Guan et al. worked with mul-

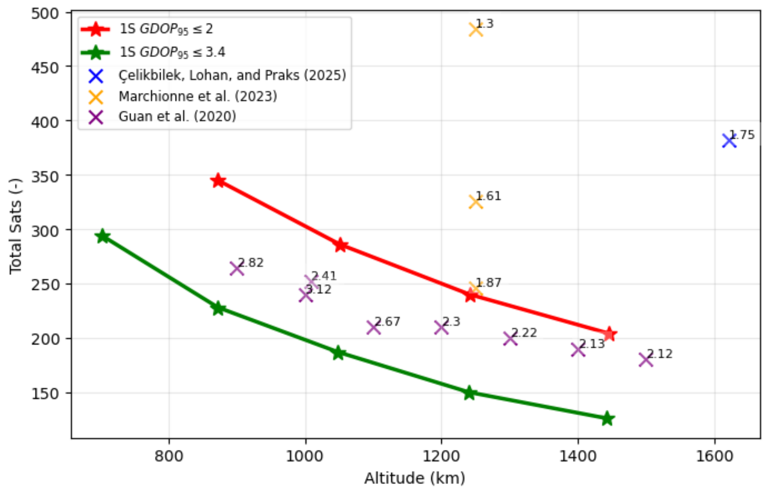

5

Figure 5.4: Comparison of the SOO results with state-of-the-art constellations [26, 106, 71]

tiple shells. This suggests that for better-performing GDOPs (less than 2), a multi-shell approach may be more effective. With this in mind, the results obtained in this chapter are promising and show that the single-shell Walker constellation can meet the mission requirements. The next step is to perform a multi-objective optimisation to further improve the performance of the constellation and explore the design space more thoroughly.

6

Multi-Objective Optimisation (MOO)

In comparison to a Single-Objective Optimisation (SOO), a Multi-Objective Optimisation (MOO) problem is defined by multiple objectives that need to be optimised simultaneously. The solution to an MOO problem is not a single point but a set of points known as the Pareto front. A MOO should be set up in such a way that the objectives are conflicting, meaning that improving one objective may worsen another. In this chapter, the optimisation performed in chapter 5 is modified to handle not only the number of satellites as an objective, but also switch the GDOP constraint to a multi-objective formulation. The chapter redefines the problem in section 6.1 and introduces the NSGA-III optimiser in section 6.2. The results of the MOO optimisation are presented in section 6.3.

6.1. Problem Definition

The problem is defined similarly as the SOO problem, but with the following modifications:

The objective functions are minimising simultaneously the total number of satellites and the maximum 95th percentile GDOP. The objective functions are defined as follows:

$$f_1(\mathbf{x}) = T \tag{6.1}$$

$$f_2(\mathbf{x}) = \max_{u \in \mathcal{U}} P_{95}(\mathrm{GDOP}_u) \tag{6.2}$$

These are competing objectives, as seen in the chapter 4, where, by setting stricter requirements on the mission, the number of satellites required also increases.

On the other hand, to limit the design area, two constraints are introduced:

$$g_1(\mathbf{x}) = \max_{u \in \mathcal{U}} P_{95}(\mathrm{GDOP}_u) - 4.5 \leq 0 \tag{6.3}$$

$$g_2(\mathbf{x}) = T - 500 \leq 0 \tag{6.4}$$

Equation 6.3 ensures that the maximum 95th percentile GDOP does not exceed 4.5. Four is categorised as a good GDOP, and exploring options around this limit without setting a strong constraint on exactly four can be advantageous. Equation 6.4 ensures that the total number of satellites does not exceed 500. Having more than 500 satellites, even if possible, is not within the objectives of most navigation missions, especially since the performance improvement drops rapidly below two. This is implemented for the final results, and not during tuning.

The remaining aspects of the problem, such as free variables and their bounds, are defined similarly to the SOO problem. A Walker star constellation is used as the default for high inclination orbits, while a Walker delta constellation is used for the second shell.

The naming convention explained in the SOO problem is also applied here, with the addition of the extra objectives to minimise and an index to refer to the Pareto front point going from least to most satellites required. For example, the third point in a two-shell star-delta configuration, minimising the number of satellites (T) and GDOP (G) for altitude 850 km (b), would be named *2SDTGb_3*.

6.2. Optimiser

6

The problem defined previously is solved using the NSGA-III optimiser, which is a popular algorithm for solving MOO problems, especially in the context of LEO-PNT constellation design [26, 71]. Other studies used a previous version of the algorithm, NSGA-II [106, 29]. This section introduces the algorithm, and a first batch of results was run along with the tuning performed on them.

6.2.1. NSGA-III

NSGA-III (Non-dominated Sorting Genetic Algorithm III) is an evolutionary algorithm designed for solving multi-objective optimisation problems, created by Deb and Jain (2014)[38], as an evolution of their previous model NSGA-II. The NSGA family works in the following way:

- A population of solutions is randomly generated.
- The population is evaluated based on the defined objective functions.
- The population is sorted into non-dominated fronts. A non-dominated front exists when an objective cannot be improved without worsening another objective. Several fronts are created, with the first front being the best solution for that population.
- For the next generation, start by adding the best fronts. If a full front does not fit into the population, the remaining slots are filled based on some selection criteria.
  - Crowd control (NSGA-II): This method selects solutions based on their rank and crowding distance, which measures how close solutions are to each other

in the objective space. For three or more objectives, the metric loses its meaning as most solutions are the best performing for some objective, and computing the crowding distance becomes more complex.

  – Reference points (NSGA-III): This method uses a set of reference points in the objective space to guide the selection process. The reference points are evenly distributed across the objective space, and solutions are selected based on their distance to these points, picking solutions from underrepresented areas.

- New solutions are generated through crossover and mutation.

- The process is repeated until a stopping criterion is met, such as a maximum number of generations or convergence to a stable solution.

The NSGA family algorithms are chosen for this problem for several reasons. The first one is given by Deb (2001)[41], which highlights the NSGA-II algorithm's ability to find a diverse set of solutions along the Pareto front. It also converges faster than other algorithms and can be parallelised. Since NSGA-III is based on NSGA-II, it inherits these advantages while also introducing improvements in handling many-objective problems. At the current stage, only two objectives are used, but more are added as the problem evolves, and it is better to have a consistent approach. Finally, from the state of the art, four out of seven chose either NSGA-II or NSGA-III as their MOO optimiser, which shows that it is a popular choice in the field [26, 106, 71, 29].

6.2.2. OPTIMISER TUNING

Tuning is performed to obtain optimal hyperparameters that ensure robust convergence to the true Pareto front. The quality of the final solution depends on two critical factors: population diversity and convergence criteria. Insufficient population diversity can cause the algorithm to converge prematurely to suboptimal solutions, while overly strict convergence criteria may terminate the optimisation before reaching the true Pareto front. Therefore, these two aspects are assessed through separate analyses.

To find the best performing set of hyperparameters in terms of time and quality of the solutions, a grid search is performed over a predefined set of hyperparameters. The performance of each set of hyperparameters is evaluated based on the quality and quantity of the solutions found. To keep it simple, the search is limited to the following hyperparameters:

- **Population size**: The number of solutions in the population. The range goes from 15 to 100.

- **Period**: The number of generations after which the population is assumed to have converged due to lack of improvement. The range goes from 10 to 50.

Other parameters, such as the number of generations and evaluations, are left at 200 and 200,000, respectively. The creation of the direction references uses the "das-dennis" method, already implemented in the software. Other variations, such as "uniform" or "energy", give the same distribution. The tolerances are the same as the ones used for SOO, except for the objective tolerance "ftol", because now GDOP is also an objective. The accuracy looked for is in the order of 0.1, so the **ftol** is set to 0.05 to give some margin. Duplicates are eliminated.

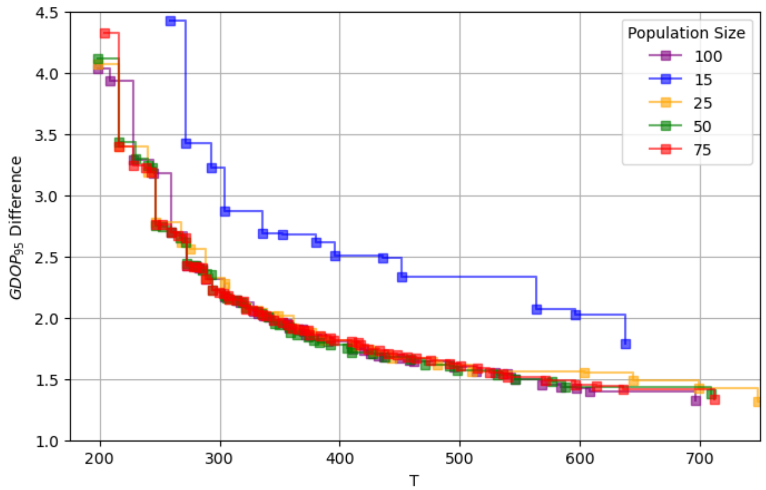

Figure 6.1: Pareto front for different populations and a period of 20

Figure 6.1 shows the Pareto front results for all populations. In general, there are slight differences between periods, but they are minimal. Therefore, only one scenario is shown here. The first conclusion that can be drawn is that a population of 15 is not enough to find a dominating Pareto front. Larger populations appear to all converge to the same Pareto front, with slight differences and better performing cases depending on the area of interest. Taking this into consideration, there is an interest in finding the Pareto front with the most points, as it shows better distribution for later analysis, while maintaining a decent running time.

Figure 6.2 shows the relationship between the size of the Pareto front and the running time for different populations. As expected, the larger the population and the period, the longer the running time. However, this is not necessarily a linear relationship with how many points in the front are found. The area of interest is the bottom right, where the time is low, but the Pareto front is still relatively large. Three especially interesting points are the red circle, the green circle, and the green circle and square. These correspond to a population of 75 and a period of 10, as well as a population of 50 and periods of 10 and 20. In order to select the best configuration, the Pareto fronts are compared.

Figure 6.3 shows that the green circle front (pop:50, per:10) tends to be slightly behind in the overall performance. The green square (pop:50, per:20) and red circle (pop:75, per:10) fronts show almost the same results. Even if the red line is faster, the circle square

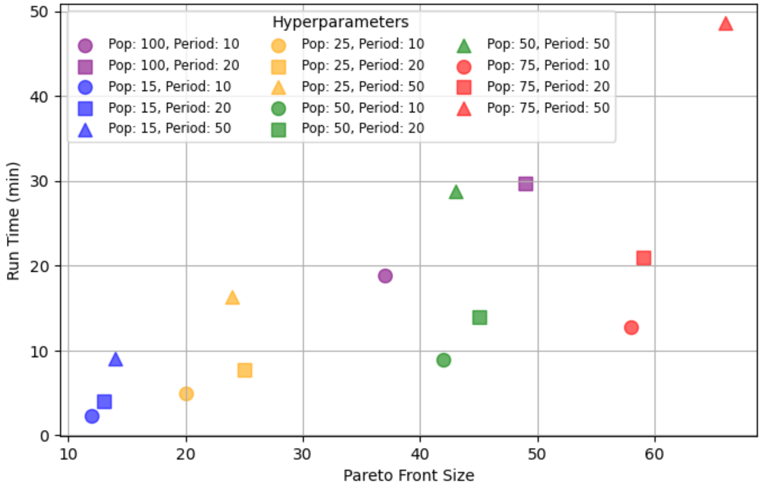

Figure 6.2: Pareto front size against running time

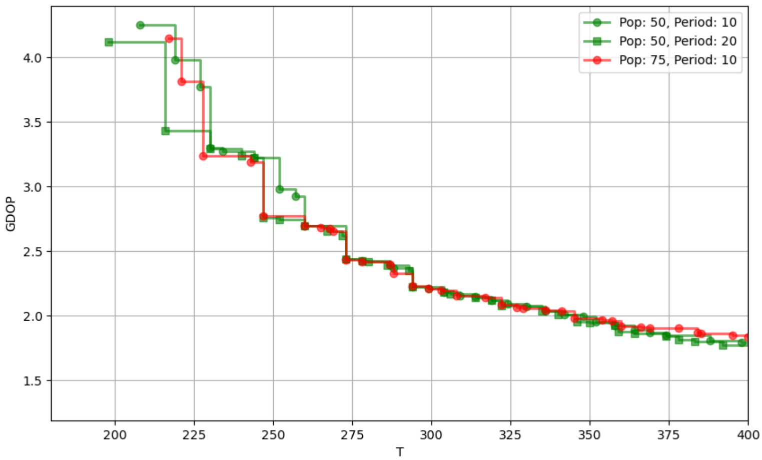

Figure 6.3: Final Pareto front comparison

front manages to find a much better performance for a GDOP of 3.4. Since this is an interesting point for research, given its similarity to Galileo, the population of 50 with a period of 20 configuration is chosen to be explored further.

In terms of the convergence of results, the history of the values is recorded and analysed. The results themselves are analysed in the next section, but the convergence is shown in Appendix C. The history of both single and double shells is studied. Convergence is better achieved for a double shell, having less average movement in the objective space. In the single shell, the convergence is less stable, especially for cases A (1250 km) and

E (1450 km). This could be due to having more combinations yielding similar results and allowing for more exploration of the objective space. Nevertheless, this only shows part of the picture, as the average value does not describe whether the Pareto front is changing or simply its distribution. Therefore, a visual analysis is also made, showing that once the optimal front has been reached, the distribution is done mainly within the front, rather than improving it. The final parameters chosen for the MOO are therefore:

Table 6.1: Optimiser and termination parameters for the MOO optimisation

Parameter	**Value**
Population size	50
Reference Directions	das-dennis (50 points)
Period	20
Max generations	$2 \cdot 10^3$
Max evaluations	$2 \cdot 10^5$
Design Variable Tolerance (xtol)	1
Constraint Tolerance (cvtol)	0.01
Objective Tolerance (ftol)	0.05

6.3. Results of the MOO Optimisation

The results of the MOO are presented in this section. Similar to the SOO, the results are divided into single-shell and double-shell configurations, followed by a comparison to state-of-the-art methods. Finally, some potential extensions of the MOO are discussed.

6.3.1. Single Shell Results

The single shell results are presented in Figure 6.4. In comparison to the SOO results, these cannot be presented in a table. Given that each Pareto front has between 10 and 24 points. The specific configurations, along with their GDOP, are presented in Appendix C.

As expected, higher altitude configurations demonstrate better performance in terms of both satellite count and GDOP, shown by these scenarios appearing closer to the lower left corner of the Pareto front. The black marks indicate the single shell SOO values obtained in the previous chapter. These points align well with the Pareto front, confirming that both optimisation approaches have converged to similar solutions.

The distribution of points along the Pareto fronts reveals some interesting characteristics. At GDOPs below 2.5, the fronts show relatively dense point distribution with smooth transitions between solutions. However, at higher GDOPs (above 2.5), the fronts exhibit sparser point distribution with occasional gaps. In the denser regions, small configuration changes, such as adding one plane or increasing satellites per plane, yield significant GDOP improvements at the cost of only 6-10 additional satellites. Conversely, the gaps in point distribution result in larger jumps of 33-57 satellites between adjacent Pareto points.

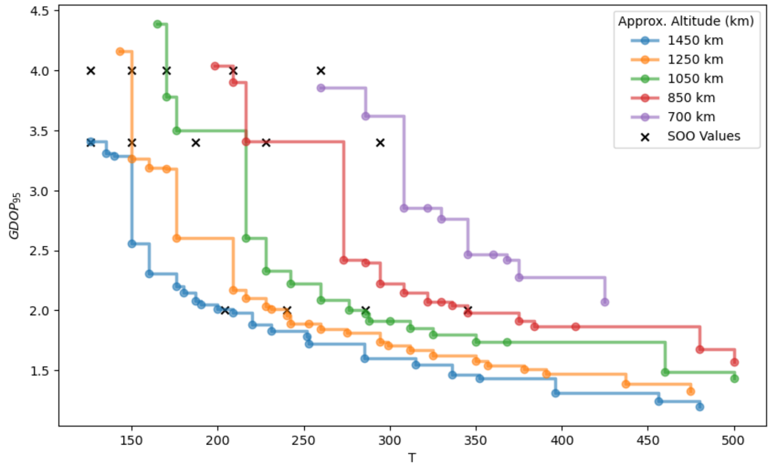

Figure 6.4: Single shell Pareto fronts

While these larger jumps are expected and justified at lower GDOPs, where substantial constellation modifications are necessary for meaningful performance improvements, their occurrence at higher GDOPs suggests that intermediate solutions may exist in these regions. This pattern indicates that the current optimisation parameters may not fully explore all potential solutions in the higher GDOP range. Although the existing results remain valid and intermediate points can be estimated through interpolation, future work could benefit from refined search strategies to achieve more uniform point distribution across the entire Pareto front.

The number of satellites per plane varies between scenarios. However, in 104 of the 107 Pareto-optimal solutions, this number is at least the total number of planes plus 4. On average, the satellites per plane equal approximately $P + 7.5$, where P is the number of planes. This suggests a trend towards more satellites per plane with fewer planes overall, which could be beneficial not only for the performance but also for the mission's cost and deployment strategy.

As a further analysis, case 'a' was rerun, aiming to minimise the total number of planes as an extra objective. The reason for this would be to improve the deployment strategy by reducing the number of launches required, assuming each launcher can reach and deploy an entire plane. This is further studied in the next chapter, but Figure 6.5 shows an initial attempt. The Pareto front is less robust in this case, only 18 instead of 24 points. The figure shows peaks, representing points that are in the optimal front of the number of planes' front, indicating a trade-off between the number of planes and the overall performance. Seven constellation configurations were compared on the basis of their similarity in GDOP. Four of them converged to the same configuration, while two improved by reducing two or three planes at virtually no increase in the total number of satellites. Finally, one converged to an even higher number of planes and satellites, suggesting convergence was not reached. In case of implementing such a scenario in the future, it might be beneficial to explore a smaller design space and increase the running time to find more optimal solutions.

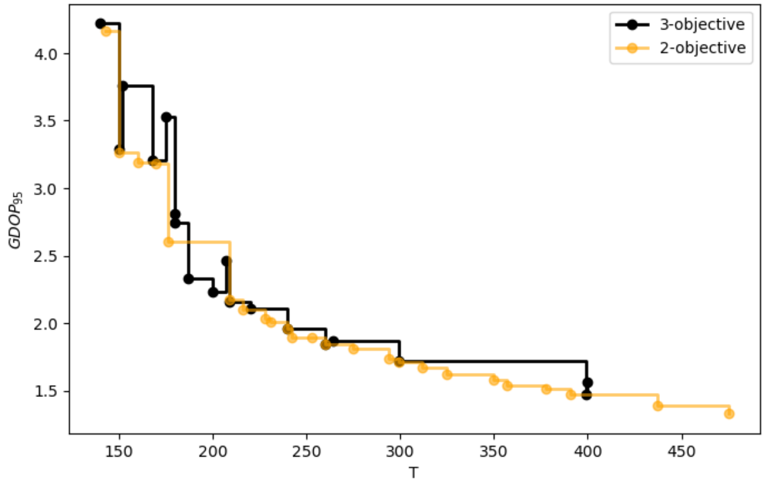

Figure 6.5: Case 'a' with number of planes as an extra objective

6.3.2. Two Shells Results

The results for the two shell configurations are shown in Figure 6.6. The two-shell SOO are also shown for comparison. The results show similar performance to the single shell. However, there are fewer empty regions in the Pareto front, indicating a more robust optimisation process. When analysing the SOO points, they are generally located in the same area as the MOO points, suggesting convergence. However, the high altitude scenario 'e' at 1450 km does not seem to converge to the same points for high GDOP. Something similar happens for the extreme points of the low altitude scenario 'd' at 700 km. This could suggest difficulties at extreme altitudes for the NSGA-III optimiser to find the best solutions. The recommendation would be to run SOO around those locations to improve the results.

The double-shell configuration requires significantly more planes than the single shell. While the single shell averages 13.4 planes, the double shell averages 19.8 planes. This increase likely results from the additional flexibility in shell design. Despite the larger number of planes, the total number of satellites remains roughly constant along the same Pareto front.

The difference between single shell and double shell Pareto fronts can be seen in Figure 6.7a. The two of them complement each other. Even though they both reach the same fronts, they cover different areas. The double shell is slightly better at low GDOPs, reaching better performances, while the single shell finds better solutions at high GDOPs.

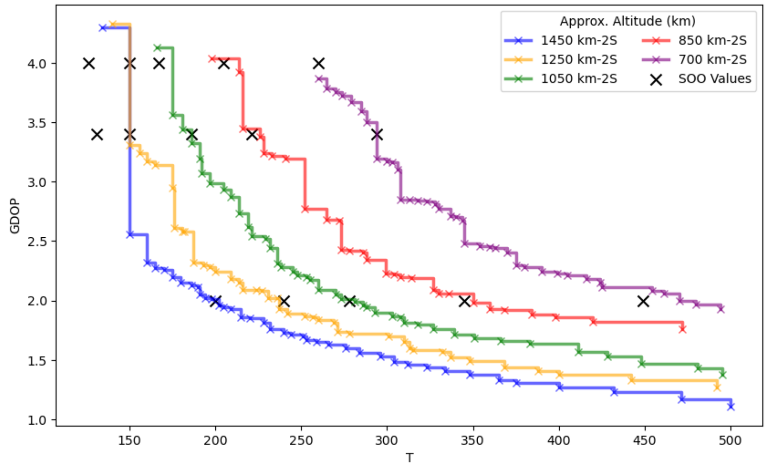

Figure 6.6: Two shell Pareto fronts

There is also a range of GDOP where both are possible and result in the same solution, which is great for flexibility in mission design. In some cases, the solution even converges to a single shell. 15% of all solutions returned to a single shell, and 35% of all solutions have less than 10 satellites in the second shell. This suggests that the double shell is not always necessary, and a single shell can be used instead. Figure 6.7b shows what percentage of the constellation is located on the second shell. The results show that when aiming for a $GDOP \geq 2.5$, the second shell is almost not required, with less than 10% of the constellation being located on it, with 0-20 satellites.

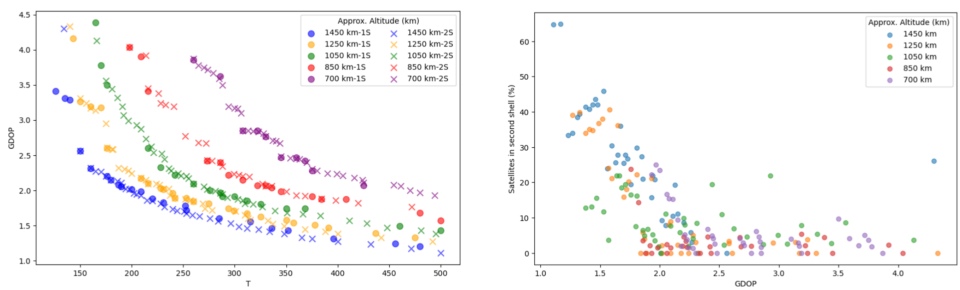

(a) Comparison of single shell and double shell Pareto fronts

(b) T2 analysis of satellite distribution

Figure 6.7: Pareto front comparison and satellite distribution analysis

Similarly to the previous subsection, a three-objective MOO was performed on case ‘a’ to see if any improvements could be made to the number of planes. From the 11 points that match GDOPs in both the 2- and 3-objective scenarios, four of them converged to the same solution, while the others all show an improvement in the number of planes.

The maximum improvement was a reduction of 10 planes. This generally comes with an increase in the number of total satellites required. On average, a reduction of 2.9 planes is achieved, while the satellite increase is of 20 elements. This could be studied further to find a good economic and feasibility balance.

6.3.3. COMPARISON TO THE LITERATURE

Taking the Pareto fronts, it is easier to compare with other cases found in the literature because there are more points closer to the solutions found in the state of the art. Figure 6.8 shows this comparison. It uses colour coding to differentiate the altitudes. These points are taken from different SOO and MOO studies found in the literature, as previously summarised in Table 2.12.

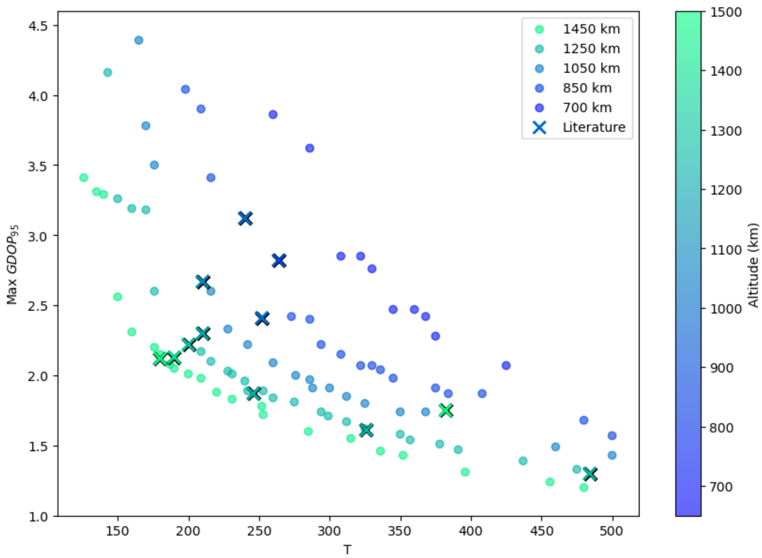

Figure 6.8: Comparison of MOO Pareto fronts to state of the art

The goal is to assess whether the literature values are dominated by the new Pareto front obtained in this study. If so, this would demonstrate the advantages of the new approach and its potential impact. Visually, this can be identified when a literature point's colour (altitude) does not match that of its neighbouring points on the Pareto front. Such a mismatch indicates that the constellation's altitude does not align with the performance of similar configurations.

For example, the green cross near the bottom right corresponds to a constellation at ~ 1450 km altitude but achieves performance comparable to an 850 km configuration. The solutions found in this thesis could improve GDOP by up to 0.6, which corresponds to shifting this point vertically downward until it aligns with the corresponding new Pareto front (colour).

Aside from this outlier, most literature points appear to align closely with the new Pareto front, suggesting that the proposed solutions achieve competitive performance across different altitudes. For a more detailed assessment, Table 6.2 provides a numerical comparison. This was obtained by taking each literature point, identifying the two nearest single-shell Pareto fronts, interpolating each to match the literature point's total number of satellites, and then performing a linear interpolation between the two fronts to determine the equivalent value.

Table 6.2: Comparison between literature points and the obtained Pareto front. A GDOP difference within ±0.05 is considered equivalent (on the Pareto front) [67, 26, 106, 71]

Literature Point	GDOP	Satellites	Altitude (km)	Difference
Ge	6.97	240	1000	−4.51 (Dominated)
Çelikbilek	1.75	382	1621	−0.40 (Dominated)
Marchionne_1	1.30	484	1250	(Not interpolated)
Marchionne_2	1.61	326	1250	0.00 (On PF)
Marchionne_3	1.87	246	1250	0.02 (On PF)
Guan_1	2.41	252	1008	−0.11 (Dominated)
Guan_2	2.82	264	900	−0.32 (Dominated)
Guan_3	3.12	240	1000	−0.66 (Dominated)
Guan_4	2.67	210	1100	−0.08 (Dominated)
Guan_5	2.30	210	1200	−0.02 (On PF)
Guan_6	2.22	200	1300	−0.01 (On PF)
Guan_7	2.13	190	1400	−0.00 (On PF)
Guan_8	2.12	180	1500	0.03 (On PF)

The table starts presenting the state-of-the-art solutions, including the number of satellites, altitude and max $GDOP_{95}$. The difference is computed as the relative improvement in GDOP with respect to the value shown in the table. A negative value indicates a better GDOP is achieved with the same number of satellites at that altitude, indicating domination. As shown in Table 6.1, the optimiser is limited to a GDOP accuracy of 0.05. Therefore, any point that is within this range can be considered equivalent in performance. With this in mind, out of the 13 literature points, six are dominated by the new Pareto front, while the other six are on the Pareto front. One point, Marchionne_1, is not interpolated because it has a GDOP too low to compare with the new Pareto front.

The results show that the new Pareto front meets or improves upon the state of the art in terms of max $GDOP_{95}$ performance. Marchionne et al. (2023)[106] is probably the best comparison to be made, as they also optimised, among other targets, for the same performance metric. Both studies show the same Pareto front, validating results. Nevertheless, an improvement with respect to it is the fact that for this comparison, only one inclination is used, while their optimised solutions required three different shells. The current results have a simplified configuration, potentially improving the deployment strategy.

The results shown by Guan et al. (2020)[71] further show the improvement against current literature. They were one of the few studies to consider single shell configurations, and their results are mostly dominated by the new Pareto front. Finally, Çelikbilek, Lohan, and Praks (2025)[26] and Ge et al. (2020)[67] were also dominated, especially for the second one, which was an analytical approach to the design.

6.3.4. POTENTIAL MOO EXTENSIONS

In the last two chapters, the performance against the number of satellites has been analysed and improved. However, these results are limited in terms of feasibility. They do not consider aspects such as limiting altitudes due to drag or radiation, have no consideration of the mass of the satellites, and do not account for the costs that would be incurred in deploying and maintaining these satellite configurations. In the next chapter, it will be explored how to extend the MOO and analyse the current Pareto fronts to include these additional constraints and factors. In this way, a stronger proposal for a LEO-PNT constellation can be made.

7

Feasibility Analysis

In this chapter, the objective is to assess the best-performing constellations in more realistic scenarios for future LEO-PNT constellations. The translation is done by analysing several aspects of the constellation unrelated to its performance. These feasibility aspects are related to external spacecraft and environmental factors, such as the space environment, cost, or time. Some of them are implemented directly into the optimiser, while others are analysed separately, and conclusions can be drawn for sets of orbits. The goal of the following chapters is to demonstrate how the feasibility of constellations can be assessed in conjunction with their performance.

The chapter starts by studying the satellites in section 7.1 and section 7.2, especially in terms of mass and Δv. Then, section 7.3 discusses the optimal deployment scenarios, considering cost and time. An analysis of the space debris risk is given in section 7.4. There is an approximation of the production and deployment cost in section 7.5, finalising with a new optimisation and analysis of the results in section 7.8.

7.1. Satellite Characterisation

Satellites come in all shapes and forms. However, they generally follow a pattern, and such patterns have been deeply studied to perform initial assessments on preliminary design. Wertz, Everett, and Puschell (2011) [174] works by taking historical data and identifying trends and correlations between different satellite parameters.

This section is formed by taking first-order approximations of the mass, geometry, instruments on boards, etc. It is important to highlight that this is a simplified approach, and real-world designs may vary significantly. The methodology can be maintained, but the specific values and configurations will need to be adjusted based on the actual design choices made during the development process.

7.1.1. MASS

The first parameter to compute is the dry mass. While Wertz, Everett, and Puschell (2011)[174] provides an approximation for LEO satellites with propulsion systems, yielding an average of 2344 kg, this value significantly exceeds what the New Space industry typically targets. Modern LEO constellations aim for much smaller satellites: micro (10-100 kg) and mini (100-500 kg) satellites [65].

To find a more appropriate approach, similar constellations can serve as inspiration for LEO-PNT systems. Communication constellations such as Starlink, OneWeb, and Kuiper share similar design principles and operational constraints. Starlink satellites have evolved over generations, with initial versions weighing between 200 and 300 kg, while the second version increased to around 1250 kg [134]. OneWeb satellites are considerably lighter at approximately 150 kg [148]. Kuiper satellites fall in the middle range at around 570 kg [93]. These examples suggest that a LEO-PNT satellite should target a mass range between 150-570 kg, depending on the specific mission requirements and technology choices.

However, to achieve a more systematic approach beyond simple analogy, a parametric model is needed. This leads to exploring power-based scaling laws that relate satellite mass to payload power requirements.

Springmann and Weck (2004)[155] devised a power law relating payload power to satellite mass using empirical data from several communication satellites. Given the similarity between LEO-PNT and communication satellites, this provides a reasonable starting point. The original empirical relation is shown in Equation 7.1, where P_{PL} is the payload power in watts, and m_{dry} is the dry mass in kg.

$$m_{dry} = 7.5 \cdot P_{PL}^{0.65} \tag{7.1}$$

However, this relation has several limitations that necessitate modifications. First, the data is based on satellites launched between 1990-1999, meaning technology improvements over the past 25 years are not reflected. Second, the regression fit shows only moderate accuracy with an R^2 value of 0.73, resulting in a standard deviation exceeding 500 kg. Finally, the satellites used in the original dataset may not be fully representative of modern LEO-PNT systems.

To validate and calibrate this equation for current applications, a comparison is made with the Iridium constellation, which was included in the original dataset and serves as an analogue for LEO-PNT systems due to similar operational environments and design constraints. Iridium satellites, launched in 1990, have a dry mass of 299.4 kg and a payload power of 686 W. Applying Equation 7.1 yields an estimated dry mass of 523.2 kg, which is 1.7 times higher than the actual mass.

This discrepancy suggests the original coefficient is too high by approximately a factor of 1.7. Additionally, accounting for 25 years of technological advancement in satellite miniaturisation and efficiency improvements, a further 30% mass reduction is assumed. These corrections lead to the modified relation shown in Equation 7.2:

$$m_{dry} = 3 \cdot P_{PL}^{0.65} \tag{7.2}$$

where the coefficient has been reduced from 7.5 to 3, representing both the calibration to Iridium data (a reduction factor of 1.7) and technological improvements (an additional 25% reduction). This adjusted equation is used for the subsequent mass estimations.

While detailed mass-power data for recent commercial constellations such as Starlink or Kuiper are not publicly available, the adjusted coefficient in Equation 7.2 was cross-checked against representative contemporary systems. Furthermore, the scaling remains within the typical range reported for modern LEO communication platforms of comparable size, giving confidence that the modified relation provides a realistic first-order approximation for present-day LEO-PNT satellites.

Drawing inspiration from Pereira and Selva (2019)[128], an expression for the payload power is derived. In their scenario, they work with fully independent GNSS constellations at MEO. For a LEO constellation, some requirements are relaxed, such as the need for a highly stable clock or the reduction in the transmission power, as well as less thermal requirements.

Table 7.1: Payload Power Requirements

Payload Comp	**Units**	**P (W)**	**Ref.**
Clock	2	10	[107]
ISL	2-4	60-80	[163]
NSGU	1	35	[128]
FGUU	1	22	[91]
RTU	1	12	[128]
Thermal	-	10%	[128]
Transmission	-	68%	[44]

Table 7.1 shows the different components required for a LEO-PNT satellite, along with their power consumption. The clock is a Chip Scale Atomic Clock (CSAC) [107], which is a low-power atomic clock, suitable for small satellites. Two of them are chosen for redundancy purposes. One key element of the LEO-PNT constellations is the potential use of ISL. Some commercially available terminals are the TESAT SCOT80 [163] and the Mynaric Condor Mk3 [113]. Only the SCOT80 had information on its power consumption. Depending on the design, the number of terminals will vary. For a simple LEO-PNT system, two terminals are enough to connect to the nearest satellites, which is assumed here.

The remaining elements are the Navigation Signal Generation Unit (NSGU), in charge of creating the code and modulating the carrier; the Frequency Generation/Upconversion

Unit (FGUU), capable of translating baseband to RF; and the Remote Terminal Unit (RTU), taking care of the interface and power usage. The values shown are outdated, but they provide an appropriate estimate, and more recent data was not publicly available. Even though the thermal power is part of the thermal subsystem, it has an effect in maintaining the payload, and Pereira and Selva (2019)[128] uses 15% of the payload power. Nevertheless, they work with satellites in MEO, which undergo a harsher environment and may require more power than LEO. Finally, the transmission power is improved using a Travelling Wave Tube Amplifier (TWTA), with an efficiency of 68% [44].

The total payload power consumption can be estimated by summing the individual components, leading to Equation 7.3

$$P_{PL} = 2 \cdot P_{clock} + P_{NSGU} + P_{FGUU} + P_{RTU} + P_{thermal} + P_T = \left(\frac{P_T}{0.68} + 249\right) / (1 - 0.10) \quad (7.3)$$

The only unknown in this equation is the transmission power P_T. The transmission power is a function of the link budget, which is a function of the orbit. It can be calculated using the following equation:

$$P_R = \frac{P_T G_t G_R}{L_{ex} L_{ant}} \cdot {\frac{\lambda}{4\pi r}}^{2} \quad (7.4)$$

where P_R is the received power, P_T is the transmission power, G_t and G_R are the transmitter and receiver antenna gains respectively, L_{ex} represents external losses, L_{ant} accounts for antenna losses, λ is the wavelength, and r is the distance between transmitter and receiver. The second part of the equation represents the free-space path loss (FSPL), which accounts for the loss of signal strength as it propagates through free space [21].

The values used for the transmission power calculation are calculated as follows. Even though the typical minimum value for a received power is -157 dBW for systems like GPS [20], a LEO-PNT system aims for a stronger signal. An improvement of a couple of decibels already improves the system against noise; therefore, P_R is set to -150 dBW. The transmitter antenna gain is slightly reduced from a typical GNSS of 10-20 dBi [1] to 7 dBi, due to the need for a more spread signal over the area [159]. Users on the ground do not have special antennas capable of improving the signal, and therefore, the receiver gain is 0 dBi.

The atmospheric loss is computed using Equation 7.5, obtained from Steigenberger, Thoelert, and Montenbruck (2018)[156], where R_e is the Earth radius in km and α is the elevation angle. The antenna and excess losses are based on Pereira and Selva (2019)[128].

$$L_{atm} = 0.07 \cdot \frac{1 + a/2}{\sin\alpha + \sqrt{\sin^2\alpha + 2a + a^2}}, \quad a = \frac{6}{R_e} \quad (7.5)$$

The distance (r) is given by Equation 3.18, and the wavelength can be computed from the frequency f using:

$$\lambda = \frac{c}{f} \tag{7.6}$$

where c is the speed of light. Following FrontierSI (2024)[65], some of the frequency bands of interest for these systems to operate in include:

- E1: 1575.42 MHz
- E5: 1191.795 MHz
- E6: 1278.75 MHz
- C band: ~ 5 GHz [140]
- UHF band: ~ 450 MHz [65]

For a European LEO-PNT constellation, the E1, E5, and E6 bands are particularly relevant as they align with the existing Galileo frequency allocation, providing potential interoperability. The final mission will probably not use all those frequencies, but this provides a conservative estimate of the power. The total transmission power can be computed for each frequency and summed up.

An overview of the values used in the transmission power calculation is shown in Table 7.2.

Table 7.2: Values for Transmission Power Calculation

Parameter	Value
P_R	-150 dBW
G_t	7 dBi
G_R	0 dBi
L_{atm}	0.38 dB
L_{ex}	0.5 dB
L_{ant}	2 dB

The results of this approximation can be seen in Table 7.3. As expected, the transmission power increases with altitude as the distance between the satellite and the receiver increases. For this same reason, the dry mass increases. The dry mass is computed using Equation 7.2.
From such results, the volume can be approximated following other empirical relations. Wertz, Everett, and Puschell (2011)[174] suggests a simple relation between wet mass and volume shown in Equation 7.7.

$$V_{s/c} = 0.01 \cdot m_{wet} \tag{7.7}$$

So far, only the dry component of the satellite mass has been computed. The total propellant mass is calculated through an iterative approach. As an initial approximation,

Table 7.3: Payload Power and Dry Mass Results

Case	Alt. (km)	P_{PL} (W)	Dry Mass (kg)
e	1450	826.3	236.2
a	1250	734.3	218.7
c	1050	645.9	201.2
b	850	561.2	183.7
d	700	500.5	170.5

the propellant mass is estimated to be approximately 10% of the dry mass, based on preliminary calculations. This initial estimate allows for the computation of the wet mass and volume, which are then used to assess mass effects from solar radiation and other environmental factors. The propellant requirements are subsequently refined through detailed Δv calculations presented in section 7.2, providing more accurate values for the final mass budget.

SOLAR RADIATION

The space environment changes with altitude and inclination. As the spacecraft increases in altitude, there is a high chance that its mass also increases. This can be due to higher power requirements or a riskier environment. As mentioned in section 4.2, solar radiation increases with altitude. The radiation causes a lifetime reduction in the electronic components when not dealt with appropriately. In a more advanced stage of the mission design, the components would be compared to study any increase in weight, along with other changes required.

7

For this preliminary stage, it has been decided to follow Pereira and Selva (2019)[128]. Their idea was to consider "careful COTS" components at the centre of a sphere of the same volume as the original spacecraft. According to Sinclair and Dyer (2013)[151], "Careful COTS" components are Commercial off-the-shelf components which were not designed with space radiation in mind, but that have been tested and proved to be able to sustain certain radiation levels. This provides an agile approach to constellation design through faster and inexpensive components, compared to the traditional radiation-hardened/space-grade counterparts.

Then, Pereira and Selva aimed to limit the radiation received by a satellite to a maximum of 30 kRad over the mission's lifetime (10 years) by adding an outer shell of aluminium ($\rho = 2700$ kg/m^3). They considered a spacecraft at two different altitudes in a polar orbit (87°). Then, they added an outer aluminium shell of a specific thickness to reduce the impact. Table 7.4 shows the results.

Table 7.4: Required Aluminium Thickness for careful COTS components

Altitude (km)	Al. Thickness (mm)
780	3
1250	7

To apply this protection approach to the current satellite design, the shielding is not applied to the entire spacecraft but rather to the electronics within it. For reference, the Juno spacecraft with an approximate volume of 30 m^3 [117] has its electronics shielded within a box of approximately 1 m^3 [115]. This extreme example protects only 3% of the total volume, but a similar approach can be adapted here. For the LEO-PNT satellites, the electronics are assumed to occupy 10% of the computed spacecraft volume, requiring protection within this smaller space.

The shielding thickness values in Table 7.4 represent a conservative approach, as they were derived for a 10-year mission lifetime, while LEO-PNT is expected to have a shorter mission. Based on the analysis, satellites operating below 700 km altitude require no additional radiation shielding. Above this threshold, the required aluminium thickness increases approximately linearly with altitude.
To model this dependence, a linear regression is derived from the data in Table 7.4, under the constraint that no shielding is required at $h = 700$ km. The general form of the relation is:

$$t(h) = m \cdot h + b \tag{7.8}$$

where t(h) is the required aluminium thickness in millimetres and h is the orbital altitude in kilometres. The slope m is determined from the two reference points $(h_1, t_1) = (780, 3)$ and $(h_2, t_2) = (1250, 7)$:

$$m = \frac{t_2 - t_1}{h_2 - h_1} = \frac{7-3}{1250-780} = 8.51 \times 10^{-3}, \mathrm{mm/km} \tag{7.9}$$

To ensure that $t(700) = 0$, the intercept b is calculated as:

$$b = -m \cdot 700 = -5.96, \mathrm{mm} \tag{7.10}$$

The resulting piecewise relation for the aluminium shielding thickness is therefore:

$$t(h) = \begin{cases} 8.51 \times 10^{-3}, h - 5.96, & h > 700, \mathrm{km} \\ 0, & h \leq 700, \mathrm{km} \end{cases} \tag{7.11}$$

Taking Equation 7.11 into account, the additional mass can be calculated for different altitudes. The approach to it is done by taking a sphere 10% of the volume of the spacecraft, and adding an aluminium shell to it. The additional mass is then computed by subtracting the original mass from the new one, assuming a constant aluminium density of 2700 kg/m^3. This mass is part of the dry mass, and will be up to 34.5 kg additional at an altitude of 1450 km.

MASS OVERVIEW

The mass budget is then built upon the dry mass, additional mass from radiation shielding, and the expected propellant mass. This results in a wet mass that can be used for further analysis. Table 7.5 shows the mass budget for the different altitudes. The propellant mass is only an approximation from what is computed in the section 7.2. The exact value is calculated in each simulation.

7

Table 7.5: Mass Budget for Different Altitudes

Case	Alt. (km)	Dry (kg)	Shield (kg)	Fuel (kg)	Total (kg)
e	1450	236.2	34.5	~ 23.6	~ 294.3
a	1250	218.7	23.9	~ 21.9	~ 264.5
c	1050	201.2	14.3	~ 20.1	~ 235.6
b	850	183.7	5.8	~ 18.4	~ 207.9
d	700	170.5	0	~ 17.1	~ 187.6

7.1.2. SATELLITE GEOMETRY

The next aspect to consider is the dimensions of the spacecraft. Taking into consideration the expected mass, the volume oscillates between 1.9 and 2.9 m^3. For simplicity, the volume is assumed to be constant at 2.5 m^3 when computing performance-related aspects, such as drag or collision avoidance manoeuvres. Taking this as input, a spacecraft of dimensions 1.5x1.5x1.1 m is considered, given that most satellites are not cubic.

For launch aspects, the volume is studied in more detail to provide a better fit. These exact values can be studied in Table 7.6.

Table 7.6: Volume as a Function of Altitude

Case	Alt. (km)	Volume (m^3)
e	1450	2.9
a	1250	2.6
c	1050	2.4
b	850	2.1
d	700	1.9

Furthermore, such a spacecraft will require between 0.5 and 2 kW [65]. Assuming the mission needs 2 kW, considering a solar cell efficiency (η) of 20% [62] and a solar flux of 1361 W/m^2, the required solar array area can be computed in Equation 7.12.

$$A_{sa} = \frac{P_{req}}{\eta \cdot P_{sol}} = \frac{2000}{0.2 \cdot 1361} = 7.35 m^2 \tag{7.12}$$

The system's specific power is within the ranges found in Sarsfield (1998)[145]. If the area is divided over two square solar panels, the resulting dimensions are 1.9 x 1.9 m.
The cross-sectional area is obtained from an ESA software, the Cross Section of Complex Bodies (CROC) [49]. The solar panels are positioned on the sides of the spacecraft. The obtained average cross-sectional area is 6.0 m^2 and the maximum area is 9.7 m^2. These values are relevant for empirical relations in solar radiation and for space debris risk.

7.1.3. PROPULSION

To perform correction manoeuvres, desaturate reaction wheels, or completely change the orbit, the satellite requires a propulsion system. Two main options are available:

electric or chemical thrusters. In a straightforward trade-off analysis, electric propulsion systems demonstrate superior efficiency in terms of Δv, with specific impulse (I_{sp}) values approximately five times higher than chemical thrusters. While deployment time is longer for electric thrusters, this is not the driving constraint given the mission size. Electric thrusters also offer higher accuracy, supporting ADCS manoeuvres and enabling continuous low-thrust operations. Additionally, they typically exhibit longer operational lifetimes compared to chemical alternatives [2].

Several electric thrusters were evaluated: the ENPULSION NANO R3 [45], Spaceware Mini M Thruster [59], and the PPS X00 Stationary Plasma Thruster [70]. The PPS X00 was selected as the baseline thruster due to the publicly available technical data, making it representative of expected performance characteristics. Its relevant properties are presented in Table 7.7 [70].

Table 7.7: PPS X00 Stationary Plasma Thruster

Thruster property	**Value**
Nominal Power (W)	200-1000
Fuel	Xenon
Thrust (mN)	15-75
Specific Impulse (s)	1300-1600
Efficiency (%)	48

This thruster operates with different ranges of power, thrust, and specific impulse. In order to simplify the analysis, a scenario with the smallest specific impulse (I_{sp}) is considered. The smallest I_{sp} represents a less efficient satellite, requiring more fuel, but also providing a more powerful thrust. Such a case provides an upper limit. Therefore, by taking an arbitrarily small power (P) of 350 watts, and an I_{sp} of 1300 seconds, the corresponding thrust (T) is 26 mN following Equation 7.13, where η is the thruster efficiency.

$$T = \frac{2\eta P}{g_0 I_{sp}} \tag{7.13}$$

7.1.4. OTHER PROPERTIES

Finally, the remaining values were assigned arbitrarily. According to a compilation of 11 LEO satellites' datasheets made by TU Delft Faculty of Aerospace Engineering (2020) [165], LEO satellites considered have a lifetime ranging between 3 and 7 years. Therefore, the target lifetime is set to 7 years. It is beneficial to extend the lifetime as much as possible to make it a competitive service, reduce replacement needs, and spread the initial investment over a longer period.

The drag coefficient is set to 2.2, which is a common value for LEO satellites [129]. The radiation coefficient is set to 1.0, a worst-case scenario used for a black body which absorbs all radiation [24].

7

Table 7.8 shows the initial values used to perform the remaining analysis in the chapter.

Table 7.8: Basic LEO-PNT Spacecraft Properties

s/c property	Value
Dry mass (kg)	170.1 - 229.9
Bus Dim. (m)	1.5x1.5x1.1
Solar Array Dim. (m)	1.9x1.9
Lifetime (yrs)	7
Drag Coefficient	2.2
Radiation Coefficient	1.0

7.2. DELTA V ANALYSIS

This section studies the fuel requirements for the mission. It is composed of the analysis of the Δv budget for the different mission phases. These phases include the (potential) initial orbit raising and plane changing, the operational phase considering stationkeeping and collision avoidance manoeuvres (CAMs), and the end-of-life (EOL) phase. Here, the stationkeeping and EOL are analysed, while the CAMs are studied in section 7.4. The deployment strategy, along with the Δv trade-off it entails, is in section 7.3. Finally, safety margins are applied to the Δv budget to account for uncertainties.

The computation of these manoeuvres is performed inversely, starting from the desired end state and working backwards to determine the necessary thrust and fuel requirements.

Conversion from Δv to fuel mass is done using the Tsiolkovsky rocket equation [164], shown in Equation 7.14, where m_0 is the mass at the start of the manoeuvre, m_f is the mass after the manoeuvre, I_{sp} is the specific impulse, and g_0 is the standard gravity (9.81 m/s^2). The difference between m_0 and m_f gives the fuel mass required for the manoeuvre.

$$\Delta v = I_{sp} \cdot g_0 \cdot \ln\left(\frac{m_0}{m_f}\right) \tag{7.14}$$

7.2.1. END OF LIFE STRATEGY

Now that the dry mass has been computed, the process of computing the wet mass starts with the EOL manoeuvres. These manoeuvres are essential to ensure the satellite can be safely deorbited or moved to a graveyard orbit at the end of its operational life. According to Agency (2023)[7], any mission should deorbit within 5 years of the end of its operational life.

The software used to compute the required Δv is the Orbital SpaceCraft Active Removal (OSCAR) [51]. Developed by ESA for EOL mission analysis, it simulates the deorbiting process by considering various factors such as atmospheric drag, solar radiation pressure, and gravitational perturbations. It allows for a delayed de-orbit process, potentially using thrusters to meet the 5-year objective.

The spacecraft parameters detailed in the previous part are used as input values for the software. The average possible cross-sectional area is used, and the mass is assumed to be the dry mass plus the additional mass from the aluminium shell. The orbits are simulated as circular, using an average altitude based on the mission profiles used in previous chapters. The inclination is considered at 84°, being an average of the high inclinations used. The results were compared to a low inclination (35°), showing that high inclinations require slightly more Δv. Therefore, all EOL calculations are performed at 84° to have a conservative estimate.

The orbit is propagated for up to 25 years using the ECSS sample solar cycle following the guidelines set by the ECSS Secretariat (2020)[43]. The recommendation suggests working with solar cycle 23 because of its accurate representation of average solar activity. OSCAR propagates the orbit throughout the entire solar cycle, including its effects on atmospheric density. The software then computes the required ΔV to deorbit within 5 years of the end of life. The results are shown in Table 7.9.

Table 7.9: EOL Δv and Fuel Mass for Different Altitudes

Alt (km)	Dry Mass (kg)	Δv (m/s)	Fuel (kg)	Disposal Duration (days)
1450	271	432.79	9.32	52.91
1250	243	335.66	6.48	36.79
1050	216	243.29	4	22.74
850	190	128.88	1.93	10.96
700	171	46.36	0.62	3.5

The table shows that at higher altitudes there is an increasing trend in the required Δv for deorbiting, which is expected due to the lower atmospheric drag and the need for more significant manoeuvres to overcome the increased orbital energy within the deorbit time frame. Nevertheless, the fuel mass is relatively small, being between 0.3% and 3.4% of the dry mass. Taking these values, a simple regression line is fitted to obtain a continuous function, helpful to adapt to the specific altitudes. It is made by a linear regression analysis, resulting in Equation 7.15.

$$\Delta v_{EOL}(h) = 0.5041 \cdot h - 300.98, \qquad R^2 = 0.9992 \tag{7.15}$$

Furthermore, the disposal duration represents the time it takes to manoeuvre after the five years have passed to ensure the satellite re-enters the atmosphere safely. This is a short period, lasting between 3 and 53 days.

7.2.2. STATIONKEEPING

In LEO, one of the limiting aspects is the atmospheric drag. It was studied in section 4.2, but is further expanded here. The values from Table 4.1 can be used to estimate the Δv

requirements for stationkeeping manoeuvres. The table shows values for the solar maxima and minima. Given the mission lifetime of 7 years, and a solar cycle of 11 years [43], the average solar activity can be considered. The satellite uses a cross-sectional area of 6 m^2, as approximated earlier, and a mass of 250 kg. Figure 7.1 shows the average Δv per year as a function of altitude, along with a fitted regression model to interpolate between points.

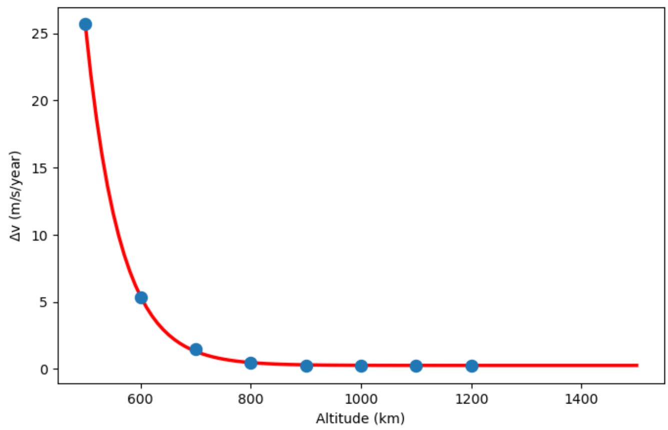

Figure 7.1: Average Annual SK Δv vs Altitude

7

The resulting fitted line is described by Equation 7.16, which is an exponential decay plus a constant, similar to the traditional atmospheric models. The model has a very high R^2 value, showing a strong fit. The equation can be used to compute the required Δv for station keeping and adapted to the timeline of the mission. For a seven-year mission at low altitude (700 km), the required Δv is less than 10 m/s, which is manageable within the mission constraints.

$$\Delta v_{SK}(h) = 7.38 \times 10^4\, e^{-0.0159h} + 0.263 \text{ (m/s/yr)}, \qquad R^2 = 0.9992 \tag{7.16}$$

7.2.3. SAFETY MARGINS

Safety margins are useful in this early stage of the design. They help model a conservative scenario, accounting for uncertainties in the design. Margins have already been applied to the dry mass of 10%, but they can also be applied to the Δv budget.

For the Δv budget, the margins vary based on the uncertainty of the calculations. For the values obtained using ESA software, such as the EOL and CAMs, a margin of 5% is considered appropriate given the high accuracy of such models. Similarly, for a transfer manoeuvre explained in section 7.3, a margin of 5% is applied, since the transfer itself follows a well-defined trajectory. However, for stationkeeping at any stage: operation, transfer or deployment, a margin of 200% is applied to account for the random nature of the environment, potential perturbations, and simplifications in the calculations.

7.3. LAUNCH AND DEPLOYMENT STRATEGY

The launch and deployment strategy plays a crucial role in the feasibility and cost of a constellation. It encompasses defining the launch profile, including the choice of launch vehicle, launch site, and deployment sequence.

7.3.1. LAUNCHER ANALYSIS

The choice of a launch vehicle is a function of cost, availability, and capacity. The current market is dominated by SpaceX's Falcon 9, which has a high launch cadence and a competitive price [97]. Nevertheless, having in mind a European LEO-PNT constellation, the launchers should be provided by European companies.

Among the European launchers, the most famous ones are Avio, with its Vega rocket family, and Arianespace, known for the Ariane family. There are other companies, such as Isar Aerospace or Rocket Factory Augsburg, but they are still in development and have not yet performed an orbital launch [127]. Therefore, they are not considered for this analysis.

Therefore, the potential rockets are Vega-C, Ariane 62 and Ariane 64. Vega-C is a small-lift launch vehicle, capable of launching up to 3.3 tons to LEO, with a fairing diameter of 3.5 m according to Arianespace (2025)[14]. Such a small launcher cannot provide the capabilities required for the constellation. Some of the optimised constellations have 15 satellites per plane, and this launcher would not be capable of filling the plane in a single launch. Therefore, it is not considered for this analysis.

7

The Ariane 6 launchers are a much better option. They have a higher payload capacity and can accommodate more satellites per launch. Table 7.10 shows an overview of the relevant specifications for the Ariane 6 variants, as defined by Arianespace (2021)[13].

Table 7.10: Ariane 62 and 64 Capabilities and Fairing Dimensions

Parameter	**Ariane 62**	**Ariane 64**
Payload capacity (LEO)	10.3 t	21.6 t
Fairing outer dimensions	5.4 m ⌀ × 14 m / 20 m	5.4 m ⌀ × 20 m
Internal diameter	4.6 m[1]	4.6 m
Internal height (cylindrical)	5 m[10] / 11 m	11 m
Internal height (with cone)	12 m / 18 m	18 m

When launching a rocket, the launch site plays a crucial role in mission performance and cost. According to Curtis (2013)[36], while all launch sites can reach inclinations ranging from their latitude to polar orbits, additional considerations must be taken into account. Equatorial locations provide a performance advantage due to Earth's higher rotational velocity, which is particularly beneficial for low inclination orbits. High inclination orbits have less benefit from this effect, as the launch trajectory must be directed

[1] The volume capacity can be extended to 6.1 m internal height if the diameter is reduced to 4.33 m

more north-south rather than east-west. Additionally, safety regulations and geopolitical considerations influence launch site selection, with high latitude sites often preferred for polar orbits to avoid overflying populated areas.

The Ariane rocket family launches from the Guiana Space Centre in French Guiana [52]. While this equatorial location is not ideal for the high inclination or polar orbits required for this mission, all LEO inclinations remain achievable from this site. The deployment accuracy for an 800 km polar orbit is within 2.5 km in semi-major axis, 3.5×10^{-4} in eccentricity, 0.04° in inclination, and 0.03° in ascending node. The total launch duration to LEO is approximately 1.5 hours [13].

Even though European launchers are the only ones considered, it is handy to compare them with other options. Most rockets present similar payload capacities for LEO. For instance, SpaceX's Falcon 9 can launch up to 23 tons to LEO [10], comparable to the Ariane 64. Other rockets are Delta IV Heavy (29 tons), Proton M (23 tons) and Atlas V (21 tons). An exception is Falcon Heavy, which can launch up to 64 tons to LEO.

7.3.2. PAYLOAD CAPACITY

The launching capacity is computed based on the maximum payload mass and the volume of the satellites. The volume is generally the limiting factor when defining the payload capacity. Therefore, the approximated volumes of the satellites computed in Table 7.6 are taken, and a 5% margin is applied to account for possible stowed solar panels. Afterwards, the mass from the Table 7.5 is taken as is.

Before the computations, some assumptions are made. The first one is that the satellite's dimensions can be modified to fit better in the launcher as long as they maintain the same volume. The satellites can only fit in the cylindrical part of the fairing and shall be positioned around a central axis. This central axis is a structural hollow tube of 1.5 m diameter and a thickness of 5 mm, made out of Carbon Fibre Reinforced Polymer (CFRP). This material has an average density of 1600 kg/m^3 [84]. Taking this into account, the mass of the central tube weighs 188 kg for the short fairing in Ariane 62, and 414 kg for the longer fairing in Ariane 62 and Ariane 64. The satellites can be placed on top of each other, leaving a 20 cm gap between them for structural purposes and to avoid damage during launch. These are from now onwards referred to as levels.

The satellites' placement will require adapters and other structural elements to ensure proper fit and support within the fairing. Therefore, to each satellite's mass, 25 kg are added, as well as some space left between the main column and the satellite to accommodate the connection port.

With these considerations in mind, five different configurations are defined to place the satellites within the fairing's floor. These different designs trade off the floor area occupied vs the number of levels required and the height of each satellite. The options are placing 4 or 5 rectangular satellites, or 5-7 trapezoidal satellites. Each scenario is compared per altitude for all five options. Given the large data volume, the specific results per altitude can be found in Appendix D. However, it is seen that in almost all scenarios, using the seven trapezoidal satellite structure, as shown in Figure 7.2, yields the best results. It is not surprising, given that it is the configuration that maximises the use of the fairing's cross-sectional area.

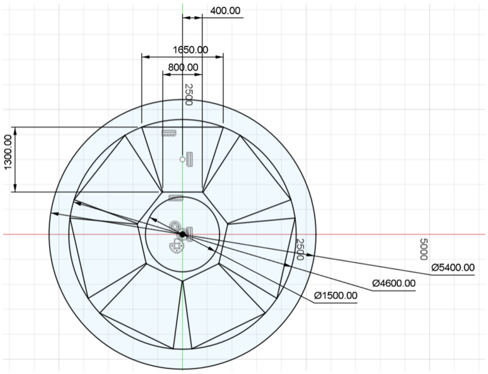

Figure 7.2: Seven Trapezoidal Satellites Configuration

Taking the specific design and multiplying it by the level's capacity (the capability to stack satellites vertically), the maximum number of satellites that can be launched per rocket is computed. Table 7.11 shows these results, along with the total mass and volume used. The values are rounded down to the nearest integer, as partial satellites cannot be launched.

Table 7.11: Launcher Capacity for Different Altitudes and Launchers

Altitude (km)	**Launcher**	**Levels**	**Total Sats**	**Total M_{PL} (kg)**
1450	A62 Low	2	14	4700
	A62 High	5	30	10000
	A64	5	35	11600
1250	A62 Low	2	14	4200
	A62 High	5	30	8900
	A64	5	35	10300
1050	A62 Low	2	14	3800
	A62 High	6	36	9600
	A64	6	42	11100
850	A62 Low	3	21	5100
	A62 High	6	42	10000
	A64	6	42	10000
700	A62 Low	3	21	4700
	A62 High	7	42	9100
	A64	7	49	11000

A result is that the Ariane 64 is potentially the best option for all altitudes except 850 km, given its capacity to launch heavier payloads compared to the Ariane 62. Nevertheless, the Ariane 62 with a longer fairing is also a viable option, being generally close in performance, but limited by the payload mass capacity. The shorter fairing could be useful if fewer satellites need to be launched, but it does not provide a real advantage in terms of performance and cost.

In the next stages, the Ariane 62 with a long fairing and Ariane 64 can be used for optimising the launch strategy.

7.3.3. DEPLOYMENT OPTIONS

The deployment strategy is a crucial aspect of constellation design, as it directly impacts the time and cost of deployment. There are two main strategies to consider: direct deployment and indirect deployment.

Cornara et al. (1999)[35] discusses the orbit injection and transfer strategies for constellations. The first method is the direct injection, where the satellites are taken to their final orbit using the launch vehicle. This method is common because it's faster, allows for a lighter satellite, and can be cheaper when all satellites are launched to the same target orbit.

A second option is the indirect injection. The launcher targets a lower altitude than the operational one, and the Earth's oblateness (J_2) effect can be used to drift the satellite in the Right Ascension of the Ascending Node (RAAN) over time. This allows for the population of several planes in one launch. This is a useful strategy when launching a large number of satellites, as it allows for a higher capacity of the launcher. Some disadvantages are the longer deployment period, increased propellant, and more complex operations.

7

7.3.4. DEPLOYMENT TIMELINE

Given the size of the constellation, considering 150+ satellites, finding a strategy to populate the constellation as fast as possible is desired. This is a function of the deployment strategy chosen, the potential drift altitude, the manufacturing cadence, and the launching capabilities of the provider.

In the New Space era, the idea of a satellite assembly line has been gaining traction. Large constellation companies like SpaceX and OneWeb are investing in high-throughput manufacturing lines to increase production rates and reduce costs [42, 61].

In the same spirit, a LEO-PNT constellation would benefit from a high manufacturing cadence. Current attempts at building a communications constellation show that they are much larger than navigation ones. This occurs because of the lower altitudes, stricter latency and broadband requirements, etc. Nevertheless, these constellations can be used for inspiration. Starlink has a manufacturing cadence of 280 satellites per month [42].

On the other hand, OneWeb has a cadence between 40-60 satellites per month [61]. The assembly lines listed here are in the USA, but there is an effort to develop similar ones in Europe. Aerospacelab (2024)[3] is developing a megafactory in Belgium, aiming to produce 500 satellites per year starting in 2026. This is equivalent to 42 satellites per month. Assuming LEO-PNT are manufactured by them at a slightly lower cadence, a manufacturing rate of 30 satellites per month is considered.

A more constraining factor is the launch cadence. According to David Cavaillolès, the chief executive of Arianespace, the company aims to reach a cadence of 9-10 launches per year with the Ariane 6 [64]. This is an extremely low cadence compared to competitors like SpaceX, launching more than 130 satellites in 2024 alone [74].

Nevertheless, a European LEO-PNT constellation would probably be launched using a European launcher. Therefore, the Ariane 6 cadence is used. The 10 launches per year need to be divided among different customers. It is expected that European governments are anchor customers, but there is also a market for commercial launches. With sufficient political will, it is assumed that 4 launches per year can be dedicated to the constellation. This is equivalent to one launch every three months.

The constellations studied in the previous chapter have at least 7 planes. Performing a direct insertion would require a launch per plane, resulting in a deployment time of at least 21 months. This is considered a long time, especially given the seven-year lifetime per satellite. Therefore, a direct insertion is not preferred, except when the number of satellites per plane does not allow for multiple planes to be launched.

7

In the optimisation process, an algorithm is created using dynamic programming. This algorithm aims to find the optimal launching strategy, assuming a launcher can only launch complete planes. The algorithm's objectives in order of priority are:

- Minimise the total number of launches.
- Minimise total unused capacity.
- Under a tie, prefer A64 over A62.

The algorithm is explained in more detail in Appendix D. The algorithm does not directly deal with time, but with the allocation of satellites to planes and launches. The time is then computed based on the manufacturing and launching cadence, as well as drifting and deployment. The last objective makes sure that the more capable launcher is used when possible, given that it is generally more time-effective. For example, when launching four planes over two launches, it is faster to launch three planes in the first launch and one in the second using an Ariane 64, rather than launching two planes in each launch using an Ariane 62 because the drifting is faster and the second launch is a direct insertion.

When studying the cadence of both manufacturing and launching, it is seen that the manufacturing cadence is higher than the launching cadence. Table 7.11 says that a maximum of 49 satellites can be launched in a single Ariane 64 launch. That would take approximately 1.5 months to manufacture, which is lower than the three months between launches. Therefore, the manufacturing cadence is not a limiting factor in this analysis.

INDIRECT INSERTION METHOD CALCULATIONS

The indirect insertion method has several phases: launch, drifting, and orbit raising. The launch phase is performed by the launcher, taking the satellites to the "drift altitude". At this point, the satellites separate from the launch vehicle and start drifting in RAAN due to the J_2 effect. The launch is assumed to deliver several planes at the right inclination at Ω_0, corresponding to the first plane's RAAN. At this stage, the first plane raises its orbit to the operational altitude, while the remaining planes drift in RAAN. When a plane is sufficiently separated in RAAN, it raises its orbit to the operational altitude. This process is repeated until all planes are deployed.

A Walker constellation with P planes will need a separation of $360/P$ degrees in RAAN for a Walker Delta and $180/P$ degrees for a Walker Star. The time required to drift this amount of degrees can be computed using Equation 7.17, where $\dot{\Omega}$ is the rate of change of RAAN due to the J_2 effect, computed using Equation 3.11, for the drift and target altitudes. $\Delta\Omega$ is the required separation in RAAN. Even though the rates change as the orbit is raised, given that both planes perform the same manoeuvres at a different time, the overall time cancels out the differences. Therefore, the relevant rates are only the drift and nominal altitude. A full proof can be found in Appendix D.

7

$$\Delta t_{drift} = \frac{\Delta\Omega}{\dot{\Omega}_{alt,nom} - \dot{\Omega}_{alt,drift}} \tag{7.17}$$

Equation 7.17 can be used for two or more planes by simply adding the required separations with respect to the first plane. For example, for a 3-plane deployment of a total of 10 planes in Walker star requires a separation of $180/10 = 18°$ for the second plane, and $36°$ for the third one. Therefore, the total time required to deploy these three planes is the time required to drift 36 degrees.

During the drifting stage, the satellite is at a lower altitude and therefore requires station-keeping manoeuvres to maintain its orbit. The Δv required for this is computed using Equation 7.16, and scaled to the time spent in drift. Furthermore, when the satellite raises its orbit to the operational altitude, it requires a transfer manoeuvre. The manoeuvre is computed assuming a continuous low-thrust manoeuvre, using the electric thruster defined earlier. This manoeuvre is more realistic than a Hohmann transfer, given the low-thrust nature of the propulsion system. It assumes a continuous spiral thrust, slowly increasing the satellite's altitude. Bettinger and Black (2014) [19] shows that the Δv required for such a manoeuvre can be computed using Equation 7.18, where a_0 is the initial orbit radius, and a_1 is the final orbit radius. The equation shows that as the number of orbits (N) increases, the Δv approaches a constant value.

$$\lim_{N\to\infty} \Delta v_{Hohmann} = \Delta v_{continuous} = \left(\frac{\mu}{a_0}\right)^{1/2}\left[1-\left(\frac{a_1}{a_0}\right)^{1/2}\right] \tag{7.18}$$

The equation computed is practically identical to the Hohmann transfer, with differences smaller than 1 m/s for the study cases. Nevertheless, there is a time component to consider, as well as the stationkeeping during the transfer. The time required to perform the transfer is computed starting from the basic Gaussian Planetary Equations, which give the Keplerian rates of change as a function of the perturbing accelerations.
The change in semi-major axis is computed using Equation 7.20, where a is the semi-major axis, e the eccentricity, n the mean motion, and f the true anomaly. Other Keplerian elements are not relevant for the analysis, and small deviations are assumed to be corrected by stationkeeping.
The perturbing acceleration in the tangential direction (F_θ) is computed as the thrust divided by the mass of the satellite, assumed constant during the transfer. There is no acceleration in the radial direction ($F_r = 0$). The equation assumes a circular orbit ($e = 0$), which is valid for this analysis given the long transfer period. The angular momentum is given by

$$h = \sqrt{(1-e^2)\mu a} = \sqrt{\mu a}. \tag{7.19}$$

Starting from the Gaussian equation for the semi-major axis:

$$\frac{da}{dt} = a\cdot\frac{2h}{\mu(1-e^2)}\left[e\sin f\, F_r + (1+e\cos f)\, F_\theta\right], \tag{7.20}$$

for $e = 0$ and $F_r = 0$ this reduces to

$$\frac{da}{dt} = a\cdot\frac{2h}{\mu}F_\theta. \tag{7.21}$$

Substituting $h = \sqrt{\mu a}$ gives

$$\frac{da}{dt} = \frac{2a^{3/2}}{\sqrt{\mu}}F_\theta. \tag{7.22}$$

Rearranging and integrating over the transfer time:

$$\int_0^t dt = \frac{\sqrt{\mu}}{2F_\theta}\int_{a_0}^{a_1} a^{-3/2}\, da, \tag{7.23}$$

which yields

$$\Delta t = \frac{\sqrt{\mu}}{F_\theta}\left(\frac{1}{\sqrt{a_0}} - \frac{1}{\sqrt{a_1}}\right). \tag{7.24}$$

Finally, substituting $F_\theta = \frac{T}{m}$:

$$\Delta t_{transfer} = \frac{m\sqrt{\mu}}{T}\left(\frac{1}{\sqrt{a_0}} - \frac{1}{\sqrt{a_1}}\right). \tag{7.25}$$

To use this transfer time, the satellite's thrusting capabilities need to be defined. Given that the satellite uses an electric propulsion system, there is a possibility that it may not be thrusting during eclipse periods if the batteries cannot handle the power requirements. The approximate eclipse time is computed by taking the radius of the Earth and assuming that if the orbit is behind the Earth, it is in eclipse. This results in an eclipse for 30% to 37% of the orbit, depending on the altitude (500-1500 km), suggesting it is not negligible. The thruster requires 350 W to operate, as explained in subsection 7.1.3. From a back-of-the-envelope analysis, this would require a battery between 3.8 and 5.0 kg, depending on the energy density of the battery. Furthermore, the satellite already has a payload budget of at least 500 W, which is more than enough to power the thruster during eclipse, especially since during eclipse, the payload is not operating. Therefore, it is assumed that the satellite can thrust continuously during the entire orbit.

Using the time computed, the stationkeeping during the transfer can be approximated. Equation 7.25 can be used to define the time the satellite spent at each altitude. Figure 7.3 shows the transfer from a drift altitude of 400 km to an operational altitude of 1200 km over a month. The orange line shows a simplification assuming the orbit raising altitude is linearly increasing. The maximum difference between the accurate and simplified model is 15 km or ~ 2%, which is negligible in the context of stationkeeping. Therefore, the linear model is used to compute the altitude for the stationkeeping during the transfer.

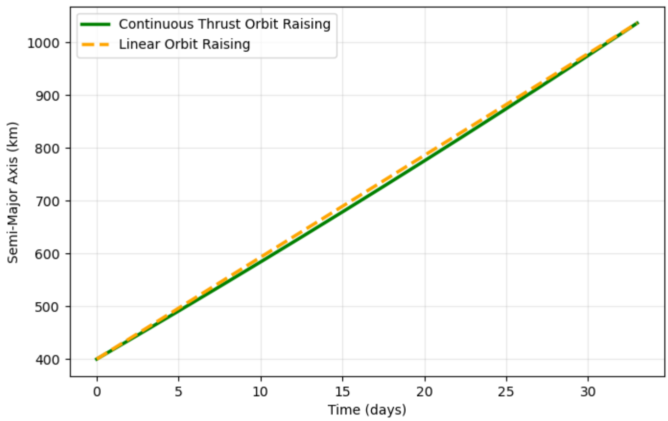

Figure 7.3: Orbit Raising Altitude Profile

From Equation 7.16 it is shown that the delta V required for stationkeeping can be modelled as an exponential decay function of the form:

$$\Delta v_{SK}(h) = Ae^{Bh} + C, \tag{7.26}$$

where A, B and C are constants. This should be in the same time units as the altitude change. Furthermore, the simplified orbit raising altitude profile is a linear function of time:

$$h(t) = h_{drift} + \frac{(h_{target} - h_{drift})}{\Delta t_{transfer}} t, \tag{7.27}$$

where h_{drift} is the initial drift altitude, h_{target} is the final target altitude, and $\Delta t_{transfer}$ is the total transfer time. By combining both equations and integrating over the transfer time, the total Δv required for stationkeeping during the transfer can be computed:

$$\Delta v_{SK,transfer} = \left[\frac{A}{B \cdot (h_{target} - h_{drift})} \cdot \left(e^{B \cdot h_{target}} - e^{B \cdot h_{drift}} \right) + C \right] \cdot \Delta t_{transfer} \tag{7.28}$$

The total time required to deploy a certain number of planes is the sum of the individual components. The total time is given by Equation 7.29, where N_{launch} is the number of launches required, Δt_{launch} is the time between launches, $\Delta t_{drift,i}$ is the drift time for the i-th plane, and $\Delta t_{transfer,i}$ is the transfer time for the i-th plane. In reality, only the last launch is composed of the drift and transfer time, as the previous launches can be performed while the first planes are drifting or transferring.

$$\Delta t_{total} = N_{launch} \cdot \Delta t_{launch} + \Delta t_{drift,N} + \Delta t_{transfer,N} \tag{7.29}$$

The total Δv per satellite of this particular stage is the sum of the stationkeeping during drift, the transfer Δv, and the stationkeeping during transfer, all multiplied by their respective margins. The total Δv is given by Equation 7.30.

$$\Delta v_{deployment} = \Delta v_{SK,drift} + \Delta v_{continuous} + \Delta v_{SK,transfer} \tag{7.30}$$

7

DRIFT ALTITUDE SELECTION

The previous formulas explain the indirect insertion method in terms of deployment time and Δv required. However, these results are a direct function of the drift altitude chosen. A lower drift altitude will result in a faster deployment due to the higher J_2 effect, but it will also require more Δv for stationkeeping and orbit raising. Therefore, a trade-off analysis is required to find the optimal drift altitude.

In order to make a decision, several drift altitudes are considered for all scenarios. The minimum allowable drift altitude is 400 km, as lower altitudes would require too much stationkeeping. The maximum allowable drift altitude is set at 90% of the operational altitude, as higher altitudes would not provide a significant J_2 effect and would take too long to deploy.

The results of the analysis are shown in Figure 7.4, where the deployment time is plotted against the total Δv required for deployment for the different altitudes. Each point represents a different drift altitude, varying by 50 km. The plot shows a bold line, the scenario where two planes are deployed per launch, and a dotted line, where three planes are deployed per launch. The direct insertion method is not shown, since it is represented by a zero Δv and effectively no deployment time.

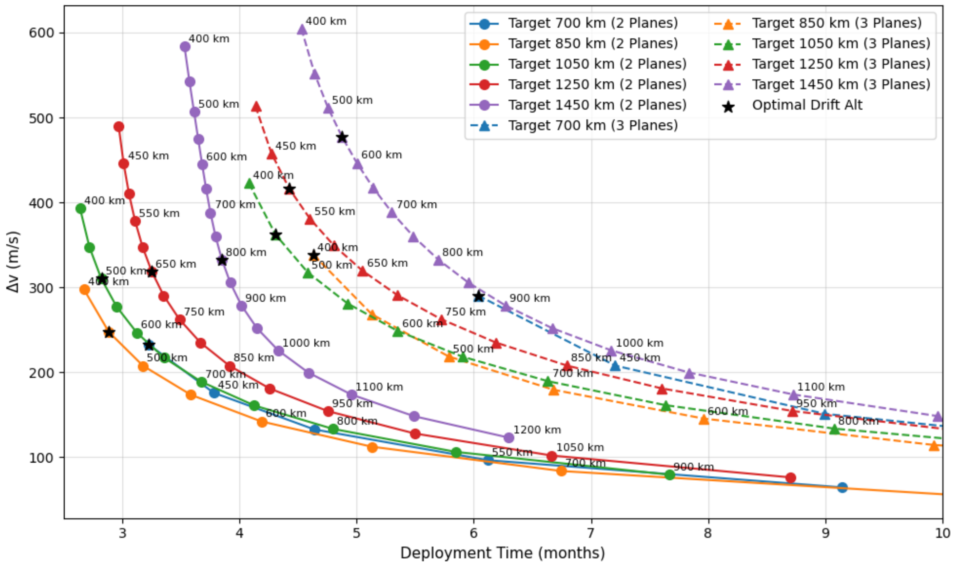

Figure 7.4: Deployment Time vs Δv for Different Drift Altitudes

The plot shows that the fastest deployment time is neither the lowest nor the highest drift altitude. It is in between, where the J_2 effect is still significant, but the transfer time is not too high. As well, the deployment time of three planes per launch is higher than that of two planes per launch, given the longer drift times required. However, it is more cost/time efficient from a global perspective, as it requires fewer launches.

For example, for an operational altitude of 1450 km and a drift altitude of 400 km, the best two-plane deployment time is 3.5 months, while the best three-plane deployment time is 4.5 months. If there are six planes in the constellation, the two-plane deployment would require three launches, taking a total of 10.5 months. The three-plane deployment would require two launches, taking a total of 7.5 months. Therefore, the three-plane deployment is preferred. This is a simplification assuming the manufacturing and launch cadence are not limiting factors, and that three planes can fit in a launcher.

The optimal drift altitudes are marked with a black star in the plot. The values are summarised in Table 7.12. The driving factor here is the deployment time, as the Δv corresponds to a relatively small propellant mass, ranging between 0.9 and 15.5 kg. Therefore, the optimal drift altitude is chosen as the one that minimises the fuel consumption within 10% of the minimum deployment time (400 km).

For the launching strategy, there is a trade-off to be made in order to find the fastest deployment. For example, a single launch would be direct, requiring no deployment time, but it might be more convenient to have it at the start to reduce the manufacturing time required and launch as soon as possible. Something similar happens with two

Table 7.12: Optimal Drift Altitudes and Deployment Times

Case	Target Alt. (km)	Two Planes		Three Planes	
		Drift Alt. (km)	Δt_{dep} (mo)	Drift Alt. (km)	Δt_{dep} (mo)
e	1450	800	3.9	550	4.9
a	1250	650	3.3	500	4.4
c	1050	500	2.8	450	4.3
b	850	450	2.9	400	4.6
d	700	400	3.2	400	6.0

and three planes. Therefore, it is preferred to place the longer deployment and manufacturing launches (three planes) in the middle of the timeline to perform tasks in parallel, and the lower deployment and manufacturing launches on the edges. Nevertheless, for a small number of launches (<7), a brute force method can be used to find the optimal launch sequence. Finally, given that the deployment is the main driver, the lowest deployment time is chosen as the last to be launched.

Two-Shell Deployment

The strategy discussed previously can easily be extended to two or more shell constellations. In order to implement such a strategy, some decisions were made regarding the deployment. The first one is that the shells are deployed sequentially, such that the first shell is fully deployed before the second one starts. By doing this, the constellation can start operating sooner, even if it is limited to a certain latitude or a poorer coverage. Furthermore, there is no preference for the order of deployment of the shells, as they are assumed to be independent. Nevertheless, given the manufacturing and deployment times, a shell might be preferred to be launched first.

In the optimisation, both shells' timelines are optimised independently and combined afterwards. The combination occurs by assessing when the manufacturing and launch of the second shell can start, given the manufacturing cadence and the launch cadence. The manufacturing of the second shell can start as soon as the manufacturing of the first shell is completed. The launch of the second shell can start as soon as there is a free launch slot, given the launches already scheduled for the first shell. The most limiting of both factors is taken as the start of the second shell, which, for our scenario, is always the launch cadency.

Finally, given the large differences between inclinations, a launcher may only carry satellites for one shell, not both. This is a representation of reality, where a modification of inclination would require very high amounts of Δv, making it unfeasible. As a back-of-the-envelope analysis, changing the inclination by 40° at 700 km altitude requires approximately 5000 m/s of Δv.

7.4. Space Debris Analysis

Space debris is a growing concern in the space industry. The current trend of constellation deployments in LEO is worsening the issue, increasing the risk of Kessler syndrome

[87]. Therefore, it is essential to consider the risk of collision with existing debris when designing a constellation. The risk is generally higher at lower altitudes, where the density of debris is greater.

In order to analyse this, the Meteoroid and Space Debris Terrestrial Environment Reference (MASTER) by European Space Agency (2024)[50] can be used to estimate the debris environment. Figure 7.5 shows the debris density as a function of altitude. It shows all particles larger than 1 cm, which are the most relevant for collision risk [47]. The analysis is done over historical data as of November 1st, 2024.

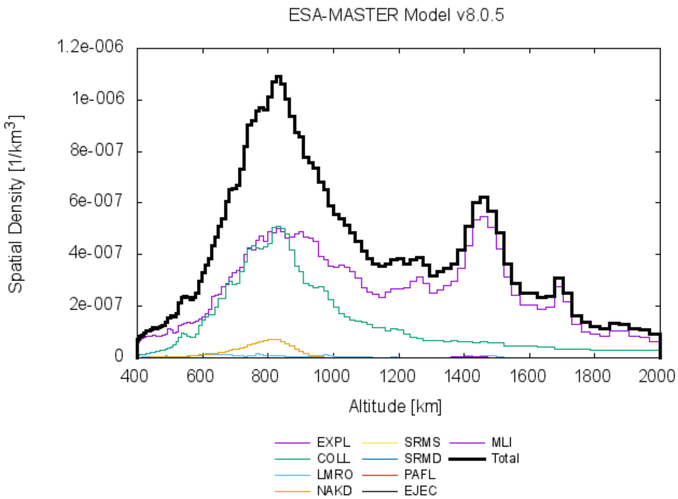

Figure 7.5: Debris Density vs Altitude

The figure shows two specific areas of interest. The first one is the peak around 850 km, which is caused mostly by collisions and explosions. The second one is the increasing trend at 1500 km, which is caused once again by explosions. Nevertheless, the spatial density and variation between altitudes are small.

Similarly, Figure 7.6 shows the spatial debris density as a function of altitude and inclination. The plot shows that the debris density is higher at high inclinations, but all within a range of 5×10^{-7} to 4×10^{-6} particles per cubic km.

Taking these results as input, the Assessment of Risk Event Statistics (ARES) by European Space Agency (2024)[48] can be used to estimate the collision risk, along with any required mitigation measures. The tool is used for the same altitudes as presented in the EOL strategy, and for a high inclination of 84°, as it has been shown to have the highest risk.

The software works with the parameters introduced previously and is concerned only

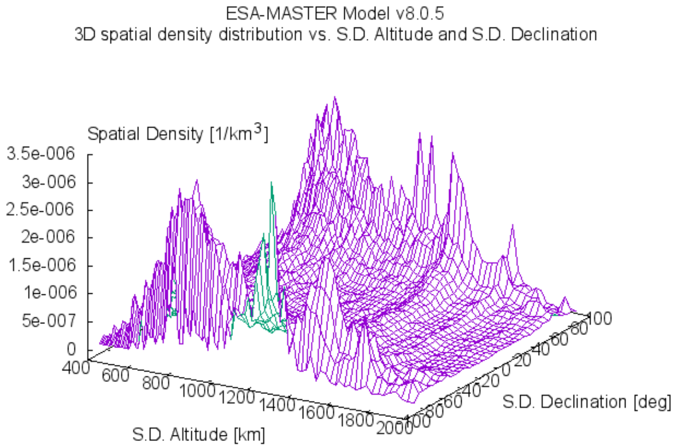

Figure 7.6: Debris Density vs Altitude and Inclination

with objects capable of damage (>1 cm) and smaller than 100 m. The software propagates the satellite using a beginning date of August 1st, 2024, at the different altitudes of the cases presented in previous chapters. The spacecraft radius is computed from the reference average area of 6 m and assuming a circle of similar area, resulting in a radius of ~ 1.4 m.

Following Agency (2023)[7], a satellite shall perform a collision avoidance manoeuvre (CAM) when the predicted collision probability exceeds 10^{-4}. After manoeuvring, this risk shall be reduced to below 10^{-6}. The results are shown in Table 7.13.

Table 7.13: CAMs and Δv for Different Altitudes

Alt (km)	**#man/yr**	**Δv (m/s)**
1450	3.22×10^{-2}	4.42×10^{-3}
1250	1.69×10^{-2}	3.57×10^{-3}
1050	4.37×10^{-2}	7.96×10^{-3}
850	1.27×10^{-1}	2.37×10^{-2}
700	1.25×10^{-1}	2.80×10^{-2}

The number of manoeuvres per year is minimal per satellite, but given the constellation size, they can add up. The Δv per manoeuvre is also minimal, being in the order of mm/s. The values help predict how much Δv is required for the mission, and how many CAMs will be performed per constellation. More importantly, it is of interest to reduce the number of manoeuvres to avoid interruptions in service.

One final thing to have in mind is the future debris environment and the upcoming LEO constellations. Some constellations have already been highlighted in Table 2.3.3. Table 7.14 shows the number and planned altitude of some of the upcoming constellations that are within the studied ranges (700-1500 km). This places an additional risk to cases ‘a’ at 1250 km and ‘b’ at 850 km, as they are within the altitudes of the new constellations.

Table 7.14: Upcoming LEO Constellations

Constellation	#Sats	Alt (km)	Reference
Qianfan	12000	800	[83]
Guowang	12992	600/1145	[30]
OneWeb	648	1200	[58]

7.5. MISSION COST

The main aspect of a feasibility analysis is related to the mission cost. As shown above, there are some general constraints, maybe due to radiation, debris, or deployment time. However, these constraints can usually be surpassed with a higher budget. Therefore, usually cost is the main constraint in a mission and a great indicator of feasibility.

The mission cost is divided into several parts. Different authors divide it in different ways. Wertz, Everett, and Puschell (2011)[174] defined the division over the space segment cost, conformed by the research and development (R&D), software, first unit, and follow-on units. Then, they include the launch segment cost, followed by the ground segment cost, to finally conclude with the operations and maintenance cost.

The R&D cost is generally a fixed cost, divided over the total number of satellites. This is complex and is not taken into account in this analysis. The constellation design will have an effect on the satellite cost, and through the number of satellites, it will affect the total manufacturing and launch costs. Another aspect related to the constellation design is the ground segment cost, as a larger constellation will potentially require more ground stations. However, this is not considered in this analysis.

Before diving into the cost analysis, the Producer Price Index (PPI) must be explained. The different models developed throughout the years, as well as the expected cost of launchers like Ariane 6, are subject to the year they were developed. Therefore, in order to compare costs from different years, the PPI is used to adjust the costs to a common year. The PPI is a measure of the "average change over time in the selling prices received by domestic producers for their output" [96]. To specifically adjust the costs, the PPI for the "Aerospace Product and Parts Manufacturing" sector is used (PCU3364133641). The objective is to bring all costs to 2025 USD. The database used averages the PPI values over the months to create a more stable reference point for cost comparisons.

The Small Satellite Cost Model (SSCM), developed by The Aerospace Corporation [105], provides a way to estimate the cost of small satellites of up to 1000 kg. The model was initially developed in 1998 and has been updated several times since then. The version used in this analysis is from 2014, and it predicts the cost of a satellite based on different parameters. This model has been extracted from Karatas and Ince (2016)[86], who assumed nominal values for most parameters and left the satellite cost as a function of mass. The resulting equation is shown in Equation 7.31.

$$Cost_{TFU} = -1.2 \times 10^{-8} \cdot m^3 - 4 \times 10^{-5} \cdot m^2 + 0.096 \cdot m + 26 \tag{7.31}$$

where $Cost_{TFU}$ is the cost in million USD (M$ USD), and m is the mass in kg. Furthermore, using the PPI, the cost is adjusted to 2025 USD by multiplying it by a factor of 1.2688. Using values from previous sections, the cost of the first unit would range between 56.3 M$ USD for the lightest satellite (187.6 kg), and 66.9 M$ USD for the heaviest one (294.3 kg).

The previous result gives the cost for the theoretical first unit (TFU). However, this cost is generally much lower when produced in series. Wang and Zhang (2021)[170] proposes a learning curve for mass-produced satellites. This learning curve has a positive effect on the satellite's cost due to familiarity with the design or other types of mass customised production. The learning curve is defined by Equation 7.32, where TFU is the theoretical first unit cost, N is the number of units produced, and S is the learning curve factor. For more than 50 units, the factor can be as low as 0.85 [170]. Given the constellation size, this value is used.

$$Cost_{constellation} = TFU \cdot N^{1+\log_2(S)} \tag{7.32}$$

Using this equation, the cost of the satellite reduces drastically. For example, assuming a constellation of 150 satellites, the cost per satellite ranges between 17.4 and 20.7 M$ USD, depending on the mass. These numbers match the expected cost for a size mini-satellite constellation, as shown in FrontierSI (2024)[65]. They discuss that satellites between 100-500 kg are expected to have a cost of 15-40 M$ USD.

Now that the satellite manufacturing cost has been computed, the launch cost must be added. This would account for the total manufacturing and deployment cost, ignoring operation. The launch cost is generally discussed as a function of the payload mass. Nevertheless, that is not reliable for most missions. When developing a deep space mission, some extra kilograms will have a large effect on the cost, as the launcher will need to bring more fuel to reach the required orbit. However, for LEO missions, the launchers have a fixed cost, and they have constraints on the total mass and volume they can bring. Therefore, the launch cost is assumed to be fixed, as long as the mass and volume constraints are not exceeded.

The Ariane 6 launch cost is not clear. Given the new nature of the launcher, there is not much information available. Nevertheless, some sources have been found stating the expected cost. Smith (2018)[152] wrote an article discussing the targeted costs for Ariane 62 and 64. They mention a cost of 82 M$ US for the Ariane 62, and 134 M$ US for the Ariane 64. Last year, Ariane 6 had its inaugural launch [12] and since then it has started deploying the Ariane 62 and expects to start launching the Ariane 64 towards the end of 2025. "Next Spaceflight", a website used for tracking launches and other space-related activities, provided some information on the launch cost of Ariane 62 and 64. According to them, the CSO-3, a French military satellite, was launched using an Ariane 62 for a cost of 88 M$ USD [118]. Furthermore, some planned launches for Project Kuiper, Amazon's satellite internet constellation, are planned to be launched using Ariane 64 for a cost of 106 M$ USD per launch towards the end of the year [119]. These values are used for the analysis.

The total cost of the constellation used in the feasibility analysis is composed of the manufacturing cost of all satellites and the launch cost of all launches required. The total cost is given by Equation 7.33, where N is the number of satellites, $Cost_{sat}$ is the cost per satellite, N_{launch} is the number of launches required, and $Cost_{A62}$ and $Cost_{A64}$ is the cost per launch.

$$Cost_{total} = Cost_{constellation} + N_{launch,A62} \cdot Cost_{A62} + N_{launch,A64} \cdot Cost_{A64} \tag{7.33}$$

7.6. ROBUSTNESS AND FAILURE

One more aspect to consider is the robustness of the constellation against failure. This is important, as the constellation must be able to provide the required service even in the case of a satellite failure. This is a complex topic, where several aspects can be considered.

Cornara et al. (1999)[35] suggests three options: overpopulation by one or two satellites per plane, spare satellites in parking orbits, or on the ground. The first option is the simplest, as it does not require any extra infrastructure. However, it incurs a higher cost, as more satellites are required. The second option is more complex, as it requires extra infrastructure and the ability to manoeuvre the satellites from the parking orbit to the operational orbit. However, it is more cost-effective, as fewer satellites are required. The third option would take the longest time, and potentially the most expensive, as a new satellite would need to be manufactured and launched.

Galileo works with two spare satellites per plane, adding a total of six spare satellites [46]. These satellites are also transmitting and have the possibility of being repositioned in case of a failure in a matter of days.

The selection of spare satellites is complex and requires a proper assessment of the reliability of the constellation. It is expected that the LEO-PNT constellation has a lower reliability than Galileo, given the lower cost and New Space approach. Space Enthusiast (2023)[153] discusses the failure rate of OneWeb and Starlink. OneWeb has had a cumulative failure rate of 0.79% over its first 634 satellites. Starlink, on the other hand, has had a cumulative failure rate of 7% over its first 4789 satellites. This can be assumed to be equivalent to the individual probability of failure of a satellite over its lifetime. Both scenarios are considered for the analysis.

In this section, two basic analyses are done. The first one studies the probability of failure of n satellites throughout the mission's lifetime. The second one evaluates the impact of these failures on the overall performance of the constellation through a Monte Carlo simulation.

For the first aspect, assume that each satellite has an independent lifetime probability p of failing (either at launch, during deployment, or in operation). Let T denote the total number of satellites in the constellation, and k the number of failed satellites. The number of failures k follows the binomial probability formula:

$$P(N = k) = \binom{T}{k} p^k (1-p)^{T-k}, \tag{7.34}$$

where N is the random variable representing the number of failed satellites.
The probability that at least k satellites fail is given by:

$$P(N \geq k) = 1 - \sum_{n=0}^{k-1} \binom{T}{n} p^n (1-p)^{T-n}. \tag{7.35}$$

The expected number of failures is:

$$\mathbb{E}[N] = T p. \tag{7.36}$$

The expected number of failures for different constellation sizes is shown in Table 7.15. It shows that under the assumed failure rate, there will most likely be failures in all constellation sizes. When running Starlink's failure rate, the expected number of failures increases to 7 and 14.9 for 100 and 200 satellites, respectively. Under those scenarios, the probability of three satellites becomes almost certain.

7

Table 7.15: Expected Number of Failures and Probabilities for Different Constellation Sizes with $p = 0.79\%$ over 7 years

T	E[N]	P(N≥1)	P(N≥2)	P(N≥3)
100	0.8	54.7%	18.7%	4.5%
150	1.2	69.6%	33.2%	11.7%
200	1.6	79.5%	46.9%	21.1%

The second analysis is the Monte Carlo. The simulation simply propagates the constellation over its repeat period, assuming a certain satellite(s) has failed. Three scenarios are considered, failures between 1 and 3 satellites. The satellite(s) that fail are chosen randomly, removed from the simulation, and the performance is computed. The performance considered here are the mean, max 95th percentile, and availability (<6) GDOP.

For the single satellite failure, all satellites are considered to fail one at a time, and the performance is computed. For the two- and three-satellite failures, 1000 random combinations are considered. These are equivalent to testing 10% and 0.1% of all possible combinations, respectively. Even if the sample size is small, it can already provide some insight into the robustness of the constellation. The number of runs is limited by the computational power available. Finally, not all scenarios are tested for this analysis; only the final set of constellations is considered.

Finally, to compare them, a new metric is defined, which is an expected performance loss (EPL). It is computed by multiplying the probability of having exactly a certain number of failures by the performance loss when that number of failures occurs. Since the performance loss analysis was only defined for up to three failures, and these are the cases with the highest probabilities of occurring, the expected performance loss is only computed for these cases. Equation 7.37 shows the equation used, where $P(n)$ is the probability of having n failures, and $L(n)$ is the performance loss when n failures occur.

$$EPL = \sum_{n=1}^{3} P(N = n) \cdot L(n) \tag{7.37}$$

The expected performance loss shows what is the expected percentage degradation in the maximum 95th percentile GDOP over the constellation's lifetime. This is a simplification, as in reality, the sum should be performed over all possible numbers of failures. However, the probability of having more than three failures is generally less than 10%, and it can be assumed that even if that happens, the probability of all happening at the same time is very low. Therefore, the expected performance loss is a clear indicator of the robustness of the constellation.

7.7. ISL AND GROUND STATION ANALYSIS

The final aspect to consider in the feasibility analysis is the Inter-satellite links (ISL) and the Telemetry, Tracking, and Command (TT&C) aspects of the constellation. As explained in chapter 2, the ISL are a potential solution for several aspects of the mission. They can help reduce the total number of ground stations required, reduce the reliance on other systems such as Galileo or GPS, and help reduce the latency of the system. ISLs can improve the POD and timing of the system [65].

On the other hand, TT&C is essential for the operation of the constellation. The ground stations are used to upload commands, download telemetry, and perform ranging and Doppler measurements. The ground stations are essential for navigation constellations, as they provide the necessary data to compute the orbits of the satellites, along with any corrections required.

This section aims to provide a basic analysis of the ISL and TT&C aspects of the constellation. It does not perform a full design of the system, but rather assesses the feasibility and potential limitations of the constellation in this aspect.

The ISL stems from the idea of having a network of satellites that can communicate with each other. This can be done using different technologies, such as RF or optical links. Based on a previous section, for this scenario, optical links are considered, given their high accuracy and data rate. The main limitation of optical links is the pointing accuracy required, which can be challenging to achieve. Nevertheless, this has already been achieved by several missions, such as Project Kuiper by Amazon [9], or Starlink by SpaceX [154]. Even for the considered terminal, the TESAT Scot80 has already been used in at least 48 missions [146].

When discussing Inter-satellite links, there are two main types: intra-plane and inter-plane links. According to Chaudhry and Yanikomeroglu (2021)[28], intra-plane links are used to connect satellites within the same orbital plane, following the same path. Even though the satellites could contact with any other visible satellite in the same plane, the most common configuration is to connect with the two closest satellites, one ahead and one behind. This creates a ring topology, which is robust and easy to manage.

The second type is inter-plane links, which are used to connect satellites in different orbital planes. This is more complex, as the relative motion between the satellites is more significant. The most common configuration is to connect with the closest satellite in the adjacent plane. This creates a mesh topology, which is more complex, but allows for more flexibility and the possibility to contact any satellite in the constellation from one ground station [28].

Furthermore, ISL can also be categorised based on its temporal connection, which can be permanent or temporary. Permanent connections are always active, while temporary connections are only active when the connection can be made, or when required [28].

For a LEO-PNT system, the ISL requirements can vary depending on the objectives. For a robust system, permanent links are preferred, as they allow for continuous communication between satellites. Furthermore, to reduce the number of ground stations required, inter-plane links could provide a simplified architecture. Nevertheless, this increases the complexity of the system, as well as its latency. Therefore, at this stage of the analysis, the possibility for intra- and inter-plane links is studied, followed by a simple ground station analysis.

7.7.1. ISL Analysis

For this analysis, some more information on the ISL terminal is required. As mentioned, the TESAT Scot80 is used as a reference. This terminal allows for a maximum range of 8000 km, and the Field of Rotation (FoR) is $\pm 160°$ in azimuth and $\pm 55°$ in elevation [146]. The mission considers two terminals per satellite, allowing for two simultaneous connections. Furthermore, it is assumed that the terminals are placed on the walls of the satellite, at 0° and 180° with respect to the velocity vector. Because they are placed on the walls, they are not able to rotate freely in the azimuth direction. A limiting rotation of $\pm 80°$ is assumed.

In order to define the azimuth and elevation angles required for the ISL, the RSW frame is used. The RSW frame is a satellite coordinate system, sometimes referred to as the Gaussian coordinate system. Based on Vallado (2013)[168], the RSW frame is defined as follows:

- R (Radial): Points from the centre of the Earth to the satellite, in the direction of the position vector.
- S (Along-track): Points in the direction of the satellite's velocity vector, perpendicular to R. It does not need to be exactly aligned with the velocity vector, as it is defined as the cross product of W and R.
- W (Cross-track): Completes the right-handed coordinate system, pointing out of the orbital plane. Computed as the cross product of the position and velocity vectors.

The exact conversion from ECI to RSW can be found in Equation 7.38, where **r** and **v** are the position and velocity vectors in ECI, respectively. The transformation matrix is composed of the unit vectors of the RSW frame.

$$\begin{bmatrix} \hat{r} \\ \hat{s} \\ \hat{w} \end{bmatrix} = \begin{bmatrix} \dfrac{\mathbf{r}}{\|\mathbf{r}\|} \\ \hat{w} \times \hat{r} \\ \dfrac{\mathbf{r} \times \mathbf{v}}{\|\mathbf{r} \times \mathbf{v}\|} \end{bmatrix} \tag{7.38}$$

7

In this frame, the azimuth and elevation angles can be computed using Equation 7.40, where x_{RSW}, y_{RSW}, and z_{RSW} are the coordinates of the target satellite in the RSW frame of the observing satellite. The azimuth is defined as the angle made by the projection of the target satellite in the S-W plane, while the elevation is defined as the angle made by the target satellite with respect to the S-W plane.

$$az = \text{atan2}(z_{RSW}, y_{RSW}) \tag{7.39}$$

$$el = \text{atan2}(x_{RSW}, \sqrt{y_{RSW}^2 + z_{RSW}^2}) \tag{7.40}$$

Using these equations, the azimuth and elevation angles required for the ISL can be computed. The analysis is done by creating a set of nine satellites distributed in three planes, with three satellites per plane. Thanks to Walker's symmetry, this configuration is enough to represent the entire shell/constellation. The objective is to compute the azimuth and elevation angles required for all possible ISL combinations as seen by the central satellite in the middle plane.

Figure 7.7 shows an example of a shell with their corresponding anomaly and RAAN distribution. It is based on a Walker Star constellation with configuration 80°: 150/10/2 at 1450 km. The central satellite is marked at (0,0), intra-plane connections are marked with (0,1) and (0,-1), and inter-plane connections are the remaining ones.

For simplicity, it is assumed that the ISL terminals are placed in the +y (0°) and -y (180°) directions of the satellite in an RSW frame, which correspond to the along-track direction

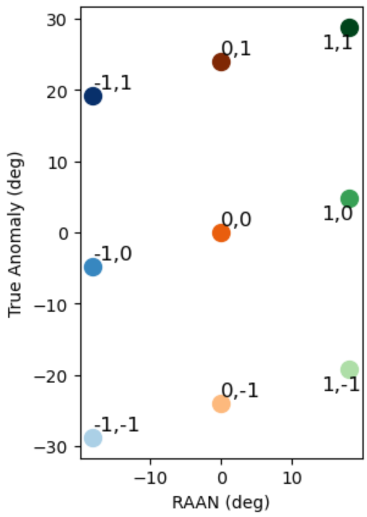

Figure 7.7: Sample Satellite Geometry for ISL Analysis, including a phasing parameter of 2

and perpendicular to the solar arrays. Therefore, the azimuth angle is limited to ±80°, as explained before. The elevation angle is limited to ±55°. Furthermore, the maximum range is set to 8000 km.

INTRA-PLANE CONNECTIONS

An intra-plane connection is the simplest one to achieve. The relative motion between satellites is minimal, as they follow the same path. The position of the target satellite in the RSW frame is therefore of the form $(x_t, y_t, 0)$, where z_t is zero, as both satellites are in the same plane. These coordinates stay constant for a circular orbit, leading to a constant azimuth with value 0°/180°, and a constant elevation angle as computed by Equation 7.40.

The limiting factor for the intra-plane connection is the distance between satellites. The maximum allowable distance is 8000 km, as per the TESAT Scot80 specifications. This distance can be computed using Equation 7.41, where a is the semi-major axis, and $\Delta\theta$ is the difference in true anomaly between the two satellites. The equation assumes a circular orbit.

$$d = 2 \cdot a \cdot \sin\left(\frac{\Delta\theta}{2}\right) \tag{7.41}$$

This equation can be rearranged to compute the maximum allowable difference in true anomaly, and therefore, the minimum number of satellites per plane. The altitude of the constellation has a direct effect on the minimum number of satellites required, as higher altitudes lead to smaller allowable differences in true anomaly. Under the limiting case in this study of an altitude of 1450 km, the minimum number of satellites per plane is 6.

The corresponding elevation is constant at $-30°$.

As long as the number of satellites per plane is higher than the minimum required, the intra-plane connection is always feasible. The elevation angle will be closer to zero as the number of satellites increases, the range will also be shorter, and the azimuth will always be zero. Therefore, the intra-plane connection is not a limiting factor for the constellation design.

INTER-PLANE CONNECTIONS

Inter-plane connections are more complex, as the relative motion between satellites is more significant. The position of the target satellite in the RSW frame is therefore of the form (x_t, y_t, z_t), where z_t is non-zero, as both satellites are in different planes. This coordinates change over time, leading to a varying azimuth and elevation angle, as computed by Equation 7.40. The satellites shown in Figure 7.7 have been propagated, and their positions in the RSW frame have been computed over time with respect to the central satellite. The planar movement of the satellites in the S-W plane is shown in Figure 7.8, where the central satellite is at the origin.

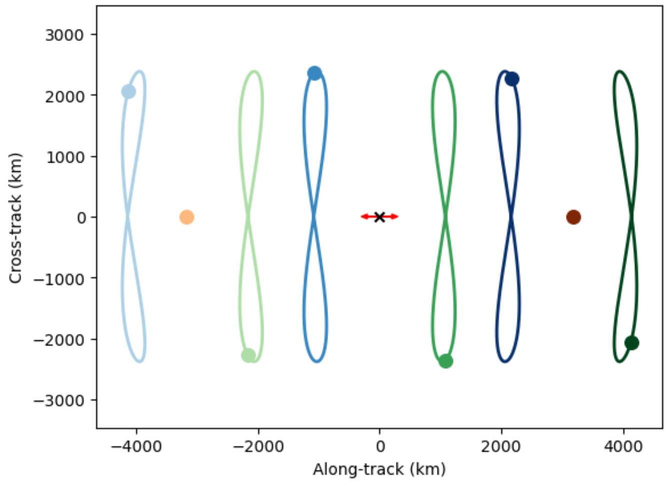

Figure 7.8: Planar Movement of Satellites in S-W Plane with respect to Central Satellite

A typical behaviour can be observed. The satellites move, creating an analemma shape, caused by the relative phase and inclination of the orbits. The relative phase is the true anomaly difference between the two planes at the ascending node of the reference plane. The relative inclination is the angle at the crossing of the two planes [173]. These parameters can also be computed using the RAAN and inclination of both planes, following Equation 7.42 and Equation 7.43, where i is the inclination of both planes, $\Delta\Omega$ is the difference in RAAN, ΔT is the time difference between the two satellites crossing their ascending nodes, n is the mean motion, and $\Delta\phi$ is the anomaly range from the ascending node to the crossing of the two planes, given by the orbit further along the RAAN.

$$\cos(i_R) = \cos^2 i + \sin^2 i \cdot \cos(\Delta\Omega) \tag{7.42}$$

$$\phi_R = \Delta T \cdot n + (180^\circ - 2\Delta\phi) \tag{7.43}$$

$$\text{where } \tan\Delta\phi = \frac{90^\circ - \Delta\Omega/2}{\cos i} \tag{7.44}$$

The analemma represents the movement the terminals (represented by the red arrows) need to perform in order to keep the connection. The limiting factor for inter-plane connections varies depending on the target satellite. The first potential constraint is the range. Similarly to the intra-plane connection, a maximum separation of 60° is allowed to maintain it within the 8000 km range. It translates to a minimum of 6 planes for a Walker Delta constellation, and 3 planes for a Walker Star constellation. This is a simple approximation, as the actual maximum distance is a function of the inclination and RAAN of both planes. The maximum angular separation (δ_{max}) can be computed using Equation 7.45 [173], which can then be used to compute the distance in meters using simple trigonometry.

$$\cos(\delta_{max}/2) = \cos(\phi_R/2) \cdot \cos(i_R/2) \tag{7.45}$$

The second potential constraint is the azimuth and elevation angles required. In order to improve the azimuth angle, it is preferable to reduce the relative inclination and increase the relative phase. In order to reduce the relative inclination, the inclination of the constellation or the RAAN spacing can be reduced. This directly translates to an increase in the number of planes. On the other hand, increasing the relative phasing can also be done by reducing the inclination, or by increasing the RAAN spacing or time between the crossings. The RAAN spacing is conflicting in both cases, as it improves one aspect while worsening the other. However, the time of the crossing is easily adjustable by choosing the right phasing parameter (F), changing the number of satellites per plane, or selecting an appropriate satellite. The elevation is never a limiting factor, as it stays within the ±55° limits for all cases studied.

This aspect is not optimised in the constellation design, but it is considered in the discussion analysis performed afterwards. The main takeaway is that both intra- and inter-plane connections are feasible for the constellation designed, at least when considering only the relative motion between satellites.

Yaw-steering Law

One final aspect that needs to be included is the feasibility of the ISL. Montenbruck et al. (2015) [109] studied different mathematical formulations for GNSS attitude control laws, including GPS, GLONASS, Galileo, among others. They all perform some form of a yaw-steering law, which consists of rotating the satellite around its radial axis (R) to keep the solar panels pointed towards the Sun as much as possible. This is essential for power generation. The reason for this is that the satellites' payload, such as the antennas, need to be pointed towards the Earth, constraining one degree of freedom.

As an initial assumption, the solar panels are placed on opposite sides of the satellite, aligned with the cross-track directions ($+W$ and $-W$) of the RSW frame. The panels can rotate around the cross-track (W) axis but are constrained in the other two directions. This configuration ensures that the panel normal vectors always lie within the radial-along-track (R-S) plane. To achieve optimal Sun alignment within these constraints, the satellite rotates around its radial (R) axis, attempting to orient the along-track (S) direction as close as possible to the Sun direction.

To compute the yaw-steering angle, the position of the Sun is required. The figures seen in this section correspond to a fictitious scenario where the Sun is at (-1 AU, 0, 0) in an ECI frame. This is useful to demonstrate the principle. Taking the position of the Sun ($\mathbf{r_{sun}}$) and the position of the satellite ($\mathbf{r_{sat}}$), the yaw-steering angle (ψ) can be computed. The first step is to get the yaw-steering frame, as defined by Montenbruck et al. (2015)[109], shown in Equation 7.46, where $\mathbf{e}$ is the unit vector pointing from the satellite to the Sun, and $\mathbf{r}$ is the satellite's position with respect to the Earth.

$$\begin{bmatrix} \hat{e_x} \\ \hat{e_y} \\ \hat{e_z} \end{bmatrix} = \begin{bmatrix} \hat{e_y} \times \hat{e_z} \\ \frac{\mathbf{e}\times\mathbf{r}}{||\mathbf{e}\times\mathbf{r}||} \\ -\frac{\mathbf{r}}{||\mathbf{r}||} \end{bmatrix} \tag{7.46}$$

This frame points towards the Earth (z-axis), perpendicular to the Sun and nadir directions (y-axis), and the x-axis completes the right-handed system with a positive projection towards the Sun. The frame is undetermined when the Sun is exactly in the radial direction. Using this frame, the yaw-steering angle is simply the angle made between the along-track direction (S) and the x-axis of the yaw-steering frame on the x-y plane. This is computed using Equation 7.47, where S_{RSW} is the along-track unit vector in the RSW frame, and $\hat{e_x}$ and $\hat{e_y}$ are the x-axis and y-axis of the yaw-steering frame.

$$\psi = \arctan 2(S_{RSW} \cdot \hat{e_y}, S_{RSW} \cdot \hat{e_x}) \tag{7.47}$$

This result is valid for all types of orbits. However, from here onwards, the analysis is performed purely on polar orbits. The resulting yaw-steering angle for the fictitious scenario is shown in Figure 7.9, where the satellite is at an altitude of $\sim$ 1450 km, with an inclination of 90°.

The first aspect to note is that the yaw-steering angle oscillates around ±90°. The sign indicates whether the satellite rotates clockwise (-) or counter-clockwise (+) around its radial axis. The yaw-steering angle varies with the RAAN. Orbits on the same plane but travelling in opposite directions will have opposite yaw-steering angles. The more aligned the orbital plane's normal vector is with the Earth-Sun line, the higher the oscillations.

Consider the example of 90°/270° RAAN scenarios. In these cases, the orbital plane is perpendicular to the Earth-Sun line. The satellite must rotate approximately 90° to keep the solar panels pointed towards the Sun at all times. As the RAAN moves towards 0°/180°, the yaw-steering angle increases its oscillations around the ±90° mark.

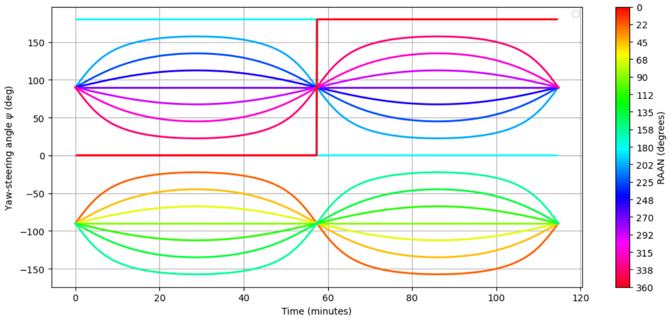

Figure 7.9: Yaw-steering Angle for 1450 km Altitude and 90° Inclination with Sun at (1 AU, 0, 0)

From this analysis, satellites at particular RAANs would need to rotate up to 180° per orbit to maintain solar panel alignment. Due to orbital plane precession, all RAANs will be encountered throughout the mission lifetime, meaning that all satellites must be designed to handle this rotation range.

From Figure 7.9, the rotation direction (clockwise or counter-clockwise) depends on the RAAN. This creates a total requirement of 180° rotation capability for the satellite. However, this requirement can be reduced by allowing the solar panels to rotate 180° around the cross-track axis (W). By rotating the panels 180°, the same pattern seen at +90° can be achieved at -90°, and vice versa.

The limiting case occurs when the orbital plane aligns with the Earth-Sun line, corresponding to 0°/180° RAAN scenarios. In this configuration, the yaw-steering angle reaches theoretical extremes of between 0° and 180°. However, with rotating panels, the satellite can maintain a fixed orientation throughout the entire orbit while keeping the panels Sun-pointed.

The key finding is that a polar orbit constellation in LEO requires a total yaw-steering capability of ±90° (180° total range) per orbit. Since the azimuth angle and yaw-steering angle operate in the same plane, the total azimuth angle required for ISL terminals is the sum of both angles. Given that the terminal is limited to ±80° in azimuth, this creates a fundamental incompatibility.

This limitation affects both inter-plane and intra-plane links. While intra-plane links are aligned with the along-track direction and nominally require no azimuth change, the yaw-steering angle can reach 90° when the plane is perpendicular to the Earth-Sun line. In such cases, the terminal would be unable to point towards the target satellite even for intra-plane connections.

What this demonstrates is that permanent ISL are not feasible with the current terminal configuration and following a yaw-steering law. Several alternatives can be considered to solve this problem:

- Relocate the terminals so they can rotate freely in azimuth (±160°), potentially enabling permanent ISLs but requiring a more complex spacecraft design.
- Relax the yaw-steering law, allowing deviations from the optimal attitude. This could enable permanent ISLs but would necessitate a detailed analysis of the control system and its impact on power generation.
- Adopt temporary ISLs, where links are only active when the yaw angle lies within the terminal limits. This simplifies the spacecraft design but requires more sophisticated network management.
- Adapt the network topology continuously, creating temporary links that adjust with orbital geometry. This could offer a quasi-permanent solution but would demand further investigation of network behaviour and management strategies.

As a secondary validation, the analysis is repeated for a more realistic orbit and with a Sun position corresponding to the 1st of January 2025. The results, shown in Appendix D, confirm the previous findings, with a maximum yaw-steering angle requirement of approximately ±90°, just at different orbital positions.

7.7.2. GROUND STATION ANALYSIS

The final analysis is performed on the ground stations. This is an extremely complex topic, and its design includes several aspects, such as the location, number, and type of ground stations. Some requirements for the ground stations could be on the latency of the system, the downlink and uplink data rates, the visibility windows, or the redundancy of the system. Especially for navigation satellites, a consistent connection to the ground segment is relevant, as it provides the necessary data for orbit determination and time synchronisation.

For this initial assessment, only the most basic aspects are considered. The visibility latitudes for some of the most common ground stations are computed, along with the number of passes per day and the average pass duration. The ground stations considered are listed in Table 7.16, along with their latitude and longitude. These locations have been chosen based on Galileo's ground stations, which stems from the idea that a European LEO-PNT system would likely use the same ground stations.

The table shows the ground stations used as uplink (ULS), telemetry, tracking, and command (TT&C), or control centres (GCC) [68]. Some stations are close to each other, such as Redu, Oberpfaffenhofen, and Fucino. However, they are all included in the analysis to provide a more comprehensive overview.

The visibility by a ground station depends on the inclination and altitude of the orbit, as well as the minimum elevation angle considered. The inclination is the main criterion. In itself, the inclination defines the maximum sub-satellite latitude achievable, given by $|i|$. However, the altitude and minimum elevation angle considered can increase this latitude. The maximum latitude visible (φ_{max}) will then be a composition of the orbit's

Table 7.16: Ground Stations Considered for Analysis [68]

Ground Station	**Latitude (deg)**	**Longitude (deg)**	**Ref.**
Svalbard, Norway	78.23	15.39	[53]
Kiruna, Sweden	67.83	21.05	[53]
Redu, Belgium	50.00	5.15	[53]
Oberpfaffenhofen, Germany	48.07	11.27	[160]
Fucino, Italy	42.00	13.60	[53]
Kourou, French Guiana	5.17	-52.70	[53]
La Reunion, France	-20.91	55.52	[53]
Noumea, New Caledonia	-21.90	165.97	[53]

inclination and a maximum central angle between the ground station and the satellite (θ_{max}). This is represented in Figure 7.10, and derived afterwards, where R_E is the Earth's radius, a is the semi-major axis of the satellite, and α is the minimum elevation angle considered.

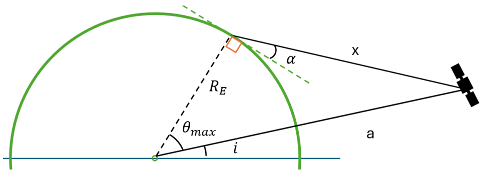

Figure 7.10: Geometry for Maximum Latitude Visible by Ground Station

Using the law of sines, the following relation can be established:

$$\frac{x}{\sin\theta_{max}} = \frac{a}{\sin(90^\circ + \alpha)} = \frac{a}{\cos\alpha} \tag{7.48}$$

where x is the distance between the satellite and the ground station. Using the law of cosines, the following relation can also be established:

$$a^2 = x^2 + R_E^2 - 2 \cdot x \cdot R_E \cdot \cos(90^\circ + \alpha) = x^2 + R_E^2 + 2 \cdot x \cdot R_E \cdot \sin\alpha \tag{7.49}$$

Combining both equations, the maximum central angle can be computed using Equation 7.50.

$$\sin\theta_{max} = \frac{\left(-R_E \sin\alpha + \sqrt{a^2 - R_E^2 \cos^2\alpha}\right) \cdot \cos\alpha}{a} \tag{7.50}$$

The final equation is then given by Equation 7.51.

$$\varphi_{max} = \min\left(|i| + \theta_{max}, 90^\circ\right) \tag{7.51}$$

For the scenarios studied here, the altitude ranges between 700 km and 1450 km, and even though the minimum elevation angle is usually set to five degrees, a more conservative value of 15 degrees is considered to ensure that the satellite is visible for longer and free of obstacles. Inputting these values into Equation 7.50, the maximum central angle ranges between 14.5° and 23.1°. This suggests that the maximum latitude visible can be increased by up to 23.1° at the highest altitudes. This means that stations like Svalbard (78° N) can see satellites at 1450 km at an inclination of ~ 55°. Anything lower would not be visible.

The constellation is propagated over one day, and the visibility of each satellite from each ground station is computed, following the same approach described in subsection 3.3.4, where a boolean visibility mask is generated for every satellite-ground station pair at different epochs. Let $V_{i,j}(t)$ be the visibility function, where

$$V_{i,j}(t) = \begin{cases} 1 & \text{if satellite } i \text{ is visible from ground station } j \text{ at time } t, \\ 0 & \text{otherwise.} \end{cases}$$

- **Maximum continuous visibility:** For each satellite–ground station pair (i, j), the longest uninterrupted visibility duration is

$$T_{i,j}^{\max} = \max_k \Delta t_k,$$

  where Δt_k is the length of the k-th contiguous interval with $V_{i,j}(t) = 1$.

- **Visibility duration statistics:** For each ground station j, compute statistics of $T_{i,j}^{\max}$ across all satellites $i = 1, \ldots, N_{\text{sat}}$:

$$T_j^{\min} = \min_i T_{i,j}^{\max}, \quad \overline{T}_j = \frac{1}{N_{\text{sat}}} \sum_{i=1}^{N_{\text{sat}}} T_{i,j}^{\max}, \quad T_j^{\max} = \max_i T_{i,j}^{\max}.$$

7

- **Satellite diversity:** The number of distinct satellites visible at least once from station j is

$$D_j = \sum_{i=1}^{N_{\text{sat}}} \left(\sum_t V_{i,j}(t) > 0 \right),$$

- **Connection opportunities:** The total number of distinct passes observed from all satellites at ground station j is

$$C_j = \sum_{i=1}^{N_{\text{sat}}} N_{i,j},$$

  where $N_{i,j}$ is the number of contiguous visibility intervals (passes) for pair (i, j).

These metrics are evaluated after the optimisation is performed to assess the feasibility of the constellation in terms of ground station visibility. The main takeaway from this analysis is that low inclination shells will require a low latitude ground station to be visible, while high inclination shells will be visible from most ground stations. Furthermore, the number and duration of connections will be maximum close to the constellation's inclination, and will decrease as the latitude difference increases.

7.8. Optimisation including Feasibility Parameters

This final section of the chapter aims to combine all the previous aspects into a single optimisation. The objective is to find a constellation that meets the performance requirements, while being feasible in terms of deployment time, Δv, and cost.

This optimisation is built on the previous ones, where the constellation parameters are optimised to meet the performance requirements. Given the complexity of the problem, this is directly tackled as a multi-objective problem, where the GDOP, deployment time, and cost are traded off. Other parameters discussed previously are indirectly included in the optimisation, such as the Δv, which is directly related to the mass of the satellite, and therefore to the cost.

7.8.1. Optimisation Setup

Similarly to the previous optimisation, the NSGA-III algorithm is used to solve the multi-objective problem. The optimisation variables are the same as in previous chapters, being the number of planes (P), the number of satellites per plane (S), and inclination (I). The altitude is related to the repeating cycle considered, and the same study cases are maintained. These are given by the number of days and orbits within the time period (n, k). This is given as an independent variable. All parameters are given in Table 7.17.

The number of planes is bounded between 5 and 20, the number of satellites per plane between 6 and 25, and the inclination between 77.5 and 87.5 degrees. The inclination is limited to a small polar range because the previous optimisations all converged to such inclinations. The constellation is assumed to be a Walker star, given the better performance shown in previous chapters. For two shell constellations, the number of planes can be between 1 and 20, while the number of satellites per plane can be between 6 and 25. The inclination is bounded between 25 and 77.5 degrees to complement the first shell. The second shell is assumed to be a Walker delta, given the lower inclination.

As mentioned, the objectives to minimise are:

- The maximum 95th percentile GDOP over the coverage area.
- The cost of the constellation, including manufacturing and launch costs, computed in billion USD.
- The total deployment time, computed in months.

The deployment time is composed of the time to manufacture the first batch of satellites, the time to launch all required launches, the drift time of the last plane, and the transfer time of the last plane. This is a simplification, knowing that the launching cadence is the limiting factor. Otherwise, the manufacturing cadence should be considered as well, and the maximum of both times should be taken.

The objectives are represented by the following equations:

$$\text{Minimise } f_1(\mathbf{x}) = \max_{u \in N_{users}} P_{95}(\text{GDOP}_u) \tag{7.52}$$

$$f_2(\mathbf{x}) = Cost_{const} + N_{launch,A62} \cdot Cost_{A62} + N_{launch,A64} \cdot Cost_{A64} \tag{7.53}$$

$$f_3(\mathbf{x}) = t_{man,1} + N_{launch} \cdot t_{launchcadence} + t_{drift,N} + t_{transfer,N} \tag{7.54}$$

where $\mathbf{x}$ is the vector of optimisation variables, N_{users} refers to the users, P_{95} is the 95th percentile function, $Cost_{const}$ is the cost of the constellation, $N_{launch,A62}$ and $N_{launch,A64}$ are the number of launches using Ariane 62 and 64 respectively, $Cost_{A62}$ and $Cost_{A64}$ are the cost per launch using Ariane 62 and 64 respectively. $t_{man,1}$ is the time to manufacture the first batch of satellites, N_{launch} is the total number of launches, t_{launch} is the time between launches, $t_{drift,N}$ is the drift time of the last launch, and $t_{transfer,N}$ is the transfer time to the target orbit performed by the last launch.

There are some constraints implemented in the optimisation to work within feasible margins. The first one is a limit on the total cost of the constellation, set to 10 B$ USD. This is arbitrarily set to force the optimiser to look for cheaper constellations. The second one is a limit on the deployment time, set to 24 months. Ideally, the constellation should be deployed within a year, but due to the low launch cadence, the constraint is relaxed to two years. Finally, there is a limit on the maximum GDOP allowed, set to 4.5. Larger values would create a constellation with poor performance.

Finally, a short overview of other relevant parameters is the manufacturing and launch cadence, the thruster settings, and satellite lifetime. For the deployment phase, up to three planes are allowed per launcher. Other surrogate models, such as the Δv required, the initial mass of the satellite, or the launcher capacity, are also included in the optimisation.

On the propagation side, the same settings as in previous chapters are used. The timestep is given by the number of observations, and the duration is related to the repeat cycle. For the performance assessment, 100 users are spread over the Northern Hemisphere.

7.8.2. TUNING

The tuning of the model is essential, especially because it represents the most complete version of the constellation design. Therefore, it is important to ensure that the optimiser can get to the best possible solutions.

Tuning has already been performed in previous chapters. This one is an improved version of the tuning done in subsection 6.2.2. This is done over more parameters, and less emphasis is put on the computing time, but rather on the quality of the solutions. It uses a more comprehensive set of metrics to evaluate the performance of the different configurations.

For this reason, three metrics are considered in order to choose the best set of parameters. In order of importance, these are:

Table 7.17: Feasibility Optimisation Setup

Free variables	Objectives	Constraints	Independent variables
Single shell			
$P \in [5, 20]$			Repeat cycle (N, K)
$S \in [6, 25]$			Launch cadence
$I \in [77.5°, 87.5°]$	f_1: Max 95th perc. GDOP	GDOP ≤ 4.5	Manufacturing cadence
Walker star	f_2: Cost (B$)	Cost $\leq$ 10 B$	Thruster settings
Extra shell	f_3: Deployment time (mo)	Time $\leq$ 24 mo	Satellite lifetime
$P \in [1, 20]$			Launcher capacity
$S \in [6, 25]$			Planes per launch
$I \in [25°, 77.5°]$			
Walker delta			

- Inverted Generational Distance (IGD): This metric measures how far the obtained Pareto front is from the true Pareto front. It is computed by taking the Euclidean distance from each point in the true Pareto front to the nearest point in the obtained Pareto front, and averaging these distances. A lower value indicates a better approximation of the true Pareto front. It was first mentioned in Coello and Sierra (2004)[33]. A problem occurs here because the true Pareto front is unknown. Therefore, an alternative is to use non-dominated solutions from all the tuning runs as a proxy for the true Pareto front.

- Hypervolume (HV): Zitzler and Thiele (1998)[183] defines this metric as a measure of the volume in the objective space that is dominated by the Pareto front. It starts by taking a reference point, usually the worst value for each objective. Then it computes the volume of the space dominated by the Pareto front and bounded by the reference point. A higher value indicates a larger dominated space, and therefore a better Pareto front.

- Time: This metric measures the total time taken by the optimisation. A lower value indicates a faster optimisation. This is important because it allows for more iterations and a more extensive exploration of the solution space. It works like a tie breaker when several sets of parameters have similar IGD and HV values.

Not that the criteria have been set, the parameters to tune are chosen. These are different from the ones in subsection 6.2.2, as then the objective was to find the best result while limiting the computational power, leading to a study of the population and period. Here, the objective is to find the best possible result, so the following parameters are tuned:

- Partitions [38]. This is the number of reference points used to divide the objective space in NSGA-III. It is common to relate the number of partitions to the population size, as the number of reference points should be similar to the population size. This is computed by Equation 7.55, where p is the number of partitions, m is the number of objectives. This range is chosen between 8, 12, and 16, which for the three objectives results in 45, 91, and 153 reference points, respectively.

$$N = \binom{p+m-1}{m-1} \tag{7.55}$$

- Simulated Binary Crossover (SBX) η and probability [39]. The distribution index η controls how far the offspring can be from the parents. A lower value allows for a wider exploration of the solution space, while a higher value focuses on exploitation. The probability controls how often crossover occurs. A higher value increases the exploration of the solution space, while a lower value focuses on exploitation. The values chosen are 15 (default) and 25 for η, taking as inspiration Deb et al. (2002)[40], where a value of 20 is selected for the study cases. The probability ranges between 0.5 (default) and 0.9. These values were chosen arbitrarily, but they allow for more variations than the default, but closer to the parents.
- Polynomial Mutation (PM) η and probability [39]. Similarly, η controls how far the mutated offspring can be from the parent. A lower value explores more, while a higher value exploits more. The probability controls the occurrence of such mutations. The values chosen are 10 and 20 (default) for η, and 0.3 and 0.9 (default) for the probability. For this scenario, more exploration is allowed for η, mainly because the probability value selected is much lower. This comes from Deb et al. (2002)[40], who suggested a probability of $1/n$, where n is the number of variables. In this case, there are three variables, so a value of 0.3 is close to the suggested one.

In the previous optimisations, chapter 5 and chapter 6, the tuning was performed over case b, which has a low altitude of 850 km. This is because it is one of the more limiting cases, requiring a large quantity of satellites to meet the performance requirements, while being sure that a solution could be found. However, for this case, the low altitude makes the tuning much longer, as the timestep is smaller and more satellites are needed, leading to more combinations to evaluate. It was also counterproductive to run cases c-e, as they work with two-day RGTs, effectively doubling the computation time. Therefore, case a, located at approximately 1250 km, is considered for this tuning.

The tuning is performed by running the optimisation with all combinations of the parameters mentioned. This results in a total of 48 combinations. Furthermore, the total number of evaluations is limited to 10,000, even if at the final optimisation, this number is increased to 100,000. This is done to reduce the computation time, as the tuning is performed over many combinations. The results of the tuning are shown in Table 7.18. These are the best five combinations, sorted by IGD, followed by their respective HV and time values.

The results show that the best combinations all have 16 partitions, which is the highest value considered. This indicates that a larger population size is beneficial for this optimisation, as it allows for a better exploration of the solution space. The first three solutions

Table 7.18: Feasibility Optimisation Tuning Results for Case a

Idx	Parts.	Prob. SBX	η SBX	Prob. PM	η PM	IGD	HV	Time (min)
1	16	0.5	25	0.9	10	0.082	39.23	31.52
2	16	0.5	15	0.3	10	0.083	39.23	31.89
3	16	0.5	15	0.9	10	0.086	39.2	31.51
4	16	0.9	25	0.9	20	0.094	39.04	31.97
5	16	0.5	25	0.3	20	0.099	39.12	32.65

are better, and they all share an η PM of 10, suggesting exploration in this parameter is beneficial. The other parameters do not show a clear trend, as they vary between the best solutions. In terms of time, all solutions are similar, and variations can be due to external factors.

Based on these results, the first combination is chosen for the final optimisation. It has the best IGD value and a high HV value. This indicates that the Pareto front obtained is close to the true Pareto front and dominates a large volume in the objective space. The time taken is on the higher end, but still acceptable. Therefore, this combination is selected for the final optimisation.

The final optimisation is run on all five cases. The following table summarises all parameters of the constellation and optimiser used for the final optimisation. This should be read in combination with Table 7.17.

Table 7.19: Constellation and mission parameters.

Parameter	Value
Repeat cycles	a(1,13), b(1,14), c(2,27), d(2,29), e(2,25)
Satellite lifetime	7 years
Thruster settings	$I_{sp} = 1300$ s, $T = 0.026$ N
Number of users	100
Minimum elevation angle	5° (GDOP), 15° (GS)
Launch cadence	4 launches per year
Maximum planes per launch	3
Launcher cost (Ariane 52)	88 M$
Launcher cost (Ariane 64)	106 M$
Manufacturing cadence	30 satellites per month
Manufacturing learning curve	85%
Fiscal year	2025

Some parameters missing in Table 7.19 are the altitude, mass, launcher capacity, duration, and timestep. These are a function of the specific repeat cycle and can be obtained from previous sections. The timestep is computed based on the number of observations by a user on Earth (20), analysis made in chapter 3.

Table 7.20: Optimiser settings.

Parameter	**Value**
Algorithm	NSGA-III
Partitions	16
Simulated Binary Crossover (SBX) probability	0.5
SBX η	25
Polynomial Mutation (PM) probability	0.9
PM η	10
Constraint tolerance (cvtol)	0.01
Function tolerance (ftol)	0.01
Variable tolerance (xtol)	1
Maximum evaluations	100,000
Random seed	1

The results of the optimisation are discussed in the following chapter.

8

Constellation Optimisation Results and Analysis

This chapter presents the final results of the multi-objective optimisation, including feasibility aspects, as described in section 7.8. This optimisation is built on the heuristic analysis performed in chapter 4, and the genetic algorithms used in chapter 5 and chapter 6. Even though the previous results show potential constellations, they were optimised for their limited set of parameters, and do not consider practical aspects such as deployment time, Δv, or cost. Therefore, this chapter takes a holistic approach and presents a more realistic constellation design that can be deployed in a reasonable timeframe and budget, while still meeting the performance requirements.

The chapter is structured as follows. First, the results of the final optimisation are presented in section 8.1, showing the Pareto front and discussing general trends. Then, some notable constellations are selected and analysed in more detail in section 8.3. Finally, a general discussion is presented in section 8.4, where aspects left out of the study are mentioned, as well as potential future work, along with recommendations for a real-world implementation.

8.1. Pareto Front Results

The results of the final optimisation are presented in this section. The optimisation is performed as described in section 7.8 for both single and double shell constellations. It trades off performance, cost, and deployment time. The running time per case ranges between 30 and 210 minutes, depending on the case and the number of shells. The resulting Pareto fronts are shown in Figure 8.1, where the trade-off between the different objectives can be observed.

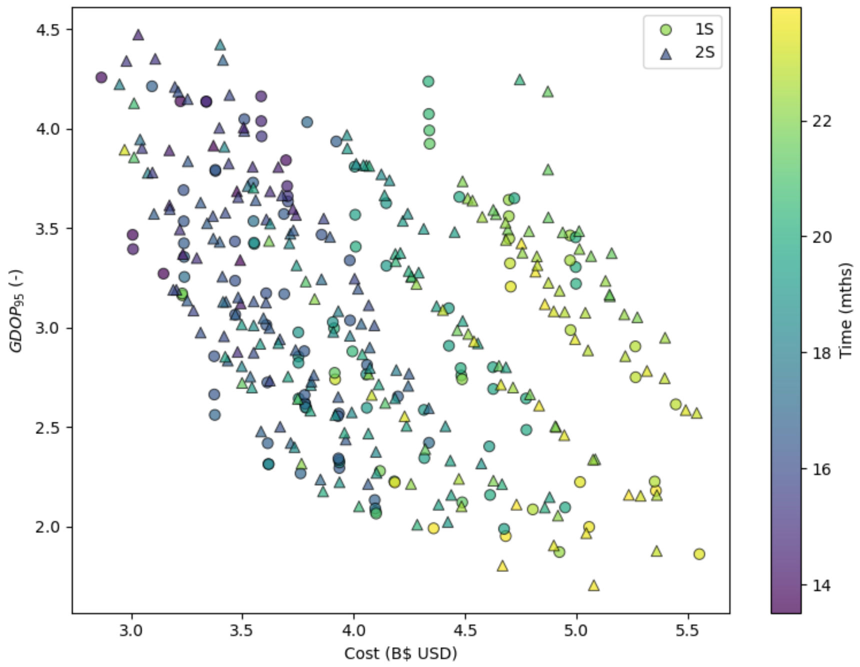

Figure 8.1: Pareto Fronts for Feasibility Optimisation

The results from the optimisation obtained a total of 377 non-dominated solutions for their particular case and number of shells, and can be found in Appendix E. The single shell case obtained 132 solutions, while the double shell case obtained 245 solutions. These do not necessarily represent the overall Pareto front, as some solutions may be dominated by solutions from other cases. However, they provide a good insight into the trade-offs between the different objectives, and there might be other reasons to choose a particular altitude over another, even if it is not the optimal solution according to this optimisation. Table 8.1 summarises the main statistics of the non-dominated solutions for each case and overall.

Table 8.1: Summary of Non-dominated Solutions for Feasibility Optimisation

		1450 km (e)	1250 km (a)	1050 km (c)	850 km (b)	700 km (d)	Combined
GDOP	min	1.70	1.90	1.86	2.15	2.57	1.70
(-)	mean	2.92	2.98	3.09	3.08	3.35	3.07
	max	4.47	4.21	4.42	4.03	4.25	4.47
Cost	min	2.87	3.09	3.34	3.79	4.33	2.87
(B$ USD)	mean	3.57	3.69	4.01	4.48	4.90	4.08
	max	5.08	4.90	5.55	5.36	5.54	5.55
Time	min	13.24	13.27	13.57	16.48	19.71	13.24
(mo)	mean	17.44	17.73	18.22	20.60	22.10	19.00
	max	23.83	23.71	23.92	23.95	23.76	23.95

Within the constraints, the area covered by the optimisation is desirable. The GDOP ranges between 1.70 and 4.47, with an average of 3.07, which is better than the 95th percentile GDOP of the Galileo constellation, which is around 3.4. The cost stays below 6 B$ USD. The deployment time is not always longer than a year, ranging between 13 and 24 months, with an average of 19 months. It would have been preferred to deploy the constellation in less than a year, but this would have required a higher launch cadence, which is not currently available. The optimisation seems to prefer higher altitudes, as the 1450 km case has the best minimum and average GDOP, cost, and deployment time.

8.1.1. OBJECTIVES TRADE-OFFS

The three objectives considered in this optimisation are the GDOP, cost, and deployment time. The GDOP is a measure of the performance of the constellation, while the cost and deployment time are measures of the feasibility of the constellation. The trade-offs between these objectives are discussed below:

- **Cost vs GDOP:** The two objectives are clearly conflicting, seen in Figure 8.2. This was already expected and seen in previous models. A better performance usually requires more satellites, which is a direct driver of cost.

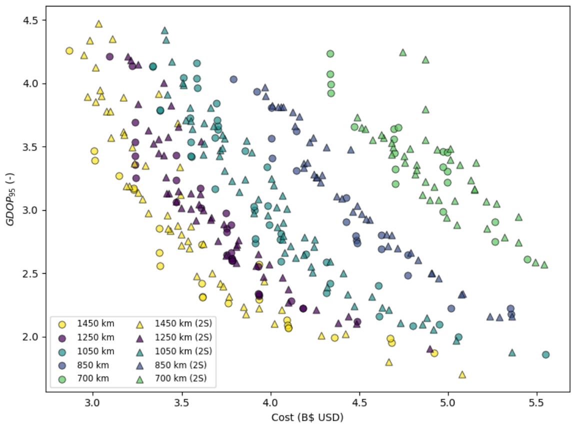

Figure 8.2: Cost vs GDOP

- **GDOP vs Deployment Time:** These two objectives are also conflicting, but the separation is not as clear. This is because of the non-linear relationship between the two aspects. The required increase in satellites or altitude for a better GDOP does not always translate to a proportional increase in deployment time, as this one is constrained to the number of launches and how they are distributed. There is also the drifting altitude component, further complicating the relationship. Figure 8.3 shows this trade-off.

- **Cost vs Deployment Time:** These two objectives are not competing, a trend observed in Figure 8.4. In fact, they are somewhat correlated, where a higher cost also translates to a higher deployment time. This is because the deployment time

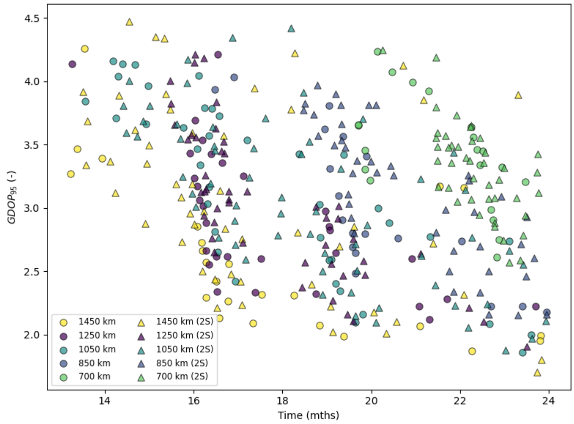

Figure 8.3: GDOP vs Deployment Time

is capped by the launch cadence, so an increase in the number of satellites will usually require more launches, and therefore a longer deployment time and directly higher cost. There are some exceptions to this, but not in the desired trend, as there are cases where, for comparable cost, the deployment time increases.

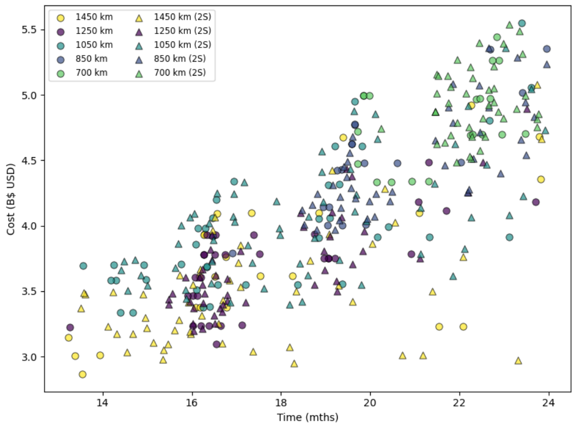

Figure 8.4: Cost vs Deployment Time

8.1.2. CONSTELLATION DESIGN PARAMETER TRENDS

In addition to the objectives, the constellation design parameters also show some interesting trends. These parameters include altitude, inclination, number of planes, number of satellites, and whether it is a single or double shell constellation. They help understand what parameters lead to better performance and feasibility.

The altitude of the solutions ranges between 700 km and 1450 km, with the best performing solutions being at the higher end of the range. This is expected, as a higher altitude allows for a larger coverage area per satellite, improving the GDOP. Furthermore, higher altitudes also allow for a more efficient deployment, either by the faster drifting or by requiring fewer satellites/planes for the same performance, leading to fewer launches and therefore a shorter deployment time and cost.

The total number of satellites ranges between 119 and 354, with an average of 212 satellites. As mentioned earlier, higher altitudes require fewer satellites, as can be seen in Figure 8.5.

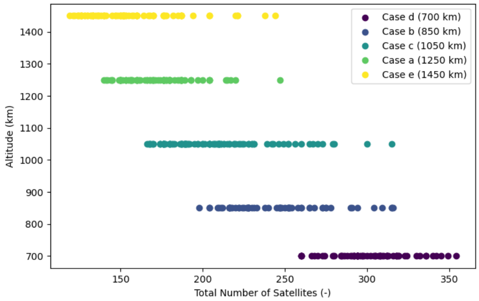

Figure 8.5: Satellite Distribution for Feasibility Optimisation

Furthermore, the distribution of the satellites over the two-shelled cases shows that most satellites are concentrated in the polar shell, with the second shell only adding a few satellites. This distribution can be seen in Figure 8.6. This suggests that a single shell constellation is sufficient for most cases, and the second shell only adds a marginal performance improvement.

8

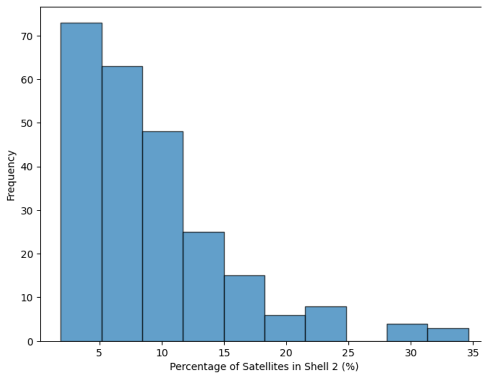

Figure 8.6: Satellite Distribution for Second Shell in Double Shell Constellations

A previous analysis made on Figure 6.7b showed that the second shell only had more relevance for low GDOPs. In that case, the optimisation was between GDOP and the number of satellites, and the second shell was able to reach lower GDOPs for the same number of satellites. However, in this case, the second shell does not provide a significant advantage, as the reduction in the number of satellites is not enough to compensate for the increase in deployment time and cost.

The double shell has more flexibility, reaching more solutions, but the overall performance is similar. The second shell is made by a Walker Delta constellation, with an average inclination of 29.5°, and 18 satellites divided between 1 and 2 planes. Even though some solutions have more satellites or planes, the average is low, helping as a complement for near-equator coverage.

The inclination of the primary shell range had already been analysed in chapter 6, and a range between 77.5-87.5° was found to be optimal. In these scenarios, the inclinations are chosen over the entire range, but the preference appears to follow a normal distribution around 82°. In terms of performance, it was shown in section 5.2 that the inclination has a small sensitivity, so the optimisation does not have a strong preference. However, for the feasibility analysis, the inclination affects the final altitude, leading to an indirect effect on the deployment time and cost through the changing mass and volume. This effect is not very strong, but it creates a complex relationship between the inclination and the objectives, leading to a wide range of inclinations being chosen.

For the single-shell configurations, the number of planes ranges from 7 to 20. The average corresponds to roughly 18 satellites per plane. Two main trends emerge: first, better performance is generally achieved with fewer planes and more satellites per plane, a tendency already noted in chapter 6. Ge et al. (2020) [67] already studied the effect of planes in a LEO constellation and did not come to sound conclusions other than the potential improvement in availability, and no improvement in the unequal distribution over the world.

A potential reason for having more satellites per plane than planes is that, for this optimisation, a Walker Star constellation is generally used. Thanks to the polar orbits considered, the planes are distributed over only 180° rather than 360°. Nevertheless, the satellites in a plane do have to cover 360°, so the space it needs to cover is simply double.

The second trend found is that the number of planes strongly influences the mission cost, since additional planes require more launches. The optimiser consistently favours configurations with more satellites per plane over those with more planes carrying fewer satellites.

The satellite distribution per plane reflects the constraints of available launch vehicles and fairing sizes listed in Table 7.11. Most solutions use about half the launcher's capacity per plane, enabling two planes to be deployed per launch. This strategy reduces both the total number of launches and the overall deployment time. For example, case 'a at 1250 km yields just under 15 satellites per plane against an Ariane 62 capacity of 30 satellites, while case 'b' at 850 km results in almost 20 satellites per plane with a launcher capacity of 42 satellites.

For the double-shell cases, the pattern remains similar. On average, the first shell contains 10.57 planes and the second 1.86, for a total of 12.43 planes. The mean number of satellites per plane is 18.4 for the first shell and 9.7 for the second, averaging to 17.1 across both shells.

8.2. COMPARISON TO LITERATURE

The given feasibility approach allows for a more realistic constellation design, considering practical aspects such as deployment time and cost. This is an improvement over previous studies that focused solely or primarily on performance metrics like GDOP. In the following paragraphs, the main results from the literature are run through the same feasibility analysis to provide a fair comparison.

Table 8.2: Feasibility Analysis of Literature Constellations

Constellation	T	alt. (km)	GDOP (-)	Cost (B$ USD)	Timeline (mo)
Ge	240	1000	6.97	5.9	37
Çelikbilek	382	1620	1.75		
Marchionne_1	484	1250	1.3	10.5	52
Marchionne_2	326	1250	1.61	7.9	46
Marchionne_3	246	1250	1.87	6.2	34
Guan_1	252	1008	2.41	4.6	21
Guan_2	264	900	2.82	5.2	34
Guan_3	240	1000	3.12	4.6	28
Guan_4	210	1100	2.67	4.0	19
Guan_5	210	1200	2.31	4.4	28
Guan_6	200	1300	2.22	4.4	28
Guan_7	190	1400	2.13	4.3	28
Guan_8	180	1500	2.12	4.3	28

Table 8.2 shows the feasibility analysis of most of the constellations found in the literature. While their performance is excellent, with an average max 95th percentile GDOP of 2.6, their cost and deployment time present significant practical challenges. A visual representation of this comparison with the results found in this work is shown in Figure 8.7. Most of the constellations would require substantially higher budgets or considerably longer deployment periods to implement.

The constellation by Ge et al. (2020)[67] was obtained analytically, and has a poor performance, with a cost slightly higher than the ones found in this thesis, but an extremely long deployment time. This deployment time is caused by the large number of planes (18), and the problem of having a shell at 90° inclination, where RAAN precession is zero, and therefore no drifting is possible.

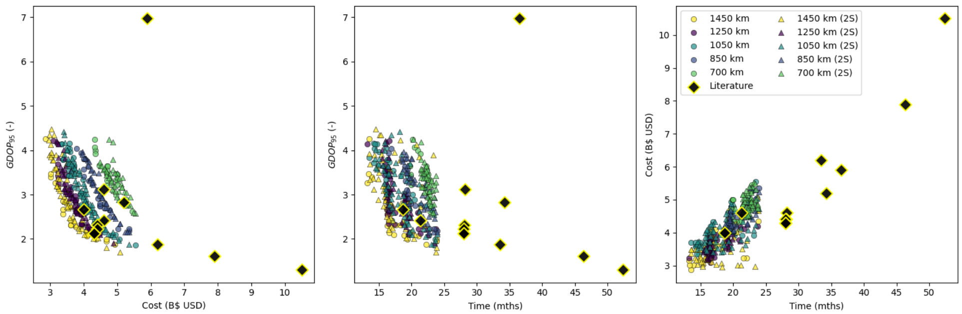

Figure 8.7: Feasibility Comparison to Literature Constellations

The constellation by Çelikbilek, Lohan, and Praks (2025)[26] could not be assessed because it is out of the altitude range considered in this work. However, it is expected that its cost and deployment time would be even higher due to the large number of satellites (382), altitude (1620 km), and planes (52). An equivalent constellation at 1450 km would have a deployment time of 4.9 years, and a cost of 9.6 B$ USD, the largest among all studied cases.

The constellations by Marchionne et al. (2023)[106] have an excellent performance, as they are optimised to minimise the same GDOP metric. The three constellations are divided among large, medium, and small constellations, a trend that also extends to the cost and deployment time. The large constellation has a large problem, which is that all planes are done through single launches, and even the first shell has one plane and 44 satellites, requiring multiple launches to deploy. This leads to a very long deployment time and a very high cost. The other two constellations also rely purely on single-plane launches (medium), and mostly on them (small). The deployment times between 2.8 and 4.3 years, and a cost between 6.2 and 10.5 B$ USD make for very difficult constellations to implement.

Finally, constellations by Guan et al. (2020)[71] have a more reasonable cost and deployment time, but most of them are still difficult to implement. A simple comparison can be made by comparing the Pareto front found in this work to the GDOP vs Cost trade-off of the literature constellations. Since the constellations operate at different altitudes than those in the optimised Pareto front, an interpolation procedure is required to enable fair comparison.

The interpolation is performed as follows: for each constellation at a specific altitude, the two closest altitude cases from this work's Pareto front are identified. Linear interpolation is then applied to estimate the GDOP that would be achieved at the constellation's altitude for the same cost. Finally, the two points computed are used in a linear regression to evaluate the GDOP at the target altitude and cost point.

While this comparison neglects the deployment time objective (which already exceeds practical limits for most Guan cases, averaging 26.8 months), it provides a meaningful assessment of performance versus cost trade-offs. The results of this comparison are presented in Table 8.3.

Table 8.3: Pareto Front Comparison based on GDOP differences

Literature Point	Difference
Guan_1	0.07 (On PF)
Guan_2	-0.66 (Dominated)
Guan_3	-0.63 (Dominated)
Guan_4	0.29 (Not Dominated)
Guan_5	-0.11 (Dominated)
Guan_6	-0.12(Dominated)
Guan_7	-0.08 (On PF)
Guan_8	-0.11(Dominated)

The values represent the differences between the interpolated GDOP from this work and the GDOP from the literature constellation. Negative values indicate that the literature constellation is performing worse than the Pareto front found in this work, and is therefore dominated. Positive values indicate that the literature constellation is performing better than the Pareto front. Values close to zero (within the optimiser accuracy of 0.1) are considered to be on the Pareto front.

Several cases are dominated by the Pareto front found in this work. Guan_1, Guan_4, and Guan_7 are either on the Pareto front or not dominated, potentially indicating attractive constellations. Guan_7 could be a feasible low GDOP constellation, as its deployment time is also not too large. However, the current work has found similar performing constellations in terms of GDOP and cost, while constraining the deployment time to be less than 2 years.

Guan_1 and Guan_4 are more difficult to assess, as they are within the potential Pareto fronts, but with a different altitude, for which interpolation is required. For these scenarios, all three objectives are interpolated and used to represent the Pareto front and compare. The results are shown in Table 8.4.

Table 8.4: Pareto Front Full Comparison based on GDOP differences

Literature Point	Difference
Guan_1	-0.03 (On PF)
Guan_4	0.03 (On PF)

Both constellations are on the Pareto front, and given that the optimiser accuracy is set to the nearest 0.1, they can be considered equivalent. They both perform deployment through two-plane launches, have sufficient Earth coverage, and have a reasonable cost. The one point of improvement for both would be the lack of repeating ground track, which would help with predictability and ground station planning, as well as a more robust performance worldwide.

This section has shown that many constellations found in literature present significant implementation challenges, particularly regarding cost and deployment time requirements. While these results may offer excellent theoretical performance, practical feasibility constraints can limit their real-world applicability. The current work has identified constellations that offer improved feasibility characteristics while maintaining comparable performance levels, and in some cases, achieving performance that meets or exceeds those found in the literature.

8.2.1. Launcher Considerations

A final consideration is the launcher. The launch vehicle selection significantly impacts deployment feasibility, representing a key factor in the analysis presented. While the current work utilises Ariane 6 as the baseline launcher due to its focus on European GNSS constellations, alternative launch systems could substantially alter the deployment landscape.

SpaceX's Falcon Heavy exemplifies this potential for improvement. With its 64,000 kg payload capacity to LEO, three times that of Ariane 64, it could dramatically reduce launch requirements and accelerate deployment timelines. At an estimated cost of 98 million USD per launch [120], Falcon Heavy also offers a better cost compared to Ariane 64. However, current launch availability remains limited to one or two missions per year [142], though future cadence increases are planned [143].

8

While launch costs typically represent a smaller fraction of total constellation expenses compared to satellite production, the reduction in required launches could yield significant benefits beyond cost savings. Fewer launches simplify logistics, reduce mission risk, and enable more flexible deployment strategies. This enhanced capability could make previously impractical constellation designs, such as multi-shell configurations or higher satellite counts, economically viable.

8.3. Analysis of Pareto-Optimal Constellations

After comparing the results to the literature and studying overall trends of the constellations, several constellations are selected for further analysis. These constellations are chosen based on notable trade-offs between the objectives, as well as potential real-world applications. In this analysis, both single and double shell constellations are combined, as well as all different altitudes. This allows for a more diverse and, therefore, complete set of constellations to be studied.

A note to mention is that for these sets of constellations, a higher accuracy is used in order to obtain the best possible results. The number of users is increased to 1000 over the entire world, and the number of observations is increased to 100, to have smaller timesteps.

To select the constellations, some categories are defined, and the best-performing constellation in each category is selected. The categories are:

- Cheapest: The constellation with the lowest cost overall.
- Best GDOP: The constellation with the lowest GDOP.
- Galileo Trade-off: The constellation that has a GDOP similar to Galileo, minimising cost and deployment time.
- Galileo Trade-off with Two Shells: The constellation that has a GDOP similar to Galileo, with low cost and deployment time, and is constrained to be a two-shelled constellation.
- Equally Weighted Optimum: The constellation that is closest to the origin in the normalised objective space, meaning it balances all objectives.

For all categories except the Low LEO constellation, a new non-dominated Pareto front (NDF) is created, allowing to get the best results overall. This new front is made of 49 potential solutions, out of which 24 are two-shelled and 25 are single-shelled. In the front, 46 solutions are at approximately 1450 km (case e), two are at 1250 km (case a), and one is at 1050 km (case c). Finally, most best performing solutions according to the criteria are single-shelled. A final case is considered in order to compare the results to the two-shell scenarios for Galileo-like constellations. The fastest deployed constellation is not considered, since it is only 10 days faster than the cheapest constellation and does not significantly impact the overall results. The selected constellations, along with the NDF and a mark on Galileo's performance, are shown in Figure 8.8.

8.3.1. CHEAPEST

The first constellation analysed is the cheapest overall. It can be found on the upper left corner of the Pareto front in Figure 8.8. This constellation maintains a GDOP below 4.5 per the constraints while minimising cost. The constellation parameters are shown in Table 8.5.

Table 8.5: Cheapest Walker constellation parameters

Type	Case (days/revs)	Altitude (km)	Inclination (°)	Pattern (T/P/F)
Walker Star	e (2/25)	1444.87	84.30	119/7/3

It is a single shell constellation with a two-day repeating ground track. A detailed view of the constellation's performance is shown in Table 8.6.

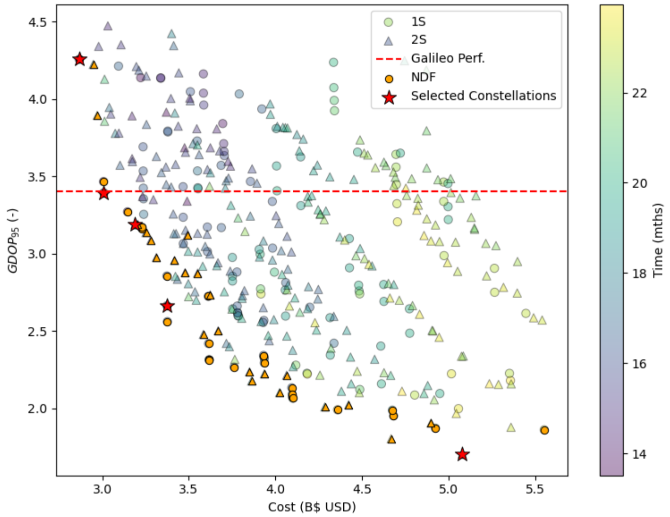

Figure 8.8: Non-Dominated Front and Selected Constellations

Table 8.6: Cheapest Constellation Performance

Metric	**GDOP**	**PDOP**	**TDOP**	**HDOP**	**VDOP**
Mean (-)	2.22	2.07	0.83	0.89	1.87
Max P95 (-)	4.27	3.94	1.66	1.34	3.70
Min. Avail. (DOP < 6) (%)	98.01	98.04	98.56	99.49	98.11

The constellation has an excellent average GDOP of 2.22, with a maximum 95th percentile GDOP of 4.27. This implies that for 95% of the time, the GDOP will be below 4.27, which is not an ideal performance, but may be sufficient for many applications. The availability here is defined as the percentage of time, the different DOPs are below 6, which is what United States Department of Defense (2020)[167] considers as a threshold. The constellation has an availability of 98.01%, meaning that for almost all the time, the GDOP is below 6. The worst availability and DOPs occur close to the equator, where the satellites move faster, and therefore the geometry is worse. This distribution can be seen in Figure 8.9.

This is an unfortunate aspect of polar constellations, where as the latitudes approach the equator, there can be some minor outages. These outages add up to a total of 1.99% of the time, which is around 30 minutes per day. This is not ideal, but it is a trade-off for having a cheap constellation.

The next aspect is the deployment time. It takes 13.55 months to produce and deploy the full constellation. Assuming a satellite lifetime of seven years, this means the constellation can be fully operational for almost 6 years before any replacements are needed. The exact deployment timeline is shown in Figure 8.10.

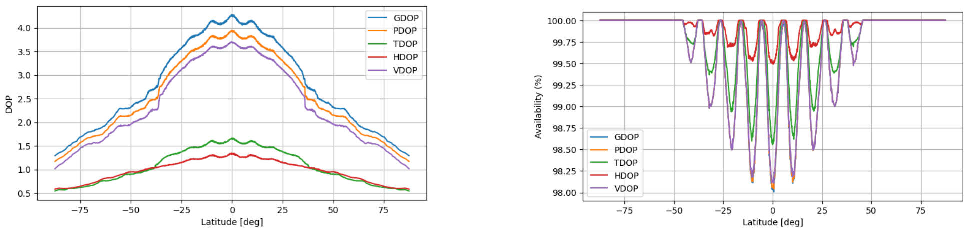

(a) 95th Percentile DOP Distribution

(b) Availability Distribution

Figure 8.9: Cheapest Constellation Performance vs Latitude

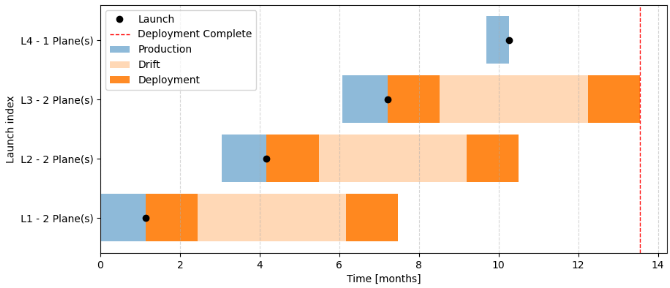

Figure 8.10: Cheapest Constellation Deployment Timeline

The timeline shows that most are two plane launches, with the final satellites being launched directly into their final orbital plane. For the first three launches, the Ariane 64 rocket is used, while for the last launch, the A62 meets the requirements. Figure 8.10 also shows that after six months since the first launch, already three planes are fully operational, and after nine months, six out of the seven planes are in place. This allows for a smooth transition to full operational capability.

The manufacturing and launching cost of the constellation is 2.87 B$ USD. This is the lowest cost found in the optimisation, and it is made by a production cost of 2.46 B$ USD, and a launch cost of 0.41 B$ USD. This leads to a cost per satellite of 20.7 M$ USD.

The most relevant parameters about the satellite are shown in Table 8.7. The satellite has a wet mass of 287.2 kg. Most constellations have shown similar characteristics, with higher mass at lower altitudes. Stationkeeping is low due to the high altitude, and the main drivers of Δv are the end-of-life disposal and the deployment. The collision avoidance manoeuvres (CAMs) expected for the entire constellation over its lifetime are expected to be ~ 27, leaving each satellite with a probability of 23% of performing a CAM over its lifetime. This leads to a negligible Δv budget for CAMs.

The final two aspects to analyse are the ISL and the ground stations. The constellation

Table 8.7: Satellite mass, power, and Δv budget (including margins).

Parameter	**Value**
Mass (kg)	
Dry	235.7
Rad. Shield	34.2
Propellant	17.3
Wet	**287.2**
Payload Power (W)	
Payload power	823.9
Δv Budget (m/s)	
EOL disposal	457.4
Station-keeping (nominal)	3.7
Collision avoidance (CAM)	0.001
Deployment	330.0
Total	**791.0**

can easily handle any connection with any of its eight surrounding neighbours, as shown in Figure 8.11. The maximum distance between satellites is 5500 km, while the maximum azimuth difference is ±74°. The azimuth difference is close to the limit (±80°), but still within the capabilities of current technology when no yaw-steering law is considered. The elevation angle is also within limits, with a minimum of −21°.

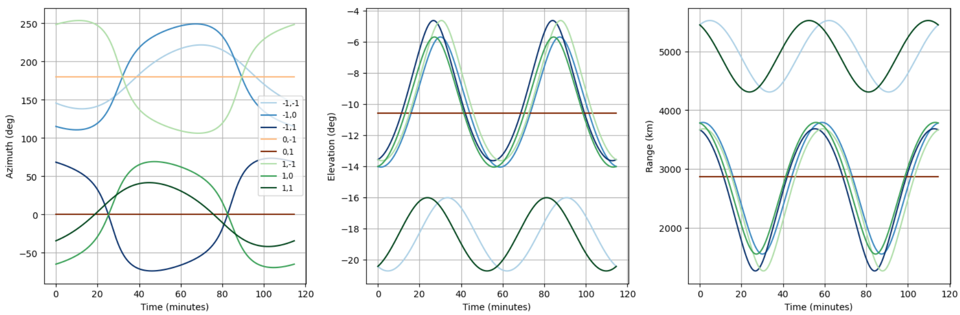

Figure 8.11: Cheapest Constellation ISL Properties

On the ground stations' side, the visibility and contact durations are crucial for maintaining communication with the satellites. For polar constellations, all ground stations are visible. They all manage to see each satellite at least once per day. The best performance is higher Northward, where contacts per day and average time are maximised. The performance of the ground stations is shown in Table 8.8.

Overall, this constellation is an attractive option for a cheap yet still performing constellation. It has some minor outages close to the equator and a poorer 95th percentile performance. It is the constellation with the lowest number of satellites (119), and therefore

Table 8.8: Ground station visibility and contact durations for Cheapest Constellation.

Ground Station	Contacts/day	Min. (min)	Mean (min)	Max. (min)
Svalbard	1505	14.67	14.81	14.83
Kiruna	1180	14.50	14.74	14.83
Redu	631	13.67	14.55	14.83
Oberpfaffenhofen	602	13.50	14.53	14.83
Fucino	530	13.50	14.50	14.83
Kourou	386	13.17	14.38	14.83
La Réunion	414	13.17	14.47	14.83
Nouméa	417	13.17	14.44	14.83

the lowest cost. It therefore has a short deployment time, allowing for a quick transition to full operational capability.

8.3.2. Best GDOP

The next constellation analysed is the one with the best GDOP overall. It can be found on the bottom right corner of the Pareto front in Figure 8.8. This constellation is a double shell constellation, with a polar shell and a low-inclined shell. The constellation parameters are shown in Table 8.9.

Table 8.9: Best GDOP Walker constellation parameters

Type	Case (days/revs)	Altitude (km)	Inclination (°)	Pattern (T/P/F)
Walker Star	e (2/25)	1444.76	84.20	204/12/6
Walker Delta	e (2/25)	1405.75	25.0	40/4/1

This constellation also follows a two-day repeating ground track. It is limited to 244 satellites, which is way less than the maximum allowable of 1000 satellites. The constraining factor is the deployment time, which is close to the two-year limit. This constellation's excellent performance is shown in Table 8.10.

Table 8.10: Best GDOP Constellation Performance

Metric	GDOP	PDOP	TDOP	HDOP	VDOP
Mean (-)	1.38	1.29	0.49	0.57	1.15
Max P95 (-)	1.71	1.59	0.63	0.69	1.45
Min. Avail. (DOP < 6) (%)	100.00	100.00	100.00	100.00	100.00

The performance is very consistent throughout the entire globe, with a mean GDOP of 1.38. On top of this, the satellites always maintain a GDOP below 6, leading to a perfect availability of 100%. The 95th Percentile DOP Distribution can be seen in Figure 8.12.

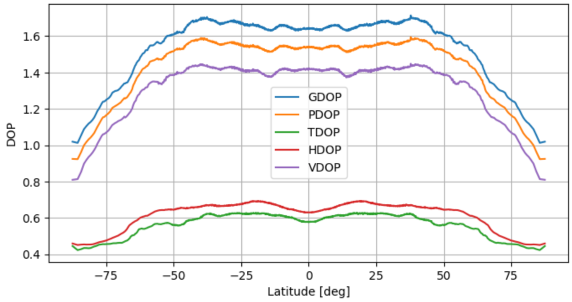

Figure 8.12: Best GDOP Constellation Performance vs Latitude

Depending on the mission, such performance could be necessary, but for most applications, it is an overdesign. This may also not lead to a significant improvement in positioning accuracy, as other error sources may dominate. Furthermore, this will have a consequence on the deployment time and cost.

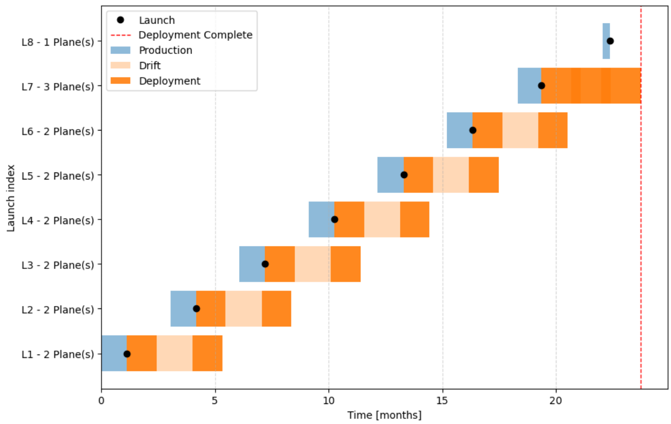

Figure 8.13: Best GDOP Constellation Deployment Timeline

The deployment time takes 23.7 months, one of the longest deployment times found. This is because the constellation requires a large number of planes (16 in total). The constellation is designed to launch into the polar orbit first in sets of two planes using Ariane 64 rockets, and then launch the low-inclination shell using Ariane 62 rockets. The low inclination shell allows for deploying three planes at a time, which helps reduce the deployment time. The deployment timeline is shown in Figure 8.13.

Following this strategy, the constellation can be built up gradually, with the first three planes being operational 4.3 months after the first launch, and adding two more planes every 3 months. Once all polar planes are launched, the constellation can be fully operational with a max 95th percentile GDOP of 2.00 and 100% availability. This is then further improved by launching the second shell.

The production cost of the constellation is 4.26 B$ USD, amounting to a cost per satellite of 17.5 M$ USD. The launch cost is 0.81 B$ USD, leading to a total cost of 5.08 B$ USD. This is among the highest costs found, but it is due to the large number of satellites (244). The cost per satellite is lower than the cheapest constellation, as the larger production scale allows for economies of scale.

The satellite characteristics are very similar to the cheapest constellation, with a wet mass of 287.2 kg. The polar shell has a payload power of 823.9 W, while the low-inclination shell has a payload power of 805.7 W due to the different altitudes. The Δv budget is the same at 791 m/s. The details are shown in Appendix E. The expected number of CAMs for its entire lifetime is 54.9, a value almost double compared to the cheapest constellation, matching the number of satellites. This should not be a challenge for the ground operations team.

In terms of the ISL, the polar shell can handle all types of connections, with maximum values of 4800 km in range, ±60° in azimuth difference, and −18° in elevation angle. On the other hand, the low-inclination shell can only handle intra-plane connections. Because there are only four planes, the inter-plane distance is up to 14000 km, which is too large to maintain any connection.

Table 8.11: Ground station visibility and contact durations for Best GDOP Constellation.

Ground Station	Polar Shell				Low-Inclination Shell			
	Conts/day	Min (min)	Mean (min)	Max (min)	Conts/day	Min (min)	Mean (min)	Max (min)
Svalbard	2579	14.67	14.81	14.83	0	0.00	0.00	0.00
Kiruna	2017	14.50	14.75	14.83	0	0.00	0.00	0.00
Redu	1081	13.67	14.57	14.83	0	0.00	0.00	0.00
Oberpfaffenhofen	1028	13.50	14.54	14.83	0	0.00	0.00	0.00
Fucino	910	13.50	14.50	14.83	123	9.50	10.20	10.50
Kourou	664	13.17	14.38	14.83	358	15.00	15.32	15.50
La Réunion	707	13.00	14.45	14.83	261	15.33	15.41	15.50
Nouméa	713	13.17	14.42	14.83	258	15.33	15.41	15.50

Table 8.11 shows the ground station performance for both shells. The polar shell can be seen by all ground stations, having better performance at higher latitudes. The low inclination can only be seen by lower latitude ground stations, starting at Fucino (42° N). If only one station is to be used, Kourou is probably the best option, as it maximises the number of contacts and the contact duration of the low inclination while having a smaller impact on the polar shell. On the other hand, Fucino is a ground station in Europe, simplifying logistics, and it has a similar performance. Furthermore, there are four times more satellites in the polar shell, so it is preferred to have four times more contacts than the low-inclination shell.

The best GDOP constellation is a great option for missions that require the best possible performance. It has perfect availability and a very low GDOP overall. However, this comes at the cost of a long deployment time and a high cost. It can be overdesigned and has some limitations in terms of ISL and ground stations due to the low-inclination shell.

8.3.3. GALILEO TRADE-OFF

This constellation takes Galileo's maximum 95th percentile GDOP of 3.4 as a reference and tries to find a constellation with a similar performance, but with a lower cost and deployment time. This is found at the leftmost side under the red horizontal line in Figure 8.8. The constellation parameters are shown in Table 8.12.

Table 8.12: Galileo Trade-off Walker constellation parameters

Type	Case (days/revs)	Altitude (km)	Inclination (°)	Pattern (T/P/F)
Walker Star	e (2/25)	1441.49	81.3	126/9/3

This is also a single shell with a two-day repeating ground track. A detailed view of the constellation's performance is shown in Table 8.13.

Table 8.13: Galileo Trade-off Constellation Performance

Metric	GDOP	PDOP	TDOP	HDOP	VDOP
Mean (-)	2.11	1.96	0.77	0.85	1.76
Max P95 (-)	3.46	3.18	1.35	1.16	2.97
Min. Avail. (DOP < 6) (%)	99.43	99.52	99.74	99.82	99.52

The constellation achieves an excellent average GDOP of 2.11, with a maximum 95th percentile GDOP of 3.46, which almost matches Galileo's performance. Its worst performance occurs at latitudes close to the equator (±25°). The availability is also high, with a minimum of 99.43%, which is equivalent to eight minutes over one day. These cases, when the DOP exceeds 6, are not concentrated in any particular latitude, though spikes can be seen around ±61°, ±48° and ±25°, as shown in Figure 8.14. These locations are not ideal, but the times the GDOP is above 6 are very brief, and the overall availability remains strong. The worst performance occurs between ±25° latitude, as expected for a polar constellation.

The deployment time is 13.93 months, a timeline very similar to the fastest and cheapest constellations. The deployment timeline is shown in Figure 8.15.

Some interesting deployment approach for such a constellation is that the first three planes can be deployed 4.3 months after launch, five planes after 7.4 months, and the final set at 13 months. Through this method, the constellation can be operational over Europe several times over one day since the beginning of the deployment. The deployment is done through five A62 launches.

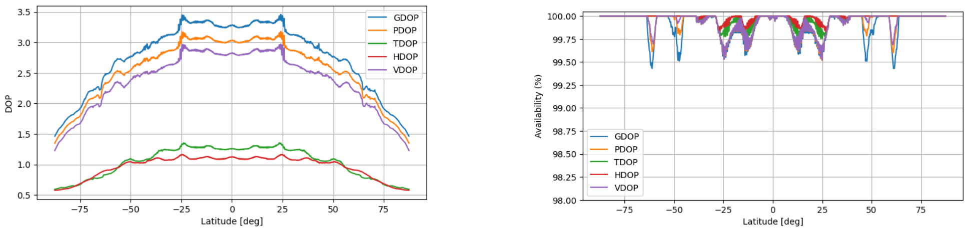

(a) 95th Percentile DOP Distribution

(b) Availability Distribution

Figure 8.14: Galileo Trade-off Constellation Performance vs Latitude

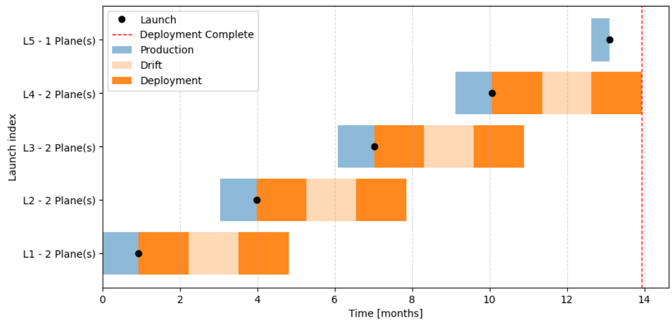

Figure 8.15: Galileo Trade-off Constellation Deployment Timeline

The cost is 3.0 B$ USD, which is a bit higher than the cheapest constellation, but still very reasonable. The cost breaks down to 2.57 B$ USD for production and 0.44 B$ USD for launch. The cost per satellite is 23.8 M$ USD, an even cheaper cost than the cheapest constellation.

The satellite characteristics are very similar to the cheapest constellation; therefore, the analysis done previously is also applicable. For the specific values, refer to Appendix E. The total number of expected CAMs is 28, with a probability of 22.5% per satellite. Similarly, all ISL connections are possible, with the highest distance being 5600 km, an azimuth difference of $\pm 61.7°$, and a minimum elevation of $-21°$. The ISL properties variation in time is also shown in the appendix.

The ground stations also see all satellites, and their performance is shown in Table 8.14. Svalbard manages to see all satellites for the maximum allowable time duration. However, all other ground stations also perform well, with high contact durations and availability.

Because of the promising results of this constellation, the robustness analysis explained in section 7.6 is performed. For this constellation, the expected number of satellite failures over its lifetime ranges between 1.0 and 8.8, depending on the failure rate assumed. Therefore, the analysis is performed for up to three simultaneous failures. The results

Table 8.14: Ground station visibility and contact durations for Galileo Trade-off.

Ground Station	Contacts/day	Min. (min)	Mean (min)	Max. (min)
Svalbard	1594	14.83	14.83	14.83
Kiruna	1157	14.50	14.77	14.83
Redu	687	13.67	14.64	14.83
Oberpfaffenhofen	640	13.67	14.63	14.83
Fucino	563	13.33	14.57	14.83
Kourou	406	13.00	14.41	14.83
La Réunion	443	13.00	14.53	14.83
Nouméa	441	12.83	14.43	14.83

are shown in Table 8.15.

Table 8.15: Robustness Analysis for Galileo Trade-off Constellation

Scenario	Mean GDOP	Max $GDOP_{95}$	Min. Avail.
Nominal	2.11	3.46	99.4
1 Failure	2.12	3.62	98.5
2 Failures	2.13	4.11	97.3
3 Failures	2.15	4.86	96.5

The constellation shows limited robustness to failures. Single-satellite failures have minimal impact, with only a 0.16 increase in maximum 95th percentile GDOP and availability reduction of less than one percentage point. However, multiple simultaneous failures cause more significant degradation. With two failures, the maximum 95th percentile GDOP increases to 4.11 (19% increase), while availability drops to 97.3%. Three failures push the maximum GDOP to 4.86 (40% increase) and availability to 96.5%, representing almost an hour of unavailability per day. While the probability of multiple simultaneous failures is low, these scenarios demonstrate that the constellation operates with relatively little margin for performance degradation.

This constellation demonstrates an effective trade-off between performance, cost, and deployment time. It manages to almost match Galileo's performance while maintaining low cost and deployment time. The times with DOP>6 could present some minor issues, but overall, the constellation represents a viable option for a GNSS constellation. There are some concerns in terms of its robustness. Potentially adding a second shell could help with the availability, but it would also increase the cost and deployment time.

8.3.4. GALILEO TRADE-OFF WITH TWO SHELLS

Except for the best GDOP configuration, all constellations analysed so far consist of a single shell. In this case, the constellation is constrained to have two shells, while still aiming to match Galileo's performance. This allows a direct comparison with the previous single-shell configuration and helps assess whether the added complexity of a second shell provides any meaningful improvement. The constellation parameters are shown in Table 8.16.

Table 8.16: Galileo trade-off with two shells - Walker constellation parameters

Type	Case (days/revs)	Altitude (km)	Inclination (°)	Pattern (T/P/F)
Walker Star	e (2/25)	1441.49	81.3	126/9/3
Walker Delta	e (2/25)	1405.77	25.1	6/1/0

The optimiser originally identified a slightly different configuration as part of the Pareto front: Walker Star: 1440.50 km, ~ 80.4°

However, for the sake of consistency, the first shell has been kept identical to the previous single-shell configuration. This adjustment slightly worsens the performance (by approximately +0.02 in the GDOP metric), but allows a fair and direct comparison between both cases.

The second shell is relatively small, accounting for less than 5% of the total satellites. It is positioned at an inclination of 25.1°, corresponding to the region of poorest performance of the polar shell. A detailed performance assessment of this configuration is presented in Table 8.17.

Table 8.17: Galileo Trade-off with Two Shells Constellation Performance

Metric	GDOP	PDOP	TDOP	HDOP	VDOP
Mean (-)	2.04	1.90	0.74	0.83	1.71
Max P95 (-)	3.19	2.95	1.23	1.10	2.75
Min. Avail. (DOP < 6) (%)	99.43	99.57	99.82	99.87	99.57

8

The additional shell provides a performance improvement, reducing the maximum 95th percentile GDOP from 3.46 to 3.19. The availability also sees a slight increase for all DOP metrics except the GDOP, which remains unchanged. The performance distribution across latitudes practically mirrors that of the single-shell configuration for the availability, as illustrated in Figure 8.16. The DOP lines become smoother, suppressing the spikes happening at ±25° latitude.

The most optimal deployment time is 16.2 months, which is 2.3 months longer than the single-shell configuration. This happens because the second shell requires an additional launch. The deployment timeline is shown in Figure 8.17.

Even though this deployment strategy is the fastest possible, it is not the most optimal in terms of operational capability. It starts by launching the low-inclination shell first. This does not allow for a gradual build-up of the constellation, as the polar shell is the one that provides most of the coverage. A better approach could be to launch the polar shell

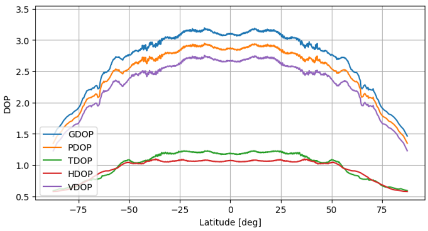

(a) 95th Percentile DOP Distribution

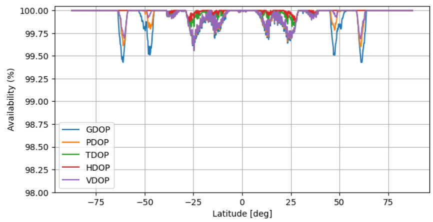

(b) Availability Distribution

Figure 8.16: Galileo Trade-off with Two Shells Constellation Performance vs Latitude

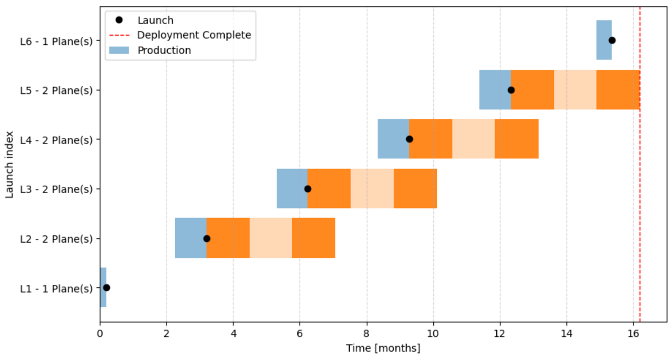

Figure 8.17: Galileo Trade-off with Two Shells Constellation Deployment Timeline

first, and then add the low-inclination shell at the end. This would add 20 to the total strategy, but it would allow for a quicker transition to full operational capability. For this to happen, the first and last launches need to be swapped. Launches are made using the Ariane 62.

The cost is 3.19 B$ USD, which is 0.19 B$ USD more expensive than the single-shell configuration. The cost breaks down to 2.66 B$ USD for production and 0.32 B$ USD for launch. The cost per satellite is 24.2 M$ USD, slightly higher than the single-shell configuration. This is because the last shell is small, and the cost of the launch is spread over fewer satellites.

The expected number of CAMs is 29.7, up to two more compared to the single shell. The ISL and ground station performance is the same for the polar shell, while the low-inclination shell can only handle intra-plane connections because it only has one plane. The ground stations are more constraining, as the low-inclination shell can only be seen by Fucino, Kourou, La Réunion, and Nouméa. The ground station performance is shown in Table 8.18.

The number of contacts for the second shell is very low, mainly due to the small num-

Table 8.18: Ground station visibility and contact durations for Galileo Trade-off Constellation with Two Shells.

Ground Station	Polar Shell				Low-Inclination Shell			
	Conts/day	Min (min)	Mean (min)	Max (min)	Conts/day	Min (min)	Mean (min)	Max (min)
Svalbard	1594	14.83	14.83	14.83	0	0.00	0.00	0.00
Kiruna	1157	14.50	14.77	14.83	0	0.00	0.00	0.00
Redu	687	13.67	14.64	14.83	0	0.00	0.00	0.00
Oberpfaffenhofen	640	13.67	14.63	14.83	0	0.00	0.00	0.00
Fucino	563	13.33	14.57	14.83	19	9.89	10.22	10.33
Kourou	406	13.00	14.41	14.83	54	15.33	15.39	15.50
La Réunion	443	13.00	14.53	14.83	39	15.33	15.36	15.50
Nouméa	441	12.83	14.43	14.83	39	15.33	15.39	15.50

ber of satellites. This could be problematic since the shell would not be reachable at all times. It would also require a low latitude ground station, preferably Kourou, to maximise the number of contacts and time.

In summary, adding a second shell does provide improvement in performance for the worst locations. The added cost and time are not too large, but the added complexity of having two shells may not be worth it. The second shell is small and would require special considerations for the ground stations. The performance improvement is not necessary to match Galileo's performance, as the single-shell configuration already does so, and in terms of availability, the improvement is equivalent to one minute over one day.

8.3.5. Equally Weighted Optimum

The final constellation to compare is the one closest to the origin. What this aims to do is to find a constellation that trades off between the three objectives, assuming they are equally important. The normalisation of the objective is done by taking the maximum and minimum found in the optimisation and scaling the values between 0 and 1. The constellation parameters are shown in Table 8.19.

Table 8.19: Equally Weighted Optimum Walker constellation parameters

Type	Case (days/revs)	Altitude (km)	Inclination (°)	Pattern (T/P/F)
Walker Star	e (2/25)	1438.25	79.30	150/10/4

This is a standard single-shell constellation with a two-day repeating ground track. However, what is interesting to see is the trade-off between the three objectives. In terms of GDOP, it is close to the excellent metric, maintaining a max 95th percentile below 3 and a mean below 2. The availability is also quite high, with a maximum of 10 min for GDOP < 6, but up to 100% availability for the other metrics (HDOP, TDOP). The constellation performance is shown in Table 8.20.

The worst availability occurs at ±56° latitude, as shown in Figure 8.18. This is not ideal as it could affect Northern Europe. The worst DOP also occurs in the range between these latitudes.

8

Table 8.20: Equally Weighted Optimum Constellation Performance

Metric	GDOP	PDOP	TDOP	HDOP	VDOP
Mean (-)	1.89	1.76	0.68	0.78	1.58
Max P95 (-)	2.69	2.54	1.00	1.09	2.40
Min. Avail. (DOP < 6) (%)	99.27	99.44	100.00	100.00	99.59

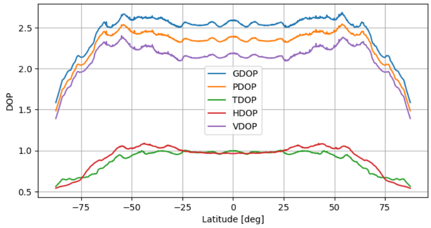

(a) 95th Percentile DOP Distribution

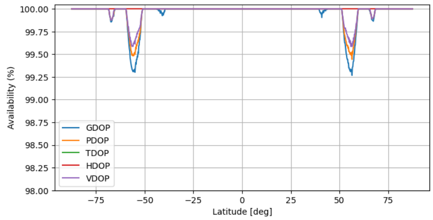

(b) Availability Distribution

Figure 8.18: Equally Weighted Optimum Constellation Performance vs Latitude

The timeline is also short for the large number of satellites, taking 16.2 months to deploy. This is faster than the two-shell Galileo trade-off constellation, even though it has more satellites. The deployment timeline is shown in Figure 8.19.

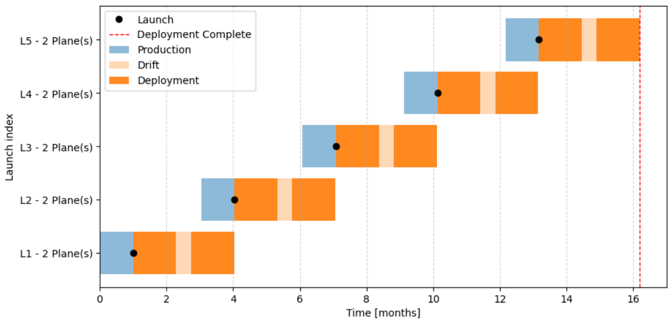

Figure 8.19: Equally Weighted Optimum Constellation Deployment Timeline

This deployment is very symmetrical, launching two planes at a time using Ariane 62, and performing a launch every time all previous satellites have reached their operational orbit. This occurs mostly out of luck, rather than design. The fact that 30 satellites can be launched at a time and that this is the same manufacturing cadence per month allows for this pattern. The result of this is that every three months, two fully operational planes are added to the constellation.

In terms of cost, it is 3.37 B$ USD, which is 10% more expensive than the single-shell Galileo trade-off constellation. The cost breaks down to 2.94 B$ USD for production and 0.44 B$ USD for launch. The cost per satellite is 19.5 M$ USD, one of the cheapest, just after the constellation with the most satellites. The satellite parameters are also very similar, with a total CAMs of 33.76.

All ISL connections are possible, with a maximum distance of 5500 km, an azimuth difference of ±60.4°, and a minimum elevation of −21°. The ground stations also see all satellites, and their performance is shown in Table 8.21. It does not vary much from the previous single-shell constellations. The higher the latitude of the ground station, the better the performance.

Table 8.21: Ground station visibility and contact durations for Equally Weighted Optimum.

Ground Station	Contacts/Day	Min (min)	Mean (min)	Max (min)
Svalbard	1712	14.83	14.87	15.00
Kiruna	1283	14.67	14.83	15.00
Redu	843	13.83	14.64	15.00
Oberpfaffenhofen	796	13.67	14.64	15.00
Fucino	689	13.33	14.61	14.83
Kourou	492	13.00	14.49	15.00
La Reunion	527	12.67	14.57	15.00
Noumea	531	12.50	14.43	15.00

This constellation is also a strong option for a GNSS constellation. The robustness analysis is also performed, with an expected 1.19 to 10.5 failures over its lifetime. The results of such failures are shown in Table 8.22.

Table 8.22: Robustness Analysis for Equally Weighted Optimum Constellation

Scenario	Mean GDOP	Max $GDOP_{95}$	Min. Avail.
Nominal	1.89	2.69	99.27
1 Failure	1.90	2.78	99.1
2 Failures	1.91	2.89	98.9
3 Failures	1.92	3.07	98.7

The constellation is relatively robust. Three satellite failures only increase the maximum 95th percentile GDOP by 14%, and the availability drops by 13 minutes over one day. This is a positive result, as it means that the constellation can handle some failures without a significant impact on performance.

This is a well-balanced constellation that manages to have an excellent performance, while still having a low cost and deployment time. The performance is more than sufficient, even though it also has some limitations at mid-latitudes. The deployment time is short, allowing for a gradual build-up of the constellation. The cost is on the low side, with a low cost per satellite. This constellation could be a strong option if all three objectives are equally important.

8.4. DISCUSSION

The five constellations presented in the previous section showcase different trade-offs between performance, cost, and deployment time. Their key characteristics are summarised in Table 8.23.

Table 8.23: Summary of Key Characteristics of Selected Constellations

Const.	Shells	Sats.	Max $GDOP_{95}$	Min. Avail.	Dep.Time (mo)	Cost (B$ USD)
Cheapest	1	119	4.27	98.01	13.55	2.87
Best GDOP	2	244	1.71	100.00	23.70	4.26
Galileo Trade-off	1	126	3.46	99.43	13.93	3.00
Galileo Trade-off 2S	2	132	3.19	99.43	16.20	3.19
Equally Weighted Optimum	1	150	2.69	99.27	16.20	3.37

The obvious question to ask is which constellation is better. The answer is clearly not straightforward, as it depends on the mission requirements and priorities. Therefore, the following discussion will take a more practical approach, analysing which constellation would be more suitable for a real-world application.

Before diving into it, a clarification on what the suitability for a real-world application means. All constellations are technically feasible, and they all provide a decent performance. However, some constellations may be overdesigned or have some limitations that make them less attractive. The goal is to find a constellation that balances the three objectives, as well as other practical considerations.

8

The most important objective is performance, as this defines the purpose of the constellation. Defining the performance requirements is a struggle, as there are no clear standards for GNSS constellations. Each constellation has its own requirements in terms of availability, DOP, accuracy, etc. For this study, the focus has been on the GDOP, a geometric indicator of the constellation's performance. The selection of the maximum 95th percentile GDOP as a metric stems from the fact that it is an indicator of the worst-case performance, while still being robust to outliers. Another metric that has been considered in the analysis but not in the optimisation is the availability, defined as the percentage of time the GDOP is below a certain threshold. This is important to ensure that the constellation can provide a reliable service.

Compared to other GNSS constellations, the availability was not set as a hard requirement. This allows for a more flexible design space, making it a nice-to-have feature. As it will be studied later, the possibility of combining the LEO-PNT constellation with other geostationary constellations can help improve the availability.

Using own simulations, the maximum 95th percentile GDOP of Galileo and GPS were found to be 3.45 and 4.70, respectively. Therefore, a constellation that can match or improve Galileo's performance would be a smart starting point. This is achieved by all constellations except for the cheapest one. On the other hand, the best GDOP constellation is clearly overdesigned, as it provides a performance that is not necessary for most applications. The other three remaining constellations provide a strong performance, with the Galileo trade-offs having slightly better availability, even if the max GDOP is slightly higher compared to the closest to the origin. Therefore, the cheapest and best GDOP constellations are not considered suitable.

A way more relevant aspect is the complexity of the constellation. This is mainly defined by the number of shells, as this increases the launch complexity, satellite design, ground stations, ISL, etc. The two-shell constellations are clearly more complex, which is why they are only better than the single-shell ones for extremely high-performance requirements. The ground stations are especially affected, as the low-inclination shell can only be seen by low-latitude ground stations. This limits the options and may require building new ground stations in remote locations. The ISL is also affected, as the connection is done within shells, not between them. This limits the options for communication, making it necessary to send two different signals to reach both shells. Furthermore, if the low-inclination shell works solely with intra-plane connections, communication is limited to the times when a plane is visible, making it impossible to have a continuous connection.

For the complexity involved and the minor performance improvement, the two-shell constellations are not considered suitable for most applications. The single-shell constellations are much simpler, and they still provide a sufficient performance. With this in mind, the single shell Galileo trade-off and the equally weighted optimum are the most suitable options. Between these two, the contact with the ground stations is practically identical, with the closest to the origin having slightly more contacts due to the larger number of satellites.

The most important feasibility parameters to consider are cost and deployment strategy. The cost is a key parameter, as it defines the budget required to deploy and maintain the constellation. However, the difference between them is not too large (370 M$ USD). The deployment time is also relevant, but to a lesser extent, as it maximises the operational lifetime by a small amount. The difference between the remaining constellations is a bit over two months, which is not too large compared to the total lifetime of the constellation (7 years). Even though the Galileo trade-off is slightly faster, the equally weighted optimum constellation is more organised, having the same launch type every time, which would facilitate planning and logistics, as well as repeatability.

In terms of sustainability-related aspects, such as space debris and EOL disposal, both constellations are practically identical. These parameters are functions of altitude and inclination, and since the two constellations maintain similar values, the results are comparable. Clearly, there will be more collision avoidance manoeuvres in the constellation closest to the origin, as it has more satellites. However, the probability of collision per satellite is the same, and the total number of expected CAMs is only six more over the constellation's lifetime.

The robustness of the system is a parameter where the constellations differ. The closest to the origin constellation has a smaller effect when satellites fail, but a higher probability of them failing compared to the Galileo trade-off constellation. The expected performance loss, as defined in section 7.6, is used here. The results are shown in Table 8.24.

Table 8.24: Expected Performance Loss for Selected Constellations for 0.76% failure rate.

Constellation	**EPL (%)**	**EPL Max GDOP$_{95}$**
Galileo Trade-off	7.3%	+0.25
Equally Weighted Optimum	3.9%	+0.10

The first column shows the expected performance degradation in percentage over the lifetime. The value next to it is the absolute increase in the maximum 95th percentile GDOP. The closest to the origin constellation has a smaller expected performance loss, an indicator of its robustness. On top of this, the performance is already better, so even if the performance degrades, it will still be better than the Galileo trade-off constellation. On top of this, if three satellites fail, the performance of the Galileo trade-off constellation degrades to a point further than GPS's performance, which is not ideal.

A parallel aspect of discussion is the possibility of working with a LEO-PNT as an augmentation system to already existing GNSS constellations. The LEO constellation would provide extra geometry, improving the DOP, faster revisit times, and improved availability at urban canyons and high latitudes [65]. This would allow for a smaller constellation, as the LEO-PNT constellation would not need to provide full coverage, but rather complement the existing systems.

This idea has certain considerations. One of the main improvements of having a LEO-PNT constellation is the improved precise point positioning (PPP) convergence. Ge et al. (2020)[67] proved that this convergence can be done within a minute, rather than the 30 minutes required by traditional GNSS constellations. The first key aspect to consider here is the need for varying inclinations. For a PPP convergence improvement, it was shown that having different inclinations is necessary in order to solve the ambiguities faster in every direction [67]. For the single-shell constellations considered here, the convergence would be fast in the latitude direction because of the polar inclination, but it would be slower in the longitude direction. This could be improved by adding a second shell with a different inclination, but as discussed before, this adds complexity.

Nevertheless, it is important to note that the PPP improvement represents only one of the potential services that a LEO-PNT constellation could provide. By designing the system purely as an augmentation to existing GNSS constellations, the constellation size could indeed be reduced, but this would come at the expense of other capabilities. In particular, the use of additional frequency bands such as C or UHF, which would enable alternative signal types and enhanced robustness, would no longer be justified in a complementary architecture and would thus offer degraded performance. In summary, while the concept of a simplified LEO-PNT augmentation system is appealing, if all objectives want to be met, then it needs to be designed as a standalone system with additional considerations for PPP, rather than as a simplified supplement to existing GNSS constellations.

With this in mind, the remaining constellations were modelled together with the Galileo constellation to see how they would perform together. The results are shown in Table 8.25.

Table 8.25: Combined Performance of Selected Constellations with Galileo

Configuration	Mean GDOP	Max $GDOP_{95}$	Avail. (%)
Galileo Only	1.91	3.44	100.00
Galileo + Galileo Trade-off	0.33	0.35	100.00
Galileo + Equally Weighted Optimum	0.31	0.32	100.00

The combination of the LEO-PNT constellation with Galileo provides a significant improvement in performance. The mean GDOP is reduced by a factor of six, and the maximum 95th percentile GDOP is reduced by a factor of ten. The availability is always met, since Galileo already meets the requirement by itself. When designing for this combination, both constellations are clearly overdesigned, and a smaller constellation could be used. However, this shows the potential of a LEO-PNT constellation to improve the performance of existing GNSS constellations and how some limitations of LEO-PNT constellations, such as the availability at mid-latitudes, can be mitigated by combining them with existing systems.

Based on the previous discussion, the most suitable constellation for a real-world application is the one closest to the origin constellation. It has been shown to have an excellent performance in terms of GDOP and availability. It is more robust against failure, and its limitations at mid-latitudes can be mitigated by combining it with existing GNSS constellations. It is more costly than the Galileo trade-off constellation (+370 M$ USD), representing an additional 12% in cost, but it is also more organised and has a clear deployment strategy without increasing it too much (+2.3 months). The satellite design is feasible, with a reasonable number of CAMs (33.76), and the ground station and ISL performance are robust. If the economic viability can be ensured, this constellation could be a strong candidate for future GNSS applications.

9

Conclusions and Recommendations

This final chapter presents the conclusions drawn from the thesis, starting from the research questions and objectives outlined in chapter 2. It also discusses the study's limitations and provides recommendations for future work in LEO-based PNT systems.

9.1. Research Questions and Objectives

The main objective of the thesis was to assess the feasibility of a LEO-based PNT system that can provide performance comparable to existing GNSS systems, while being cost-effective and leveraging New Space technologies. In order to do so, several research questions were addressed throughout the thesis. The conclusions for each research question are summarised below:

9.1.1. Geometric Performance and Practical Constraints

This subsection addresses the first set of research questions, led by the following main question:

RQ1. How do geometric performance metrics (e.g., DOP, availability) trade off with practical constraints (e.g., cost, deployment time) in a LEO-PNT system designed as an independent GNSS alternative?

The trade-off between geometric performance and practical constraints was investigated through a multi-objective optimisation of Walker constellations. The performance metric used is the maximum 95th percentile GDOP, which evaluates the overall geometric quality of the constellation while being robust to outliers. The feasibility considerations include the orbital perturbations, Δv, satellite mass and volume, launcher fitting, deployment strategy, manufacturing and launch costs, ground segment, inter-satellite links, robustness against failures, space debris, and interaction with Galileo.

RQ1.1: *How do altitude and inclination selection influence both GDOP performance and practical constraints such as orbital lifetime or launch requirements?*

A heuristic analysis demonstrated that in order to have a GDOP < 4 for the entire globe, a minimum inclination of 68°-74° is required, depending on altitude (section 4.1). Optimal values were found to be between 77.5° and 87.5°. Through a sensitivity analysis, it was shown that the inclination is not too sensitive in terms of performance (5.2.2). From a feasibility perspective, polar orbits have a smaller precession rate, leading to a longer deployment time, are more susceptible to space debris, and require high-latitude ground stations.

Through the same heuristic analysis [4.2], the altitude was found to have limits between 700 and 1500 km due to drag and radiation, respectively. Altitude is probably the most influential parameter in the constellation design, as it affects almost all aspects of the mission. A higher altitude improves the geometric performance, reduces the number of satellites required, and increases the coverage time of ground stations. However, it also increases the radiation exposure, the satellite power leading to a higher mass and volume, the ΔV required and the strategy for deployment.

Five repeating ground track orbit scenarios were tested, with approximate altitudes of 700(d), 850(b), 1050(c), 1250(a), and 1450(e) km. The repeatability of the orbits has a positive response in terms of performance, making the system more robust and feasible, improving operations from the ground segment [4.3]. It was pondered whether a higher altitude with fewer satellites or a lower altitude with more satellites would be better. The results showed that in terms of performance, cost, and deployment time, the higher altitudes performed better. It was shown that for the same performance, a constellation at 1450 km would be 33% cheaper and take 33% less time to deploy than one at 700 km.

RQ1.2: *What is the Pareto front between GDOP and the number of satellites, or other relevant design constraints?*

9

The main optimisation objectives were the maximum 95th percentile GDOP, the total cost, and the deployment time. The results show a clear competition between performance and cost or deployment time [8.1]. The clearest trade-off is between performance and cost, since they have the most direct relationship. A better performance requires more satellites and launches, which increases the cost. Usually, the deployment time also increases, but the relation is not as clear. The deployment time works on a mixed continuous (drifting time) and discrete (launch cadence) manner, which creates certain jumps in the Pareto front.

The final comparison, cost vs deployment time, shows a rough positive correlation. Usually, a longer deployment time is related to more launches due to a higher number of satellites, which together increase the cost. Furthermore, the specific altitude case generally constrains the cost and deployment time to a certain region, and as the altitude increases, both cost and deployment time tend to decrease. This reflects how the choice of altitude, launcher capacity, and constellation size jointly shape the Pareto frontier.

RQ1.3: *How does the inclusion of deployment aspects influence constellation selection?*

The inclusion of deployment aspects introduces strong coupling between the constellation geometry and the launcher configuration. The fitting of satellites per launcher directly affects the number of orbital planes that can be populated in each launch, which has a decisive influence on both deployment time and cost. The main factors impacted by these constraints are the number of planes and the total number of satellites.

In the optimisation results, it was observed that configurations enabling the deployment of two planes per launch were generally preferred when feasible. To maximise launcher utilisation, the number of satellites per plane would typically converge to values| slightly below half of the launcher capacity. This demonstrates that launcher capacity and constellation configuration must be optimised together. Notably, state-of-the-art designs identified in literature [8.2] become unfeasible when deployment time is considered, leading to deployment durations of up to 4.3 years. However, the deployment results are highly dependent on the assumed launcher and cadence model, which may evolve with New Space developments.

RQ1.4: *What is the impact of partial constellation failure on LEO-PNT geometrical performance?*

Partial constellation failure represents a significant concern for LEO constellations due to the large number of satellites involved, the harsh space environment, and the New Space approach to satellite design. Even with an optimistic satellite reliability assumption of 99.21%, the analysis revealed that the probability of at least one satellite failure over the constellation's lifetime is substantial, ranging between 55 and 80% [7.6].

The likelihood of multiple failures is also considerable, with probabilities of 20-45% for two failures and 5-20% for three failures depending on the constellation's size. These statistics highlight the importance of designing constellations that can maintain acceptable performance despite partial failures.

The impact of satellite failures on system performance was evaluated using two representative constellations: the equally weighted optimum configuration and the Galileo trade-off constellation. The results demonstrated that performance degradation can be significant. For instance, three satellite failures in the Galileo trade-off constellation resulted in an increase of +1.4 in the maximum 95th percentile GDOP and a substantial reduction in availability (-2.9%) [8.3.3].

To better assess constellation robustness, a new metric called Expected Performance Loss (EPL) was introduced [7.6]. This metric combines the probability of failure with the associated performance degradation, enabling more informed comparisons between different constellation designs and providing better awareness of system robustness characteristics.

RQ1.5: *What considerations would be needed to adapt the independent LEO-PNT system into a Galileo augmentation role?*

A potential adaptation of the constellation to work alongside Galileo was also studied [8.4]. The results show that the performance of the combined system is significantly improved, with a mean GDOP reduced by a factor of six and a maximum 95th percentile GDOP reduced by a factor of ten. However, the improvement is not worth the excessive size of the constellation. It was also mentioned that the system would augment the existing signals, but for the new signals, it needs to function as an independent system instead.

9.1.2. Influence of Walker Configuration Variations

Within the Walker constellations, there are five variations to consider: the type of Walker constellation (Delta vs Star), the number of shells, and within each the total number of satellites (T), the number of planes (P) and the relative spacing between planes (F). These parameters led to the following question:

How do variations within Walker constellation configurations affect navigation performance and system complexity?

RQ2.1: *How do specific Walker constellation parameters affect navigation performance metrics such as GDOP and availability?*

Walker Star constellations generally provide better GDOP and efficiency than Walker Delta when the entire globe is considered, as they avoid unnecessary redundancy and distribute satellites more evenly [5.2.2]. Star constellations allow slightly faster deployment, indirectly improving service continuity. From a purely geometrical point of view, a single shell constellation is generally preferred as long as the maximum 95th percentile GDOP requirement is above 2.5 [6.3.2].

9

The addition of a second shell at low inclinations can improve the overall performance, as it was seen in the comparison between the Galileo trade-off constellations [8.3.3, 8.3.4]. It can also have large benefits on other performance aspects not studied in this thesis, such as precise point positioning (PPP) convergence time [8.4]. However, it comes with an increase in complexity, and usually in cost and deployment time.

Increasing the total number of satellites (T) generally improves GDOP and robustness, but with diminishing returns after a certain point. The Pareto analysis shows optimal ranges between 119 and 354 satellites for the studied configurations [8.1.2]. The number of planes (P) tends to be less than the number of satellites per plane. This occurs because in Walker Star constellations, the planes are spaced over 180°, while the satellites per plane are spaced over 360°, leading to a more efficient distribution. The relative spacing parameter (F) was not modified, but rather a theoretical optimum was used [4.4]. It was shown that this optimum does not always match the best performance, but the differences are minor.

RQ2.2: *What qualitative implications do these configurations have for ground segment operations?*

The introduction of multiple shells increases system complexity and imposes additional requirements on the ground segment. A two-shell configuration typically requires a low-latitude and high-latitude ground station to maintain adequate coverage and data downlink capacity [8.4]. Moreover, multi-shell architectures lead to more intricate tracking and control operations, as the orbital planes differ in inclination and altitude. This also affects deployment logistics and coordination between ground stations.

In terms of deployment, the number of planes (P) plays a central role in determining the overall cost and time. Reducing the total number of planes or maximising the number of planes deployed per launch is key to achieving shorter deployment durations [7.3]. The manufacturing of satellites remains the primary cost driver, accounting for 83-87% of the total cost [8.3], further underlining the operational benefits of configurations with fewer satellites.

RQ2.3: *How do these configurations influence inter-satellite link feasibility?*

The inter-satellite link (ISL) feasibility is influenced by both the constellation geometry and the adopted attitude control law. Walker Star constellations are generally more favourable for ISL implementation due to smaller inter-plane spacing [7.7]. The relative spacing parameter (F) also plays a role: increasing F increases the relative phasing between planes, which reduces the azimuth angle between satellites in adjacent planes and improves the likelihood of maintaining line-of-sight connections [7.7.1].

However, the inclusion of multiple shells can complicate ISL feasibility, particularly when the lower shell follows a Walker Delta pattern. Additionally, attitude control strategies significantly constrain ISL performance. If the satellites follow a yaw-steering law relative to the Sun, line-of-sight loss will occur due to rotations of up to ±90° around the cross-track axis, causing intermittent ISL disconnections. As the constellation precesses, all satellites eventually experience these orientations, suggesting that an alternative attitude strategy should be considered if ISL continuity is required [7.7.1].

9.1.3. SUSTAINABILITY CONSIDERATIONS IN CONSTELLATION DESIGN

The final set of questions concerns the sustainability aspect and how it can be included in the constellation design and optimisation process. The main question is:

RQ3. How can sustainability constraints be included in the LEO-PNT constellation design and optimisation process?

In order to consider sustainability, two main aspects were studied: space debris and end-of-life disposal strategies.

RQ3.1: *What is the risk of collision for optimal constellations?*

A space debris analysis was performed to understand the space debris environment and the collision risk for the constellation [7.4]. The results show debris density peaks at 850 km and 1500 km. New large constellations are aiming for 800 and 1200 km altitudes, which could change the environment. Nevertheless, at the current state, the overall collision risk is low, especially at the optimal altitudes (~ 1450 km), with an expected 20% chance of performing a Collision Avoidance Manoeuvre (CAM) per satellite over the constellation's lifetime [8.3]. These manoeuvres also translate to a minor requirement in the Δv budget, with an expected 0.001 m/s. The main consequence of a manoeuvre is the temporary service interruption.

RQ3.2: *How can the disposal strategy be implemented in the optimal constellation?*

Post-mission disposal compliance is achieved through controlled reentry within 5 years after end-of-life [7.2.1]. This requirement is consistently achievable, needing between 45 and 430 m/s of Δv, depending on orbital altitude. The process utilises electric propulsion systems. Altitude serves as the primary driver for propellant requirements, with higher orbits demanding greater Δv. While increased inclination also increases fuel needs, its impact is secondary. The disposal strategy involves lowering the perigee altitude, allowing atmospheric drag to complete the deorbiting process. This consideration is integrated into the optimisation framework through approximation of disposal manoeuvre Δv requirements, which influence total spacecraft mass, volume, and mission cost.

9.2. LIMITATIONS AND FUTURE WORK

This thesis presented a comprehensive analysis of the feasibility of a LEO-PNT constellation, addressing several gaps in the literature. However, there are still limitations and areas for future research that could further enhance the understanding and design of such systems.

The performance metric adopted in this study is specific to the selected case. Different studies use varying approaches, from visibility criteria and DOP metrics to full signal propagation models for computing position error. Each yields slightly different results, and the choice should align with mission requirements. Future work could extend the performance formulation to combine multiple objectives or regional constraints, or to include aspects beyond geometric performance.

The feasibility metrics used are simplified and partly based on empirical formulas. The cost model, developed in 2014, does not fully capture the economic dynamics of the New Space era. Although newer models exist, they are not open source. Thanks to the simulator's modularity, the cost function could be replaced by more accurate or mission-specific data. Similarly, satellite parameters such as mass, volume, and power rely on historical correlations that carry significant variance. Future work should include a detailed satellite design, integrating more realistic subsystem models and a dedicated radiation study to improve the accuracy of both cost and launcher feasibility estimates.

The launcher used, the manufacturing, and launch cadence are all specific to this study and to a European context. The cadence models are assumptions based on available data but may not reflect future market conditions. Future work could explore alternative launch vehicles, including emerging New Space options. These changes would probably have a significant impact on the deployment time and cost results, leading to different optimal configurations.

The orbital mechanics in the simulator assume Keplerian motion with J_2 perturbation, which is an acceptable simplification for early-stage design but limits long-term accuracy. A higher-fidelity propagator would allow for a more detailed analysis of the constellation's evolution and its influence on performance and feasibility. Likewise, ΔV estimations were based on averaged solar cycle effects and safety factors, and the conversion to fuel mass assumed constant thrust and specific impulse. Future work should model propulsion systems more precisely, accounting for time-varying performance and realistic operational conditions.

The design space explored in this thesis focused on Walker constellations, inspired by previous research. However, other architectures, such as Flower constellations, could offer greater flexibility and potentially improved performance. The inclusion of non-zero eccentricity orbits might enhance regional coverage, though it introduces additional challenges such as variable signal strength and beam pointing. Further exploration of the Walker F parameter and a finer sampling of altitude levels could yield deeper insights into constellation performance and ISL feasibility. Performing a deeper sensibility analysis could also help identify critical design parameters and their impact on overall system performance.

The optimisation employed a simple Genetic Algorithm for the SOO and NSGA-III for the MOO, both commonly used in the literature. To constrain the study's scope, algorithm comparisons were not performed. However, future work could include benchmarking against alternative methods such as MOPSO or PSO to evaluate their suitability for this problem. A more systematic tuning of hyperparameters would also improve optimisation consistency and performance.

From a regulatory standpoint, this work only considered basic aspects of debris mitigation and signal usage. The legal and policy environment for LEO constellations is complex and rapidly evolving. Future research should include a detailed review of regulations related to frequency allocation, coordination among operators, and compliance with sustainability and demisibility requirements. Integrating these constraints into the system design would ensure greater realism and relevance.

Finally, at the system level, the potential augmentation of Galileo by a LEO-PNT constellation was only briefly discussed. A detailed assessment of the technical and operational synergies between both systems is needed to define how they can complement each other effectively. Extending the simulator to include signal propagation and processing would allow computation of realistic positioning errors, the ultimate performance measure.

Furthermore, several operational aspects require deeper investigation. The ISL implementation remains a major challenge, as the current analysis shows that maintaining a yaw-steering attitude conflicts with continuous ISL links. Future studies should explore alternative attitude strategies, intermittent ISL connections, or more complex inter-satellite link topologies. The ground segment analysis was also simplified; a dedicated study on ground station requirements, locations, and operations would improve system-level feasibility assessment. Additionally, spares were not included in the optimisation, though they play a key role in overall constellation robustness and system sustainability. Their inclusion in future analyses would provide a more comprehensive evaluation of system-wide resilience.

9.3. FINAL REMARKS

This thesis aimed to develop a methodology for designing and optimising LEO-PNT constellations that is fast, modular, and adaptable to diverse mission requirements. A significant knowledge gap existed in the literature regarding the practical feasibility of such missions. This work addressed this gap by integrating both performance metrics and practical constraints, while conducting parametric analyses to understand the influence of various design parameters.

The results demonstrate that a LEO-PNT constellation is indeed feasible and capable of delivering performance comparable to existing GNSS systems at reduced cost while leveraging New Space technologies. Several feasible constellations were identified and compared, ranging from cost-effective solutions to high-performance configurations, demonstrating the trade-offs between geometric performance, deployment time, and mission cost. All research questions have been successfully addressed, and the initial objective has been fulfilled. This work establishes a foundation for future studies, ultimately contributing to the advancement of global navigation systems.

Bibliography

[1] European Space Agency (ESA) (2011) *Antennas - Navipedia*, Edited by GMV. Accessed: 2025-09-04, URL: https://gssc.esa.int/navipedia/index.php/Antennas.

[2] Dawn Aerospace (2024) *A Comparison of Electric and Chemical Propulsion in the Era of Low Launch Costs*, Accessed: 2025-08-25, URL: https://www.dawnaerospace.com/latest-news/electricorchemical.

[3] Aerospacelab (2024) *Aerospacelab breaks ground on Europe's largest satellite manufacturing facility*, Accessed: 2025-09-08, URL: https://www.aerospacelab.com/blog/press-releases-1/aerospacelab-breaks-ground-on-europe-s-largest-satellite-manufacturing-facility-20.

[4] European Space Agency (2011) *Galileo Performances - Navipedia*, URL: https://gssc.esa.int/navipedia/index.php/Galileo_Performances.

[5] European Space Agency (2011) *GPS Performances - Navipedia*, URL: https://gssc.esa.int/navipedia/index.php/GPS_Performances#cite_note-SPS-Standard-1.

[6] European Space Agency (2020) *Types of orbits*, Accessed: 2025-03-18, URL: https://www.esa.int/Enabling_Support/Space_Transportation/Types_of_orbits#LEO.

[7] European Space Agency (2023) *ESA Space Debris Mitigation Requirements*, tech. rep., URL: https://technology.esa.int/upload/media/ESA-Space-Debris-Mitigation-Requirements-ESSB-ST-U-007-Issue1.pdf.

[8] European Space Agency *Galileo satellites*, URL: https://www.esa.int/Applications/Satellite_navigation/Galileo/Galileo_satellites.

[9] Amazon (2023) *Amazon's Project Kuiper completes successful test of space lasers*, Accessed: 2025-09-25, URL: https://www.aboutamazon.com/news/innovation-at-amazon/amazon-project-kuiper-oisl-space-laser-december-2023-update.

[10] Jonathan Amos (2018) *Elon Musk's huge Falcon Heavy rocket set for launch*, Accessed: 2025-10-29, BBC News, URL: https://www.bbc.com/news/science-environment-42950957.

[11] Nalineekumari Arasavali, Sasibhushana Rao Gottapu, and N Ashok Kumar (2018) "GDOP Analysis with Optimal Satellites Using GA for Southern Region of Indian Subcontinent", in: *Procedia Computer Science* 143 (), pp. 303–308, ISSN: 18770509, DOI: 10.1016/j.procs.2018.10.400.

[12] ArianeGroup (2024) *Ariane 6 inaugural launch - mission successful*, Accessed: 2025-09-12, URL: https://ariane.group/en/news/ariane-6-inaugural-launch-mission-successful/.

[13] Arianespace (2021) *ARIANE 6 USER'S MANUAL ISSUE 2 REVISION 0*, tech. rep., Arianespace, URL: https://ariane.group/app/uploads/sites/4/2024/10/Mua-6_Issue-2_Revision-0_March-2021.pdf.

[14] Arianespace (2025) *Vega C: the lightweight, high-performance launcher by Arianespace*, Accessed: 2025-08-28, Arianespace, URL: https://www.arianespace.com/vega-c/.

[15] David Arnas, Daniel Casanova, and Eva Tresaco (2018) "2D Necklace Flower Constellations", in: *Acta Astronautica* 142 (), pp. 18–28, ISSN: 00945765, DOI: 10.1016/j.actaastro.2017.10.017, URL: https://linkinghub.elsevier.com/retrieve/pii/S0094576517302801.

[16] David Arnas et al. (2017) "3-Dimensional Necklace Flower Constellations", in: *Celestial Mechanics and Dynamical Astronomy* (), DOI: 10.1007/s10569-017-9789-1.

[17] Martín E. Avendaño, Jeremy J. Davis, and Daniele Mortari (2013) "The 2-D lattice theory of Flower Constellations", in: *Celestial Mechanics and Dynamical Astronomy* 116 (4), pp. 325–337, ISSN: 0923-2958, DOI: 10.1007/s10569-013-9493-8, URL: http://link.springer.com/10.1007/s10569-013-9493-8.

[18] Javier Pérez Bartolomé et al. (2015) "Overview of Galileo System", in: pp. 9–33, DOI: 10.1007/978-94-007-1830-2_2.

[19] Robert A. Bettinger and Jonathan T. Black (2014) "Mathematical relation between the Hohmann transfer and continuous-low thrust Maneuvers", in: *Acta Astronautica* 96 (1), pp. 42–44, ISSN: 0094-5765, DOI: 10.1016/J.ACTAASTRO.2013.11.020, URL: https://www.sciencedirect.com/science/article/pii/S0094576513004232.

[20] John Betz (2010) *Link Budgets*, tech. rep., International Committee on GNSS, URL: https://www.gps.gov/multimedia/presentations/2010/10/ICG/betz.pdf.

[21] John W. Betz (2016) *Engineering satellite-based navigation and timing: Global Navigation Satellite Systems, signals, and receivers*, Wiley: IEEE.

[22] J. Blank and K. Deb (2020) "pymoo: Multi-Objective Optimization in Python", in: *IEEE Access* 8 (), pp. 89497–89509.

[23] B. R. Bowring (1976) "Transformation from Spatial to Geographical Coordinates", in: *Survey Review* 23 (181), pp. 323–327, ISSN: 17522706, DOI: 10.1179/SRE.1976.23.181.323, URL: https://www.tandfonline.com/doi/abs/10.1179/sre.1976.23.181.323.

[24] Andrea Capannolo et al. (2023) "The space environment", in: *Modern Spacecraft Guidance, Navigation, and Control: From System Modeling to AI and Innovative Applications* (), pp. 77–129, DOI: 10.1016/B978-0-323-90916-7.00003-2, URL: https://www.sciencedirect.com/science/article/pii/B9780323909167000032.

[25] Daniel Casanova, Martín Avendaño, and Daniele Mortari (2014) "Seeking GDOP-optimal Flower Constellations for global coverage problems through evolutionary algorithms", in: *Aerospace Science and Technology* 39 (), pp. 331–337, ISSN: 12709638, DOI: 10.1016/j.ast.2014.09.017, URL: https://linkinghub.elsevier.com/retrieve/pii/S1270963814001989.

[26] Kaan Çelikbilek, Elena Simona Lohan, and Jaan Praks (2025) "Optimization of a LEO-PNT Constellation: Design Considerations and Open Challenges", in: *International Journal of Satellite Communications and Networking* (), ISSN: 15420981, DOI: 10.1002/sat.1555.

[27] Navigation Center *GPS Constellation*, URL: https://www.navcen.uscg.gov/gps-constellation.

[28] Aizaz U. Chaudhry and Halim Yanikomeroglu (2021) "Laser Intersatellite Links in a Starlink Constellation: A Classification and Analysis", in: *IEEE Vehicular Technology Magazine* 16 (2), pp. 48–56, ISSN: 15566080, DOI: 10.1109/MVT.2021.3063706.

[29] Guoquan Chen et al. (2024) "Lunar Communication-Navigation Integrated Constellation: Frozen Orbit-Based HyInc Walker", in: *2024 IEEE Wireless Communications and Networking Conference (WCNC)*, IEEE, pp. 1–6, ISBN: 979-8-3503-0358-2, DOI: 10.1109/WCNC57260.2024.10570962, URL: https://ieeexplore.ieee.org/document/10570962/.

[30] Stephen Clark (2025) *China's Guowang Megaconstellation is More Than Another Version of Starlink*, Accessed: 2025-10-07, URL: https://arstechnica.com/space/2025/08/china-may-have-taken-an-early-lead-in-the-race-for-a-military-megaconstellation/.

[31] Maurice Clerc (2008) "Why does it work?", in: *International Journal of Computational Intelligence Research* 4.2 (), pp. 79–91.

[32] Maurice Clerc and James Kennedy (2002) "The particle swarm—explosion, stability, and convergence in a multi-dimensional complex space", in: *IEEE Transactions on Evolutionary Computation* 6.1 (), pp. 58–73.

[33] Carlos A. Coello Coello and Manuel Reyes Sierra (2004) "A study of the parallelization of a coevolutionary multi-objective evolutionary algorithm", in: *Proceedings of MICAI*, vol. 2972, Lecture Notes in Computer Science, Springer, pp. 688–697.

[34] Continuum Analytics (2012) *Numba: A LLVM-based Python JIT Compiler*, URL: https://numba.pydata.org/.

[35] Stefania Cornara et al. (1999) "Satellite Constellation Launch, Deployment, Replacement and End-of-Life Strategies", in: *13 th Annual AIAA/USU Conference on Small Satellites* ().

[36] Howard D. Curtis (2013) *Orbital Mechanics for Engineering Students*, 3rd, Oxford: Butterworth-Heinemann, DOI: 10.1016/B978-0-08-097747-8.00006-2.

[37] Jeremy J. Davis, Martín E. Avendaño, and Daniele Mortari (2013) “The 3-D lattice theory of Flower Constellations”, in: *Celestial Mechanics and Dynamical Astronomy* 116 (4), pp. 339–356, ISSN: 0923-2958, DOI: 10.1007/s10569-013-9494-7, URL: http://link.springer.com/10.1007/s10569-013-9494-7.

[38] Kalyanmoy Deb and Himanshu Jain (2014) “An evolutionary many-objective optimization algorithm using reference-point-based nondominated sorting approach, Part I: Solving problems with box constraints”, in: *IEEE Transactions on Evolutionary Computation* 18 (4), pp. 577–601, ISSN: 1089778X, DOI: 10.1109/TEVC.2013.2281535.

[39] Kalyanmoy Deb, Karthik Sindhya, and Tatsuya Okabe (2007) “Self-adaptive simulated binary crossover for real-parameter optimization”, in: *Proceedings of GECCO 2007: Genetic and Evolutionary Computation Conference* (), pp. 1187–1194, DOI: 10.1145/1276958.1277190, URL: https://dl.acm.org/doi/pdf/10.1145/1276958.1277190.

[40] Kalyanmoy Deb et al. (2002) “A fast and elitist multiobjective genetic algorithm: NSGA-II”, in: *IEEE Transactions on Evolutionary Computation* 6 (2), pp. 182–197, ISSN: 1089778X, DOI: 10.1109/4235.996017.

[41] Kalyanmoy. Deb (2001) *Multi-objective optimization using evolutionary algorithms*, John Wiley & Sons, Ltd, p. 479, ISBN: 978-0-471-87339-6, URL: https://www.wiley.com/en-us/Multi-Objective+Optimization+using+Evolutionary+Algorithms-p-9780471873396.

[42] TOI Science Desk (2025) *SpaceX gives rare look inside Starlink factory: 70 satellites a week and mini lasers*, Accessed: 2025-09-08, URL: https://timesofindia.indiatimes.com/science/spacex-gives-rare-look-inside-starlink-factory-70-satellites-a-week-and-mini-lasers/articleshow/123548215.cms.

[43] ECSS Secretariat (2020) *ECSS-E-ST-10-04C REv.1*, tech. rep., ECSS, URL: https://ecss.nl/wp-content/uploads/2020/07/ECSS-E-ST-10-04C-Rev.1(15June2020).pdf.

[44] Peter Ehret et al. (2005) “L-band TWTAs for navigation satellites”, in: *IEEE Transactions on Electron Devices* 52 (5), pp. 679–684, ISSN: 00189383, DOI: 10.1109/TED.2005.846355.

[45] ENPULSION (2024) *ENPULSION NANO R³ Propulsion System*, Accessed: 2025-09-01, URL: https://satsearch.co/products/enpulsion-enpulsion-nano-r3.

[46] European Space Agency (2011) *Galileo Space Segment*, ed. by GMV, Accessed: 2025-10-06, URL: https://gssc.esa.int/navipedia/index.php/Galileo_Space_Segment.

9

[47] European Space Agency (2021) *Space Debris FAQ: Frequently asked questions*, Accessed: 2025-08-27, ESA, URL: https://www.esa.int/Space_Safety/Space_Debris/Space_Debris_FAQ_Frequently_asked_questions.

[48] European Space Agency (2024) *ARES - Assessment of Risk Event Statistics (DRAMA Tool Suite)*, Developed by IRAS/TUBS, DEIMOS Space, HTG, etamax space GmbH, Belstead Research Limited. Accessed: 2025-08-25, URL: https://sdup.esoc.esa.int/drama/.

[49] European Space Agency (2024) *CROC - Cross Section of Complex Bodies (DRAMA Tool Suite)*, Developed by IRAS/TUBS, DEIMOS Space, HTG, etamax space GmbH, Belstead Research Limited. Accessed: 2025-08-25, URL: https://sdup.esoc.esa.int/drama/.

[50] European Space Agency (2024) *MASTER - Meteoroid and Space Debris Terrestrial Environment Reference*, Developed by IRAS/TUBS under ESA contract. Accessed: 2025-08-25, URL: https://sdup.esoc.esa.int/master/.

[51] European Space Agency (2024) *OSCAR - Orbital SpaceCraft Active Removal (DRAMA Tool Suite)*, Developed by IRAS/TUBS, DEIMOS Space, HTG, etamax space GmbH, Belstead Research Limited. Accessed: 2025-08-25, URL: https://sdup.esoc.esa.int/drama/.

[52] European Space Agency (2025) *Ariane 6 Overview*, Accessed: 2025-08-28, ESA, URL: https://www.esa.int/Enabling_Support/Space_Transportation/Launch_vehicles/Ariane_6_overview.

[53] European Space Agency (2025) *Galileo IOV Ground Stations*, Overview of global Galileo ground stations including location, type, and hosting organizations. Accessed: 2025-09-29, URL: https://www.esa.int/Applications/Satellite_navigation/Galileo_IOV_Ground_Stations.

[54] European Space Agency (2025) *SPENVIS: Space Environment Information System*, URL: https://www.spenvis.oma.be/intro.php.

[55] European Space Agency (2025) *The solar cycle, a heartbeat of stellar energy*, Accessed: 2025-10-01, URL: https://www.esa.int/Science_Exploration/Space_Science/The_solar_cycle_a_heartbeat_of_stellar_energy.

[56] EUSPA (2024) *EUSPA EO and GNSS Market Report*, tech. rep., EUSPA, DOI: 10.2878/73092.

[57] EUSPA *Constellation Information | European GNSS Service Centre (GSC)*, URL: https://www.gsc-europa.eu/system-service-status/constellation-information.

[58] Eutelsat Communications SA (2025) *High-speed, Low-latency LEO Satellite | Eutelsat*, Accessed: 2025-10-07, URL: https://www.eutelsat.com/satellite-network/oneweb-leo-constellation.

[59] Exotrail (2024) *spaceware™ Mini M Thruster*, Accessed: 2025-09-01, URL: https://satsearch.co/products/exotrail-spaceware-mini-m-thruster.

9

[60] Daniele Ferrara et al. (2025) "New Space Engineering Design: Characterization of Key Drivers", in: *Applied Sciences* 15 (15), p. 8138, ISSN: 2076-3417, DOI: 10.3390/APP15158138, URL: https://www.mdpi.com/2076-3417/15/15/8138/htm%20https://www.mdpi.com/2076-3417/15/15/8138.

[61] Space Florida (2016) *Space Florida Announces OneWeb Satellites To Build Manufacturing Facility At Cape Canaveral Spaceport*, Accessed: 2025-09-08, URL: https://www.spaceflorida.gov/news/space-florida-announces-oneweb-satellites-to-build-manufacturing-facility-at-cape-canaveral-spaceport.

[62] Fluxim AG (2025) *Highest Perovskite Solar Cell Efficiencies (2025 Update)*, Accessed: 2025-08-26, URL: https://www.fluxim.com/research-blogs/perovskite-silicon-tandem-pv-record-updates.

[63] Rasmus Flytkjær et al. (2023) *The economic impact on the UK of a disruption to GNSS*, tech. rep., London Economics, URL: www.londoneconomics.co.uk..

[64] Jeff Foust (2025) *Arianespace plans five Ariane 6 launches in 2025, primarily in the second half of the year*, Accessed: 2025-09-08, URL: https://spacenews.com/arianespace-plans-five-ariane-6-launches-in-2025-primarily-in-the-second-half-of-the-year/.

[65] FrontierSI (2024) "State of the Market Report, Low Earth Orbit Positioning Navigation and Timing - 2024 Edition", in: (), URL: https://frontiersi.com.au/wp-content/uploads/2025/01/FrontierSI-State-of-Market-Report-LEO-PNT-2024-Edition-v1.1.pdf.

[66] Michael P Gallaher (2019) *Economic Benefits of the Global Positioning System (GPS)*, tech. rep., RTI International, URL: www.rti.org.

[67] Haibo Ge et al. (2020) "LEO constellation optimization for LEO enhanced global navigation satellite system (LeGNSS)", in: *Advances in Space Research* 66 (3), pp. 520–532, ISSN: 18791948, DOI: 10.1016/j.asr.2020.04.031.

[68] GMV (2011) *Galileo Ground Segment*, Edited by GMV. Last updated 20 October 2022. Accessed: 2025-09-29, URL: https://gssc.esa.int/navipedia/index.php/Galileo_Ground_Segment.

[69] Inside GNSS (2010) *Measuring GNSS Signal Strength*, URL: https://insidegnss.com/measuring-gnss-signal-strength/?utm_source=chatgpt.com.

[70] Safran Group (2024) *PPSX00, Hall Effect Thruster*, Accessed: 2025-08-25, URL: https://www.safran-group.com/products-services/ppsrx00-stationary-plasma-thruster.

[71] Meiqian Guan et al. (2020) "Optimal walker constellation design of LEO-based global navigation and augmentation system", in: *Remote Sensing* 12 (11), ISSN: 20724292, DOI: 10.3390/rs12111845.

[72] Jikang Gui et al. (2023) “A Novel Analytical Method for Designing Hybrid Mega Satellite Constellations”, in: *2023 IEEE 23rd International Conference on Communication Technology (ICCT)*, IEEE, pp. 1185–1190, ISBN: 979-8-3503-2595-9, DOI: 10.1109/ICCT59356.2023.10419504, URL: https://ieeexplore.ieee.org/document/10419504/.

[73] Yi Han et al. (2021) “LEO navigation augmentation constellation design with the multi-objective optimization approaches”, in: *Chinese Journal of Aeronautics* 34 (4), pp. 265–278, ISSN: 10009361, DOI: 10.1016/j.cja.2020.09.005.

[74] Jacob Kjærsgaard Hansen (2025) *SpaceX: Launch cadence*, Accessed: 2025-09-08, URL: https://observablehq.com/@jacobkjaersgaardhansen/spacex-launch-cadence.

[75] Lina He et al. (2013) “Experimental Study on the Precise Orbit Determination of the BeiDou Navigation Satellite System”, in: *Sensors (Basel, Switzerland)* 13 (), pp. 2911–28, DOI: 10.3390/s130302911.

[76] M. Heikkinen (1982) “Geschlossene formeln zur berechnung räumlicher geodätischer koordinaten aus rechtwinkligen koordinaten”, in: *Z. Vermess* (), pp. 207–211.

[77] John H. Holland (1975) *Adaptation in natural and artificial systems : an introductory analysis with applications to biology, control, and artificial intelligence*, University of Michigan Press, viii, 183 pages : ISBN: 0472084607, URL: http://mitpress.mit.edu/catalog/item/default.asp?ttype=2&tid=8929.

[78] Akram Al-Hourani (2021) “Optimal Satellite Constellation Altitude for Maximal Coverage”, in: *IEEE Wireless Communications Letters* 10 (7), pp. 1444–1448, ISSN: 21622345, DOI: 10.1109/LWC.2021.3069751.

[79] InertialLabs (2024) *What are the limitations of GNSS?*, URL: https://inertiallabs.com/what-are-the-limitations-of-gnss/?utm_source=chatgpt.com.

[80] Oguz Kagan Isik et al. (2020) “Integrity Analysis for GPS-Based Navigation of UAVs in Urban Environment”, in: *Robotics 2020, Vol. 9, Page 66* 9 (3), p. 66, ISSN: 2218-6581, DOI: 10.3390/ROBOTICS9030066, URL: https://www.mdpi.com/2218-6581/9/3/66/htm%20https://www.mdpi.com/2218-6581/9/3/66.

[81] Taitus Software Italia *Flower constellation*, URL: https://help.taitussoftware.com/SaVoir/help/content/6.advanced/constellations/flower/flower.htm.

[82] Farha Jahanb (2016) “Implementation of GNSS/GPS Navigation and its Attacks in UAVSim Testbed”, PhD thesis, University of Toledo.

[83] Andrew Jones (2024) *Chinese Megaconstellation Launch Creates Field of Space Debris*, Accessed: 2025-10-07, URL: https://spacenews.com/chinese-megaconstellation-launch-creates-field-of-space-debris/.

[84] Kamarul Azhar Kamarudin and Iskandar Abdul Hamid (2017) "Effect of High Velocity Ballistic Impact on Pretensioned Carbon Fibre Reinforced Plastic (CFRP) Plates", in: *IOP Conference Series: Materials Science and Engineering* 165 (1), p. 012005, ISSN: 1757-899X, DOI: 10.1088/1757-899X/165/1/012005, URL: https://iopscience.iop.org/article/10.1088/1757-899X/165/1/012005%20https://iopscience.iop.org/article/10.1088/1757-899X/165/1/012005/meta.

[85] Elliott D Kaplan and C Hegarty (2006) *Understanding GPS: Principles and applications*, 2nd, Artech House, ISBN: 1580538940.

[86] Yasin Karatas and Fuat Ince (2016) "Fuzzy expert tool for small satellite cost estimation", in: *IEEE Aerospace and Electronic Systems Magazine* 31 (5), pp. 28–35, ISSN: 08858985, DOI: 10.1109/MAES.2016.140210.

[87] Donald J. Kessler and Burton G. Cour-Palais (1978) "Collision Frequency of Artificial Satellites: The Creation of a Debris Belt", in: *J Geophys Res* 83 (A6), pp. 2637–2646, ISSN: 0148-0227, DOI: 10.1029/JA083IA06P02637.

[88] Nadim Khairallah and Zaher M. Kassas (2022) "An Interacting Multiple Model Estimator of LEO Satellite Clocks for Improved Positioning", in: *IEEE Vehicular Technology Conference* 2022-June (), ISSN: 15502252, DOI: 10.1109/VTC2022-SPRING54318.2022.9860828.

[89] Nadim Khairallah and Zaher M. Kassas (2024) "Ephemeris Tracking and Error Propagation Analysis of LEO Satellites With Application to Opportunistic Navigation", in: *IEEE Transactions on Aerospace and Electronic Systems* 60 (2), pp. 1242–1259, ISSN: 15579603, DOI: 10.1109/TAES.2023.3325797.

[90] Lawrence A. Klein (2017) "Alternative sources of navigation and traffic flow data", in: *ITS Sensors and Architectures for Traffic Management and Connected Vehicles*, CRC Press, ISBN: 9781351800969, DOI: 10.1201/9781315206905/SENSORS-ARCHITECTURES-TRAFFIC-MANAGEMENT-CONNECTED-VEHICLES-LAWRENCE-KLEIN/ACCESSIBILITY-INFORMATION, URL: https://www.taylorfrancis.com/books/mono/10.1201/9781315206905/sensors-architectures-traffic-management-connected-vehicles-lawrence-klein.

[91] Kongsberg Gruppen (2014) *On Board the Galileo*, Accessed: 2025-08-29, Kongsberg Gruppen, URL: https://www.kongsberg.com/newsroom/stories/2014/9/board-galileo/.

[92] Sharbel Kozhaya, Joe Saroufim, and Zaher M. Kassas (2025) "Unveiling Starlink for PNT", in: *NAVIGATION: Journal of the Institute of Navigation* 72 (1), ISSN: 0028-1522, DOI: 10.33012/NAVI.685, URL: https://navi.ion.org/content/72/1/navi.685%20https://navi.ion.org/content/72/1/navi.685.abstract.

[93] Jack Kuhr (2025) *Kuiper Economics, Demand, and Regulatory Hurdles*, LinkedIn post. Accessed: 2025-08-25, URL: https://www.linkedin.com/posts/jack-kuhr-ab9a945b_kuiper-economics-demand-and-regulatory-activity-7323802831046500352-IekV/.

[94] Erik Kulu (2021) "Satellite Constellations-2021 Industry Survey and Trends", in: *Small Satellite Conference* (), URL: https://digitalcommons.usu.edu/smallsat/2021/all2021/218/.

[95] Stanford NAV Lab (2024) *gnss_lib_py: Open-source GNSS Library*, URL: https://github.com/Stanford-NavLab/gnss_lib_py.

[96] U.S. Bureau of Labor Statistics (2025) *Producer Price Indexes*, Accessed: 2025-09-12, URL: https://www.bls.gov/ppi/.

[97] Alyssa Lafleur (2025) *Top 10 Rocket Launch Companies To Look For in 2024*, Accessed: 2025-08-28, Space Insider, URL: https://spaceinsider.tech/2023/01/16/rocket-launch-companies/#:~:text=Read%20also:%20Top%206%20Rocket,cost%20of%20access%20to%20space..

[98] Land Information New Zealand (2025) *World Geodetic System 1984 (WGS84)*, Accessed: 2025-10-01, URL: https://www.linz.govt.nz/guidance/geodetic-system/coordinate-systems-used-new-zealand/geodetic-datums/world-geodetic-system-1984-wgs84.

[99] Thomas J. Lang and William S. Adams (1997) "A Comparison of Satellite Constellations for Continuous Global Coverage", in: *Mission Design & Implementation of Satellite Constellations*, pp. 51–62, DOI: 10.1007/978-94-011-5088-0_5.

[100] Israel Leyva-Mayorga et al. (2022) "NGSO Constellation Design for Global Connectivity", in: (), DOI: 10.48550/arXiv.2203.16597.

[101] Xingxing Li et al. (2019) "LEO constellation-augmented multi-GNSS for rapid PPP convergence", in: *Journal of Geodesy* (), DOI: 10.1007/s00190-018-1195-2.

[102] Elena Simona Lohan and Kaan Çelikbilek (2024) "On the Impact of the Number of the Constellation Shells on Standalone LEO-PNT Positioning Metrics", in: *2024 36th Conference of Open Innovations Association (FRUCT)*, IEEE, pp. 353–360, ISBN: 978-952-65246-2-7, DOI: 10.23919/FRUCT64283.2024.10749954, URL: https://ieeexplore.ieee.org/document/10749954/.

[103] R. David Luders (1961) "Satellite Networks for Continuous Zonal Coverage", in: *ARS Journal* 31 (2), pp. 179–184, ISSN: 1936-9972, DOI: 10.2514/8.5422.

[104] Fujian Ma et al. (2020) "Hybrid constellation design using a genetic algorithm for a LEO-based navigation augmentation system", in: *GPS Solutions* 24 (2), p. 62, ISSN: 1080-5370, DOI: 10.1007/s10291-020-00977-0, URL: http://link.springer.com/10.1007/s10291-020-00977-0.

[105] Eric Mahr and Greg Richardson (2003) "Development of the Small Satellite Cost Model (SSCM) Edition 2002", in: *Greg Richardson Senior Member of the Technical Staff Gregory.G.Richardson@aero.org* (310), pp. 336–6791.

[106] Lorenzo Marchionne et al. (2023) "Striking a Balance: Performance and Cost Optimization of LEO-PNT Constellation for Hybrid Users Using a Meta-Heuristic Approach", in: *2023 IEEE 10th International Workshop on Metrology for AeroSpace, MetroAeroSpace 2023 - Proceedings* (), pp. 609–614, DOI: 10.1109/METROAEROSPACE57412.2023.10189946.

[107] Microchip Technology Inc. (2025) *CSAC-SA65 | Microchip Technology*, Accessed: 2025-08-29, Microchip Technology, URL: https://www.microchip.com/en-us/product/csac-sa65#Documentation.

[108] Mike1024 *Local Plane Tangent Coordinates*, URL: https://en.wikipedia.org/wiki/Local_tangent_plane_coordinates#/media/File:ECEF_ENU_Longitude_Latitude_relationships.svg.

[109] O. Montenbruck et al. (2015) "GNSS satellite geometry and attitude models", in: *Advances in Space Research* 56 (6), pp. 1015–1029, ISSN: 0273-1177, DOI: 10.1016/J.ASR.2015.06.019, URL: https://www.sciencedirect.com/science/article/pii/S0273117715004378?via%3Dihub.

[110] Oliver Montenbruck, Peter Steigenberger, and Andre Hauschild (2020) "Comparing the 'Big 4' - A User's View on GNSS Performance", in: *2020 IEEE/ION Position, Location and Navigation Symposium, PLANS 2020* (), pp. 407–418, DOI: 10.1109/PLANS46316.2020.9110208.

[111] Ruben Morales-Ferre et al. (2020) "GDOP-based analysis of suitability of LEO constellations for future satellite-based positioning", in: *2020 IEEE International Conference on Wireless for Space and Extreme Environments (WiSEE)*, IEEE, pp. 147–152, ISBN: 978-1-7281-6451-9, DOI: 10.1109/WiSEE44079.2020.9262624, URL: https://ieeexplore.ieee.org/document/9262624/.

[112] Daniele Mortari, Matthew P. Wilkins, and Christian Bruccoleri (2004) "The Flower Constellations", in: *The Journal of the Astronautical Sciences* 52 (1-2), pp. 107–127, ISSN: 0021-9142, DOI: 10.1007/BF03546424.

[113] Mynaric (2025) *Condor Mk3 - Optical Communication Terminal for Space-Based Applications*, Accessed: 2025-09-04, URL: https://mynaric.com/products/space/condor-mk3/.

[114] NanoAvionics (2025) *How Many Satellites are in Space?*, Accessed: 2025-03-18, URL: https://nanoavionics.com/blog/how-many-satellites-are-in-space/.

[115] NASA (2017) *Juno Armored Up to Go to Jupiter*, Archived from the original on 2017-01-07., URL: https://www.nasa.gov.

[116] NASA "Spherical Harmonic Representation of the Gravity Field Potential", in: (), URL: https://spsweb.fltops.jpl.nasa.gov/portaldataops/mpg/MPG_Docs/Source%20Docs/gravity-SphericalHarmonics.pdf.

[117] NASA Jet Propulsion Laboratory (2025) *Jupiter Orbit Insertion Press Kit - Fast Facts*, California Institute of Technology, Accessed: 2025-09-01, URL: https://www.jpl.nasa.gov/news/press_kits/juno/facts/.

[118] Next Spaceflight (2025) *Ariane 62 | CSO-3*, Accessed: 2025-09-12, URL: https://nextspaceflight.com/launches/details/917.

[119] Next Spaceflight (2025) *Ariane 64 | Project Kuiper*, Accessed: 2025-09-12, URL: https://nextspaceflight.com/launches/details/6930.

[120] Next Spaceflight (2025) *Falcon Heavy | Griffin Mission One*, Accessed: 2025-09-12, URL: https://nextspaceflight.com/launches/details/917.

[121] NumPy Developers (2025) *NumPy Documentation*, Accessed: 2025-10-01, URL: https://numpy.org/doc/2.3/index.html.

[122] China Satellite Navigation Office (2017) "Update on BeiDou Navigation Satellite System", in: *Twelfth Meeting of the International Committee on Global Navigation Satellite Systems* ().

[123] China Satellite Navigation Office (2019) "Development of the BeiDou Navigation Satellite System", in: (), Accessed: 2025-09-01, URL: http://www.beidou.gov.cn/xt/gfxz/201912/P020191227430565455478.pdf.

[124] Lorenzo Olivieri and Alessandro Francesconi (2020) "Large constellations assessment and optimization in LEO space debris environment", in: *Advances in Space Research* 65 (1), pp. 351–363, ISSN: 18791948, DOI: 10.1016/j.asr.2019.09.048.

[125] René Oosterlinck and Laurent Gauthier (2001) *EGNOS: The first European implementation of GNSS-Project Status*, tech. rep., European Space Agency, URL: http://www.egnos-pro.esa.int/Publications/IAF%5C%202001/EGNOS%5C%20Status%20Paper%5C%20-%5C%20IAF%5C%20-%5C%20October%5C%202001.pdf.

[126] Deng Pan et al. (2018) "LEO Constellation Optimization Model with Non-uniformly Distributed RAAN for Global Navigation Enhancement", in: pp. 769–778, DOI: 10.1007/978-981-13-0005-9_63, URL: https://link.springer.com/10.1007/978-981-13-0005-9_63.

[127] Andrew Parsonson (2025) *Top European Launch Companies of 2024*, Accessed: 2025-08-28, European Spaceflight, URL: https://europeanspaceflight.com/top-european-launch-companies-of-2024/.

[128] Filipe Pereira and Daniel Selva (2019) "Exploring the Architecture Trade Space of NextGen Global Navigation Satellite Systems", in: *2019 IEEE Aerospace Conference*, vol. 2019-March, IEEE, pp. 1–13, ISBN: 978-1-5386-6854-2, DOI: 10.1109/AERO.2019.8741849, URL: https://ieeexplore.ieee.org/document/8741849/.

[129] David Mostaza Prieto, Benjamin P. Graziano, and Peter C.E. Roberts (2014) "Spacecraft drag modelling", in: *Progress in Aerospace Sciences* 64 (), pp. 56–65, ISSN: 0376-0421, DOI: 10.1016/J.PAEROSCI.2013.09.001, URL: https://www.sciencedirect.com/science/article/pii/S0376042113000754?via%3Dihub.

[130] CSIS Aerospace Security Project (2022) *Cost of space launches to low Earth orbit*, URL: https://ourworldindata.org/grapher/cost-space-launches-low-earth-orbit#reuse-this-work.

[131] Fabricio S. Prol et al. (2023) "Simulations using LEO-PNT systems: A Brief Survey", in: *2023 IEEE/ION Position, Location and Navigation Symposium, PLANS 2023* (), pp. 381–387, DOI: 10.1109/PLANS53410.2023.10140118.

9

[132] Fabricio S. Prol et al. (2024) "Simulations of Dedicated LEO-PNT Systems for Precise Point Positioning: Methodology, Parameter Analysis, and Accuracy Evaluation", in: *IEEE Transactions on Aerospace and Electronic Systems* 60 (5), pp. 6499–6516, ISSN: 0018-9251, DOI: 10.1109/TAES.2024.3404909, URL: https://ieeexplore.ieee.org/document/10538397/.

[133] QZSS *Quasi-Zenith Satellite Orbit (QZO)*, URL: https://qzss.go.jp/en/technical/technology/orbit.html.

[134] Guinness World Records (2025) *Largest Satellite Constellation*, Accessed: 2025-08-25., URL: https://www.guinnessworldrecords.com/world-records/628755-largest-satellite-constellation.

[135] I Reda and A Andreas (2008) "Solar Position Algorithm for Solar Radiation Applications (Revised)", in: *NREL* (), DOI: 10.2172/15003974, URL: https://research-hub.nrel.gov/en/publications/solar-position-algorithm-for-solar-radiation-applications-revised/.

[136] Tyler Reid (2017) "Orbital Diversity for Global Navigation Satellite Systems", PhD thesis.

[137] Sergey Revnivykh (2009) *GLObal Navigation Satellite System (GLONASS)*, tech. rep., 4-th meeting of International Committee on GNSS, pp. 13–18, URL: https://www.unoosa.org/documents/pdf/icg/activities/2009/icg4/01.pdf.

[138] L. Rider (1985) "Optimized Polar Orbit Constellations for Redundant Earth Coverage", in: *Journal of Astronautical Sciences* 33 (2), pp. 147–161, URL: https://ui.adsabs.harvard.edu/abs/1985JAnSc..33..147R/abstract.

[139] L. Rider (1986) "Analytic design of satellite constellations for zonal earth coverage using inclined circular orbits", in: *Journal of the Astronautical Sciences* 34 (), pp. 31–64, ISSN: 0021-9142, URL: https://ui.adsabs.harvard.edu/abs/1986JAnSc..34...31R/abstract.

[140] Lionel Ries, Marco Anghileri, and Roberto Prieto-Cerdeira (2023) *Extension of RNSS C-band*, Accessed: 2025-09-04, URL: https://www.unoosa.org/documents/pdf/icg/2023/ICG-17/icg17_wgs_03_02rev.pdf.

[141] Lionel Ries et al. (2023) "LEO-PNT for Augmenting Europe's Space-based PNT Capabilities", in: *2023 IEEE/ION Position, Location and Navigation Symposium, PLANS 2023* (), pp. 329–337, DOI: 10.1109/PLANS53410.2023.10139999.

[142] RocketLaunch.Live (2025) *Falcon Heavy Launch History*, Accessed: 2025-10-29, URL: https://www.rocketlaunch.live/?pastOnly=1&filter=falcon-heavy.

[143] RocketLaunch.Live (2025) *Falcon Heavy Launch Schedule*, Accessed: 2025-10-29, URL: https://www.rocketlaunch.live/?filter=falcon-heavy.

[144] Marina Ruggieri et al. (2008) *The Flower Constellation Set and its Possible Applications*, tech. rep., European Space Agency, URL: http://www.esa.int/act.

[145] Liam P. Sarsfield (1998) *The Cosmos on a Shoestring: Small Spacecraft for Space and Earth Science*, Santa Monica, CA: RAND Corporation, URL: https://www.rand.org/pubs/monograph_reports/MR864.html.

[146] Hanno Scheife (2024) *TESAT-Standard Optical Network Products for Space - Opportunities for PICs*, Presented at EPIC Technology Meeting on Photonic Integration and Packaging at Fraunhofer IZM, Accessed: 2025-09-25, URL: https://epic-photonics.com/wp-content/uploads/2023/07/1.3-Hanno-Scheife-TESAT.pdf.

[147] SciPy Steering Council (2025) *SciPy*, Accessed: 2025-10-01, URL: https://scipy.org/.

[148] Peter B. de Selding (2015) "Competition To Build OneWeb Constellation Draws 2 U.S., 3 European Companies", in: *SpaceNews* (), Accessed: 2025-08-25, URL: https://spacenews.com/competition-to-build-oneweb-constellation-draws-2-u-s-3-european-companies/.

[149] Renhe Shi et al. (2018) "Multidisciplinary modeling and surrogate assisted optimization for satellite constellation systems", in: *Structural and Multidisciplinary Optimization* 58 (5), pp. 2173–2188, ISSN: 16151488, DOI: 10.1007/s00158-018-2032-1.

[150] Jan Van Sickle and John A. Dutton *The Navigation Message | GEOG 862: GPS and GNSS for Geospatial Professionals*, URL: https://www.e-education.psu.edu/geog862/node/1734.

[151] Doug Sinclair and Jonathan Dyer (2013) "SSC13-IV-3 Radiation Effects and COTS Parts in SmallSats", in: *27th Annual AIAA/USU Conference on Small Satellites* (), URL: https://digitalcommons.usu.edu/cgi/viewcontent.cgi?article=2934&context=smallsat.

[152] Rich Smith (2018) *Europe Complains: SpaceX Rocket Prices Are Too Cheap to Beat*, Accessed: 2025-09-12, URL: https://www.fool.com/investing/2018/06/02/europe-complains-spacex-rocket-prices-are-too-chea.aspx.

[153] Space Enthusiast (2023) *OneWeb Satellite Internet: Review, Pros, Cons, Availability*, Accessed: 2025-10-06, URL: https://orbitaltoday.com/2023/08/29/%D0%BEneweb-satellite-internet-review-pros-cons-availability/.

[154] SpaceX (2025) *Starlink | Technology*, Accessed: 2025-09-25, URL: https://www.starlink.com/technology.

[155] Philip N. Springmann and Olivier L. De Weck (2004) "Parametric Scaling Model for Nongeosynchronous Communications Satellites", in: *American Institute of Aeronautics and Astronautics Inc.* 41 (3), pp. 472–477, ISSN: 15336794, DOI: 10.2514/1.6220, URL: /doi/pdf/10.2514/1.6220.

[156] Peter Steigenberger, Steffen Thoelert, and Oliver Montenbruck (2018) "GNSS satellite transmit power and its impact on orbit determination", in: *Journal of Geodesy* 92 (6), pp. 609–624, ISSN: 14321394, DOI: 10.1007/S00190-017-1082-2/FIGURES/11, URL: https://link.springer.com/article/10.1007/s00190-017-1082-2.

[157] J. Sanz Subirana, J.M. Zornoza, and M. Hernandez (2011) *Transformations between ECEF and ENU coordinates*, URL: https://gssc.esa.int/navipedia/index.php/Transformations_between_ECEF_and_ENU_coordinates.

9

[158] Taehyun Sung and Jaemyung Ahn (2023) “Optimal deployment of satellite mega-constellation”, in: *Acta Astronautica* 202 (), pp. 653–669, ISSN: 00945765, DOI: 10.1016/j.actaastro.2022.10.027.

[159] SBG Systems (2025) *Antenna Gain - GNSS Glossary*, Accessed: 2025-09-04, URL: https://www.sbg-systems.com/glossary/antenna-gain-gnss/.

[160] Tageo.com (2025) *oberpfaffenhofen Geography Population Map cities coordinates location*, Includes geographic coordinates, nearby towns, and satellite map links. Accessed: 2025-09-29, URL: https://www.tageo.com/index-e-gm-v-02-d-m2542706.htm.

[161] Mahdia Tahsin et al. (2015) “Analysis of DOP and its preciseness in GNSS position estimation”, in: *2nd International Conference on Electrical Engineering and Information and Communication Technology, iCEEiCT 2015* (), DOI: 10.1109/ICEEICT.2015.7307445.

[162] Tudat Team (2025) *Tudat*, URL: https://docs.tudat.space/en/latest/index.html.

[163] Tesat (2025) *SCOT80 Optical Communication Terminal for Satellite Networks*, Version 2025-03. Accessed: 2025-09-04, URL: https://www.tesat.de/images/tesat/products/250820_DataSheet_SCOT80_A4.pdf.

[164] Konstantin E. Tsiolkovsky (1903) *Exploration of Outer Space by Means of Rocket Devices*, Kaluga, Russia: Imperial Russian Technical Society.

[165] TU Delft Faculty of Aerospace Engineering (2020) *Spacecraft Design and Sizing*, Brightspace course platform, Course reader for AE1222-II Aerospace Design & Systems Engineering Elements, TU Delft.

[166] Andrew Turner (2002) “Constellation Design Using Walker Patterns”, in: *AIAA/AAS Astrodynamics Specialist Conference and Exhibit*, American Institute of Aeronautics and Astronautics, ISBN: 978-1-62410-124-3, DOI: 10.2514/6.2002-4636, URL: https://arc.aiaa.org/doi/10.2514/6.2002-4636.

[167] United States Department of Defense (2020) *Global Positioning System Standard Positioning Service Performance Standard*, tech. rep., Accessed: 2025-10-02, Department of Defense, URL: https://www.gps.gov/sites/default/files/2025-07/2020-SPS-performance-standard.pdf.

[168] David A Vallado (2013) “9.6.1 Central Body Analysis”, in: *Fundamentals of Astrodynamics and Applications*, Fourth, Microcosm Press, pp. 647–654.

[169] J. C. Walker (1970) *Circular Orbit Patters Providing Continuous Whole Earth Coverage*, tech. rep., Royal Aircraft Establishment, URL: https://apps.dtic.mil/sti/tr/pdf/AD0722776.pdf.

[170] Xuefeng Wang and Shijie Zhang (2021) “Cost Analysis for Mass Customized Production of Satellites Based on Modularity”, in: *IEEE Access* 9 (), pp. 13754–13760, ISSN: 21693536, DOI: 10.1109/ACCESS.2020.3048845.

[171] Xiaofang Wei et al. (2023) "A discrete design method of repeat ground track orbit for Earth observation satellites", in: *Aerospace Systems* 6 (2), pp. 199–206, ISSN: 25233955, DOI: 10.1007/S42401-022-00188-0/TABLES/5, URL: https://link.springer.com/article/10.1007/s42401-022-00188-0.

[172] Yanbo Wei, Huaijian Li, and Xiaojing Du (2020) *An Efficient LEO Global Navigation Constellation Design Based on Walker Constellation*, tech. rep.

[173] James Richard Wertz (2001) *Mission geometry: orbit and constellation design and management: spacecraft orbit and attitude systems*, Microcosm Press : Kluwer Academic Publishers, ISBN: 978-0-7923-7148-9.

[174] James Richard Wertz, David F. Everett, and Jeffery John Puschell (2011) *Space mission engineering: The new smad*, Microcosm Press.

[175] Luke Winternitz (2017) *Introduction to GPS and other Global Navigation Satellite Systems*, URL: www.gps.gov/governance/advisory/meetings/2015-06/leveson.pdf.

[176] Wei Xie et al. (2019) "Characteristics and Performance Evaluation of QZSS Onboard Satellite Clocks", in: *Sensors* 19 (), p. 5147, DOI: 10.3390/s19235147.

[177] Xin Xie et al. (2018) "Design and validation of broadcast ephemeris for low Earth orbit satellites", in: *GPS Solutions* 22 (2), pp. 1–11, ISSN: 15211886, DOI: 10.1007/S10291-018-0719-9/FIGURES/6, URL: https://link.springer.com/article/10.1007/s10291-018-0719-9.

[178] Xoneca (2013) *Geometric Dilution Of Precision.svg*, URL: https://commons.wikimedia.org/wiki/File:Geometric_Dilution_Of_Precision.svg.

[179] Fuzhan Yue et al. (2022) "A Satellite Augmentation System based on LEO mega-constellation", in: *2022 International Conference on Artificial Intelligence, Information Processing and Cloud Computing (AIIPCC)*, IEEE, pp. 221–225, ISBN: 978-1-6654-6287-7, DOI: 10.1109/AIIPCC57291.2022.00055, URL: https://ieeexplore.ieee.org/document/10070149/.

[180] Chen Zhang et al. (2018) "LEO constellation design methodology for observing multi-targets", in: *Astrodynamics* 2 (2), pp. 121–131, ISSN: 2522-008X, DOI: 10.1007/s42064-017-0015-4.

[181] J. Zhu (1994) "Conversion of Earth-centered Earth-fixed coordinates to geodetic coordinates", in: *IEEE Transactions on Aerospace and Electronic Systems* 30.3 (), pp. 957–961, DOI: 10.1109/7.303772.

[182] Qinyu Zhu et al. (2022) "Laser Inter-Satellite Link Visibility and Topology Optimization for Mega Constellation", in: *Electronics (Switzerland)* 11 (14), ISSN: 20799292, DOI: 10.3390/electronics11142232.

[183] Eckart Zitzler and Lothar Thiele (1998) "Multiobjective optimization using evolutionary algorithms — A comparative case study", in: *Parallel Problem Solving from Nature — PPSN V*, ed. by Agoston E. Eiben et al., Berlin, Heidelberg: Springer Berlin Heidelberg, pp. 292–301.

A

SIMULATOR APPENDIX

PERTURBATION ANALYSIS

This section presents additional information regarding the perturbation analysis performed in section 3.2. These analyses are performed with the following spacecraft settings:

- Mass: 260 kg
- Surface area: 1.0 m^2
- Drag coefficient: 1.2
- Reflectivity coefficient: 1.0

The values used were chosen to represent a small LEO satellite, but are not representative of a specific satellite design developed in this work.

The figures below show the error evolution for the higher LEO orbit case at 1500 km.

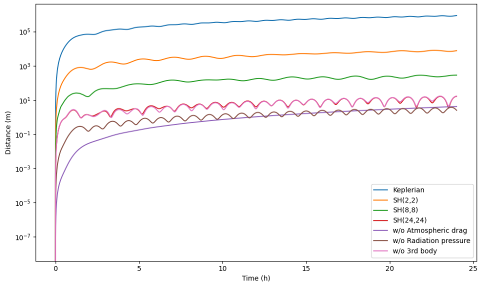

(a) Short Term Effect

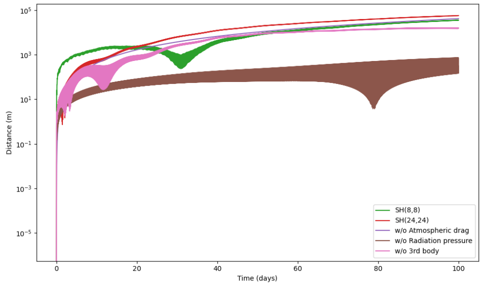

(b) Long Term Effect

Figure A.1: 1500km Orbit Error with respect to High Fidelity Scenario

B

Single Objective Optimisation Appendix

Single shell Initial Results

The initial results of the single-objective optimisation for the one-shell constellations are presented in Table B.1. These are used for tuning in later stages. The most important outcome is that Star constellations consistently outperform Delta ones in terms of GDOP, often requiring fewer satellites to meet the performance criteria.

Table B.1: Initial results of the SOO one shell constellations

Scenario	**Type**	**T**	**P**	**F**	**a**	**i**	**$GDOP_{95}$**
1D4Ta	Delta	171	9	7	1,248.27	84.67	3.48
1S4Ta	Star	150	10	4	1,239.43	77.87	3.80
1D4Tb	Delta	299	13	2	869.08	77.44	3.76
1S4Tb	Star	198	11	3	877.37	83.07	3.98
1D4Tc	Delta	242	11	10	1,041.55	72.47	3.76
1S4Tc	Star	170	10	2	1,055.33	82.51	3.82
1D4Td	Delta	375	15	4	706.42	84.48	3.86
1S4Td	Star	260	13	5	709.20	83.26	3.92
1D2Ta	Delta	323	17	14	1,242.26	80.06	1.97
1S2Ta	Star	240	12	3	1,247.86	84.36	1.95
1D2Tb	Delta	n.a.	n.a.	n.a.	~800	~85	n.a.
1S2Tb	Star	345	15	6	878.68	83.96	1.98
1D2Tc	Delta	399	19	16	1,046.19	75.89	1.91
1S2Tc	Star	280	14	7	1,058.74	84.97	2
1D2Td	Delta	n.a.	n.a.	n.a.	~700	~85	n.a.
1S2Td	Star	500	20	14	711.61	84.80	2.00

TWO SHELL INITIAL RESULTS

The initial results of the single-objective optimisation for the two shell constellations are presented in Table B.2.

B

Table B.2: Initial results of the SOO two-shell constellations

Scenario	**Type**	**T**	**P**	**F**	**a**	**i**	$GDOP_{95}$
2SD4Ta	Star	108	9	5	1,246.27	83.14	3.87
	Delta	48	6	3	1,190.04	31.38	
2SD4Tb	Star	187	11	4	876.82	82.70	3.93
	Delta	25	5	4	812.54	30.07	
2SD4Tc	Star	150	10	4	1,058.60	84.87	3.95
	Delta	30	6	0	1,000.01	36.22	
2SD4Td	Star	180	15	2	709.44	83.42	4.00
	Delta	240	12	3	671.46	58.03	
2SD2Ta	Star	140	10	5	1,248.67	84.98	1.97
	Delta	120	8	0	1,192.88	35.19	
2SD2Tb	Star	247	13	6	879.09	84.24	1.98
	Delta	140	14	3	822.14	40.80	
2SD2Tc	Star	240	12	3	1,053.39	81.11	2.00
	Delta	60	10	3	1,018.11	53.93	
2SD2Td	Star	300	15	9	711.93	85	1.98
	Delta	300	15	9	654	44.20	

C

Multi-Objective Optimisation Appendix

The following sections present additional figures related to the multi-objective optimisation process described in subsection 6.2.2. It shows the convergence history of the Pareto front, as well as the evolution of the two objectives: number of satellites and 95th percentile GDOP, for both the single shell and double shell configurations.

C

SINGLE SHELL

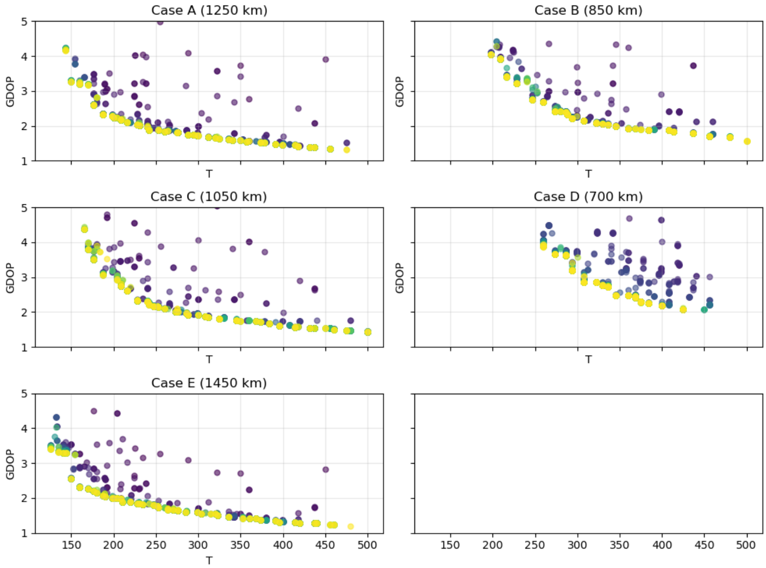

Figure C.1: Pareto front history for the single shell configuration

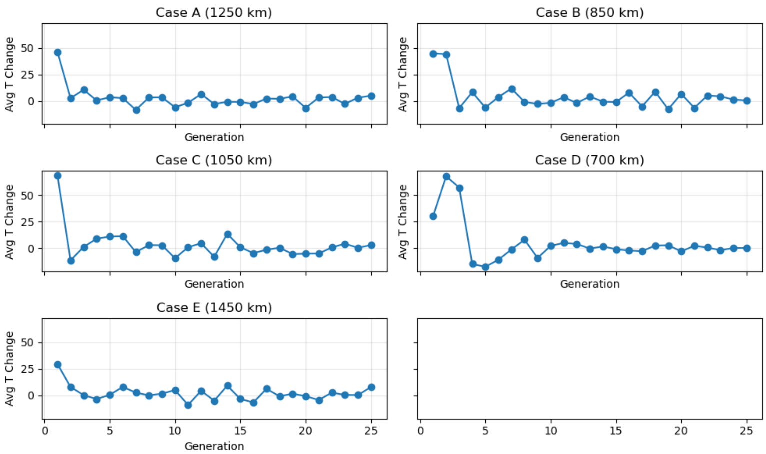

Figure C.2: Number of satellites history for the single shell configuration

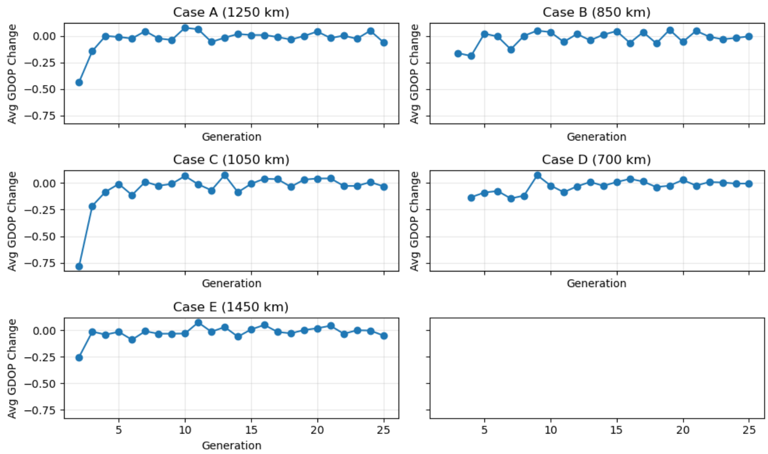

Figure C.3: 95th Percentile GDOP history for the single shell configuration

Double Shell

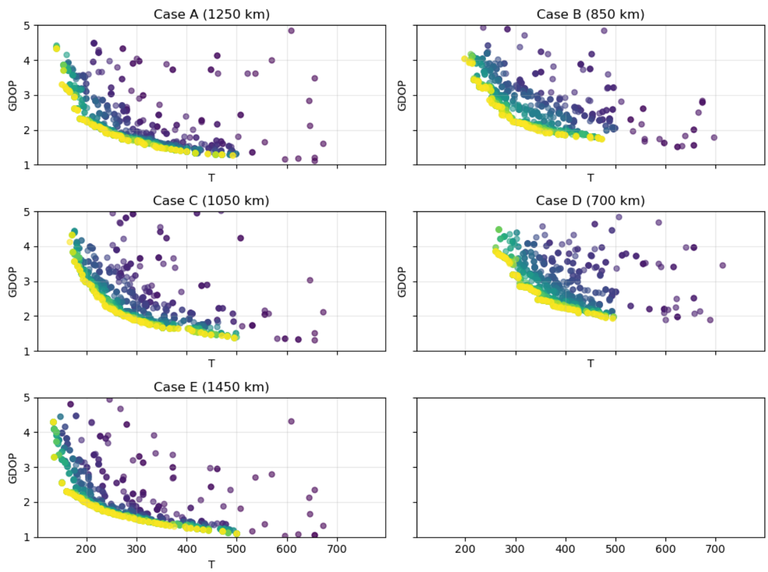

Figure C.4: Pareto front history for the double shell configuration

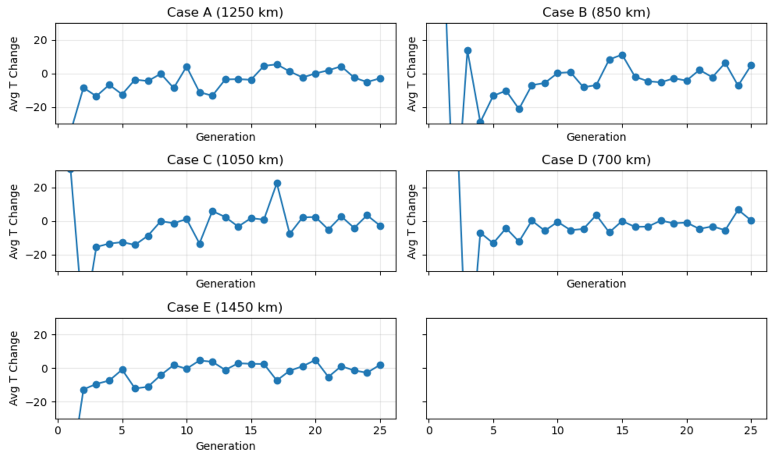

Figure C.5: Number of satellites history for the double shell configuration

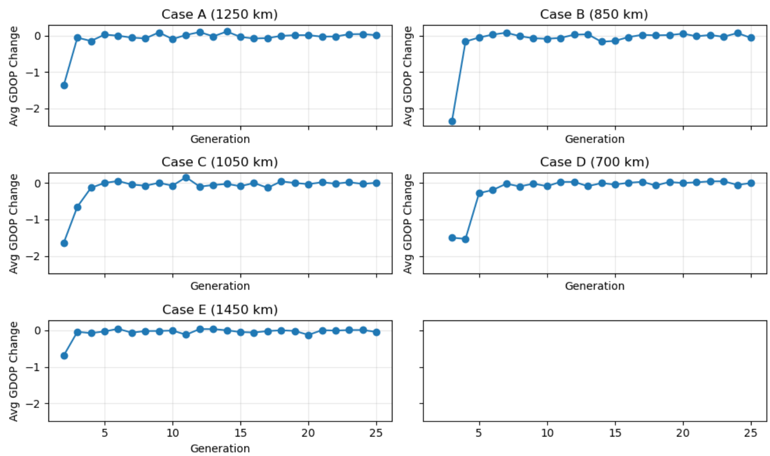

Figure C.6: 95th Percentile GDOP history for the double shell configuration

MOO Pareto Configurations

The following tables list the Pareto optimal configurations obtained from the multi-objective optimisation for both the single shell and double shell cases. The cases are labelled according to the naming convention described in subsection 5.1.1. As a reminder, the letter corresponds to the approximate altitude and repeatability (N, K) of the shell(s):

- a: 1250 km (1, 13)
- b: 850 km (1, 14)
- c: 1050 km (2, 27)

- d: 700 km (2, 29)
- e: 1450 km (2, 25)

As a note, the exact altitude can be computed using the inclination and the repeatability conditions and filling in Equation 4.3. Furthermore, the phasing parameter F follows the optimal values explained in section 4.4.

Table C.1: Pareto optimal configurations for single shell constellations

Case	T	P	I	GDOP
$1STGa_1$	143.0	11	84.9	4.16
$1STGa_2$	150.0	10	83.0	3.26
$1STGa_3$	160.0	10	82.0	3.19
$1STGa_4$	170.0	10	84.7	3.18
$1STGa_5$	176.0	11	84.4	2.6
$1STGa_6$	209.0	11	83.2	2.17
$1STGa_7$	216.0	12	84.1	2.1
$1STGa_8$	228.0	12	84.8	2.03
$1STGa_9$	231.0	11	83.5	2.01
$1STGa_{10}$	240.0	12	83.6	1.96
$1STGa_{11}$	242.0	11	84.3	1.89
$1STGa_{12}$	253.0	11	83.2	1.89
$1STGa_{13}$	260.0	13	84.8	1.84
$1STGa_{14}$	275.0	11	84.1	1.81
$1STGa_{15}$	294.0	14	84.9	1.74
$1STGa_{16}$	299.0	13	85.0	1.71
$1STGa_{17}$	312.0	13	84.9	1.67
$1STGa_{18}$	325.0	13	85.0	1.62
$1STGa_{19}$	350.0	14	84.9	1.58
$1STGa_{20}$	357.0	17	84.9	1.54
$1STGa_{21}$	378.0	18	81.6	1.51
$1STGa_{22}$	391.0	17	82.2	1.47
$1STGa_{23}$	437.0	19	84.2	1.39
$1STGa_{24}$	475.0	19	84.2	1.33
$1STGb_1$	198.0	11	83.3	4.04
$1STGb_2$	209.0	11	81.3	3.9
$1STGb_3$	216.0	12	83.2	3.41
$1STGb_4$	273.0	13	82.3	2.42
$1STGb_5$	286.0	13	81.9	2.4
$1STGb_6$	294.0	14	84.7	2.22
$1STGb_7$	308.0	14	84.7	2.15
$1STGb_8$	322.0	14	83.3	2.07
$1STGb_9$	330.0	15	84.5	2.07
$1STGb_{10}$	336.0	14	83.3	2.04

Continued on next page

C

C

Table C.1 – continued from previous page

Case	T	P	I	GDOP
$1STGb_{11}$	345.0	15	84.6	1.98
$1STGb_{12}$	375.0	15	84.9	1.91
$1STGb_{13}$	384.0	16	84.7	1.87
$1STGb_{14}$	408.0	17	85.0	1.87
$1STGb_{15}$	480.0	20	84.3	1.68
$1STGb_{16}$	500.0	20	84.3	1.57
$1STGc_{1}$	165.0	11	83.6	4.39
$1STGc_{2}$	170.0	10	81.1	3.78
$1STGc_{3}$	176.0	11	84.9	3.5
$1STGc_{4}$	216.0	12	81.8	2.6
$1STGc_{5}$	228.0	12	81.9	2.33
$1STGc_{6}$	242.0	11	85.0	2.22
$1STGc_{7}$	260.0	13	84.5	2.09
$1STGc_{8}$	276.0	12	84.2	2.0
$1STGc_{9}$	286.0	13	83.3	1.97
$1STGc_{10}$	288.0	12	84.9	1.91
$1STGc_{11}$	300.0	12	83.4	1.91
$1STGc_{12}$	312.0	13	84.9	1.85
$1STGc_{13}$	325.0	13	85.0	1.8
$1STGc_{14}$	350.0	14	84.6	1.74
$1STGc_{15}$	368.0	16	85.0	1.74
$1STGc_{16}$	460.0	20	82.6	1.49
$1STGc_{17}$	500.0	20	82.6	1.43
$1STGd_{1}$	260.0	13	85.0	3.86
$1STGd_{2}$	286.0	13	81.3	3.62
$1STGd_{3}$	308.0	14	82.0	2.85
$1STGd_{4}$	322.0	14	81.8	2.85
$1STGd_{5}$	330.0	15	83.3	2.76
$1STGd_{6}$	345.0	15	82.9	2.47
$1STGd_{7}$	360.0	15	82.2	2.47
$1STGd_{8}$	368.0	16	85.0	2.42
$1STGd_{9}$	375.0	15	82.7	2.28
$1STGd_{10}$	425.0	17	84.9	2.07
$1STGe_{1}$	126.0	9	81.1	3.41
$1STGe_{2}$	135.0	9	81.1	3.31
$1STGe_{3}$	140.0	10	84.7	3.29
$1STGe_{4}$	150.0	10	82.0	2.56
$1STGe_{5}$	160.0	10	84.7	2.31
$1STGe_{6}$	176.0	11	82.1	2.2
$1STGe_{7}$	180.0	10	81.6	2.15
$1STGe_{8}$	187.0	11	85.0	2.08
$1STGe_{9}$	190.0	10	84.9	2.05

Continued on next page

Table C.1 – continued from previous page

Case	T	P	I	GDOP
$1STGe_{10}$	200.0	10	81.7	2.01
$1STGe_{11}$	209.0	11	81.2	1.98
$1STGe_{12}$	220.0	11	84.7	1.88
$1STGe_{13}$	231.0	11	82.8	1.83
$1STGe_{14}$	252.0	14	80.4	1.78
$1STGe_{15}$	253.0	11	84.7	1.72
$1STGe_{16}$	285.0	15	82.0	1.6
$1STGe_{17}$	315.0	15	81.2	1.55
$1STGe_{18}$	336.0	16	84.6	1.46
$1STGe_{19}$	352.0	16	82.3	1.43
$1STGe_{20}$	396.0	18	84.8	1.31
$1STGe_{21}$	456.0	19	83.9	1.24
$1STGe_{22}$	480.0	20	83.9	1.2

Table C.2: Pareto optimal configurations for double shell constellations

Case	T1	P1	I1	T2	P2	I2	GDOP	T
$2STGa_{1}$	140	10	81.7	0	0	0.0	4.33	140
$2STGa_{2}$	150	10	84.7	0	0	0.0	3.31	150
$2STGa_{3}$	150	10	80.9	6	6	38.0	3.24	156
$2STGa_{4}$	160	10	81.4	0	0	0.0	3.17	160
$2STGa_{5}$	160	10	81.4	5	5	49.4	3.14	165
$2STGa_{6}$	170	10	84.2	5	5	42.7	2.95	175
$2STGa_{7}$	176	11	84.8	0	0	0.0	2.61	176
$2STGa_{8}$	176	11	84.8	5	5	52.1	2.58	181
$2STGa_{9}$	176	11	84.7	6	6	40.7	2.58	182
$2STGa_{10}$	187	11	84.9	0	0	0.0	2.32	187
$2STGa_{11}$	187	11	84.7	6	6	48.8	2.3	193
$2STGa_{12}$	187	11	84.8	10	5	45.5	2.28	197
$2STGa_{13}$	200	10	84.7	0	0	0.0	2.24	200
$2STGa_{14}$	209	11	84.9	0	0	0.0	2.18	209
$2STGa_{15}$	209	11	84.4	5	5	46.3	2.15	214
$2STGa_{16}$	216	12	84.7	0	0	0.0	2.09	216
$2STGa_{17}$	204	12	81.9	20	5	26.9	2.09	224
$2STGa_{18}$	209	11	84.1	18	6	41.8	2.08	227
$2STGa_{19}$	231	11	84.5	0	0	0.0	2.02	231
$2STGa_{20}$	231	11	84.6	5	5	47.4	2.02	236
$2STGa_{21}$	187	11	84.3	50	5	26.2	1.93	237
$2STGa_{22}$	242	11	84.7	0	0	0.0	1.89	242
$2STGa_{23}$	242	11	84.6	10	5	39.5	1.87	252
$2STGa_{24}$	242	11	84.9	15	5	42.0	1.86	257

Continued on next page

C

C

Table C.2 – continued from previous page

Case	T1	P1	I1	T2	P2	I2	GDOP	T
$2STGa_{25}$	260	13	84.9	0	0	0.0	1.84	260
$2STGa_{26}$	209	11	84.7	60	15	40.7	1.81	269
$2STGa_{27}$	216	12	84.7	55	5	29.6	1.74	271
$2STGa_{28}$	228	12	84.9	50	5	26.3	1.72	278
$2STGa_{29}$	253	11	84.7	48	6	39.1	1.7	301
$2STGa_{30}$	198	11	84.9	112	16	37.7	1.65	310
$2STGa_{31}$	247	13	84.9	66	6	26.3	1.6	313
$2STGa_{32}$	187	11	85.0	128	16	40.6	1.58	315
$2STGa_{33}$	252	14	84.6	80	16	28.5	1.57	332
$2STGa_{34}$	209	11	84.7	128	16	40.7	1.52	337
$2STGa_{35}$	220	11	84.7	128	16	40.7	1.49	348
$2STGa_{36}$	240	12	84.7	128	16	40.6	1.44	368
$2STGa_{37}$	252	12	84.7	136	17	39.1	1.41	388
$2STGa_{38}$	264	12	84.7	136	17	39.1	1.38	400
$2STGa_{39}$	266	14	84.6	176	16	43.2	1.33	442
$2STGa_{40}$	300	15	83.6	192	16	43.2	1.27	492
$2STGb_{1}$	198	11	83.1	0	0	0.0	4.04	198
$2STGb_{2}$	209	11	81.9	5	5	47.3	3.92	214
$2STGb_{3}$	216	12	82.8	0	0	0.0	3.45	216
$2STGb_{4}$	216	12	83.1	10	10	52.2	3.38	226
$2STGb_{5}$	228	12	80.7	0	0	0.0	3.24	228
$2STGb_{6}$	228	12	80.7	5	5	52.0	3.22	233
$2STGb_{7}$	228	12	80.7	13	13	42.2	3.19	241
$2STGb_{8}$	247	13	83.2	5	5	52.4	2.77	252
$2STGb_{9}$	260	13	82.9	5	5	42.4	2.68	265
$2STGb_{10}$	260	13	82.9	12	12	52.2	2.67	272
$2STGb_{11}$	273	13	82.9	0	0	0.0	2.43	273
$2STGb_{12}$	273	13	82.7	5	5	36.7	2.42	278
$2STGb_{13}$	273	13	82.5	13	13	42.6	2.4	286
$2STGb_{14}$	288	12	83.9	0	0	0.0	2.34	288
$2STGb_{15}$	294	14	82.7	5	5	42.3	2.23	299
$2STGb_{16}$	294	14	82.7	10	5	52.3	2.22	304
$2STGb_{17}$	294	14	83.1	14	14	42.7	2.2	308
$2STGb_{18}$	308	14	81.8	6	6	52.2	2.19	314
$2STGb_{19}$	322	14	82.9	5	5	42.3	2.09	327
$2STGb_{20}$	322	14	82.7	8	8	53.4	2.06	330
$2STGb_{21}$	336	14	82.8	0	0	0.0	2.06	336
$2STGb_{22}$	345	15	82.9	5	5	42.3	1.98	350
$2STGb_{23}$	360	15	83.1	0	0	0.0	1.93	360
$2STGb_{24}$	360	15	83.1	8	8	52.2	1.92	368
$2STGb_{25}$	384	16	82.8	0	0	0.0	1.88	384
$2STGb_{26}$	384	16	82.5	14	14	42.6	1.86	398

Continued on next page

Table C.2 – continued from previous page

Case	T1	P1	I1	T2	P2	I2	GDOP	T
$2STGb_{27}$	360	15	83.8	60	12	55.2	1.82	420
$2STGb_{28}$	360	15	82.8	112	14	52.7	1.76	472
$2STGc_{1}$	160	10	83.2	6	6	26.1	4.13	166
$2STGc_{2}$	160	10	84.8	15	5	26.1	3.56	175
$2STGc_{3}$	176	11	84.4	5	5	27.8	3.44	181
$2STGc_{4}$	176	11	84.8	10	5	33.7	3.32	186
$2STGc_{5}$	176	11	84.5	15	5	27.4	3.19	191
$2STGc_{6}$	187	11	81.9	5	5	33.4	3.07	192
$2STGc_{7}$	187	11	81.9	10	5	33.4	2.99	197
$2STGc_{8}$	160	10	84.6	45	5	27.8	2.93	205
$2STGc_{9}$	204	12	83.3	5	5	30.1	2.87	209
$2STGc_{10}$	204	12	83.0	10	5	27.7	2.73	214
$2STGc_{11}$	204	12	84.9	15	5	33.8	2.62	219
$2STGc_{12}$	216	12	81.7	5	5	28.7	2.54	221
$2STGc_{13}$	204	12	84.7	25	5	29.1	2.52	229
$2STGc_{14}$	187	11	83.0	45	5	27.7	2.44	232
$2STGc_{15}$	216	12	82.3	20	5	28.6	2.31	236
$2STGc_{16}$	228	12	82.9	10	5	27.7	2.28	238
$2STGc_{17}$	240	12	81.7	5	5	30.7	2.24	245
$2STGc_{18}$	228	12	82.3	20	5	29.6	2.21	248
$2STGc_{19}$	228	12	82.3	25	5	29.6	2.2	253
$2STGc_{20}$	240	12	82.9	15	5	31.8	2.17	255
$2STGc_{21}$	240	12	82.9	20	5	29.7	2.09	260
$2STGc_{22}$	240	12	83.4	30	5	30.0	2.05	270
$2STGc_{23}$	273	13	83.4	0	0	0.0	2.01	273
$2STGc_{24}$	276	12	82.9	5	5	27.5	1.99	281
$2STGc_{25}$	276	12	84.7	10	5	31.5	1.96	286
$2STGc_{26}$	273	13	84.5	15	5	32.2	1.94	288
$2STGc_{27}$	273	13	83.0	20	5	29.7	1.9	293
$2STGc_{28}$	288	12	84.8	15	5	32.2	1.87	303
$2STGc_{29}$	288	12	84.8	20	5	32.2	1.86	308
$2STGc_{30}$	260	13	84.6	50	5	29.4	1.81	310
$2STGc_{31}$	294	14	84.9	24	6	28.7	1.8	318
$2STGc_{32}$	273	13	84.9	54	6	28.9	1.76	327
$2STGc_{33}$	273	13	84.9	66	6	28.1	1.71	339
$2STGc_{34}$	286	13	83.9	65	5	31.5	1.68	351
$2STGc_{35}$	286	13	84.8	80	5	31.5	1.66	366
$2STGc_{36}$	299	13	84.5	84	7	32.3	1.64	383
$2STGc_{37}$	396	18	84.6	15	5	34.1	1.57	411
$2STGc_{38}$	378	18	84.5	50	5	27.8	1.53	428
$2STGc_{39}$	378	18	84.6	70	7	27.8	1.47	448
$2STGc_{40}$	418	19	84.6	63	7	31.4	1.43	481

Continued on next page

C

Table C.2 – continued from previous page

Case	T1	P1	I1	T2	P2	I2	GDOP	T
$2STGc_{41}$	432	18	84.6	63	7	27.4	1.38	495
$2STGd_{1}$	260	13	84.7	0	0	0.0	3.87	260
$2STGd_{2}$	260	13	84.7	5	5	34.3	3.78	265
$2STGd_{3}$	260	13	84.4	10	10	34.4	3.75	270
$2STGd_{4}$	260	13	84.6	14	7	44.5	3.72	274
$2STGd_{5}$	273	13	83.8	6	6	34.4	3.67	279
$2STGd_{6}$	273	13	83.7	12	6	31.0	3.59	285
$2STGd_{7}$	260	13	83.0	28	7	37.3	3.5	288
$2STGd_{8}$	294	14	84.4	0	0	0.0	3.19	294
$2STGd_{9}$	294	14	83.8	6	6	44.3	3.17	300
$2STGd_{10}$	294	14	83.8	9	9	44.3	3.16	303
$2STGd_{11}$	294	14	83.7	12	6	31.0	3.1	306
$2STGd_{12}$	308	14	82.1	0	0	0.0	2.85	308
$2STGd_{13}$	308	14	82.3	5	5	43.9	2.85	313
$2STGd_{14}$	308	14	82.0	10	5	37.7	2.84	318
$2STGd_{15}$	308	14	82.3	15	5	37.8	2.83	323
$2STGd_{16}$	308	14	82.9	20	10	30.5	2.81	328
$2STGd_{17}$	330	15	84.1	0	0	0.0	2.77	330
$2STGd_{18}$	330	15	83.9	7	7	39.4	2.71	337
$2STGd_{19}$	330	15	83.8	10	5	32.1	2.7	340
$2STGd_{20}$	330	15	84.9	14	7	41.4	2.67	344
$2STGd_{21}$	345	15	83.8	0	0	0.0	2.48	345
$2STGd_{22}$	345	15	83.4	9	9	37.0	2.46	354
$2STGd_{23}$	345	15	83.8	15	5	38.1	2.45	360
$2STGd_{24}$	345	15	84.8	18	6	38.5	2.44	363
$2STGd_{25}$	345	15	83.8	25	5	32.3	2.4	370
$2STGd_{26}$	375	15	84.9	0	0	0.0	2.3	375
$2STGd_{27}$	375	15	83.7	5	5	36.9	2.28	380
$2STGd_{28}$	384	16	84.2	6	6	39.3	2.24	390
$2STGd_{29}$	384	16	85.0	15	5	40.7	2.23	399
$2STGd_{30}$	384	16	84.4	21	7	34.0	2.21	405
$2STGd_{31}$	408	17	84.2	8	8	44.2	2.18	416
$2STGd_{32}$	384	16	83.8	40	5	38.1	2.15	424
$2STGd_{33}$	360	15	84.3	65	5	25.5	2.11	425
$2STGd_{34}$	384	16	84.4	70	7	39.4	2.08	454
$2STGd_{35}$	384	16	84.1	77	7	39.5	2.06	461
$2STGd_{36}$	360	15	84.9	110	10	29.0	2.0	470
$2STGd_{37}$	360	15	84.8	120	10	33.5	1.97	480
$2STGd_{38}$	384	16	84.9	110	10	35.6	1.93	494
$2STGe_{1}$	99	9	79.5	35	5	45.7	4.3	134
$2STGe_{2}$	150	10	82.7	0	0	0.0	2.56	150
$2STGe_{3}$	160	10	82.9	0	0	0.0	2.32	160

Continued on next page

Table C.2 – continued from previous page

Case	T1	P1	I1	T2	P2	I2	GDOP	T
$2STGe_4$	160	10	82.8	5	5	28.4	2.27	165
$2STGe_5$	160	10	83.4	10	5	36.0	2.26	170
$2STGe_6$	160	10	83.8	15	5	34.1	2.2	175
$2STGe_7$	160	10	83.8	20	5	33.9	2.15	180
$2STGe_8$	150	10	84.5	36	12	35.9	2.13	186
$2STGe_9$	170	10	83.4	20	5	35.9	2.11	190
$2STGe_{10}$	176	11	83.8	15	5	29.9	2.05	191
$2STGe_{11}$	176	11	83.0	18	6	34.2	2.02	194
$2STGe_{12}$	198	11	83.7	0	0	0.0	2.01	198
$2STGe_{13}$	160	10	83.6	42	14	36.2	1.96	202
$2STGe_{14}$	160	10	83.6	45	15	36.0	1.94	205
$2STGe_{15}$	176	11	81.7	33	11	33.6	1.93	209
$2STGe_{16}$	170	10	83.6	45	15	34.0	1.86	215
$2STGe_{17}$	160	10	84.2	60	15	35.9	1.85	220
$2STGe_{18}$	160	10	83.5	68	17	35.9	1.81	228
$2STGe_{19}$	187	11	83.3	45	15	34.0	1.76	232
$2STGe_{20}$	176	11	84.2	64	16	35.1	1.73	240
$2STGe_{21}$	176	11	83.6	68	17	36.2	1.71	244
$2STGe_{22}$	187	11	83.9	64	16	41.6	1.7	251
$2STGe_{23}$	162	18	83.8	91	13	41.6	1.67	253
$2STGe_{24}$	187	11	83.4	72	18	35.9	1.65	259
$2STGe_{25}$	198	11	83.9	68	17	41.0	1.63	266
$2STGe_{26}$	192	12	83.7	84	12	34.5	1.6	276
$2STGe_{27}$	216	12	83.1	68	17	36.2	1.56	284
$2STGe_{28}$	160	10	83.1	136	17	47.8	1.53	296
$2STGe_{29}$	176	11	83.8	128	16	47.6	1.48	304
$2STGe_{30}$	176	11	83.8	136	17	43.7	1.46	312
$2STGe_{31}$	187	11	83.8	136	17	47.8	1.44	323
$2STGe_{32}$	198	11	83.0	136	17	47.8	1.41	334
$2STGe_{33}$	204	12	83.6	144	18	47.9	1.38	348
$2STGe_{34}$	221	13	83.8	144	18	47.9	1.33	365
$2STGe_{35}$	231	11	83.9	144	18	47.9	1.31	375
$2STGe_{36}$	264	12	83.9	136	17	47.9	1.27	400
$2STGe_{37}$	288	12	84.1	144	18	50.1	1.23	432
$2STGe_{38}$	165	11	83.0	306	17	59.0	1.17	471
$2STGe_{39}$	176	11	83.2	324	18	59.1	1.11	500

D

Feasibility Appendix

D.1. Launcher Satellite Placement

Several placement strategies were considered for placing the satellites within a launcher's payload capacity. The following figures show a top view of the different strategies evaluated. The two main shapes considered were rectangular and trapezoidal, as they are the most common shapes for satellite buses.

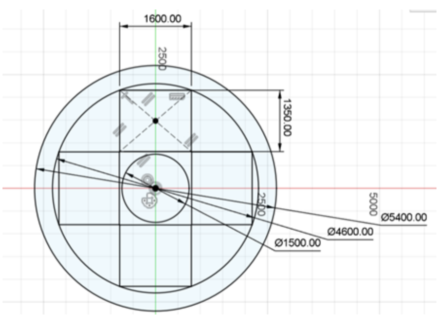

(a) Four Satellites Placement

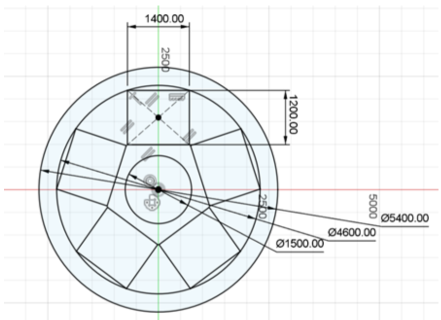

(b) Five Satellites Placement

Figure D.1: Rectangular Satellite Placement Strategies

Furthermore, the actual capacity for the different launchers was evaluated based on the satellite mass and volume. The following table summarises the results for the different configurations and altitudes considered in this work. The first row shows the capacity for the Ariane 62 with a lower fairing, while the second row shows the capacity for the Ariane 64. The second row can also be considered for the Ariane 62 with the longer fairing, as long as the mass does not exceed 10.3 tonnes. The limiting factor is in italics. The chosen configurations for the feasibility analysis are highlighted in bold. The values are shown in Table D.1.

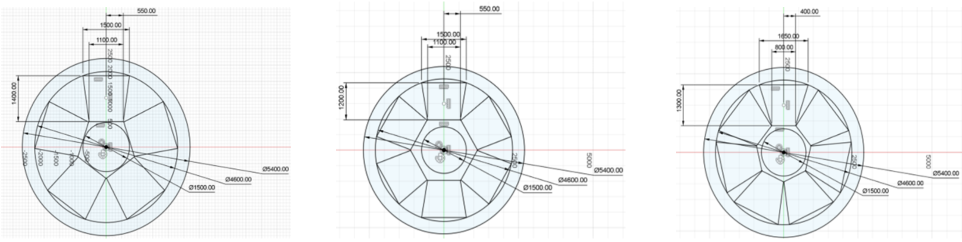

(a) Five Satellites Placement (b) Six Satellites Placement (c) Seven Satellites Placement

Figure D.2: Trapezoidal Satellite Placement Strategies

Table D.1: Launcher capacity for different altitudes and configurations.

Altitude [km]	Launcher	Rec. 4	Rec. 5	Trap. 5	Trap. 6	Trap. 7
1450	Ariane 62	12	10	10	12	**14**
	Ariane 64	24	25	25	***30***	**35**
1250	Ariane 62	12	10	10	12	**14**
	Ariane 64	28	30	30	***30***	**35**
1050	Ariane 62	12	10	15	12	**14**
	Ariane 64	32	30	30	***36***	**42**
850	Ariane 62	16	15	15	18	**21**
	Ariane 64	36	35	35	36	***42***
700	Ariane 62	16	15	15	18	**21**
	Ariane 64	36	35	40	***42***	**49**

D.2. LAUNCH STRATEGY DYNAMIC PROGRAMMING

The dynamic programming algorithm developed to find the optimal launch strategy aims to minimise the total number of launches required, followed by minimising the unused launcher capacity, and, under a tie, preferring Ariane 64 over Ariane 62. The problem consists of finding the best combination of launches that distributes all satellites into complete planes, given the constraints of launcher capacity.

In dynamic programming, the global problem (launching all orbital planes) is decomposed into smaller subproblems (launching a subset of planes). For a given number of remaining planes, the algorithm evaluates all possible launch options by testing both Ariane 62 and Ariane 64, and considering launching between 1 and the maximum number of planes that fit within the launcher's capacity. Each possible action is defined as a state, characterised by the number of planes left to launch, the launcher type, and the number of satellites launched in that action. The algorithm then recursively computes the optimal strategy for each state and stores the results in memory to avoid redundant calculations.

Through this process, the algorithm constructs a decision tree of possible launch sequences, evaluating the total number of launches and unused capacity for each sequence. By comparing these sequences according to the defined objectives, the algorithm identifies the optimal launch strategy. The final output is the sequence of launches that minimises the total number of launches, minimises unused capacity, and prefers Ariane 64 when equivalent options exist, ensuring an efficient deployment of the constellation.

D.3. RAAN SEPARATION AFTER SEQUENTIAL DRIFT AND RAISE

We consider two satellites initially co-located at a drift altitude h_d (semi-major axis $a_d = R_E + h_d$). Satellite 1 is raised immediately to the target altitude h_t ($a_t = R_E + h_t$) following some altitude profile $a_{\text{raise}}(\tau)$ of duration T, while Satellite 2 remains at a_d drifting for time t before following the same raise profile, simply delayed by t.
The secular RAAN rate for circular orbits under the J_2 perturbation is given by Equation 3.11, but repeated here for convenience:

$$\dot{\Omega}(a) = -\frac{3}{2} J_2 R_E^2 \sqrt{\frac{\mu}{a^7}} \cos i \Rightarrow K a^{-7/2},$$

where a is the semi-major axis, i the inclination, μ the Earth's gravitational parameter, R_E the Earth radius, and J_2 the second zonal harmonic.

The accumulated RAAN difference between the two satellites at the end of both manoeuvres is

$$\Delta\Omega = \int_0^{t+T} \left[\dot{\Omega}_2(\tau) - \dot{\Omega}_1(\tau)\right] d\tau. \tag{D.1}$$

Now, the integral can be split into intervals ($[0,T]$, $[T,t]$, $[t,t+T]$), where it is assumed that $t > T$, meaning that the raise is completed before the second satellite starts its raise manoeuvre. The piecewise definitions of $a_1(\tau)$ and $a_2(\tau)$ are:

$$a_1(\tau) = \begin{cases} a_{\text{raise}}(\tau), & 0 \le \tau \le T, \\ a_t, & \tau > T, \end{cases} \tag{D.2}$$

$$a_2(\tau) = \begin{cases} a_d, & 0 \le \tau < t, \\ a_{\text{raise}}(\tau - t), & t \le \tau \le t+T, \\ a_t, & \tau > t+T. \end{cases} \tag{D.3}$$

Thus, the RAAN difference can be expressed as

$$\frac{1}{K}\Delta\Omega = \int_0^T \left[a_d^{-7/2} - a_{\text{raise}}(\tau)^{-7/2}\right] d\tau + \int_T^t \left[a_d^{-7/2} - a_t^{-7/2}\right] d\tau + \tag{D.4}$$

$$\int_t^{t+T} \left[a_{\text{raise}}(\tau - t)^{-7/2} - a_t^{-7/2}\right] d\tau. \tag{D.5}$$

By performing a change of variable in the last integral ($u = \tau - t$), so $u \in [0,T]$, we can combine the first and last integrals, cancelling the raising profile terms:

$$\int_0^T \left[a_d^{-7/2} - a_{\text{raise}}(u)^{-7/2}\right] du + \int_0^T \left[a_{\text{raise}}(u)^{-7/2} - a_t^{-7/2}\right] du = T\left[a_d^{-7/2} - a_t^{-7/2}\right]. \tag{D.6}$$

Then, adding the middle integral, given by:

$$\int_T^t \left[a_d^{-7/2} - a_t^{-7/2}\right] d\tau = (t-T)\left[a_d^{-7/2} - a_t^{-7/2}\right], \tag{D.7}$$

we obtain the final result:

$$\Delta\Omega = K(T + (t-T))\left[a_d^{-7/2} - a_t^{-7/2}\right] = Kt\left[a_d^{-7/2} - a_t^{-7/2}\right]. \tag{D.8}$$

This shows that the RAAN separation depends only on the drift time t and not on the raise profile or duration T, as long as the two satellites follow the same profile. The same result can be obtained for the case $t < T$.

D

D.4. YAW-STEERING LAW

This section works as a validation for what subsection 7.7.1 presented regarding the yaw-steering angle requirements for inter-satellite links in polar LEO constellations.

D.4.1. POSITION OF THE SUN

According to Reda and Andreas (2008) [135], the Julian Day (JD) corresponding to a calendar date $(Y, M, D, H, \text{Min}, S)$ is computed as

$$\begin{aligned}
\text{if } M \le 2: \quad & Y \leftarrow Y-1, \quad M \leftarrow M+12, \\
A &= \left\lfloor \frac{Y}{100} \right\rfloor, \\
B &= 2 - A + \left\lfloor \frac{A}{4} \right\rfloor, \\
JD &= \lfloor 365.25(Y+4716) \rfloor + \lfloor 30.6001(M+1) \rfloor + D + B - 1524.5 \\
&\quad + \frac{H + \frac{\text{Min}}{60} + \frac{S}{3600}}{24}.
\end{aligned} \tag{D.9}$$

The number of days since J2000.0 is

$$n = JD - 2451545.0. \tag{D.10}$$

The Sun's mean longitude and mean anomaly (in degrees) are

$$L = 280.46^\circ + 0.9856474^\circ\, n, \qquad \theta = 357.528^\circ + 0.9856003^\circ\, n. \tag{D.11}$$

The ecliptic longitude is then

$$\lambda = L + 1.915^\circ \sin\theta + 0.020^\circ \sin(2\theta). \tag{D.12}$$

The obliquity of the ecliptic is approximated as

$$\varepsilon = 23.439^\circ - 0.0000004^\circ\, n. \tag{D.13}$$

In ecliptic coordinates, the position of the Sun (in astronomical units) is

$$\begin{aligned} x_{\text{ecl}} &= \cos\lambda, \\ y_{\text{ecl}} &= \cos\varepsilon \sin\lambda, \\ z_{\text{ecl}} &= \sin\varepsilon \sin\lambda. \end{aligned} \tag{D.14}$$

Finally, converting to kilometres (with 1 AU = 149,597,870.7 km), the solar position vector in the Earth-Centred Inertial (ECI) frame is

$$\vec{r}_{\text{ECI}} = \text{AU}_{\text{km}} \begin{bmatrix} x_{\text{ecl}} \\ y_{\text{ecl}} \\ z_{\text{ecl}} \end{bmatrix}. \tag{D.15}$$

D

D.4.2. YAW-STEERING ANGLE COMPUTATION FOR REALISTIC EXAMPLE

In a similar manner to what is shown in the main text, the yaw-steering angle is computed for a more realistic orbit and Sun position. The orbit considered has an altitude of 1450 km, an inclination of 45°. The Sun position corresponds to January 1st, 2025, at 12:00 UTC. The results are shown in Figure D.3.

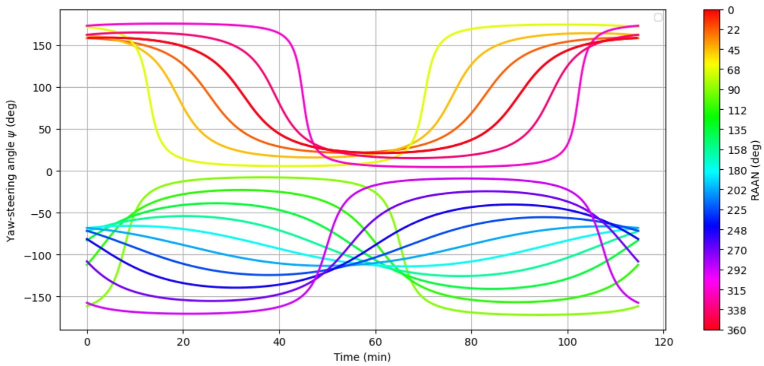

Figure D.3: Yaw-steering angle for a 1450 km altitude, 45° inclination orbit on January 1st, 2025.

The results confirm that a maximum yaw-steering angle of approximately ±90° is required, oscillating around ±90° depending on the RAAN.

E

Constellation Optimisation Results and Discussion Appendix

E.1. Analysis of Pareto Optimal Constellations

This section presents additional information regarding the analysis of the three selected Pareto optimal constellations presented in section 8.3. It shows the satellite characteristics for each constellation and their respective mass, power, and Δv budgets.

Table E.1: Satellite mass, power, and Δv budget (including margins) for selected Pareto optimal constellations

Param.	**Best GDOP Constellation (Polar/Low-Inc.)**	**Galileo Trade-off**	**Galileo Trade-off 2 Shells (Polar/Low-Inc.)**	**Closest to Origin Constellation**
		Mass (kg)		
Dry	235.7	235.5	235.4	235.2
Rad. Shield	34.0	34.0	34.0	33.8
Propellant	17.3	17.2	17.2	17.1
Wet	**287.2**	**286.6**	**286.6**	**286.1**
		Payload Power (W)		
Payload power	823.8/805.7	822.3	822.3/805.7	820.8
		Δv Budget (m/s)		
EOL disposal	457.3/436.2	455.6	455.6/436.3	453.8
Station-keeping (nominal)	3.7	3.7	3.7	3.7
Collision avoidance (CAM)	0.001	0.001	0.001	0.001
Deployment	329.9/451.5	328.3	328.3/0.0	326.8
Total	**790.9/891.4**	**787.6**	**787.6/439.9**	**784.3**

E.2. Complete Pareto Fronts

Table E.2: Pareto optimal configurations for single shell constellations

Case	T	P	F	h	I	GDOP	Cost	Time
$1SGCLa_1$	204	12	6	1246.1	87.4	2.22	4.18	23.7
$1SGCLa_2$	187	11	4	1239.0	81.6	2.34	3.93	16.5
$1SGCLa_3$	150	10	4	1237.9	80.7	3.42	3.24	16.4
$1SGCLa_4$	187	11	4	1236.5	79.5	2.55	3.93	16.3
$1SGCLa_5$	140	10	5	1239.0	81.6	4.21	3.09	16.5
$1SGCLa_6$	200	20	9	1242.5	84.5	2.28	4.12	21.7
$1SGCLa_7$	187	11	4	1241.8	84.0	2.33	3.93	17.4
$1SGCLa_8$	160	10	3	1235.9	79.0	3.06	3.47	16.1
$1SGCLa_9$	180	18	7	1234.6	77.8	2.98	3.75	19.0
$1SGCLa_{10}$	160	10	3	1234.2	77.5	3.43	3.47	15.9
$1SGCLa_{11}$	220	20	8	1238.6	81.3	2.12	4.49	21.3
$1SGCLa_{12}$	176	11	5	1242.3	84.4	2.6	3.78	17.5
$1SGCLa_{13}$	150	10	4	1239.1	81.7	3.35	3.24	16.6
$1SGCLa_{14}$	187	11	4	1244.2	85.9	2.32	3.94	18.7
$1SGCLa_{15}$	144	9	1	1235.8	78.9	4.14	3.22	13.3
$1SGCLa_{16}$	176	11	5	1240.1	82.6	2.62	3.78	16.8
$1SGCLa_{17}$	176	11	5	1235.3	78.5	2.88	3.78	16.3
$1SGCLa_{18}$	170	10	2	1236.0	79.1	3.01	3.61	16.2
$1SGCLa_{19}$	180	18	7	1235.5	78.6	2.82	3.75	19.1
$1SGCLa_{20}$	150	10	4	1236.8	79.8	3.53	3.24	16.2
$1SGCLa_{21}$	176	11	5	1239.2	81.8	2.62	3.78	16.5
$1SGCLa_{22}$	150	10	4	1235.7	78.8	3.69	3.24	16.0
$1SGCLa_{23}$	180	18	7	1235.3	78.5	2.85	3.75	19.1
$1SGCLa_{24}$	180	18	7	1236.6	79.6	2.64	3.75	19.2
$1SGCLa_{25}$	176	11	5	1237.4	80.3	2.66	3.78	16.3
$1SGCLa_{26}$	150	10	4	1240.8	83.1	3.25	3.24	17.1
$1SGCLa_{27}$	160	10	3	1235.1	78.3	3.23	3.47	16.0
$1SGCLa_{28}$	176	11	5	1246.0	87.3	2.6	3.79	20.9
$1SGCLa_{29}$	204	12	6	1243.7	85.5	2.23	4.18	21.1
$1SGCLa_{30}$	170	10	2	1235.0	78.2	3.17	3.61	16.1
$1SGCLb_1$	252	12	2	867.9	80.3	3.1	4.43	19.3
$1SGCLb_2$	216	12	5	867.7	80.2	3.81	4.0	19.0
$1SGCLb_3$	273	13	4	870.0	81.9	2.49	4.77	19.6
$1SGCLb_4$	228	12	4	867.5	80.0	3.31	4.15	19.1
$1SGCLb_5$	247	13	6	872.2	83.5	2.8	4.48	19.9
$1SGCLb_6$	216	12	5	871.8	83.2	3.41	4.01	19.9
$1SGCLb_7$	247	13	6	876.3	86.4	2.74	4.49	22.0
$1SGCLb_8$	294	14	6	873.9	84.7	2.22	5.01	23.4
$1SGCLb_9$	315	15	8	875.4	85.8	2.18	5.36	24.0
$1SGCLb_{10}$	252	12	2	868.4	80.7	2.91	4.43	19.3
$1SGCLb_{11}$	216	12	5	869.6	81.6	3.57	4.01	19.4

Continued on next page

E

Table E.2 – continued from previous page

Case	T	P	F	h	I	GDOP	Cost	Time
1SGCLb$_{12}$	198	11	3	871.1	82.7	4.03	3.79	16.9
1SGCLb$_{13}$	209	11	2	868.7	80.9	3.93	3.92	16.5
1SGCLb$_{14}$	260	13	5	868.3	80.6	2.8	4.62	19.6
1SGCLb$_{15}$	260	13	5	869.2	81.3	2.69	4.63	19.6
1SGCLb$_{16}$	273	13	4	868.8	81.0	2.64	4.77	19.6
1SGCLb$_{17}$	228	12	4	866.5	79.3	3.62	4.15	18.9
1SGCLb$_{18}$	247	13	6	874.2	84.9	2.76	4.48	20.6
1SGCLb$_{19}$	315	15	8	872.2	83.5	2.23	5.35	22.7
1SGCLc$_{1}$	216	12	5	1047.7	80.9	2.6	4.06	19.1
1SGCLc$_{2}$	273	13	4	1048.5	81.5	2.1	4.95	19.6
1SGCLc$_{3}$	204	12	6	1052.4	84.5	3.0	3.91	20.2
1SGCLc$_{4}$	204	12	6	1056.1	87.3	2.74	3.92	23.1
1SGCLc$_{5}$	176	11	5	1052.1	84.3	3.53	3.55	17.2
1SGCLc$_{6}$	180	9	6	1049.6	82.4	4.16	3.58	14.2
1SGCLc$_{7}$	228	12	4	1047.0	80.3	2.59	4.31	19.1
1SGCLc$_{8}$	216	12	5	1045.9	79.4	2.76	4.06	18.8
1SGCLc$_{9}$	176	11	5	1054.2	85.9	3.43	3.55	18.4
1SGCLc$_{10}$	210	10	8	1044.5	78.3	3.34	3.98	16.1
1SGCLc$_{11}$	204	12	6	1046.3	79.8	3.03	3.91	18.8
1SGCLc$_{12}$	252	12	2	1047.1	80.4	2.4	4.61	19.2
1SGCLc$_{13}$	168	8	2	1049.0	81.9	4.14	3.34	14.4
1SGCLc$_{14}$	252	12	2	1050.4	83.0	2.16	4.61	19.8
1SGCLc$_{15}$	210	10	8	1045.9	79.4	3.04	3.98	16.3
1SGCLc$_{16}$	189	9	5	1049.6	82.4	3.71	3.7	14.2
1SGCLc$_{17}$	189	9	5	1043.7	77.6	3.84	3.7	13.6
1SGCLc$_{18}$	170	10	2	1047.2	80.5	3.79	3.38	16.2
1SGCLc$_{19}$	204	12	6	1054.5	86.1	2.77	3.91	21.3
1SGCLc$_{20}$	210	10	8	1055.4	86.8	2.88	3.99	20.4
1SGCLc$_{21}$	220	11	1	1047.3	80.6	2.65	4.2	16.5
1SGCLc$_{22}$	168	8	2	1049.9	82.6	4.13	3.34	14.7
1SGCLc$_{23}$	260	13	5	1056.0	87.2	2.09	4.8	22.7
1SGCLc$_{24}$	231	11	0	1050.3	82.9	2.42	4.34	16.9
1SGCLc$_{25}$	180	9	6	1051.8	84.1	3.96	3.59	15.0
1SGCLc$_{26}$	180	9	6	1050.0	82.7	4.04	3.58	14.3
1SGCLc$_{27}$	189	9	5	1051.6	83.9	3.66	3.7	14.9
1SGCLc$_{28}$	180	10	1	1045.9	79.4	4.05	3.51	16.1
1SGCLc$_{29}$	170	10	2	1048.1	81.2	3.79	3.38	16.4
1SGCLc$_{30}$	189	9	5	1053.2	85.1	3.63	3.7	15.8
1SGCLc$_{31}$	228	12	4	1048.6	81.6	2.34	4.32	19.3
1SGCLc$_{32}$	187	11	4	1046.0	79.5	3.17	3.69	16.3
1SGCLc$_{33}$	187	11	4	1044.3	78.1	3.57	3.69	16.3
1SGCLc$_{34}$	280	14	7	1053.8	85.6	2.0	5.06	23.6

Continued on next page

E

Table E.2 – continued from previous page

Case	T	P	F	h	I	GDOP	Cost	Time
1SGCLc$_{35}$	176	11	5	1050.1	82.8	3.73	3.55	16.6
1SGCLc$_{36}$	315	15	8	1053.7	85.5	1.86	5.55	23.4
1SGCLc$_{37}$	176	11	5	1055.3	86.7	3.42	3.55	19.4
1SGCLc$_{38}$	200	10	9	1044.6	78.4	3.47	3.86	16.1
1SGCLc$_{39}$	209	11	2	1046.7	80.1	2.81	4.06	16.5
1SGCLd$_{1}$	312	13	1	700.0	81.0	3.3	5.0	19.8
1SGCLd$_{2}$	260	13	5	703.5	83.4	4.07	4.34	20.5
1SGCLd$_{3}$	312	13	1	699.7	80.8	3.45	5.0	19.8
1SGCLd$_{4}$	336	14	3	701.0	81.7	2.75	5.26	22.9
1SGCLd$_{5}$	294	14	6	700.2	81.1	3.45	4.7	22.5
1SGCLd$_{6}$	345	15	6	701.2	81.8	2.61	5.44	22.8
1SGCLd$_{7}$	294	14	6	698.6	80.0	3.64	4.7	22.2
1SGCLd$_{8}$	336	14	3	700.3	81.2	2.9	5.26	22.7
1SGCLd$_{9}$	312	13	1	700.7	81.5	3.22	5.0	20.0
1SGCLd$_{10}$	294	14	6	698.9	80.2	3.56	4.7	22.3
1SGCLd$_{11}$	294	14	6	702.2	82.5	3.32	4.7	22.9
1SGCLd$_{12}$	308	14	5	699.4	80.6	3.34	4.97	22.4
1SGCLd$_{13}$	286	13	3	699.9	80.9	3.65	4.72	19.7
1SGCLd$_{14}$	273	13	4	700.4	81.3	3.66	4.47	19.7
1SGCLd$_{15}$	294	14	6	703.9	83.7	3.2	4.7	23.5
1SGCLd$_{16}$	308	14	5	700.7	81.5	2.99	4.97	22.7
1SGCLd$_{17}$	260	13	5	702.5	82.7	4.24	4.33	20.1
1SGCLd$_{18}$	308	14	5	699.0	80.3	3.46	4.97	22.4
1SGCLd$_{19}$	260	13	5	705.4	84.7	3.92	4.34	21.3
1SGCLd$_{20}$	260	13	5	704.7	84.2	3.99	4.34	20.9
1SGCLe$_{1}$	160	10	3	1437.6	77.7	2.72	3.61	16.2
1SGCLe$_{2}$	187	11	4	1446.5	85.7	2.08	4.1	18.8
1SGCLe$_{3}$	160	10	3	1443.7	83.3	2.31	3.62	17.5
1SGCLe$_{4}$	204	12	6	1448.4	87.3	1.99	4.36	23.8
1SGCLe$_{5}$	119	7	3	1444.9	84.3	4.26	2.87	13.5
1SGCLe$_{6}$	160	10	3	1439.9	79.8	2.42	3.61	16.5
1SGCLe$_{7}$	150	10	4	1437.4	77.5	2.86	3.37	16.1
1SGCLe$_{8}$	221	13	8	1448.6	87.5	1.95	4.68	23.8
1SGCLe$_{9}$	140	10	5	1448.3	87.2	3.17	3.23	21.5
1SGCLe$_{10}$	221	13	8	1441.2	81.0	1.99	4.67	19.4
1SGCLe$_{11}$	150	10	4	1441.5	81.3	2.56	3.38	16.8
1SGCLe$_{12}$	150	10	4	1438.3	78.3	2.66	3.37	16.2
1SGCLe$_{13}$	135	9	2	1437.5	77.6	3.27	3.15	13.2
1SGCLe$_{14}$	126	9	3	1441.5	81.3	3.39	3.01	13.9
1SGCLe$_{15}$	170	10	2	1440.8	80.7	2.27	3.76	16.8
1SGCLe$_{16}$	126	9	3	1438.9	78.9	3.47	3.01	13.4
1SGCLe$_{17}$	160	10	3	1445.2	84.6	2.31	3.62	18.3

Continued on next page

E

Table E.2 – continued from previous page

Case	T	P	F	h	I	GDOP	Cost	Time
$1SGCLe_{18}$	187	11	4	1443.7	83.3	2.09	4.1	17.3
$1SGCLe_{19}$	176	11	5	1439.5	79.5	2.29	3.93	16.3
$1SGCLe_{20}$	187	11	4	1448.3	87.2	2.06	4.1	21.1
$1SGCLe_{21}$	238	14	10	1441.1	80.9	1.87	4.92	22.3
$1SGCLe_{22}$	176	11	5	1437.5	77.6	2.57	3.93	16.3
$1SGCLe_{23}$	187	11	4	1440.8	80.7	2.13	4.09	16.6
$1SGCLe_{24}$	140	10	5	1448.5	87.4	3.16	3.23	22.1

E

Table E.3: Pareto optimal configurations for double shell constellations

Case	T1	P1	F1	h1	I1	T2	P2	F2	h2	I2	GDOP	Cost	Time
$2SGCLa_{1}$	150	10	4	1239.3	81.9	27	3	2	1199.8	25.8	2.75	3.7	19.6
$2SGCLa_{2}$	150	10	4	1239.9	82.4	12	2	1	1199.6	25.1	3.01	3.5	19.3
$2SGCLa_{3}$	170	10	2	1240.3	82.7	8	1	0	1200.8	29.4	2.73	3.81	17.1
$2SGCLa_{4}$	150	10	4	1239.1	81.7	18	3	2	1199.7	25.4	2.92	3.58	19.2
$2SGCLa_{5}$	135	9	2	1238.4	81.1	10	1	0	1218.3	61.2	4.15	3.25	16.0
$2SGCLa_{6}$	187	11	4	1242.3	84.4	60	6	1	1199.8	25.6	1.9	4.9	23.5
$2SGCLa_{7}$	144	9	1	1235.7	78.8	9	1	0	1218.9	61.9	3.82	3.44	15.5
$2SGCLa_{8}$	160	10	3	1237.9	80.7	13	1	0	1200.5	28.3	2.89	3.74	16.5
$2SGCLa_{9}$	187	11	4	1238.1	80.9	6	1	0	1200.9	29.6	2.37	4.1	18.4
$2SGCLa_{10}$	190	19	8	1240.1	82.6	14	2	0	1199.6	25.0	2.21	4.26	22.2
$2SGCLa_{11}$	144	9	1	1236.3	79.3	6	1	0	1199.7	25.3	4.0	3.4	15.5
$2SGCLa_{12}$	150	10	4	1241.0	83.3	6	1	0	1199.7	25.3	3.13	3.41	17.2
$2SGCLa_{13}$	170	10	2	1237.3	80.2	9	1	0	1199.6	25.0	2.76	3.82	16.4
$2SGCLa_{14}$	144	9	1	1235.3	78.5	12	2	1	1232.0	75.5	3.65	3.48	15.6
$2SGCLa_{15}$	150	10	4	1241.2	83.5	39	3	1	1199.8	25.8	2.47	3.96	19.9
$2SGCLa_{16}$	150	10	4	1237.0	79.9	16	2	1	1199.8	25.7	3.01	3.55	18.8
$2SGCLa_{17}$	150	10	4	1237.2	80.1	6	1	0	1199.7	25.4	3.26	3.41	16.3
$2SGCLa_{18}$	135	9	2	1240.1	82.6	10	1	0	1199.7	25.2	3.83	3.26	16.5
$2SGCLa_{19}$	170	10	2	1238.7	81.4	16	2	1	1200.0	26.4	2.56	3.92	19.1
$2SGCLa_{20}$	187	11	4	1241.0	83.3	6	1	0	1200.0	26.6	2.27	4.1	19.1
$2SGCLa_{21}$	135	9	2	1235.9	79.0	22	2	0	1219.7	62.8	3.58	3.42	16.0
$2SGCLa_{22}$	135	9	2	1240.0	82.5	16	2	1	1199.7	25.4	3.52	3.34	16.7
$2SGCLa_{23}$	135	9	2	1239.7	82.2	14	2	0	1200.0	26.4	3.63	3.31	16.5
$2SGCLa_{24}$	150	10	4	1237.1	80.0	16	1	0	1199.6	25.0	3.13	3.55	16.2
$2SGCLa_{25}$	187	11	4	1241.8	84.0	28	4	0	1200.4	28.0	2.1	4.48	22.5
$2SGCLa_{26}$	135	9	2	1239.0	81.6	6	1	0	1200.8	29.1	4.21	3.2	16.0

Continued on next page

Table E.3 – continued from previous page

Case	T1	P1	F1	h1	I1	T2	P2	F2	h2	I2	GDOP	Cost	Time
$2SGCLa_{27}$	160	10	3	1236.6	79.6	8	1	0	1201.6	31.8	2.94	3.67	16.2
$2SGCLa_{28}$	170	10	2	1238.2	81.0	27	3	2	1199.6	25.1	2.47	4.07	19.4
$2SGCLa_{29}$	150	10	4	1236.7	79.7	24	3	0	1200.2	27.3	2.92	3.66	19.0
$2SGCLa_{30}$	150	10	4	1239.4	82.0	33	3	0	1199.7	25.3	2.58	3.8	19.8
$2SGCLa_{31}$	150	10	4	1238.6	81.3	21	1	0	1200.9	29.7	3.0	3.62	16.5
$2SGCLa_{32}$	150	10	4	1239.7	82.2	7	1	0	1199.8	25.7	3.13	3.43	16.8
$2SGCLa_{33}$	135	9	2	1239.7	82.2	20	2	1	1200.1	26.8	3.43	3.4	16.7
$2SGCLa_{34}$	176	11	5	1237.5	80.4	9	1	0	1199.6	25.0	2.57	3.99	18.5
$2SGCLa_{35}$	144	9	1	1235.5	78.6	21	3	1	1216.2	58.5	3.54	3.61	15.9
$2SGCLa_{36}$	150	10	4	1239.7	82.2	10	1	0	1199.7	25.3	3.07	3.47	16.8
$2SGCLa_{37}$	204	12	6	1239.3	81.9	13	1	0	1199.7	25.3	2.16	4.44	19.5
$2SGCLa_{38}$	135	9	2	1239.5	82.1	7	1	0	1199.7	25.3	4.19	3.21	16.2
$2SGCLa_{39}$	135	9	2	1237.2	80.1	18	3	2	1202.9	35.3	3.56	3.37	16.0
$2SGCLa_{40}$	150	10	4	1239.7	82.2	19	1	0	1205.5	41.4	3.05	3.59	16.8
$2SGCLa_{41}$	150	10	4	1243.0	84.9	30	3	1	1200.3	27.4	2.64	3.75	21.1
$2SGCLa_{42}$	150	10	4	1237.3	80.2	11	1	0	1199.7	25.3	3.15	3.48	16.3
$2SGCLa_{43}$	170	10	2	1237.5	80.4	17	1	0	1214.5	56.2	2.65	3.93	16.5
$2SGCLa_{44}$	160	10	3	1237.8	80.6	18	2	0	1200.1	27.0	2.71	3.81	19.0
$2SGCLa_{45}$	187	11	4	1240.1	82.6	27	3	2	1200.2	27.3	2.11	4.38	19.6
$2SGCLa_{46}$	135	9	2	1239.7	82.2	18	2	0	1199.7	25.3	3.45	3.37	16.6
$2SGCLa_{47}$	150	10	4	1236.4	79.4	20	1	0	1199.7	25.2	3.13	3.61	16.2
$2SGCLb_{1}$	247	13	6	869.5	81.5	6	1	0	823.8	26.4	2.81	4.65	21.4
$2SGCLb_{2}$	252	12	2	869.2	81.3	13	1	0	823.4	25.1	2.8	4.68	19.6
$2SGCLb_{3}$	216	12	5	871.0	82.6	8	1	0	828.1	36.7	3.37	4.21	19.7
$2SGCLb_{4}$	247	13	6	875.3	85.7	21	3	1	823.4	25.0	2.61	4.83	23.7
$2SGCLb_{5}$	168	8	2	872.3	83.6	48	4	3	823.9	26.6	3.82	4.01	18.5
$2SGCLb_{6}$	260	13	5	871.7	83.1	30	2	0	823.6	25.6	2.34	5.07	22.4

Continued on next page

Table E.3 – continued from previous page

Case	T1	P1	F1	h1	I1	T2	P2	F2	h2	I2	GDOP	Cost	Time
2SGCLb$_{7}$	216	12	5	872.5	83.7	11	1	0	823.5	25.3	3.28	4.25	20.1
2SGCLb$_{8}$	198	11	3	873.6	84.5	14	2	0	823.8	26.3	3.81	4.07	20.1
2SGCLb$_{9}$	216	12	5	870.6	82.3	15	1	0	823.4	25.0	3.28	4.29	19.6
2SGCLb$_{10}$	216	12	5	872.1	83.4	6	1	0	831.0	42.1	3.37	4.19	20.0
2SGCLb$_{11}$	216	12	5	872.1	83.4	12	2	1	823.4	25.0	3.26	4.26	22.2
2SGCLb$_{12}$	216	12	5	873.5	84.4	12	1	0	823.6	25.7	3.26	4.26	20.5
2SGCLb$_{13}$	198	11	3	870.7	82.4	6	1	0	851.1	66.4	3.97	3.97	18.8
2SGCLb$_{14}$	228	12	4	869.2	81.3	10	1	0	823.4	25.1	3.11	4.37	19.5
2SGCLb$_{15}$	198	11	3	871.8	83.2	12	1	0	823.5	25.3	3.82	4.04	19.3
2SGCLb$_{16}$	260	13	5	875.2	85.6	18	3	2	823.4	25.0	2.46	4.94	23.5
2SGCLb$_{17}$	216	12	5	871.9	83.3	14	2	0	823.6	25.6	3.22	4.28	22.2
2SGCLb$_{18}$	240	12	3	869.5	81.5	14	1	0	823.5	25.3	2.92	4.56	19.5
2SGCLb$_{19}$	216	12	5	873.0	84.1	24	2	1	823.4	25.2	3.09	4.4	22.9
2SGCLb$_{20}$	247	13	6	875.6	85.9	6	1	0	823.7	26.1	2.71	4.66	23.4
2SGCLb$_{21}$	209	11	2	869.6	81.6	11	1	0	823.4	25.0	3.74	4.16	18.7
2SGCLb$_{22}$	294	14	6	875.0	85.5	10	1	0	823.4	25.0	2.16	5.23	24.0
2SGCLb$_{23}$	198	11	3	871.0	82.6	20	2	1	824.3	27.9	3.66	4.14	19.3
2SGCLb$_{24}$	294	14	6	871.4	82.9	22	1	0	827.8	36.1	2.16	5.36	22.6
2SGCLb$_{25}$	216	12	5	873.3	84.3	6	1	0	823.4	25.0	3.33	4.19	20.4
2SGCLb$_{26}$	209	11	2	868.7	80.9	18	3	2	824.9	29.3	3.57	4.24	18.8
2SGCLb$_{27}$	198	11	3	872.1	83.4	6	1	0	823.9	26.7	3.9	3.97	19.2
2SGCLb$_{28}$	228	12	4	869.1	81.2	18	2	0	823.9	26.6	2.99	4.46	21.7
2SGCLb$_{29}$	294	14	6	873.6	84.5	15	1	0	823.4	25.0	2.15	5.29	23.3
2SGCLb$_{30}$	209	11	2	869.7	81.7	24	3	0	825.2	30.3	3.5	4.31	19.2
2SGCLb$_{31}$	216	12	5	873.5	84.4	36	3	2	824.1	27.2	2.93	4.54	23.5
2SGCLb$_{32}$	209	11	2	868.5	80.8	36	3	2	830.7	41.5	3.48	4.45	19.4
2SGCLb$_{33}$	198	11	3	873.3	84.3	13	1	0	823.4	25.0	3.81	4.06	19.9

Continued on next page

Table E.3 – continued from previous page

Case	T1	P1	F1	h1	I1	T2	P2	F2	h2	I2	GDOP	Cost	Time
2SGCLb$_{34}$	273	13	4	870.8	82.5	18	3	2	823.4	25.0	2.34	5.08	21.8
2SGCLb$_{35}$	260	13	5	873.7	84.6	15	1	0	823.7	25.9	2.5	4.91	22.6
2SGCLb$_{36}$	198	11	3	870.0	81.9	27	3	2	823.4	25.2	3.54	4.22	19.3
2SGCLb$_{37}$	228	12	4	871.4	82.9	22	2	0	823.4	25.2	2.97	4.51	22.3
2SGCLb$_{38}$	247	13	6	870.8	82.5	18	3	2	823.4	25.0	2.66	4.79	21.8
2SGCLb$_{39}$	247	13	6	873.6	84.5	11	1	0	823.8	26.2	2.7	4.71	22.5
2SGCLb$_{40}$	209	11	2	868.9	81.1	8	1	0	823.4	25.0	3.77	4.12	18.5
2SGCLb$_{41}$	260	13	5	870.6	82.3	15	1	0	823.4	25.0	2.5	4.9	21.8
2SGCLb$_{42}$	228	12	4	869.9	81.8	20	1	0	823.9	26.5	3.03	4.49	19.5
2SGCLc$_{1}$	228	12	4	1049.9	82.6	18	3	2	1006.5	27.0	2.23	4.63	21.9
2SGCLc$_{2}$	189	9	5	1047.0	80.3	24	2	1	1006.4	26.6	3.01	4.09	16.1
2SGCLc$_{3}$	198	11	3	1049.0	81.9	21	3	1	1007.1	28.9	2.64	4.18	18.9
2SGCLc$_{4}$	189	9	5	1049.2	82.1	36	3	2	1006.1	25.8	2.71	4.24	16.9
2SGCLc$_{5}$	160	10	3	1051.7	84.0	16	2	1	1008.0	31.4	3.7	3.55	19.8
2SGCLc$_{6}$	168	8	2	1050.9	83.4	36	4	2	1005.9	25.0	2.96	3.98	18.0
2SGCLc$_{7}$	252	12	2	1051.1	83.5	18	3	2	1005.9	25.0	2.05	4.92	22.2
2SGCLc$_{8}$	216	12	5	1051.6	83.9	26	2	0	1005.9	25.1	2.24	4.47	22.6
2SGCLc$_{9}$	147	7	6	1053.8	85.6	21	3	1	1006.3	26.4	4.34	3.41	16.9
2SGCLc$_{10}$	189	9	5	1046.8	80.2	22	2	0	1007.2	29.2	3.11	4.07	16.0
2SGCLc$_{11}$	240	12	3	1051.8	84.1	9	1	0	1006.7	27.7	2.21	4.66	20.2
2SGCLc$_{12}$	189	9	5	1046.6	80.0	17	1	0	1005.9	25.1	3.25	4.0	15.8
2SGCLc$_{13}$	168	8	2	1050.4	83.0	15	1	0	1005.9	25.1	3.68	3.62	14.9
2SGCLc$_{14}$	147	7	6	1054.9	86.4	20	2	1	1005.9	25.0	4.42	3.4	18.2
2SGCLc$_{15}$	216	12	5	1050.1	82.8	23	1	0	1010.3	37.0	2.33	4.43	19.6
2SGCLc$_{16}$	170	10	2	1047.7	80.9	12	2	1	1006.0	25.5	3.52	3.62	18.6
2SGCLc$_{17}$	168	8	2	1049.5	82.3	33	3	0	1007.3	29.5	3.24	3.85	17.3
2SGCLc$_{18}$	189	9	5	1050.8	83.3	8	1	0	1006.8	28.1	3.45	3.89	16.5

Continued on next page

Table E.3 – continued from previous page

Case	T1	P1	F1	h1	I1	T2	P2	F2	h2	I2	GDOP	Cost	Time
$2SGCLc_{19}$	168	8	2	1049.2	82.1	23	1	0	1006.7	27.8	3.6	3.73	14.5
$2SGCLc_{20}$	209	11	2	1048.6	81.6	21	3	1	1006.1	25.8	2.5	4.41	18.9
$2SGCLc_{21}$	198	11	3	1048.9	81.8	12	1	0	1005.9	25.1	2.8	4.07	18.6
$2SGCLc_{22}$	204	12	6	1054.2	85.9	11	1	0	1005.9	25.1	2.62	4.14	21.1
$2SGCLc_{23}$	176	11	5	1055.6	86.9	14	2	0	1005.9	25.1	3.14	3.82	22.1
$2SGCLc_{24}$	252	12	2	1049.6	82.4	15	1	0	1005.9	25.2	2.15	4.88	19.6
$2SGCLc_{25}$	189	9	5	1048.2	81.3	6	1	0	1006.0	25.4	3.55	3.86	15.7
$2SGCLc_{26}$	204	12	6	1054.0	85.7	18	2	0	1006.1	25.8	2.55	4.23	23.4
$2SGCLc_{27}$	160	8	3	1049.6	82.4	40	4	1	1006.6	27.4	3.08	3.93	18.0
$2SGCLc_{28}$	170	10	2	1048.4	81.4	20	1	0	1006.8	28.0	3.49	3.73	16.5
$2SGCLc_{29}$	168	8	2	1050.8	83.3	9	1	0	1006.1	25.9	3.81	3.55	15.0
$2SGCLc_{30}$	160	10	3	1053.8	85.6	6	1	0	1005.9	25.0	3.91	3.42	18.5
$2SGCLc_{31}$	273	13	4	1053.2	85.1	27	3	2	1006.8	28.0	1.88	5.36	23.0
$2SGCLc_{32}$	160	8	3	1052.6	84.7	9	1	0	1005.9	25.0	4.17	3.44	15.9
$2SGCLc_{33}$	160	10	3	1055.7	87.0	21	3	1	1005.9	25.2	3.43	3.62	21.9
$2SGCLc_{34}$	252	12	2	1051.4	83.8	13	1	0	1006.0	25.3	2.1	4.86	20.1
$2SGCLc_{35}$	240	12	3	1053.0	85.0	39	3	1	1005.9	25.0	1.97	5.04	23.6
$2SGCLc_{36}$	210	10	8	1047.2	80.5	14	1	0	1008.1	31.8	2.77	4.25	16.6
$2SGCLc_{37}$	147	7	6	1048.1	81.2	39	3	1	1007.8	30.9	3.81	3.66	14.4
$2SGCLc_{38}$	144	8	5	1055.3	86.7	44	4	0	1006.0	25.3	3.42	3.71	18.4
$2SGCLc_{39}$	168	8	2	1052.5	84.6	6	1	0	1007.1	28.9	3.99	3.51	15.9
$2SGCLc_{40}$	216	12	5	1052.2	84.4	40	4	1	1006.6	27.4	2.11	4.73	23.9
$2SGCLc_{41}$	160	10	3	1052.4	84.5	14	1	0	1006.9	28.2	3.71	3.52	17.6
$2SGCLc_{42}$	176	11	5	1055.2	86.6	33	3	0	1006.2	26.1	2.77	4.07	22.3
$2SGCLc_{43}$	204	12	6	1050.8	83.3	9	1	0	1006.1	25.6	2.71	4.11	19.6
$2SGCLc_{44}$	210	10	8	1052.2	84.4	9	1	0	1005.9	25.0	2.79	4.19	17.9
$2SGCLc_{45}$	160	8	3	1051.2	83.6	51	3	0	1006.1	25.7	2.9	4.07	16.9

Continued on next page

Table E.3 – continued from previous page

Case	T1	P1	F1	h1	I1	T2	P2	F2	h2	I2	GDOP	Cost	Time
$2SGCLc_{46}$	187	11	4	1049.8	82.5	10	1	0	1006.6	27.5	2.98	3.91	18.7
$2SGCLc_{47}$	168	8	2	1049.5	82.3	6	1	0	1010.2	36.9	4.01	3.51	14.6
$2SGCLc_{48}$	176	11	5	1054.8	86.3	11	1	0	1006.0	25.5	3.23	3.78	21.1
$2SGCLc_{49}$	168	8	2	1052.1	84.3	19	1	0	1005.9	25.0	3.66	3.68	15.6
$2SGCLc_{50}$	170	10	2	1049.6	82.4	21	3	1	1006.4	26.7	3.31	3.74	19.3
$2SGCLc_{51}$	216	12	5	1050.7	83.2	7	1	0	1006.6	27.4	2.51	4.24	19.7
$2SGCLc_{52}$	189	9	5	1049.4	82.2	18	1	0	1006.1	25.8	3.19	4.02	16.4
$2SGCLc_{53}$	204	12	6	1056.1	87.3	6	1	0	1009.9	36.1	2.66	4.08	23.1
$2SGCLc_{54}$	170	10	2	1048.2	81.3	7	1	0	1006.2	26.2	3.64	3.56	16.4
$2SGCLc_{55}$	189	9	5	1049.4	82.2	42	3	0	1006.2	26.1	2.59	4.34	17.2
$2SGCLc_{56}$	160	8	3	1050.9	83.4	48	3	1	1006.4	26.9	3.02	4.03	17.0
$2SGCLc_{57}$	168	8	2	1050.0	82.7	24	1	0	1007.0	28.6	3.57	3.74	14.7
$2SGCLc_{58}$	231	11	0	1050.1	82.8	12	2	1	1006.6	27.3	2.32	4.57	18.9
$2SGCLc_{59}$	168	8	2	1050.8	83.3	22	2	0	1005.9	25.2	3.47	3.72	17.3
$2SGCLc_{60}$	216	12	5	1048.2	81.3	14	2	0	1007.0	28.7	2.39	4.32	21.4
$2SGCLc_{61}$	187	11	4	1052.4	84.5	20	2	1	1006.2	26.2	2.87	4.04	19.9
$2SGCLd_{1}$	286	13	3	700.2	81.1	6	1	0	651.0	25.0	3.55	4.87	21.5
$2SGCLd_{2}$	336	14	3	702.0	82.4	18	1	0	652.4	28.6	2.57	5.54	23.1
$2SGCLd_{3}$	260	13	5	704.5	84.1	36	3	2	651.0	25.0	3.28	4.81	23.7
$2SGCLd_{4}$	312	13	1	701.0	81.7	30	3	1	661.2	44.7	2.95	5.4	22.4
$2SGCLd_{5}$	312	13	1	701.5	82.0	6	1	0	655.0	34.4	3.16	5.15	21.7
$2SGCLd_{6}$	294	14	6	703.4	83.3	10	1	0	651.0	25.0	3.08	4.9	23.3
$2SGCLd_{7}$	273	13	4	701.0	81.7	7	1	0	654.2	32.7	3.57	4.64	21.7
$2SGCLd_{8}$	260	13	5	705.0	84.4	30	3	1	651.6	26.5	3.42	4.75	23.7
$2SGCLd_{9}$	294	14	6	701.5	82.0	25	1	0	651.0	25.0	2.89	5.05	22.8
$2SGCLd_{10}$	273	13	4	700.9	81.6	12	2	1	651.5	26.4	3.49	4.69	21.8
$2SGCLd_{11}$	322	14	4	701.7	82.2	18	1	0	651.7	26.8	2.75	5.39	23.0

Continued on next page

Table E.3 – continued from previous page

Case	T1	P1	F1	h1	I1	T2	P2	F2	h2	I2	GDOP	Cost	Time
2SGCLd$_{12}$	299	13	2	700.3	81.2	6	1	0	651.2	25.4	3.48	5.01	21.5
2SGCLd$_{13}$	294	14	6	700.4	81.3	24	1	0	651.2	25.4	3.07	5.04	22.6
2SGCLd$_{14}$	286	13	3	699.4	80.6	6	1	0	654.1	32.5	3.79	4.87	21.4
2SGCLd$_{15}$	294	14	6	701.9	82.3	8	1	0	655.0	34.4	3.22	4.87	22.9
2SGCLd$_{16}$	312	13	1	702.6	82.8	12	2	1	661.4	45.0	3.07	5.21	22.2
2SGCLd$_{17}$	299	13	2	702.2	82.5	17	1	0	651.1	25.2	3.23	5.13	22.3
2SGCLd$_{18}$	286	13	3	701.3	81.9	19	1	0	651.0	25.1	3.39	5.01	22.1
2SGCLd$_{19}$	260	13	5	703.1	83.1	8	1	0	652.7	29.3	3.65	4.51	22.3
2SGCLd$_{20}$	260	13	5	702.3	82.6	24	2	1	653.7	31.7	3.44	4.68	22.6
2SGCLd$_{21}$	312	13	1	700.0	81.0	7	1	0	671.4	57.2	3.37	5.16	21.5
2SGCLd$_{22}$	264	12	1	701.5	82.0	24	1	0	652.3	28.4	4.25	4.74	20.2
2SGCLd$_{23}$	294	14	6	701.5	82.0	15	1	0	651.0	25.0	3.08	4.95	22.8
2SGCLd$_{24}$	273	13	4	700.3	81.2	6	1	0	657.0	38.1	3.59	4.63	21.5
2SGCLd$_{25}$	322	14	4	703.4	83.3	10	1	0	651.2	25.4	2.78	5.32	23.4
2SGCLd$_{26}$	273	13	4	700.2	81.1	21	3	1	660.8	44.2	3.48	4.79	22.0
2SGCLd$_{27}$	273	13	4	703.6	83.5	24	3	0	651.3	25.7	3.31	4.82	23.0
2SGCLd$_{28}$	312	13	1	700.4	81.3	6	1	0	654.9	34.2	3.17	5.15	21.5
2SGCLd$_{29}$	294	14	6	700.3	81.2	13	1	0	651.3	25.9	3.18	4.92	22.6
2SGCLd$_{30}$	299	13	2	701.0	81.7	11	1	0	651.1	25.3	3.36	5.06	21.8
2SGCLd$_{31}$	260	13	5	702.8	82.9	10	1	0	653.4	31.0	3.64	4.53	22.2
2SGCLd$_{32}$	273	13	4	701.7	82.2	18	3	2	651.0	25.0	3.38	4.76	22.2
2SGCLd$_{33}$	336	14	3	702.9	83.0	13	1	0	651.9	27.4	2.58	5.49	23.3
2SGCLd$_{34}$	294	14	6	703.9	83.7	19	1	0	651.0	25.1	2.94	4.99	23.5
2SGCLd$_{35}$	260	13	5	701.2	81.8	24	3	0	655.6	35.5	3.53	4.68	22.3
2SGCLd$_{36}$	286	13	3	700.6	81.4	12	2	1	652.0	27.7	3.48	4.94	21.7
2SGCLd$_{37}$	286	13	3	698.7	80.1	6	1	0	651.3	25.7	4.19	4.87	21.4
2SGCLd$_{38}$	312	13	1	700.6	81.4	18	3	2	660.0	43.0	3.05	5.27	21.9

Continued on next page

Table E.3 – continued from previous page

Case	T1	P1	F1	h1	I1	T2	P2	F2	h2	I2	GDOP	Cost	Time
$2SGCLd_{39}$	260	13	5	703.1	83.1	14	2	0	652.0	27.8	3.56	4.58	22.5
$2SGCLd_{40}$	308	14	5	701.2	81.8	15	1	0	651.6	26.5	2.86	5.22	22.8
$2SGCLd_{41}$	260	13	5	702.2	82.5	6	1	0	652.2	28.1	3.73	4.49	21.9
$2SGCLd_{42}$	294	14	6	704.7	84.2	6	1	0	651.3	25.7	3.12	4.86	23.8
$2SGCLd_{43}$	273	13	4	702.2	82.5	24	2	1	651.0	25.1	3.36	4.82	22.5
$2SGCLe_{1}$	140	10	5	1447.4	86.5	12	2	1	1405.9	25.7	2.72	3.5	21.4
$2SGCLe_{2}$	119	7	3	1442.3	82.0	38	2	0	1405.8	25.0	2.73	3.62	15.7
$2SGCLe_{3}$	90	6	2	1442.5	82.2	42	6	4	1406.3	27.5	3.57	3.1	16.7
$2SGCLe_{4}$	150	10	4	1444.5	84.0	32	4	3	1405.8	25.1	2.1	4.02	20.6
$2SGCLe_{5}$	119	7	3	1444.5	84.0	9	1	0	1405.8	25.1	3.78	3.1	15.5
$2SGCLe_{6}$	119	7	3	1442.8	82.5	22	2	0	1406.9	29.5	3.35	3.3	15.0
$2SGCLe_{7}$	150	10	4	1445.9	85.2	18	1	0	1406.2	26.8	2.4	3.73	18.6
$2SGCLe_{8}$	144	9	1	1440.6	80.5	7	1	0	1405.8	25.0	2.87	3.55	16.0
$2SGCLe_{9}$	140	10	5	1448.5	87.4	30	3	1	1406.1	26.6	2.32	3.77	22.1
$2SGCLe_{10}$	119	7	3	1441.9	81.7	14	2	0	1410.1	39.0	3.89	3.17	14.3
$2SGCLe_{11}$	140	10	5	1445.6	84.9	12	1	0	1406.0	25.9	2.81	3.5	18.3
$2SGCLe_{12}$	119	7	3	1443.3	82.9	17	1	0	1405.8	25.1	3.49	3.22	15.0
$2SGCLe_{13}$	119	7	3	1444.5	84.0	6	1	0	1405.8	25.1	3.9	3.05	15.4
$2SGCLe_{14}$	140	10	5	1446.7	85.9	15	1	0	1405.8	25.0	2.7	3.54	19.3
$2SGCLe_{15}$	119	7	3	1442.8	82.5	14	2	0	1406.9	29.7	3.61	3.17	14.7
$2SGCLe_{16}$	126	9	3	1441.4	81.2	22	2	0	1405.8	25.1	2.83	3.43	16.7
$2SGCLe_{17}$	126	9	3	1438.5	78.5	7	1	0	1406.4	27.7	3.19	3.2	15.6
$2SGCLe_{18}$	126	9	3	1440.5	80.4	14	2	0	1405.8	25.0	2.97	3.31	16.2
$2SGCLe_{19}$	96	6	1	1442.9	82.6	28	4	0	1405.8	25.2	4.47	3.03	14.5
$2SGCLe_{20}$	85	5	2	1448.5	87.4	36	3	2	1406.6	28.4	3.89	2.97	23.3
$2SGCLe_{21}$	119	7	3	1440.9	80.8	18	3	2	1406.3	27.2	3.37	3.23	14.1
$2SGCLe_{22}$	176	11	5	1445.0	84.4	18	3	2	1406.2	27.0	2.01	4.28	20.3

Continued on next page

Table E.3 – continued from previous page

Case	T1	P1	F1	h1	I1	T2	P2	F2	h2	I2	GDOP	Cost	Time
2SGCLe$_{23}$	150	10	4	1442.5	82.2	17	1	0	1405.8	25.2	2.42	3.72	17.0
2SGCLe$_{24}$	90	6	2	1447.6	86.6	40	5	1	1405.9	25.6	3.78	3.08	18.2
2SGCLe$_{25}$	150	10	4	1441.7	81.5	8	1	0	1405.8	25.1	2.48	3.58	16.8
2SGCLe$_{26}$	136	8	6	1440.7	80.6	17	1	0	1405.8	25.0	3.12	3.49	14.2
2SGCLe$_{27}$	160	10	3	1442.4	82.1	10	1	0	1405.9	25.8	2.24	3.85	17.1
2SGCLe$_{28}$	187	11	4	1441.5	81.3	17	1	0	1409.0	36.3	2.02	4.42	19.1
2SGCLe$_{29}$	160	10	3	1440.4	80.3	16	2	1	1425.9	65.2	2.22	3.94	19.1
2SGCLe$_{30}$	136	8	6	1437.4	77.5	17	1	0	1405.9	25.6	3.34	3.49	13.6
2SGCLe$_{31}$	104	8	2	1444.6	84.1	18	3	2	1406.0	25.9	4.22	2.95	18.3
2SGCLe$_{32}$	119	7	3	1441.8	81.6	33	3	0	1406.8	29.4	2.88	3.48	14.9
2SGCLe$_{33}$	119	7	3	1445.0	84.4	14	2	0	1407.7	32.3	3.59	3.17	16.0
2SGCLe$_{34}$	150	10	4	1442.8	82.5	27	3	2	1406.1	26.3	2.18	3.86	20.1
2SGCLe$_{35}$	90	6	2	1448.5	87.4	36	4	2	1406.6	28.6	3.86	3.01	21.2
2SGCLe$_{36}$	187	11	4	1448.1	87.1	33	3	0	1406.0	26.1	1.8	4.67	23.8
2SGCLe$_{37}$	84	6	3	1444.2	83.7	40	5	1	1406.4	27.8	4.34	2.98	15.3
2SGCLe$_{38}$	135	9	2	1439.3	79.3	12	2	1	1406.0	25.9	2.96	3.42	15.9
2SGCLe$_{39}$	117	9	4	1446.5	85.7	30	3	1	1405.8	25.0	2.85	3.42	19.6
2SGCLe$_{40}$	85	5	2	1443.6	83.2	45	5	0	1410.3	39.5	4.35	3.11	15.1
2SGCLe$_{41}$	128	8	7	1437.4	77.5	17	1	0	1406.2	26.8	3.91	3.37	13.5
2SGCLe$_{42}$	90	6	2	1448.4	87.3	36	3	2	1406.6	28.5	4.13	3.01	20.7
2SGCLe$_{43}$	204	12	6	1444.8	84.2	40	4	1	1405.8	25.0	1.7	5.08	23.7
2SGCLe$_{44}$	126	9	3	1442.4	82.1	10	1	0	1405.8	25.0	3.14	3.25	16.6
2SGCLe$_{45}$	136	8	6	1437.6	77.7	16	1	0	1406.6	28.3	3.68	3.48	13.6
2SGCLe$_{46}$	126	9	3	1438.0	78.1	12	2	1	1432.6	72.7	3.09	3.28	15.7
2SGCLe$_{47}$	119	7	3	1444.5	84.0	32	4	3	1405.8	25.2	2.75	3.54	17.1
2SGCLe$_{48}$	170	10	2	1439.5	79.5	15	1	0	1435.9	76.0	2.21	4.06	16.5
2SGCLe$_{49}$	160	10	3	1439.6	79.6	18	1	0	1406.2	26.9	2.44	3.96	16.5

Continued on next page

Table E.3 – continued from previous page

Case	T1	P1	F1	h1	I1	T2	P2	F2	h2	I2	GDOP	Cost	Time
$2SGCLe_{50}$	104	8	2	1442.3	82.0	24	3	0	1409.3	37.0	3.94	3.04	17.4
$2SGCLe_{51}$	126	9	3	1440.5	80.4	6	1	0	1405.8	25.1	3.19	3.19	16.0
$2SGCLe_{52}$	150	10	4	1438.3	78.3	14	1	0	1437.0	77.1	2.5	3.67	16.2